Université de Liège
Faculté des Sciences Appliquées
Département ArGEnCo
Architecture, Géologie, Environnement et Constructions
Unité Géo^3
Géotechnologies, Hydrogéologie, Prospection géophysique

Groundwater flow and contaminant transport in an alluvial aquifer: *in-situ* investigation and modelling of a brownfield with strong groundwater – surface water interactions

Thèse de doctorat

présentée par Jordi BATLLE-AGUILAR

en vue de l'obtention du grade de Docteur en Sciences de l'Ingénieur

Soutenue devant le jury composé de :

Robert CHARLIER, Université de Liège (Belgique) - Président
Alain DASSARGUES, Université de Liège (Belgique) - Promoteur
Serge BROUYÈRE, Université de Liège (Belgique) - Co-promoteur
Stoyan GAYDARDZHIEV, Université de Liège (Belgique)
Frédéric NGUYEN, Université de Liège (Belgique)
Ludo DIELS, VITO (Belgique)
Henri HALEN, SPAQuE (Belgique)
Daniel HUNKELER, Université de Neuchâtel, (Suisse)
René THERRIEN, Université Laval (Canada)

Juillet 2008

Université de Liège
Faculté des Sciences Appliquées
Département ArGEnCo
Architecture, Géologie, Environnement et Constructions
Unité Géo^3
Géotechnologies, Hydrogéologie, Prospection géophysique

Groundwater flow and contaminant transport in an alluvial aquifer: *in-situ* investigation and modelling of a brownfield with strong groundwater – surface water interactions

Thèse de doctorat

présentée par Jordi BATLLE-AGUILAR

en vue de l'obtention du grade de Docteur en Sciences de l'Ingénieur

Soutenue devant le jury composé de :

Robert CHARLIER, Université de Liège (Belgique) - Président
Alain DASSARGUES, Université de Liège (Belgique) - Promoteur
Serge BROUYÈRE, Université de Liège (Belgique) - Co-promoteur
Stoyan GAYDARDZHIEV, Université de Liège (Belgique)
Frédéric NGUYEN, Université de Liège (Belgique)
Ludo DIELS, VITO (Belgique)
Henri HALEN, SPAQuE (Belgique)
Daniel HUNKELER, Université de Neuchâtel, (Suisse)
René THERRIEN, Université Laval (Canada)

Juillet 2008

ABSTRACT

The continuous demand on new residential and economic areas of the modern society has to face up with problems posed by polluted sites related to former industrial activities, typically located in suburbs areas. These sites, known as brownfields, are often located nearby navigable rivers to facilitate transport operations of industrial manufacturing, which increase their potential environmental threat due to the possible migration of pollutants in groundwater to surface water bodies through groundwater discharge.

In this context, the objective of this research, performed in the scope of the FP6-IP AquaTerra project, was to contribute to a better assessment of the risk of groundwater contaminant dispersion for a brownfield located next to the Meuse River (Belgium), in a context where strong groundwater – surface water interactions prevail.

The brownfield of interest corresponds to the site of the former coke factory of Flémalle. Resulting from industrial activities, soils and groundwater located in the alluvial aquifer are heavily contaminated with various types of organic (BTEX, PAHs, mineral oils...) and inorganic (As, Zn, Cd...) pollutants.

To do so, detailed characterisation campaign was performed, consisting of, on the one hand, classical field experiments such as pumping tests, injection tests and tracer experiments; on the other hand, advanced and original field experiments such as a detailed monitoring of groundwater – surface water interaction and dynamics, and the development and application of an innovative tracer technique, the Finite Volume Point Dilution Method (FVPDM), used to quantify and monitor groundwater fluxes.

Monitoring and field works data was subsequently used to develop and calibrate a groundwater flow model using the finite difference code MODFLOW, with an automatic parameter estimation approach based on an original combined regional scale (zonation) and local scale (pilot points) approach. A transport model was also developed using MT3DMS and calibrated using tracer experiments performed in the brownfield.

This groundwater flow and transport model was used to better quantify the dynamics of groundwater – surface water interactions and to model various scenarios of contaminant dispersion through the aquifer – river system. For these scenarios, benzene was considered because it is one of the main pollutants encountered in the site, its large solubility and mobility in groundwater and its acute toxicity.

These scenarios were established considering various groundwater flow conditions (steady state *vs*. transient) and various hydrodispersive processes possibly affecting the mobility of

benzene in groundwater, namely advection, hydrodynamic dispersion, sorption – desorption and, as evidenced by the research results of the University of Neuchâtel (Switzerland), benzene degradation under sulphate reducing conditions.

These simulations indicate that benzene attenuation is mainly controlled by ongoing benzene degradation processes, aquifer heterogeneity and river stage fluctuations. Based on this analysis, the risk of benzene dispersion is low, and monitored natural attenuation (MNA) is a valuable option with (1) monitoring benzene at control planes downstream from the sources; (2) further investigation on risk of sulphate depletion in the alluvial aquifer; and (3) further investigation on mobilisation/immobilisation of heavy metals related to dynamics of organic pollutant plumes.

Keywords: brownfield; groundwater – surface water interaction; groundwater pollution; groundwater flow and contaminant transport; contaminant attenuation; dispersion; biodegradation; risk assessment.

RÉSUMÉ

La demande continue de nouveaux terrains à usages résidentiels ou économiques des sociétés modernes est confrontée aux problèmes posés par les sites contaminés liés aux anciennes activités industrielles, souvent localisées en zone périurbaine. Ces sites, dénommés en anglais *brownfields* (friche industrielle), sont souvent situés près de cours d'eau navigables pour faciliter les opérations de transport des matières premières, ce qui augmente leur menace potentielle pour l'environnement à cause de la migration possible des contaminants présents dans les eaux souterraines vers les eaux de surface.

Dans ce contexte, l'objectif de cette recherche, réalisée dans le cadre du projet FP6-IP AquaTerra, est de contribuer à une meilleure estimation du risque de dispersion des contaminants présents dans la nappe aquifère pour un site contaminé localisé près de la rivière Meuse (Belgique), dans un contexte où de fortes interactions existent entre les eaux souterraines et de surface.

Le site contaminé étudié correspond à l'ancienne cokerie de Flémalle. En conséquence des activités industrielles, les sols et eaux souterraines de l'aquifère alluvial sont fortement contaminés par différents types de polluants organiques (BTEX, HAP, huiles minérales…) et inorganiques (As, Zn, Cd…).

Une campagne de caractérisation a été réalisée, consistant, d'une part, en des essais de pompage, des tests d'injection et des essais de traçage, d'autre part, en des essais de terrain plus originaux comme le suivi détaillé de la dynamique et des interactions entre les eaux souterraines et les eaux de surface et le développement et l'application d'une technique innovante de traçage, appelée « *Finite Volume Point Dilution Method (FVPDM)* », utilisée pour quantifier les flux d'eau souterraine.

Les travaux de terrain ont été par la suite utilisés pour développer et calibrer un modèle d'écoulement des eaux souterraines à l'aide du code différences finies MODFLOW, avec une approche d'estimation automatique des paramètres basée sur une combinaison originale d'une approche régionale (zonation) et locale (points pilotes). Un modèle de transport de solutés a aussi été développé avec le code MT3DMS et calibré à l'aide des essais de traçage réalisés sur le site.

Ce modèle écoulement - transport a été utilisé pour mieux quantifier la dynamique des interactions entre les eaux souterraines et de surface et pour modéliser différents scénarios de dispersion de contaminants au travers du système eau souterraine – eau de surface. Pour ces scénarios, le benzène a été pris en compte car il est un des polluants principaux rencontrés sur

le site, il est fortement soluble et mobile dans les eaux souterraines et il est toxique. Ces scénarios ont été établis en considérant différentes conditions d'écoulement (régime permanent *vs* régime transitoire) et différents processus de transport régissant potentiellement la mobilité du benzène dans l'eau souterraine, tels que l'advection, la dispersion hydrodynamique, la sorption-désorption et, comme mis en évidence par les travaux de l'Université de Neuchâtel, la dégradation en conditions sulfato-réductrices.

Ces simulations indiquent que l'atténuation du benzène est principalement contrôlée par les processus de biodégradation, l'hétérogénéité de l'aquifère et les fluctuations du niveau de la rivière. Sur base de cette analyse, le risque de dispersion du benzène est faible et l'atténuation naturelle contrôlée (*monitored natural attenuation*) peut être considérée comme une option valable de remédiation, moyennant (1) un suivi des concentrations en benzène en aval des sources de pollutions ; (2) une étude sur le risque de diminution des teneurs en sulphates ; et (3) une étude supplémentaire sur la mobilisation/immobilisation des métaux lourds liée à la dynamique des panaches de polluants organiques.

Mots clés : friche industrielle ; interactions eaux souterraines – eaux de surface ; pollution des eaux souterraines ; écoulement souterrain et transport de polluants ; atténuation de polluants ; dispersion ; biodégradation ; analyse du risque.

RESUM

La continua demanda de la societat actual per a nous espais destinats a la vivenda i centres econòmics ha de fer front a una problemàtica cada vegada més freqüent: zones contaminades on antigament es duren a terme activitats industrials, típicament ubicades a les afores dels nuclis urbans. Aquestes zones contaminades, conegudes amb el nom de "*brownfields*", estan sovint situades prop de rius que en el passat servien com a mitjà de transport de matèries primeres, incrementant així el risc mediambiental d'aquestes àrees com a conseqüència d'una possible dispersió de contaminants presents en els aqüífers vers les aigües superficials.

En aquest particular context, l'objectiu d'aquesta recerca, duta a terme en el marc del projecte europeu AquaTerra FP6-IP, és de contribuir a un millor coneixement del risc de dispersió de substàncies contaminants dissoltes en l'aigua subterrània en un *brownfield* ubicat a la vora del riu Meuse (Bèlgica), amb un context favorable per a les interaccions entre les aigües subterrànies i superficials.

El "*brownfield*" en qüestió correspon a l'antiga fàbrica de producció de *coke* de Flémalle (Est de Liège, Bèlgica). Com a resultat de les activitats industrials relacionades amb la producció d'aquest producte (*coke*), el sòl i l'aqüífer al·luvial es troben fortament contaminats per un seguit de substàncies d'origen orgànic (BTEX, HAP, olis minerals...) i inorgànic (As, Zn, Cd...).

Detallades campanyes de caracterització han estat dutes a terme, per una banda, realitzant assajos de camp clàssics com ara assajos de bombeig, d'injecció i de traçador en radial convergent; per altra banda, experiments més avançats i originals han estat també duts a terme, com ara un seguiment continu de la interacció aigües subterrànies – aigües superficials i la seva dinàmica, així com el desenvolupament i aplicació d'una nova tècnica de traçador, anomenada "*Finite Volume Point Dilution Method* (FVPDM)", amb l'objectiu d'avaluar i quantificar el flux d'aigua subterrània.

Les dades obtingudes durant les tasques de control i assajos de camp han estat utilitzades posteriorment per la realització i calibració d'un model de flux subterrani, fent ús del codi de diferències finites MODFLOW, alhora que l'estimació dels paràmetres del model ha estat duta a terme de forma automàtica en base a una combinació, a escala regional i local, de les tècniques de zonació (*zonation*) i punts pilots (*pilot points*). Posteriorment, un model de transport de substàncies dissoltes en l'aigua subterrània ha estat elaborat fent us del codi MT3DMS, utilitzant els assajos de traçador realitzats en el camp per a la seva calibració.

L'ús conjunt dels models de flux d'aigua subterrània i de transport permet una millor comprensió de la dinàmica temporal de les interaccions aigües subterrànies – aigües superficials, alhora que diferents escenaris de dispersió de contaminants en l'aqüífer poden ésser avaluats. Per a la realització d'aquests escenaris, el benzè fou la substància contaminant escollida, pel fet que és un dels principals contaminants en el "*brownfield*" estudiat, la seva solubilitat és de les més importants entre les substàncies contaminants d'origen orgànic, i perquè la seva toxicitat és prou elevada com per ésser considerat extremadament perillós per a la salut de les persones.

Aquests escenaris de contaminació foren duts a terme considerant fluxos subterranis constants i variables en el temps, i diversos processos hidrodispersius susceptibles d'afectar la mobilitat del benzè en l'aqüífer, com ara l'advecció, la dispersió hidrodinàmica, i els efectes d'adsorció – desorció foren considerats, així com la degradació del benzè, procés lligat a condicions sulfato-reductores i posat de manifest en el "*brownfield*" estudiat gràcies a la recerca duta a terme per l'equip d'hidrogeologia de la Universitat de Neuchâtel (Suïssa).

Els resultats del model indiquen que l'atenuació del benzè en el medi subterrani és principalment controlada pels processos de degradació, heterogeneïtat de l'aqüífer i les fluctuacions del riu adjacent. Gràcies a aquests resultats, el risc de dispersió del benzè és lleu, alhora que el seguiment de l'atenuació natural (*Monitored Natural Attenuation*) és una opció vàlida de descontaminació mitjançant (1) el seguiment de la degradació del benzè aigües avall de la font de contaminació; (2) el seguiment del contingut en sulfat en el aqüífer (producte responsable de la degradació en el cas estudiat); i (3) l'estudi de la mobilitat dels metalls pesants en relació a la dinàmica dels contaminants orgànics presents.

Paraules clau: *brownfield*; interacció aigües subterrànies – aigües superficials; contaminació de les aigües subterrànies; flux d'aigua subterrània; transport de contaminants dissolts; atenuació de substàncies contaminants; dispersió; biodegradació; anàlisi de risc.

ACKNOWLEDGEMENTS

I would like to express my considerable thanks to Alain Dassargues, Ph.D promotor, and Serge Brouyère, Ph.D co-promotor and supervisor. Their guidance during these years has been really valuable. I'm also grateful for the anticipating reading of the work they have done, as well as for proposals and suggestions to improve its quality.

Special thanks are addressed to Serge Brouyère, direct supervisor but, also now, really a friend of mine: you taught me how to address field works in the best conditions, you transmitted the pleasure of the research, telling me the things as they are, good or bad, but as they are. Thanks Serge!

My thanks are also due to Robert Charlier, Stoyan Gaydardzhiev, Frédéric Nguyen, Ludo Diels, Henri Halen, Daniel Hunkeler and René Therrien to accept being part of the jury.

I will have happy memories of Philippe Orban, Ph.D researcher in the Hydrogeology Unit and colleague of bureau, but in top of that, a very good friend and confident, always ready to help at any time, in and out of the work. Plenty of souvenirs I will keep: Cargese, Tübingen, sampling and field works… Thanks for these great times Phil!

I'm really indebted to all the colleagues of the Hydrogeology Unit that, in one way or another, have contributed to this work, either in the field, in the lab or just to take a break for a beer (or just a coke for some of them)! I'm specially thinking to Ingrid Ruthy, Nicolas Gardin, Piotr Wojda, Pascal Goderniaux, Julie Gesels, Laurent Thomas, Laurent Soh Angaman, Julie Couturier, Samuel Wildemeersch, Tanguy Robert, Gaelle Lorenzini, David Catherina, Jean Beaujean, Jean Michel Lemieux, Vincent Henrion, Laurent Piront, Marie Dachy, Ileana-Cristina Popescu, Sébastien Papin and Julien Monfort.

Thanks to Philippe Meus (EWTS) and Bernard Belot, for dye and salt tracer analysis; thanks are also due to Annick Anceau and the staff of the Earth Science library, always ready to help me in the research of an article or a map. Many thanks to Martine, Christiane and Nadia, the qualified secretary staff of the ArGEnCo department, for many aspects of practical information, bills, invoices…or just to play a joke!

Special thanks to the FP6 AquaTerra project (nº 505428), who funded for a large part my Ph.D grant, and specially to Johannes Barth, for its continuous support and encouragement in the research activities within the project; thanks to University of Liège, who financed part of my conference travels; thanks also to the research funds of the Aquapôle ULg, helping to acquire valuable field devices; thanks to the project FRAC-WECO, for its scientific support

and funds; and finally, thanks to the SPAQuE and specially to André Lox, Delphine Léonard, Vincent Vandenheede and Henri Halen, for providing a free access to the Flémalle site and to available data.

Sincere thanks to Daniel Hunkeler, Barbara Morasch, Karolien Vanbroekhoven and Ludo Diels for their valuable comments and guidance in geochemical aspects related to organic and inorganic pollutants.

I wish to express my gratitude to Stéphane Muguet (URS-Corps, Belgium); Robert Halleux and Philippe Tomsin (CHST, University of Liège); Pierre Theunissen (SPE – TGV Seraing); Alain Louis, Patrick Ledoux, Jan Hernrivaux, Philippe Dierick, Lahoucine El Haouti and Théodore Droixhe (MET); Thierry Hosay (IRCEL/CELINE); Jerôme Brixko (AIDE); Jeffry Davis and the technical staff of EMS-i, (Environmental Modeling Software); Paul Barlow and M.C. Hill (US Geological Survey).

I would like to gratefully thank the fire brigade of Huy, Flémalle and Seraing, who supplied with more than 200 meters of flexible pipe to perform pumping tests.

Special thanks also to Julie Gesels, Julie Couturier, Laurent Thomas and Jean-Michel Lemieux, who spent a piece of their time to read and to propose corrections to this work, improving its quality.

Of course, I will never forget the support of my best friends, Vadó, Gerard and Vicenç, for whom the distance between Belgium and Catalonia was not a problem to keep in touch. *Gràcies companys*! Special thanks are also due to Alex, an amazing catalan guy that I met here in Liège. Thanks *Pixa* and I hope to see you soon somewhere in Europe!

And finally, but not least, I would like to sincerely acknowledge my parents for their unending support in good and not so good moments,… *gràcies papa, gràcies mama*! This work is dedicated to you!

Jordi Batlle-Aguilar

July 2008

KNOWLEDGE DISSEMINATION

List of publications

- Batlle-Aguilar, J., Brouyère, S., Dassargues, A., Diels, L., Vanbroekhoven, K., Hunkeler, D., Morasch, B. and H. Halen. Natural attenuation of contaminants in groundwater and risk assessment of surface water contamination by groundwater discharge. Manuscript in preparation for submission to *Journal of Hydrology* (July 2008).

- Batlle-Aguilar, J., Pessel, M., Schneider, S., Coquet, Y., Tucholka, P. and P. Vachier. Axisymetrical infiltration in soil imaged by non-invasive electrical resistivimetry. *Soil Sci. Soc. Am. J.* Accepted with minor changes (May 2008).

- Barth, J.A.C., Grathwohl, P., Fowler, H., Bellin, A., Gerzabek, M.H., Lair, G., Barceló, D., Petrovic, M., Navarro, A., Négrel, Ph., Petelet-Giraud, E., Darmendrail, D., Rijnaarts, H., Langenhoff, A., de Weert, J., Slob, A., van der Zaan, B.M., Gerritse, J., Frank, E., Gutierrez, A., Kretzschmar, R., Gocht, T., Steidle, D., Garrido, F., Jones, K.C., Meijer, S., Moeckel, C., Marsman, A., Klaver, G., Vogel, T., Bürger, C., Kolditz, O., Broers, H.P., Baran, N., Joziasse, J., Von Tümpling, W., Van Gaans, P., Merly, C., Chapman, A., Brouyère, S., Batlle-Aguilar, J., Orban, Ph., Tas, N. and H. Smidt. (2008). Mobility, turnover and storage of pollutants in soils, sediments and waters: achievements and results by the EU project AquaTerra. A review. *Agronomy for Sustainable Development*. DOI: 10.1051/agro:2007060.

- Barth, J.A.C., Kalbus, E., Schmidt, C., Bayer-Raich, M., Reinstorf, F., Schirmer, M., Thiéry, D., Dubus, I.G., Gutierrez, A., Baran, N., Mouvet, C., Petelet-Giraud, E., Négrel, Ph., Banton, O., Batlle-Aguilar, J., Brouyère, S., Goderniaux, P., Orban, Ph., Rozemeijer, J.C., Visser, A., Bierkens, M.F.P., Van der Grift, B., Broers, H.P., Marsman, A., Klaver, G., Slobodnick, J. and P. Grathwohl. (2007). Selected groundwater studies of EU project AquaTerra leading to large-scale basin considerations. *Water Practice and Technology.* **2**(3). doi: 10.2166/WPT.2007062.

- Brouyère S., Batlle-Aguilar, J., Goderniaux, P. and A. Dassargues (2008). A new tracer technique for monitoring groundwater fluxes: The Finite Volume Point Dilution Method. *J. Contam. Hydrol.* **95**: 121-140.

- Batlle-Aguilar, J., Orban, P., Dassargues, A. and S. Brouyère (2007). Identification of groundwater quality trends in a chalk aquifer threatened by intensive agricultures. *Hydrogeology Journal* **15**: 1615-1627.

Conference proceedings (with oral presentation)

- Batlle-Aguilar, J., Brouyère, S., Dassargues, A., Diels, L., Vanbroekhoven, K., Hunkeler, D., Morasch, B. and H. Halen. Hydrodynamic characterisation of a groundwater – surface water system and evaluation of BTEX, PAHs decay and heavy metals fate. *In* Proceedings of the 10th International conference on Soil-Water systems, ConSoil 2008, Milan (Italy), 3 - 6 June, 2008.

- Batlle-Aguilar, J. and S. Brouyère. Assessing groundwater – surface water interaction and groundwater discharge in a contaminated site in an industrial, sub-urbanized area. *In* Proceedings of the conference Groundwater Quality 2007 – Securing Groundwater Quality in Urban and Industrial Environments. Fremantle (Western Australia), 2 – 7 December, 2007.

- Brouyère, S., Batlle-Aguilar, J., Goderniaux, P. and A. Dassargues. The finite volume point dilution method: a tracer technique for monitoring transient Darcy fluxes. *Geophysical Research Abstracts, Vol. 9, 02145, European Geosciences Union (EGU).* Vienna (Austria), 15-20 April, 2007.

- Batlle-Aguilar, J., Coquet, Y., Tucholka, P. and P. Vachier. Axisymetrical water infiltration in soil imaged by non-invasive electrical resistivimetry. *Geophysical Research Abstracts, Vol. 6, 01343, European Geosciences Union (EGU).* Nice (France), 25-30 April, 2004.

Conference proceedings (with poster presentation)

- Brouyère, S., Batlle-Aguilar, J., Goderniaux, P. and A. Dassargues. A new single well tracer test: the Finite Volume Point Dilution Method. Theory, field application and model validation. *In* Proceedings of the 6th International Conference on Calibration and Reliability in Groundwater Modelling, ModelCARE 2007. Copenhagen (Denmark), 9 – 13 September, 2007.

- Batlle-Aguilar, J., Orban, Ph., Dassargues, A. and S. Brouyère. Identification of groundwater quality trends in a chalky aquifer threatened by intensive agriculture. *In* Proceedings of the conference Diffuse inputs into the groundwater: Monitoring – Modelling – Management. Graz (Austria), 29 – 31 January, 2007.

Generic scientific dissemination (with oral presentation)

- Contribution of site characterisation and modelling to understand organic pollutant fate in a brownfield. Oral presentation in the Second ENVITAM PhD Day, University of Liège, Belgium. **January 2008**.

- New approach in aquifer characterization and their interaction with adjacent rivers: tools development. Oral presentation in Aquapôle, University of Liège, Sart Tilman, Belgium. **September 2007**.

- Groundwater tracer technique aiming the study of a groundwater – river system: example of the Flémalle test site (Belgium). Oral presentation in Seminar EIER, Ouagadougou, Burkina Faso. **June 2007**.

- Groundwater tracer technique aiming the study of a groundwater – river system: example of the Flémalle test site (Belgium). Oral presentation in the Bilateral cooperation project Walloon Region – Romania (CGRI – APEFE). University of Bucharest (Romania). **April 2007**.

- Quantifying possible pollutant discharging into a river from a contaminated alluvial aquifer prevailing groundwater – surface water interaction. Poster presentation in EDT Envitam kick off event and first PhD student day. UCL, Louvain-la-Neuve, Belgium. **February 2007**.

- Groundwater characterisation in a polluted site. Oral presentation in the Seminar of the Doctoral School RP2E. UHP-Nancy, France. **January 2006**.

AquaTerra project reports (Deliverables)

- Hérivaux, C., Orban, P., Batlle-Aguilar, J., Goderniaux, P. and S. Brouyère. Socio-economic analysis integrating soil-water system modelling for the Geer catchment (Meuse, Walloon Region) – diffuse nitrate pollution in groundwater. **May 2008**. Aquaterra -Integrated Project of the 6th EU RTD Framework Programme. Project no. 505428. 45 pp.

- Batlle-Aguilar, J. and S. Brouyère. Groundwater flow and transport for the former Flémalle cokery site. Deliverable R3.25, **May 2008.** Aquaterra -Integrated Project of the 6th EU RTD Framework Programme. Project no. 505428. 34 pp.

- Dubus, I.G., Pinault, J.L., Surdyk, N., Guyonnet, D., Broers, H.P., Visser, A., Orban, Ph., Batlle-Aguilar, J., Goderniaux, P. and S. Brouyère. Report with comparison of statistical and physically deterministic methods of trend assessment and extrapolation in terms of data requirements, costs and accuracy. Deliverable T2.11, **January 2008**. Aquaterra -Integrated Project of the 6th EU RTD Framework Programme. Project no. 505428. 33 pp.

- Broers, H.P., Visser, A., Heerdink, R., Van der Grift, B., Surdyk, N., Dubus, I.G., Amaoui, N., Orban, Ph., Batlle-Aguilar, J., Goderniaux, P. and S. Brouyère. Report which describes the physically-deterministic determination and extrapolation of time trends at selected test locations in Dutch part of the Meuse Basin, the Brévilles catchement and the Geer catchment. Deliverable T2.10, **January 2008**. Aquaterra -Integrated Project of the 6th EU RTD Framework Programme. Project no. 505428. 47 pp.

- Batlle-Aguilar, J. and S. Brouyère. Update on field experiments and description of the groundwater flow and transport model for the Flémalle cokery site. Deliverable Basin R3.19, **December 2006**. Aquaterra -Integrated Project of the 6th EU RTD Framework Programme. Project no. 505428. 50 pp.

- Broers, H.P, Visser, A., van der Grift, B., Dubus, I.G., Gutierrez, A., Mouvet, C., Baran, N., Orban, Ph., Batlle-Aguilar, J. and S. Brouyère. Input data sets and short report describing the subsoil input data for groundwater and reactive transport modelling at test locations in Dutch part of the Meuse basin, the Brévilles catchment and the Geer catchment. Deliverable Trend T2.5, **May 2006**. Aquaterra -Integrated Project of the 6th EU RTD Framework Programme. Project no. 505428. 23 pp.

- Broers, H.P., Visser, A., Pinault, J.-L., Guyonnet, D., Dubus, I.G., Baran, N., Gutierrez, A., Mouvet, C., Batlle-Aguilar, J., Orban, Ph. and S. Brouyère. Report on extrapolated time trends at test sites. Deliverable Trend T2.4, **November 2005**. Aquaterra -Integrated Project of the 6th EU RTD Framework Programme. Project no. 505428. 81 pp.

- Broers, H.P., Visser, A., Dubus, I.G., Baran, N., Morvan, X., Normand, M., Gutierrez, A., Mouvet, C., Batlle-Aguilar, J., Brouyère, S., Orban, Ph., Dautrebande, S., Sohier, C., Korcz, M., Bronder, J., Dlugosz, J. and M. Odrzywolek. Deliverable Trend T2.2, **November 2005**. Aquaterra -Integrated Project of the 6th EU RTD Framework Programme. Project no. 505428. 63 pp.

- Batlle-Aguilar, J. and S. Brouyère. Documentation of site equipment and description of experiments performed and still planned in the Flémalle former cokery test site. Deliverable Basin R3.15, **October 2005**. Aquaterra -Integrated Project of the 6th EU RTD Framework Programme. Project no. 505428. 23 pp.

- Batlle-Aguilar, J., Wojda, P. and S. Brouyère. Compilation of data collected and fed into a hydrogeological database in the Walloon Meuse catchment region. Deliverable Basin R.311, **May 2005**. Aquaterra -Integrated Project of the 6th EU RTD Framework Programme. Project no. 505428. 44pp.

- Broers, H.P., Baran, N., Batlle-Aguilar, J., Bierkens, M., Bronder, J., Brouyère, S., Dlugosz, J., Dubus, I.G., Gutierrez, A., Korcz, M., Mouvet, C., Slowikowski, D. and A. Visser. Deliverable Trend T2.1, **November 2004**. Aquaterra -Integrated Project of the 6th EU RTD Framework Programme. Project no. 505428. 97 pp.

- Batlle-Aguilar, J., Popescu, I.-C., Orban, Ph. and S. Brouyère. Synthesis of data availability for the river Meuse and the aquifer located in the alluvial plain in the Walloon Meuse catchment region. Deliverable Basin R3.4, **August 2004**. Aquaterra - Integrated Project of the 6th EU RTD Framework Programme. Project no. 505428. 6 pp.

Other scientific reports

- Batlle-Aguilar, J., Brouyère, S., Gardin, N. Mise en oeuvre et résultats des essays de traçage réalisés à Nasso, dans le bassin du Kou (Bobo Dioulasso, Burkina Fasso). **February 2008**. Appui à la gestion et à la protection des resources en eaux souterraines dans la région de Bobo-Dioulasso. Cooperation project ULg – APEFE. 50 pp.

- Batlle-Aguilar, J., Brouyère, S., Garrido, F., Joulian, C., Lucas, L., Jauzein, M., Joubert,A., Morasch, B., Höhener, P., Hunkeler, D., Bastiaens, L., Dejonghe, W., Diels, L., Gemoets, J., Seuntjens, P. and K. Vanbroekhoven. **December 2006**. Field and laboratory experiments performed in the Flémalle cokery site by AquaTerra partners during the period 2005-2006. Unpublished report, 75 pp

TABLE OF CONTENTS

LIST OF SYMBOLS

Symbol	Dimension	Definition
b	[L]	Mean saturated thickness of the aquifer
c	[L]	Instantaneous step change in river water level
C	[M L^{-3}]	Dissolved solute concentration
$\overline{C}$	[M M^{-1}]	Contaminant concentration sorbed on the subsurface solids
C_{DL}	[M L^{-3}]	Tracer concentration representing the device detection limit
C_{in}	[M L^{-3}]	Concentration of the tracer injection fluid
C_{im}	[M L^{-3}]	Solute concentration in the immobile domain
$\overline{C}_{im}$	[M M^{-1}]	Sorbed concentration in the immobile phase
C_m	[M L^{-3}]	Solute concentration in the mobile domain
$\overline{C}_m$	[M M^{-1}]	Sorbed concentration in the mobile phase
C_s	[M L^{-3}]	Contaminant concentration at the source and sink
C_{SL}	[M L^{-3}]	Tracer concentration representing the device saturation limit
C_t	[M L^{-3}]	Tracer concentration in the transit flux intercepted by the well screen
C_w	[M L^{-3}]	Tracer concentration in the injection well
C_w^*	[-]	Non-dimensional tracer concentration in the injection well
d	[L]	Width of the riverbank material
D	[L^2 T^{-1}]	Hydrodynamic dispersion coefficient
D^*	[-]	Effective molecular diffusion coefficient
e	[-]	Weighted residual
e_{scr}	[L]	Screen length of the well
f	[-]	Fraction of sorption in contact with the mobile phase
f_{oc}	[-]	Fraction of soil organic carbon
F	[L]	System input
F'	[L T^{-1}]	Time rate of change of system input
g	[-]	Unknown values of the hydraulic property to be estimated
g_o	[-]	Initial values of the hydraulic property to be estimated
h	[L]	Groundwater head
h^{obs}	[L]	Observed groundwater head being matched
h^{sim}	[L]	Simulated groundwater head
h_{rec}	[L]	Groundwater head during the recovery period
h_w	[L]	Height of the water column in the well
H	[L]	River water level
H_D	[-]	Dimensionless unit-step response solution
H_i	[L]	Initial river water level
H_0	[L]	River water level after the step change
k	[-]	Time variable of integration (time step)
K	[L T^{-1}]	Hydraulic conductivity of the aquifer
K_d	[L^3 M^{-1}]	Distribution coefficient between sorbed and dissolved phases
K_{draw}	[L T^{-1}]	Estimated hydraulic conductivity during the drawdown period
K_{oc}	[L^3 M^{-1}]	Soil adsorption coefficient for soil organic carbon
K_{rec}	[L T^{-1}]	Estimated hydraulic conductivity during the recovery period
K_s	[L T^{-1}]	Hydraulic conductivity of the riverbank material
K_y	[-]	Ratio of vertical to horizontal hydraulic conductivity
l	[L]	Characteristic length between one point to another
L	[L]	River reach length
N	[-]	Number of the unknown parameters of the hydraulic property to be estimated
ND	[-]	Number of observations
NH	[-]	Number of hydraulic head observations

NQ	[-]	Number of flow observations
p	[-]	Fraction of sorption in contact with the immobile phase
p_i	[-]	Model parameters
P_e	[-]	Peclet number
q	[T^{-1}]	Volumetric flow rate per unit volume of aquifer
q_j^{obs}	[$L^3 T^{-1}$]	*jth* observed flow being matched in the objective function
q_j^{sim}	[L^3T^{-1}]	Simulated flow corresponding to q_j^{obs}
$q_s^{'} = \partial\theta/\partial t$	[T^{-1}]	Rate of change in transient groundwater storage
Q_{cr}	[$L^3 T^{-1}$]	Critical injection flow rate
Q_{in}	[$L^3 T^{-1}$]	Injection flow rate
Q_{out}	[$L^3 T^{-1}$]	Flow rate leaving the well through the screens
Q_p	[$L^3 T^{-1}$]	Pumping rate
Q_{riv}	[$L^3 T^{-1}$]	Seepage rate from (or to) one side of the river
Q_t	[$L^3 T^{-1}$]	Transit flow rate crossing the screen well
Q_t^{in}	[$L^3 T^{-1}$]	Groundwater flow dynamically dependant on the injection rate (Q_{in})
r_{gp}	[L]	Radius of the gravel pack
r_w	[L]	Radius of the well casing
R^2	[-]	Coefficient of determination
R_{GW}	[$L T^{-1}$]	Groundwater recharge
Rf	[L]	Rainfall
R_{fc}	[-]	Retardation factor
R_{inf}	[L]	Radius of influence
R_s	[-]	Ratio of the heavy isotope to the light isotope
R_{std}	[-]	Standard of the heavy isotope to the light isotope
S	[-]	Storage coefficient
$S_{1,2,3,4}$	[-]	Orthogonal transect (slide) of aquifer
S_y	[-]	Specific yield coefficient
t	[T]	Time
t'	[T]	Time since the cessation of pumping
T	[$L^2 T^{-1}$]	Aquifer transmissivity
T_{min}	[T]	Time of the first arrival
T_{mod}	[T]	Time of the modal arrival (concentration peak)
u	[-]	Vector containing values of the parameters being estimated
V_{in}	[L^3]	Volume of injected tracer fluid
V_w	[L^3]	Volume of water in the well
W	[L]	River channel height
x	[L]	Horizontal coordinate
x_0	[L]	Distance from the middle of the river to the river-aquifer boundary
x_D	[-]	Dimensionless distance (x/x_0)
z	[L]	Vertical coordinate
α	[T^{-1}]	First-order transfer between the mobile and immobile water
α_L	[L]	Longitudinal dispersivity
α_{LK}	[L]	Riverbank leakance (or riverbank resistance)
α_R	[$L^2 T^{-1}$]	Riverbank coefficient (or river conductance)
α_T	[L]	Transverse dispersivity
β	[$L^2 T^{-1}$]	Aquifer diffusivity
δ	[-]	Isotope ratio
Δt	[T]	Time step size
ε	[-]	Enrichment factor
ζ_i^{obs}	[-]	Observation value being matched
ζ_i^{sim}	[-]	Simulated equivalent value corresponding to ζ_i^{obs}
$\eta_i^{g_0}$	[-]	Interpolation weight for initial values

η_i^{PP}	[-]	Interpolation weight for pilot points
θ	[-]	Total aquifer porosity
θ_{im}	[-]	Immobile porosity
θ_m	[-]	Mobile porosity
κ	[-]	Fraction of the substrate remaining after a time
λ	[T^{-1}]	Linear decay constant
λ_1	[T^{-1}]	First-order reaction rate for the dissolved phase
λ_2	[T^{-1}]	First-order reaction for the sorbed (solid) phase
λ_B	[T^{-1}]	Biodegradation rate coefficient
v	[$L\ T^{-1}$]	Groundwater effective velocity
v_{ap}	[$L\ T^{-1}$]	Apparent Darcy flux
v_D	[$L\ T^{-1}$]	Darcy flux
ρ_b	[$M\ L^{-1}$]	Bulk density
τ	[T]	Time variable of integration
Φ	[-]	Weighted least-squares objective function
ψ^g	[-]	Interpolation function used to parameterise the undefined hydraulic property *g*
ω_h	[-]	Weight for the *ith* head observation
ω_q	[-]	Weight for the *jth* flow observation
χ	[T]	Birsoy – Summer's parameter

LIST OF ACRONYMS

ADE	Advection dispersion equation
a.s.l.	above sea level
AIDE	Association intercommunale pour le démergement et l'épuration
BRGM	Bureau des recherches géologiques et minières (France)
BTC	Breakthrough curve
BTEX	Benzene, toluene, ethylbenzene and xylène
CATTI	Computer aided tracer test interpretation
CHYN	Centre for hydrogeology, University of Neuchâtel (Switzerland)
DO	Dissolved oxygen
EA	Electron acceptor
ED	Electron donor
EWTS	European water tracing services (Belgium)
GMS	Groundwater modeling software
GW - SW	Groundwater – surface water
IPT	Integral pumping tests
IRCEL/CELINE	Intergewestelijke cel voor het leefmilieu/Céllule interégionale de l'environnement (Belgian interegional environment agency)
LIMOS	Laboratoire des interactions micro-organismes, minéraux et matières organiques dans les sols, Université Henri Poincaré, Nancy (France)
LNAPL	Light non-aqueous phase liquid
MET	Ministère wallon de l'equipement et des transports (walloon ministry of transports and equipements)
MIM	Mobile – immobile water
MNA	Monitoring natural attenuation
MODFLOW	Modular finite difference groundwater flow model
MTEs	Metal trace elements
MT3DMS	Modular three-dimensioanl multispecies transport model
PAHs	Polyaormatic hydrocarbons
REV	Representative elementary volume
RT3D	Reactive multispecies transport in 3-dimensional groundwater systems
SPAQuE	Société publique d'aide à la qualité de l'environnement
SPE-TGV	Belgian Electricity Producer Company
STOMP	Subsurface transport over multiple phases
TCE	Trichloroethylene
USEPA	United States environmental protection agency
USGS	United States geological survey
VC	Vynil chloride (chloroethylene)
VITO	Vlaamse instellin voor technologisch onderzoek - Flemish institute for technological research- (Belgium)
VPDB	Vienna Pee Dee Belemnite

I was born not knowing and have had only a little time to change that here and there.

Richard P. Feynman

Physicist (1918-1988)

1. INTRODUCTION

1.1. Context of the research

Groundwater is used daily by billions of persons in the world as drinkable water. At the same time, increasing contamination and threatening of aquifers is experiencing a serious worldwide environmental issue due to, among others, urbanisation and industrial development.

Since groundwater is part of the hydrologic cycle (Figure 1.1), contaminants in other parts of the cycle, such as atmosphere or surface water bodies, can be transferred to groundwater. Unfortunately groundwater is not always naturally protected by soil, and pollutants affecting soil and surface water can end up in the aquifer. It is thus recognised that physical and chemical interactions between rivers and groundwater must be considered, and that water in general should be considered as a single resource.

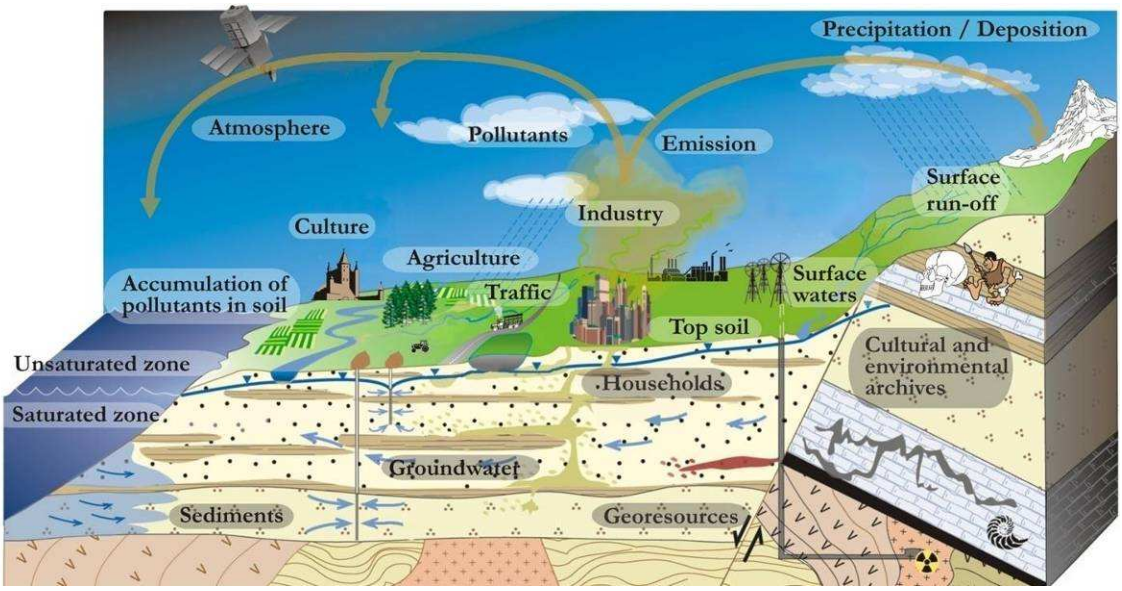

Figure 1.1. Schematisation of the hydrologic cycle (http://www.attempto-projects.de/aquaterra/).

Once groundwater has become obviously affected by pollution, large volumes of aquifer are usually polluted. Cleanup measures are very expensive and often technically complex and challenging.

Industrial zones have been traditionally located in the suburbs of the cities. Due to the increasing urbanisation pressures, cities are growing and consequently expanding to zones historically occupied by industries. Practically this means that former industrial sites are at present becoming residential and/or commercial zones reaffected to new economic activities. Indeed, this trend has to face up with environmental problems due to uncontrolled pollutant

releases in these zones in the past. Brownfields[1] are clear examples of these former contaminated sites.

Environmental contamination due to brownfields can potentially affect soil and groundwater quality, as well as, indirectly, human health and ecosystems. Pollutants related to chemical and metallurgical industries are typically encountered in these sites.

Industrial activities are often located nearby navigable rivers to facilitate transport operations of industrial manufacturing. This has resulted in the existence of numerous contaminated sites close to rivers and in relatively urbanised areas, posing a major risk of contaminant dispersion in the environment, particularly by possible migration to surface water, through groundwater discharge. Because of that, and in order to develop new economic activities in these areas, such sites often need detailed investigations aiming at defining the actual risk posed by the presence of contaminants and defining which remediation measures have to be taken. Referring to that, natural attenuation is a fashionable and efficient way to reduce the contaminant risk of pollutant substances. However, natural attenuation in groundwater is only effective when contaminant degrading microorganisms are present and/or when geochemical conditions of the system are favourable. To evaluate this effectiveness, many site-specific factors have to be considered, among which the dynamics of groundwater fluxes, groundwater – surface water interactions and biogeochemical processes.

It is known that ground- and surface water are not independent systems, being intimately related one to each other. Changes in surface water levels (or groundwater) are likely to cause changes on groundwater levels (or surface water) in the adjacent aquifer (or river/stream), as well as water fluxes flowing from one system to the other. Understanding aquifer responses to external stresses (i.e. rainfall, river stage variations) contributes to a better understanding of its dynamics and, as one of the consequences, to a better estimate of groundwater fluxes flowing out to the adjacent river/stream.

This research focuses on a brownfield located next to the Meuse River, in an urbanised and industrialised area, in Belgium. Due to past industrial activities, the soil and alluvial aquifer are both highly contaminated by organic pollutants, mainly BTEX and PAHs, as well as other components such as mineral oils, sulphates, cyanide and heavy metals. Pollutant substances encountered in the aquifer are seriously toxic. Some of them, reported as carcinogenic, are

[1] Brownfields are defined as sites that have been affected by the former uses of the site and surrounding land, are derelict or underused, have real or perceived contamination problems and are mainly in developed urban areas (see Chapter 2 for details).

likely to reach the Meuse River and population living just at some tens of meters far from the site.

1.2. A research in the scope of the AquaTerra project

This research thesis has been funded by the AquaTerra project (http://www.attempto-projects.de/aquaterra/), an integrated project of the 6th EU RTD Framework Programme, and one of the first environmental Integrated Project in the EU FP6, active since the 1st June 2004 for a time period of 5 years. The project consortium is formed by 45 partner organisations in 13 EU countries as well as in Switzerland and Serbia.

AquaTerra integrates multiple disciplines, from geosciences, environmental engineering and chemistry to socio-economic sciences, from the catchment to the regional scale with case studies located in major European river basins. It involves practitioners and end-users to elaborate operational tools for the different stakeholders[2] (policy-makers, river basin managers, regional and urban land planners…).

AquaTerra aims to a better understanding of the river-sediment-soil-groundwater system as a whole by identifying relevant processes, quantifying the associated parameters and developing numerical models of the groundwater-soil-sediment-river system to identify adverse trends in soil functioning, water quantity and quality. The main objectives of the project are 1) to provide better understanding of the river-sediment-soil-groundwater system at various temporal and spatial scales; 2) to provide the scientific basis for improved river basin management; 3) to develop specific tools for water and soil quality monitoring; and 4) to develop models for impact evaluation of pollution as well as climate and land-use changes for definition of long-term management schemes. These objectives must be achieved through 11 sub-projects, most consisting in several work packages.

AquaTerra works on different scales, from micro-scales investigated in the laboratory to river basins (Figure 1.2). These are integrated into numerical models, to provide comprehensive and advanced management tools for catchment areas and river basins.

Within the sub-project BASIN, in the scope of which this research was conducted, five contrasting European river basins (Brévilles, Ebro, Meuse, Elbe and Danube) are investigated focusing on: 1) soil-groundwater-river processes and; 2) floodplain-sediment-river interactions near the mouths of rivers. Each basin constitutes a “work package”, R1 to R5 respectively, R3 corresponding to the work package of the Meuse basin. Two research areas

[2] Someone who may be affected by, or may affect, a decision that has to be made or its implementation.

are addressed within R3, namely a Belgian/Walloon catchment, where several contamination problems of groundwater and sediments by old industrial activities exist, and a Dutch floodplain, where the Dommel flowing through a zinc production area, with cadmium as the main contaminant in the sediments. The research presented here focuses on the first one.

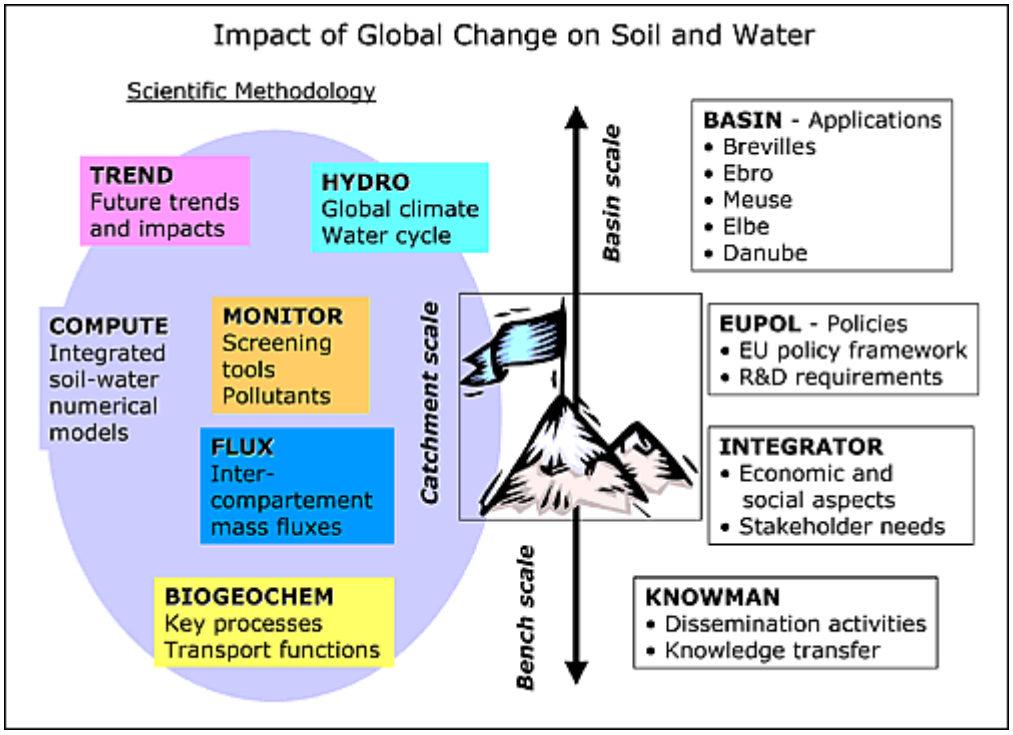

Figure 1.2. Overview of AquaTerra project structure (http://www.attempto-projects.de/aquaterra/).

The study site concerned in this research was also the focus of research activities of three other AquaTerra partners: 1) VITO (Vlaamse Instellin voor Technologisch Onderzoek - Flemish Institute for Technological Research-, Belgium) who have focused on the study of heavy metals mobility and possible bioprecipitation in the aquifer; 2) CHYN (Center for Hydrogeology, University of Neuchâtel, Switzerland) who have focused on natural attenuation of organic pollutants in the aquifer; and 3) LIMOS (Laboratoire des Interactions Micro-organismes, Minéraux et Matières organiques dans les Sols, Nancy University, France) who have focused on heavy metals and MTEs (Metal Trace Elements) turnover in the soils.

AquaTerra results integration and dissemination for future use in environmental EU policies is done by EUPOL and INTEGRATOR sub-projects (Figure 1.3). Objectives of integration are ambitious: 1) a common representation of the functioning of the soil-water resource system for all stakeholders involved in its management; 2) a shared integrated conceptual representation of the river basin functioning for integration of all scientific results of the

project; and 3) a conceptual impact assessment integrated model at the river basin scale, providing a framework to characterise and assess direct and indirect impacts of global change on soil and water resources.

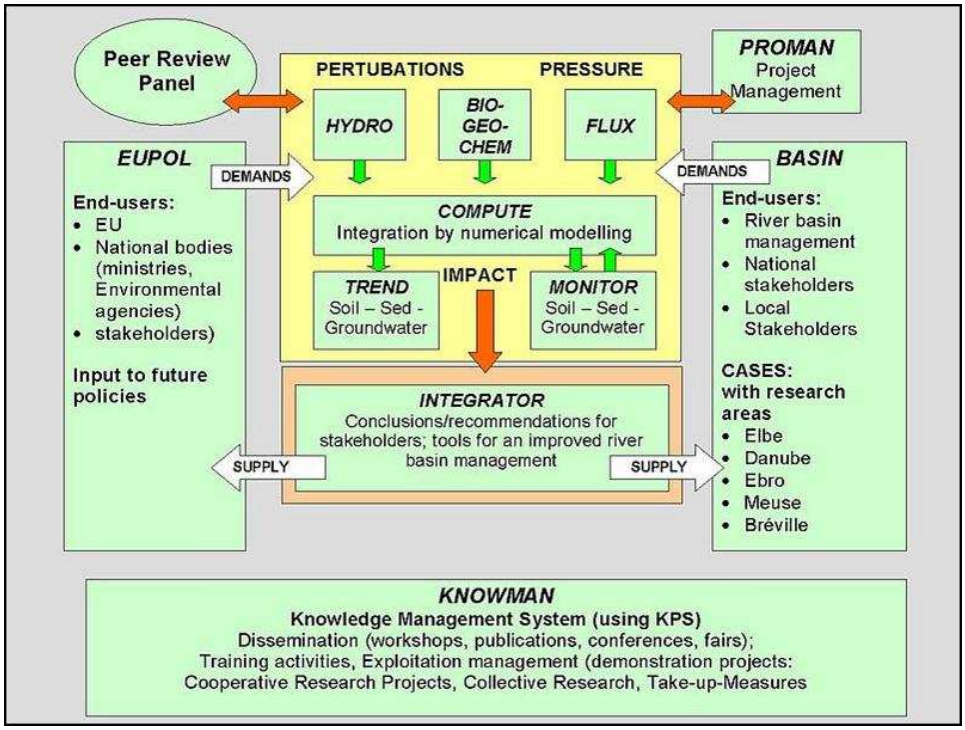

Figure 1.3. Structure and major elements of the project. Each rectangular box represents a sub-project consisting of 2 to 5 packages.

1.3. Objectives of the research

Although soil and groundwater are both highly polluted in the site of concern, research activities presented in this work focuses on the alluvial aquifer system, particularly on the study of hydrodynamics of the river-aquifer system and on the dispersion of the organic pollutants dissolved in the alluvial aquifer.

This work contributes to a better comprehension of the river – alluvial aquifer system dynamism, at the same time that the risk of groundwater pollutant dispersion in an alluvial aquifer adjacent to a river is evaluated.

The specific objectives of this work can be enumerated as follows:

1. To evaluate whether, at the level of the studied brownfield, an interaction exists between groundwater and the neighbouring Meuse River, and, if so, to assess the dynamics of such interactions;
2. To estimate average and transient (ground)water fluxes flowing from the aquifer to the river (or from the river to the aquifer);
3. To characterise hydrodynamic and hydrodispersive parameters in the alluvial aquifer of the studied site;
4. To perform groundwater flow and transport modelling to characterise organic pollutant behaviour versus transient aquifer conditions and to understand the present contaminant state of the aquifer;
5. In terms of risk assessment of contaminant dispersion off-site, to evaluate and, as much as possible, to quantify the relative importance of factors possibly influencing the natural attenuation for organic pollutants.

The research performed is structured as follows: Chapter 2 presents the study site from a regional to local point of view, as well as the quality status of the aquifer; Chapter 3 offers an overview of the research state concerning river – aquifer interactions, organic pollutant degradation in aquifers and inverse modelling in hydrogeology; Chapter 4 describes monitoring and field works campaigns; Chapter 5 present efforts in groundwater and transport modelling; and finally, Chapter 6 summarises the main conclusions in conjunction with future perspectives.

The most exciting phrase to hear in science, the one that heralds new discoveries, is not "Eureka!" (I found it!), but rather "That's funny..."

Isaac Asimov

Writer (1920-1992)

2. COKE AND GASWORK PLANTS: THE FLÉMALLE SITE. A CASE STUDY

2.1. Introduction

Past economical activities in industrialised areas have resulted nowadays in the existence of numerous abandoned polluted sites in urbanised areas near roads, rail tracks and navigable rivers, where industries were preferentially located for an easier manufacturing transport. Modern urbanised societies experience increased pressures on land use and its associated environmental quality. Solutions for this increased stress on urbanised environments may be found in a better management of polluted sites. A polluted site is defined as a property that has soil, groundwater, or surface water containing contaminants at levels that exceed those considered as safe by regulators (De Sousa, 2001).

This research has focused on a polluted site located in an urbanised area, where former coke and gas production works were carried out in the past. The chapter is organised as follows:

- Section 2.2 presents an overview of the environmental problem issue from former industrial sites and the need for their redevelopment;
- Section 2.3 describes in general terms the functioning of a coke and gas production plant and its environmental consequences for groundwater quality;
- Section 2.4 describes the historic of the studied site, from three different points of view: geological, hydrological and hydrogeological characteristics. The evolution of the site before, during and after industrial activities is summarised, former characterisation studies presented, and finally, the present environmental state of the soil and groundwater systems is described;
- Section 2.5 summarises main conclusions arising from the complete description of the site.

2.2. Redevelopment of polluted former industrial sites

Polluted sites where industrial activities were developed in the past, are often nowadays underused, abandoned and located near urbanised areas, representing a real threat for soil and subsurface environment, as well as for humans living in surroundings. These polluted sites are known as brownfields. Ferber and Grimski (2002) define brownfields as sites that have been affected by the former uses on site and surrounding land, are often underused, have real or perceived contamination problems and are mainly in developed urban areas.

In terms of affected land area by brownfields, a total of 128,000 ha in Germany have been identified, 39,600 ha in United Kingdom, 20,000 ha in France, 14,500 ha in Belgium (among

which 9,000 in the Walloon Region and 5,500 in the Flemish Region) and between 9,000 and 11,000 ha in The Netherlands (Prokop *et al.*, 2000; Ferber and Grimski, 2002).

Due to high costs of cleaning, many brownfields have been abandoned for decades. However, redevelopment of brownfields has become more common in the first decade of the 21st century as it can help the community in many ways. Many brownfield sites are usually located in unattractive, economically depressed parts of the neighbourhood. Cleanup and redevelopment of such sites can encourage the value of the zone and create jobs, as well as impact positively the local economy by creating a safer, healthier urban space for housing and businesses activities. The continuous growing of modern cities is at the origin of an expansion to outskirts, which increases the demand of residential areas. This fact generates socio-economical problems and controversy face up to brownfields typically located in these peripheral areas. But on the top of that, drinking contaminated groundwater can have serious health effects for humans, and ecosystems can also be seriously harmed. Other long term effects, such as certain types of cancer, may also result from exposure to polluted groundwater.

A key question in brownfield redevelopment remains: how clean is clean? In particular, is it necessary to clean up the site to pristine conditions? Cleanup efforts can vary considerably depending on the type of contaminant, on the level of contamination, the extent of the contaminated area and on specific environmental standards. A key factor is also often considering the future use of the site when defining the level of required decontamination (Risk-Based Land Management). For example, if industrial activities are planned for a contaminated site, cleanup standards requirements can be less strict than if the site is intended for residential use, because in the former use the exposition level to the contaminants is expected to be lower.

Several kinds of former industrial activities can be at the origin of what is known presently as brownfields. Coke and gas production plants were numerous in industrialised countries like United Kingdom, Germany, The Netherlands and Belgium, among others. It is precisely in a former coke and gas production plant where research works here presented were performed.

2.3. Coke and gas production plants

2.3.1. How coke and gas production plants work

Coke is the remaining material from the destructive distillation of coal in an oxygen-free atmosphere after all volatile components have evaporated. Coke is mostly used in iron and steel industry processes to reduce iron ore[3] to iron. In the past, these plants were also largely used to produce town gas for heating, lighting and cooking, from where the name of gaswork plant comes (Myers, 2001).

In most cases, gaswork plants are located near waterways or train lines for easy delivery of coal. Moreover, they have been traditionally installed close to cities, to minimise the size of the network of pipes used for the gas distribution.

The process of the ironmaking occurs mainly in the blast furnace, which purpose is to chemically reduce and physically convert iron oxides into liquid iron. The blast furnace is a huge, steel stack with refractory brick, where iron ore, coke and limestone are dumped (Figure 2.1).

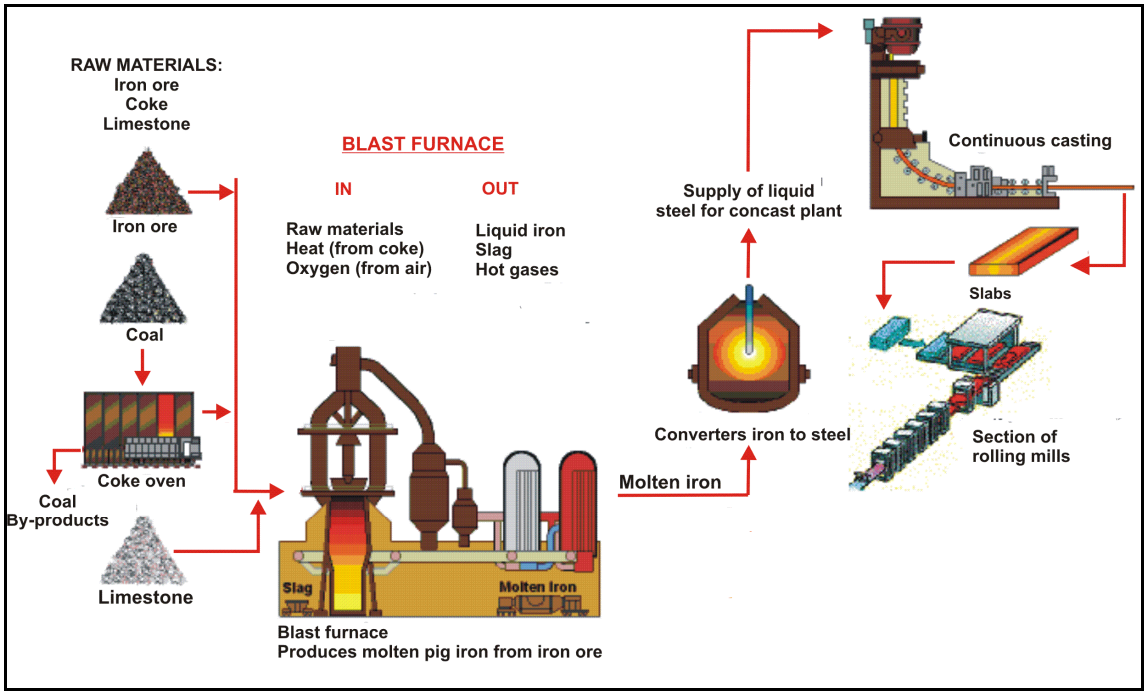

Figure 2.1 Schematic procedure of the ironmaking process (modified from http://www.thepotteries.org/shelton/how.htm).

Coal, in its basic form, is not suitable for direct use in the blast furnace, because it contains too many useless elements for the melting process, making it not strong enough to carry the

[3] Natural mineral that contains iron.

blast furnace burden (Ertem and Özdabak, 2005). It must therefore be converted to metallurgical coke. The coke is produced from a mixture of coals. The coal is crushed and loaded into a powder and then charged into a battery of individual ovens. As the oven is heated, the coal is cooked so that most of the volatile matter, such as oil and tar, are removed. Once coal is cooked, the resulting product, coke, is removed from the oven after 18 to 24 hours of reaction time. It contains 90 to 93% of carbon, some ash and sulphur, but compared to raw coal, it is very strong, with a high energy value.

The final raw material used in the ironmaking process is limestone. This can be pure high calcium limestone, dolomitic limestone containing magnesia or a blend of the two types of limestone. The purpose of the limestone is to remove sulphur and other impurities in the inronmaking process.

The three raw materials, iron ore, coke and limestone, are introduced in the blast furnace, where a series of chemical reactions of iron oxidation and sulphur removing (it is necessary to remove the sulphur before the hot metal becomes steel) occurs at around 1,000ºC. The resulting product is the molten iron and a slag[4] formed by a mixture of CaS, Silica (SiO_2), Aluminia (Al_2O_3), Magnesia (MgO) and/or Calcia (CaO).

In addition to molten iron and slag, hot dirty gases are also produced. These gases proceed (or they should) through gas cleaning equipment where particulate matter is removed from the gas and where the gas is cooled.

In summary, many chemical and physical reactions take place in the blast furnace, and the desired final product is the hot metal.

2.3.2. Groundwater pollution from coke and gas production plants

The pollution issues generated by former coke and gas production plants have become a worldwide concern from the environmental point of view.

The main problem of concern from coke-gaswork plants, disregarded of air pollution, is surface and groundwater contamination by wastewater generated in the coal coking process (Forth and Beaumont, 1999; Haerens, 2004). During the quenching of hot coke and for washing gas produced from ovens, high quantities of heavily polluted liquid effluents are produced (Ghose, 2002). The composition of this wastewater varies from one factory to another depending on the quality of the raw coal, the carbonation temperature and the methods used for by-product recovery (Zhang *et al.*, 1998). Traditionally it contains

[4] The left-overs from the ironmaking process, the impurities left when the iron is smelted.

ammonia, cyanide, thiocyanate, and many toxic organic contaminants, such as phenols, mono- and poly-cyclic nitrogen-containing aromatics, oxygen- and sulphur-containing heterocyclics compounds and polyaromatic hycrocarbons (PAHs) (Stamoudis and Luthy, 1980; Jianlong *et al.*, 2002; Li *et al.*, 2003). All these compounds can produce long-term environmental impacts and most of the heterocyclic and PAHs are reported as mutative and carcinogenic (Melcer *et al.*, 1984; Azhar and Stuckey, 1994; Jianlong *et al.*, 2002). It is therefore necessary to remove these substances from coke-plant wastewaters for reducing their harm to environment and human health.

2.3.3. Coke and gas production in the city of Liège and surroundings

As many other industrialised regions in the world, the Walloon Region of Belgium has now to face up problems related to former industrial activities, such as metallurgy and chemistry, that were and are still generally located nearby navigable rivers. This has resulted in the existence of abundant contaminated sites close to rivers and in relatively urbanised areas, posing a major risk of contaminant dispersion in the environment, particularly by possible migration to surface water through groundwater discharge.

The city of Liège and its surroundings has been traditionally an important center for the metallurgical industry and other related industries, often located next to the Meuse River. Some of these industries are still in activity nowadays, while others disappeared, closed a few tens of years ago, leaving abandoned contaminated lands contributing to dirty, polluted and bleak areas.

The site of concern in this research is one of the several brownfields in the Walloon Region (Belgium), which denotes the importance of the metallurgical industry during the past in this area. The former coke and gaswork plant of Flémalle is an example of these brownfields where new economical activities should be started again.

2.4. The former coke and gaswork plant of Flémalle

2.4.1. Site description

The studied site is located in the North bank of the Meuse River alluvial plain, upstream of the city of Liège (Belgium) (Figure 2.2a). The former coke plant was established on a surface of approximately 11 ha, from the hillslope to the Meuse River. However, the part of the site concerned by this work extends over 8 ha (400 m long and 200 m wide), close to the river (Figure 2.2b).

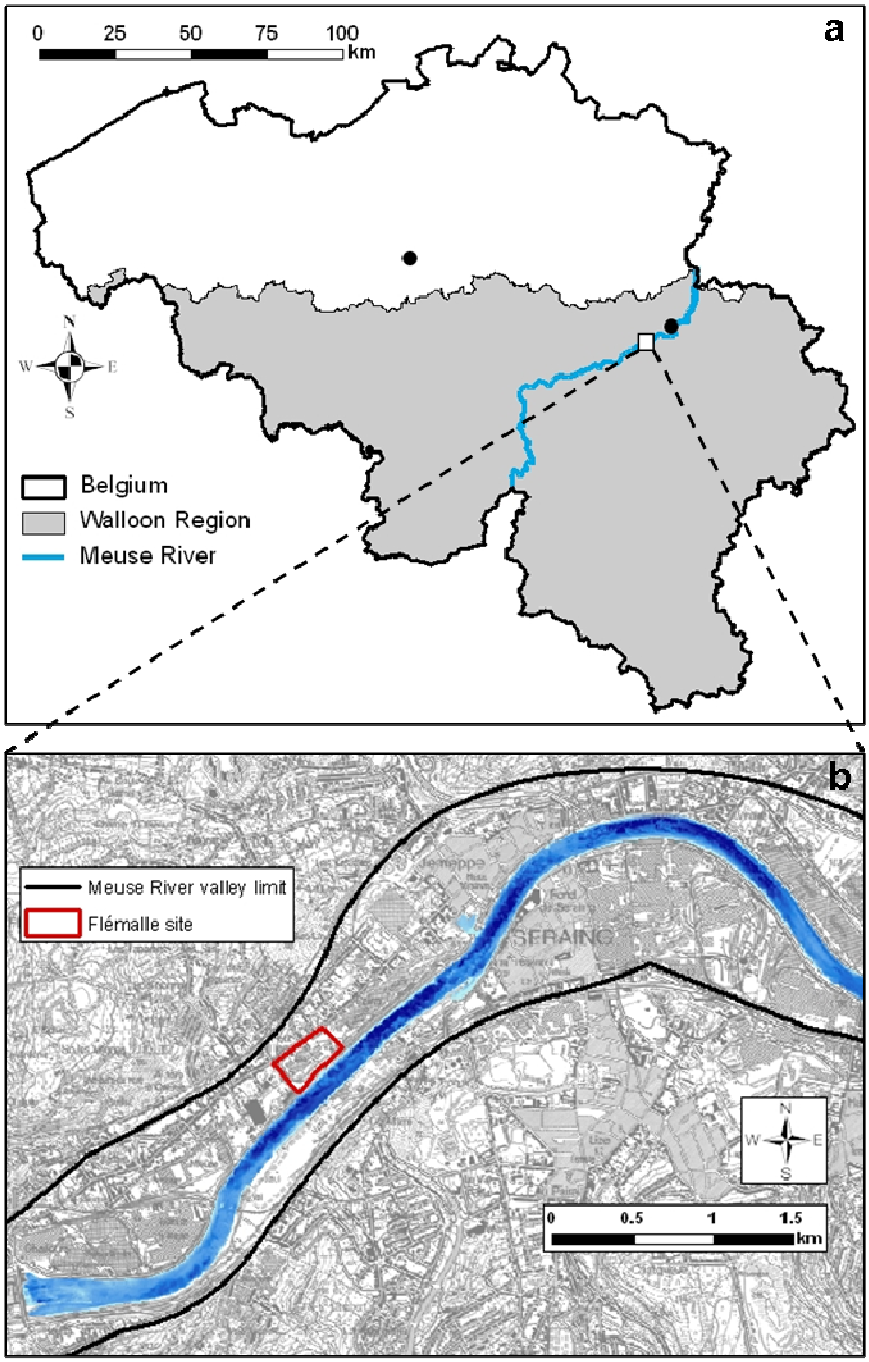

Figure 2.2 Location of the former coke and gaswork site in Flémalle.

2.4.2. Hydrography

The Meuse is the main river of the Walloon Region. The river drains the northern part of France, where riverbed and basin are not very large, and then it flows through Belgium and The Netherlands to the North Sea. The tributaries network of the Meuse basin is much more developed in Belgium than in France. In Belgium, the Meuse River water levels are artificially controlled by dams to allow boats navigation and to prevent large floods downstream.

The surface of the whole Meuse basin is around 36,000 km^2, of which 38.75% is located in the Walloon Region (about 14,000 km^2). It corresponds to 45.7% of Belgium and 75% of the Walloon Region (Haddouchi, 1987) (Figure 2.3).

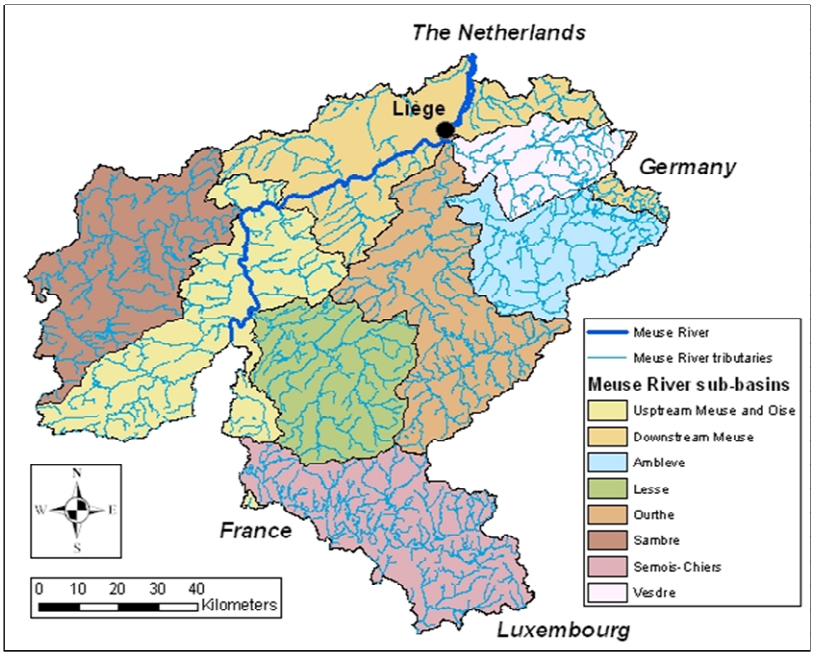

Figure 2.3. Sub-basin division and river network in the Walloon Meuse basin.

2.4.3. Meuse basin sedimentology

A total of 14 quaternary river terraces form the Meuse River basin, where three different alluvial deposits can be differentiated (Haddouchi, 1987):

- Alluvium formed by sand and gravels, deposited by dense braided river network;
- Alluvium with smaller grain size deposited during inter-glacial periods in the lower part of the basin, affected by marine transgressions;
- Alluvium poorly classified, not affected by marine transgressions and probably deposited during temperate climate.

These three different alluvium deposits are almost present in all the river terraces, and were deposited during glacial – interglacial successions as a consequence of different capacity of transport of the river.

The modern alluvium deposits, corresponding to the current course of the river and where nowadays human settlements are located, were deposited during periglacial period by braided river channels, with multiple gravel islands surrounded by ancient river channels usually filled

with less pervious materials. The denser networks of channels surrounding gravel islands were mainly located where the alluvial plain is wide, while smaller river channels filled by silty-clay alluviums were preferentially located near the hillslope.

2.4.4. Hydrogeology

2.4.4.1. Regional hydrogeology

In application of the European Framework Water Directive 2000/60/EC (EU, 2000), the aquifers of the Walloon Region have been subdivided in groundwater bodies (DGRNE, 2005), based on physical, hydrogeological and no-hydrogeological (administrative limits, hydrogeochemical status,…) criteria. Most of these groundwater bodies are included totally and/or partially in the Walloon Meuse basin (Figure 2.4).

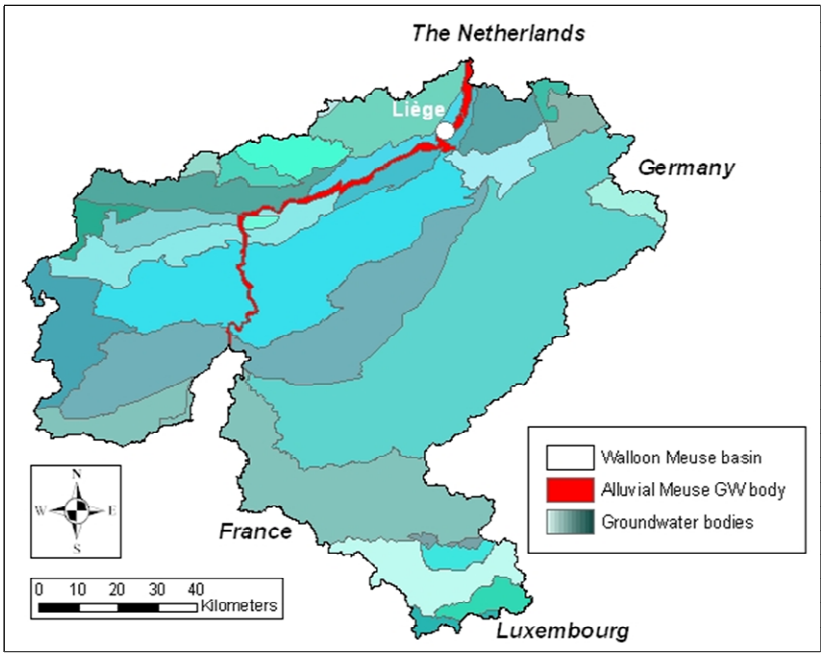

Figure 2.4. Groundwater bodies in the Walloon Meuse basin.

The site under study is located in the groundwater body number “RWM073” (Alluvions et graviers de la Meuse), classified as a threatened groundwater body with poorly qualitative status, regarding the industrial activities developed and located upstream and downstream of the city of Liège.

The alluvial aquifer of the Meuse River is mainly composed of loamy sands and gravels, conferring to this aquifer of an important groundwater resource, deposited by the Meuse River on the semipervious sandstone-shaly carboniferous bedrock.

Some kilometres upstream and downstream of the city of Liège, where industrial activities are mainly located, the alluvial aquifer of the Meuse River basin is characterised by high sulphate (SO_4^{2-}) and ammonium (NH_4^+) concentrations (up to 570 mg L^{-1} and 190 mg L^{-1}, respectively), as well as Fe and Mn (up to 0.45 mg L^{-1} and 1.4 mg L^{-1}, respectively). Dissolved oxygen concentrations are usually low, from 1 to 2.7 mg L^{-1}. High contents of sulphate, ammonium and Mn seem to be related to industrial spoilage. These artificially high concentrations of major elements make groundwater of the alluvial aquifer non drinkable in localised areas (Haddouchi, 1987).

Former hydrogeological studies performed in the alluvial aquifer have evidenced a wide range of hydraulic conductivity values. Dassargues (1994) estimated the hydraulic conductivity for the alluvial aquifer downstream of Liège city, obtaining values between 1.5×10^{-3} and 7.5×10^{-2} m s^{-1}. This values were subsequently confirmed by Brouyère (2001), who estimated high hydraulic conductivity values also downstream of Liège city, ranging from 1×10^{-2} and 6×10^{-2} m s^{-1}. Peters (1996) and Rentier (2002) observed a wider range of hydraulic conductivity values upstream of Liège, ranging from 3×10^{-4} to 1×10^{-2} m s^{-1}. It is likely that this wide range of hydraulic conductivity could be related to the braided river morphology of the river which deposited the alluvium in the past.

2.4.4.2. Local hydrogeology

The mean piezometric level in the Flémalle site is around 60 meters a.s.l. (above sea level), in relation with the mean water level in the Meuse River, at 59.4 meters a.s.l. in regular conditions. The alluvial aquifer is located at a depth of 7.5 meters in the “plateau” area, and at 5 meters depth in the “depressed” area. The mean saturated thickness is 8 meters, and the topography of the carboniferous bedrock is relatively constant between 51 and 53 meters a.s.l., at a mean depth of 15 meters (Figure 2.5).

The alluvial aquifer is overlain by a backfill layer characterised by a variable thickness and a high variability of components. This layer is mainly composed of materials originated from industrial building dismantlement, like ashes, brick fragments, iron pipes…, and even railway track. Within this backfill layer, local saturated perched zones can be noticed seasonally after rainy periods, but these perched water levels cannot be considered as a continuous aquifer because they are dry during the summer period.

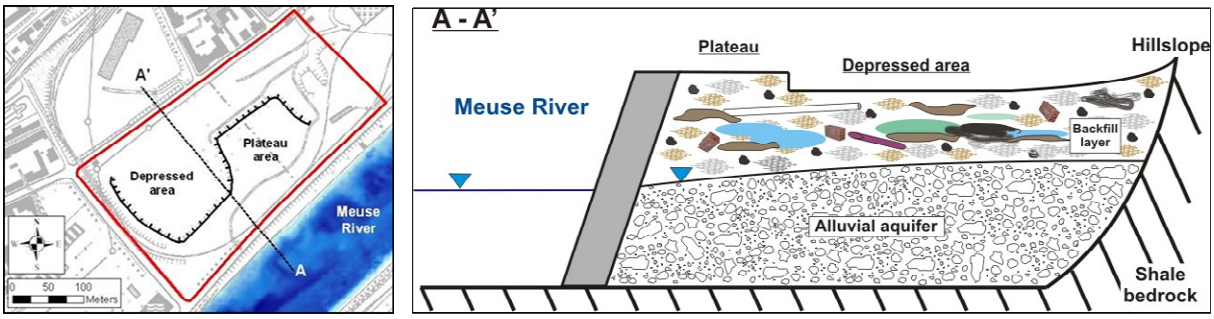

Figure 2.5. Vertical profile of the local hydrogeology in the former Flémalle cokery (not at scale).

The aquifer is recharged by rainfall and, locally, lateral infiltration from the hillslope. However, natural conditions of recharge in the studied area and surroundings are highly modified due to urbanisation. It is indeed likely that the alluvial aquifer is mostly recharged by the Meuse River upstream from a dam located on the river. The Flémalle site is located between the Ivoz-Ramet dam, 2 km upstream, and the Ile Monsin dam, 15 km downstream (Figure 2.6). The Ivoz-Ramet dam induces a difference in the Meuse River water level of 3 meters between upstream and downstream. This difference of water level is likely to infer a bypass of Meuse River water through the alluvial plain.

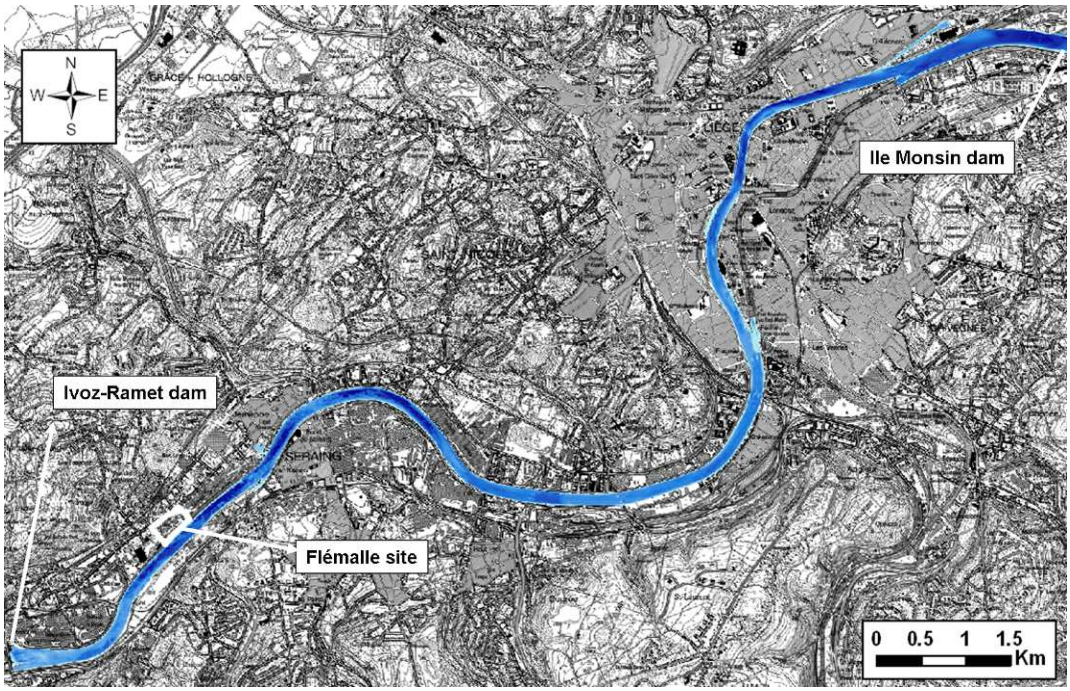

Figure 2.6. Location of the Ivoz-Ramet and Ile Monsin dams, and the Flémalle site.

2.4.5. Site history

2.4.5.1. Before the industrial activities

The only information about the site before the coke and gas production comes from ancient topographic maps. The oldest one corresponds to Ferraris (1778), depicted in Figure 2.7. From this map, it appears that the surroundings of the site were not urbanised, but mainly occupied by agricultural fields, and the Meuse River morphology was substantially different from nowadays, with a channel and a small island (Corbeaux Island, -Île aux Corbeaux-). It is likely this ancient channel was passing through the site where the coke plant was established afterwards.

A new map presented by Houbotte (1847) does not show considerable changes in the zone 70 years later. A part of this map is presented in Figure 2.8. In a subsequent geological map (IGN, 1893) the course of the Meuse River was still unchanged and the channel and the island were still present (map not shown).

Between 1908 and 1910, the channel was filled with materials of unknown origin, maybe from the Corbeaux Island (SPAQuE, 2007), and riverbanks were developed with a mixture of concrete and rocks materials in order to prevent frequent flooding of the alluvial plain.

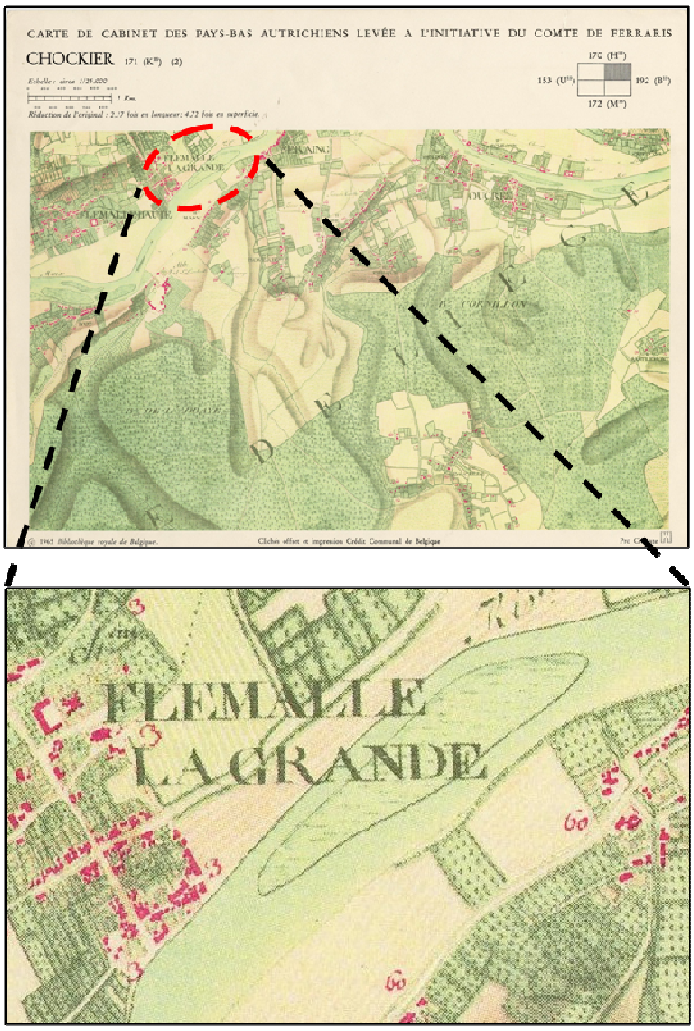

Figure 2.7. Part of the 171(2) plate map where the Flémalle site is located. The oval dashed zone indicates the approximate location of the studied site (Ferraris, 1778).

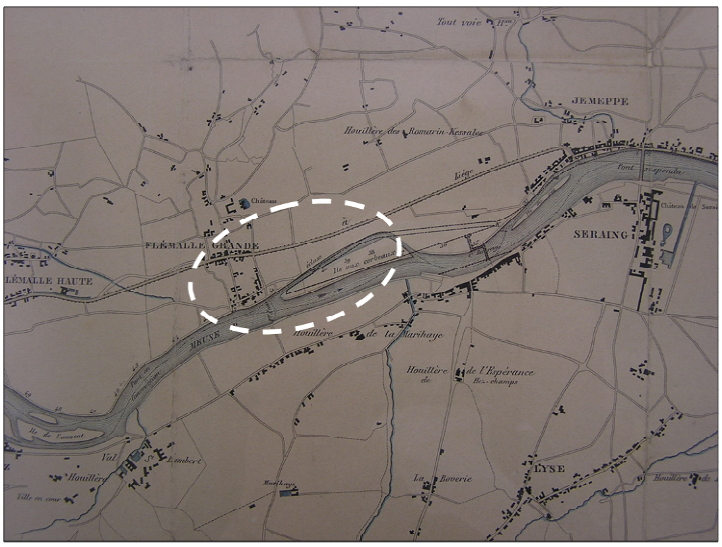

Figure 2.8. Part of the map of Houbotte (1847). The oval dashed zone indicates the approximate location of the studied site.

2.4.5.2. During industrial activities

The history of the Flémalle coke plant, officially called "Metallurgical site of Esperance Longdoz", started in 1913, date at which the building of the coke and gaswork plant started. Due to socio-political problems related to the First World War, the building of the plant was stopped many times, and it was finally in 1922 when the coke and gas production started to work continuously until 1984. During 62 years of activity, a total of 26,375 million tons of coal were introduced in the ovens, with 18,381 million tons of coke produced and more than 8,000 millions of m^3 gas produced. A summary of the Flémalle coke plant history is presented in Table 2.1.

Table 2.1 History of the former Flémalle coke plant (CHST, 1984).

Date	Event
1913	Contract agreement for construction and installation of a coal stockage, 90 coke ovens and a factory to reuse sub-products of the coal burn process.
1914 - 1918	The project was interrupted because of the First World War.
1918	Construction plant installation was restarted.
1922	End of the works. At this moment, the gaswork Flémalle site was composed of: Crane for unloading landing craft in the Meuse river; 8 coal silos with a total capacity of 10,000 tons; A crushing hall with 3 crushers (CARR type) of 40 tons/hour capacity; 90 coke ovens made of 2 groups of 22+23, able to treat 8 tons of coal; Gas treatment installation and sub-products recuperation, with the following sequence: tar production, ammonium sulphate production, distilled benzol production, washing and fractionation; Installation for desulphurisation treatment of the gas, via dry tanks; Gasometer and a power station; By that time, the production capacity of the cokery was about 560 tons of coke per day, which means a mass of 770 tons of coal in the ovens.
1928	A battery-oven of 23 ovens was added. This new battery-oven helped increasing the productivity of the cokery with about 140 tons of coke per day, reaching a total production of 700 tons of coke per day (1,000 tons per day of coal put in the oven).
1940-1945	Different factories related with the steel manufacturing were established in the neighbourhoods of the gaswork plant.
1950	The first 45 ovens were demolished, and the rest of the old ovens (between 46 and 113) were stopped. A new battery of 44 ovens (COPPEE type) was added, as well as a new line of sub-products treatment.
1951	Because of an increase in needs of coke, the ovens 46 to 113 were started again, working continuously until 1975.
1957	16 new ovens were added to the 44 modern ovens constructed in 1950, getting to the factory a capacity of 2,000 tons per day of coal in ovens, which means a final production of 1,400 tons of coke. At this time, more than 330,000 m^3 per day of gas were sold to the city of Liège and its suburbs, with peaks of 15,000 m^3/h in the winter time.
1968	The cokery gas was progressively substituted by natural gas.
1970	The last gas compressor was stopped in January 1970.
1975	The battery-ovens from 1922-28 was definitively stopped.
1984	Coke production was definitively stopped for two main reasons: the batteries age and rationalisation plans.

Figure 2.9 shows the activity of the Flémalle coke plant during its “gold period” of production, between 1928 and 1968.

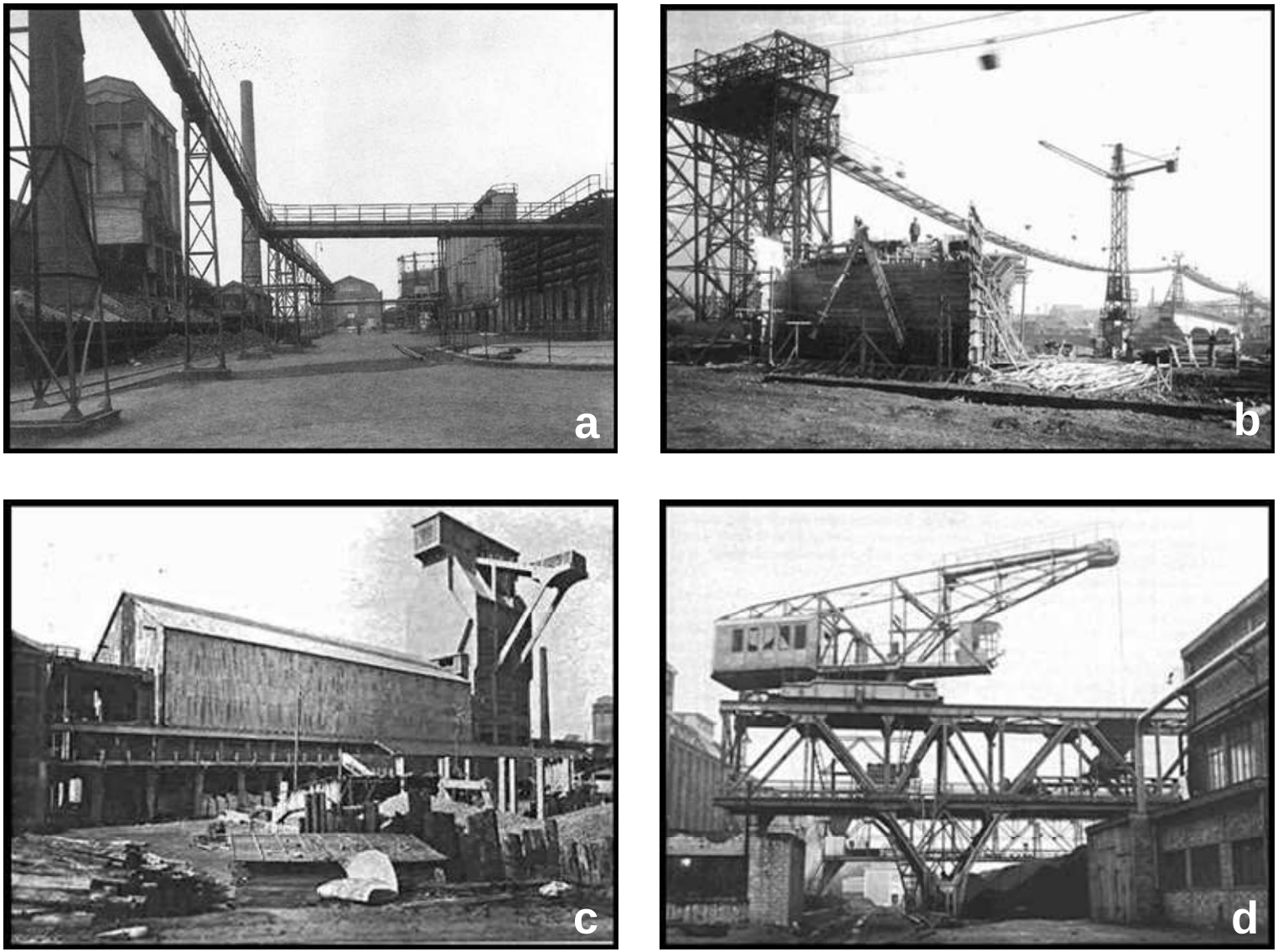

Figure 2.9. Pictures of the Flémalle coke plant at different times in the past: a) interior of the site in 1930; b) bridge building in 1948; c) oven battery building in 1950; d) bridge building in 1960 (SPAQuE, 2007).

Figure 2.10 shows aerial photographs from years 1947, 1971, 1978 and 1999 (aerial photographs before these dates were not found). The North extended area of the Flémalle site, used during the activity period for coal storage and linked to the main site by railway track, is also presented in Figure 2.10 (limited by a dashed line). A piece of evidence of the decline period in 1978 (Figure 2.10c) is the disaffection of this North extended area.

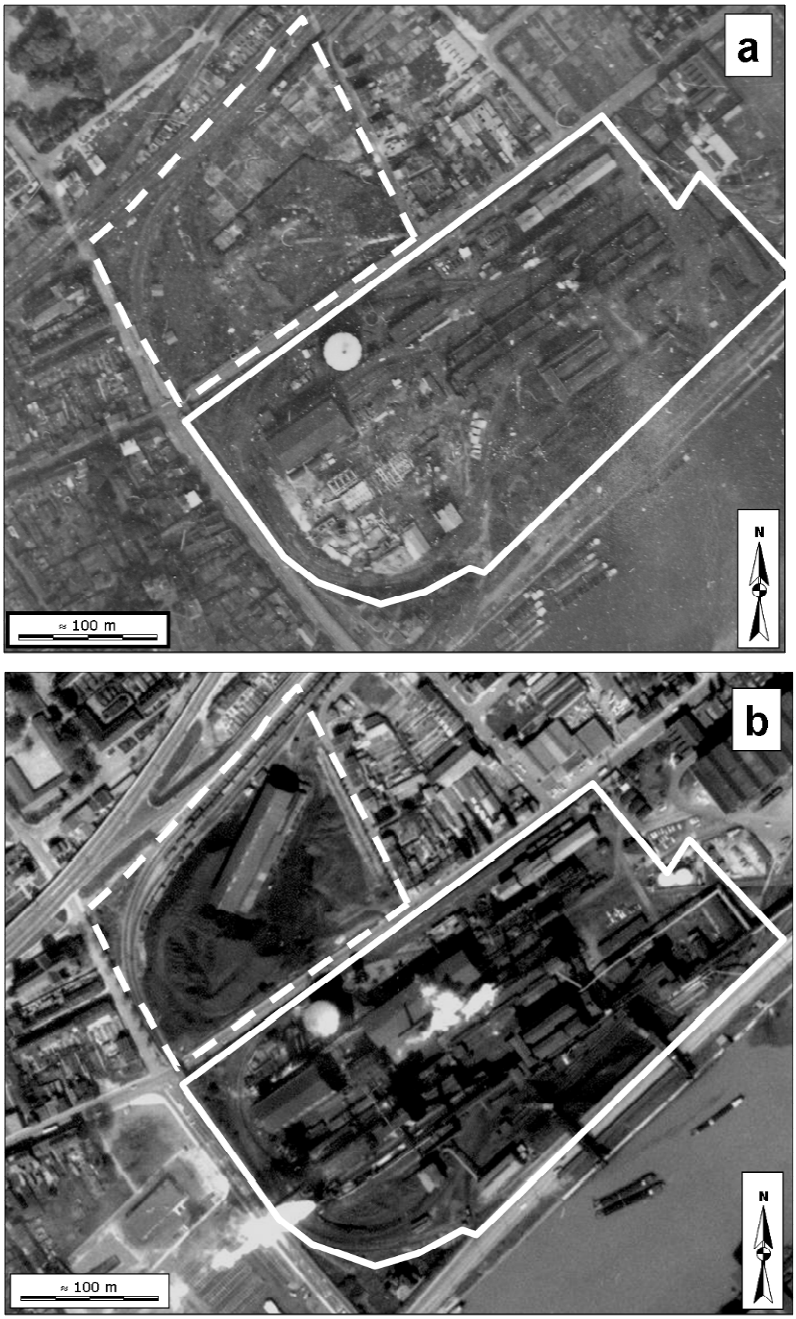

Figure 2.10. Aerial photographs of the Flémalle coke plant at four different times in the industrial activity period: 1947 (a); 1971 (b); 1978 (c); and 1999 (d). The area delimited by the dashed line corresponds to the North extended part of the coke plant area previously used as coal storage (modified from SPAQuE, 2007).

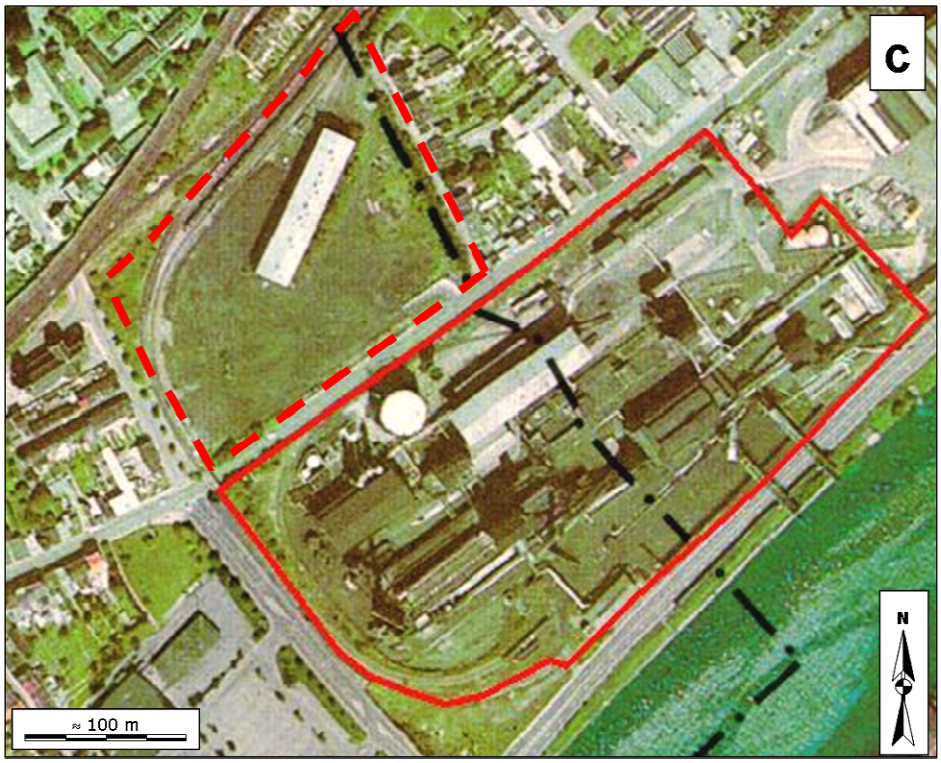

Figure 2.10. (Continuation).

2.4.5.3. After industrial activities

After the definitive stop of coke production in 1984, the site was subsequently dismantled and abandoned. Soil and groundwater pollution was noticed at the beginning of the 90's, last century. Up to now, several soil and groundwater characterisation campaigns have been carried out, starting in 1992 (details presented in the next section). The Northern extension of the site has been redeployed to iron recycling activities since year 2000.

Nowadays, the morphology of the Flémalle site is characterised by a difference of 3 meters in the topography between a "depressed" area in the centre of the site and a "plateau" area in the zone adjacent to the river (Figure 2.10d). This difference of height was probably artificially made of backfill deposits originated during the building dismantling process at the end of the industrial activity.

2.4.6. Prior characterisation studies

Five characterisation campaigns were carried out between 1992 and 2005, coordinated by the SPAQuE (Société Publique d'Aide à la Qualité de l'Environnement):

- The first characterisation campaign was performed in 1992: 64 piezometers were drilled, 10 groundwater samples were taken from the saturated perched lenses and 30 from the alluvial aquifer, and 248 soil samples were analysed;
- The second characterisation campaign was performed in 2001: 10 new piezometers were drilled. Groundwater samples from both the new and former piezometers were analysed: 6 from the saturated perched lenses and 19 from the alluvial aquifer. 9 soil samples and 5 gas samples were also analysed;
- The third characterisation campaign was carried out also in 2001: 26 new piezometers were drilled, 4 groundwater samples, 14 soil samples and 5 gas samples were analysed;
- The fourth characterisation campaign was carried out at the beginning of 2002, with 2 new piezometers drilled and groundwater samples analysed;
- The fifth and last characterisation campaign was performed in 2005 by URS Corps in collaboration with the Hydrogeology Unit of the University of Liège. A total of 58 additional piezometers were drilled, groundwater and soil samples were taken and analysed. Some of the piezometers corresponding to this campaign were drilled over the limits of the Flémalle site, in private gardens in the North part.

After the last characterisation campaign, and considering the piezometers not able to provide further information for different reasons (not found back in the field, clogged, dry,…) after an inventory work, a total of 116 piezometers screened at different depths in the alluvial aquifer are available ("deep piezometers"). Piezometers screened in the backfill layer ("shallow aquifer") are not any more considered.

Among the "deep piezometers" only 6 were drilled with a large diameter (6" ~ 0.15 m), and can be used for advanced investigations. The others are equipped with 4" diameter (~ 0.1 m) tubing and screens and their use is limited to groundwater head monitoring. Figure 2.11 presents all piezometers used during the field works performed in the scope of the present research in the Flémalle site.

It is worth noting that all piezometers were drilled and equipped without considering the possibility of sampling groundwater at different depths. Only in very specific locations two piezometers can be found, placed one next to the other, and screened at two different depths. This implies to work in depth-averaged conditions (in two dimensions) for groundwater flow and solute transport.

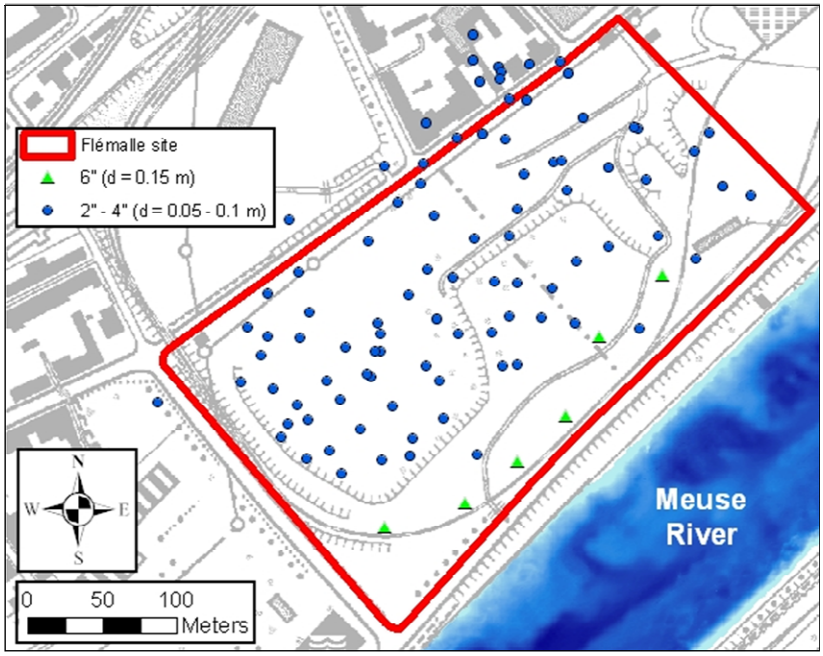

Figure 2.11 Location of piezometers used in the former Flémalle coke plant.

2.4.7. Environmental pollution originated by the former Flémalle coke plant

Up to now, there is no official regulation on soil and groundwater pollution applicable in the Walloon Region. The Walloon Soil Decree is in preparation and until it will be promulgate,

SPAQuE applies a simplified and well defined methodology (SPAQuE, 2007) based on the existing draft of regulation and on international regulations. In this methodology, maximum admissible pollutant concentrations in the soil and groundwater are established in relation to the present or future planned land use of the contaminated zone. Three quality standards are developed for soil and groundwater quality assessment on polluted sites, used to define whether the site is considered as contaminated or not, and in the affirmative case, if decontamination and/or remediation techniques must be imperatively implement. The three quality standards are defined as follows (SPAQuE, 2007; Moutier and Halen, 2008):

- The "reference value" (RV) corresponds to the value of the expected background concentrations in soil and groundwater;
- The "trigger value" (TV) is defined as a precautionary risk-based value used to differentiate between soils and groundwater which may be treated as not polluted and those requiring further investigations and, if necessary, a risk assessment;
- The "intervention value" (IV) acts as a cut-off risk: soils and groundwater concentrations above this value lead to mandatory further action, like remediation, engineering controls, land-use restrictions or monitoring;

These three quality standards values must be adapted to each contaminated site depending on different site specific parameters, such as downgradient receptors (humans, water supply pumping well, wildlife,…), future activities planned in the site…

Quality standards for soils are land-use dependent, with 5 categories of future land-use considered: natural, agricultural, residential, leisure or commercial and, industrial. For quality standards in groundwater, a single value is considered, whatever the expected land-use and considering the fact that groundwater is mobile in the underground.

In the Flémalle site, soil and groundwater are highly polluted due to past industrial activities related to coke and gas production. Contaminations by both, organic and inorganic pollutants, have been reported from former characterisation campaigns, as described here after. Location of soil and groundwater samples is presented in Figure 2.12.

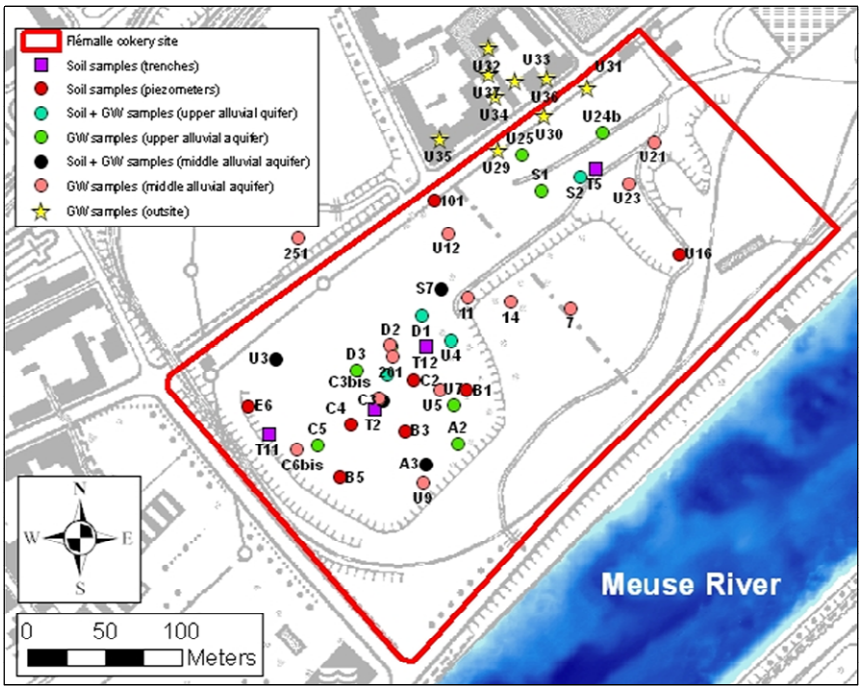

Figure 2.12. Soil and groundwater samples location.

2.4.7.1. Soil contamination

Soil samples analysed from the first (1992), second (2001) and fifth (2005) characterisation campaigns reported important soil contamination in the backfill layer (0 – 4 m depth) by organic pollutants, mainly BTEX (Benzene, Toluene, Ethylbenzene and Xylene) and PAHs (Polynuclear Aromatic Hydrocarbons), the most common petroleum hydrocarbons responsible of groundwater pollution (Alvarez and Illman, 2006). A summary of soil pollutants concentration is presented in Table 2.2. The list of analysed species is longer than presented in this table, but the more representative pollutant substances are only listed here. For example, naphthalene and fluoranthene are listed as representative compounds of PAHs, although other PAHs components are also present and often with no negligible concentration, like benzo(a)pyrene, benzo(a)anthracene and benzo(b)fluoranthene, among others. Mineral oils and cyanide are also frequently present, as well as inorganic pollutants such as arsenic (As), cadmium (Cd), zinc (Zn) and lead (Pb). Others compounds such as barium (Ba) and mercury (Hg) were also encountered locally.

Because the future use of the Flémalle site is unknown, pollutant concentrations listed in Table 2.2 are commented taking into account the corresponding intervention value for industrial use.

Almost all soil samples analysed for BTEX compounds exceed the benzene intervention value of 0.6 mg kg^{-1}. Referring to this, observation well C3 is highlighted as the one presenting the highest benzene concentrations, up to more than 140,000 mg kg^{-1}. Other BTEX compounds such as Toluene, Ethylbenzene and Xylene exceed also the intervention value, fixed at 85, 76 and 20 mg kg^{-1}, respectively.

Concerning PAHs, naphthalene and fluoranthene intervention values are fixed at 17 and 300 mg kg^{-1}, respectively. These concentrations are largely exceeded, reaching locally concentrations up to 140,000 and 25,000 mg kg^{-1}, respectively.

With concentrations up to 130,000 mg kg^{-1}, concentrations of mineral oils in the backfill layer largely exceed the intervention value, fixed at 5,000 mg kg^{-1}.

Metal trace elements (MTEs) are also present in the Flémalle site, but at lower concentrations than organic substances, even if their presence is not negligible in the backfill layer. Zn has been reported up to 3,350 mg kg^{-1}, while the intervention value corresponds to 1,300 mg kg^{-1}. The intervention values for Cd, As and Pb are fixed at 50, 300 and 1,360 mg kg^{-1} respectively. Their presence in the backfill layer does not exceed these values, but their concentrations are often beyond the reference (RV) and trigger value (TV).

Unfortunately, samples taken during the drilling process of different characterisation campaigns do not allow a comparison of concentrations in function of the time at a same location.

Table 2.2. Summary of soil contamination in the former Flémalle coke plant (As: arsenic; Cd: cadmium; Zn: zinc; Pb: lead; n.a.: not analysed; * observation well presently disappeared, clogged or broken; ** Trenches). Concentrations above the intervention value are represented in bold and grey shadow.

	ID	Depth (m)	BTEX (mg kg^{-1})				PAHs (mg kg^{-1})		Mineral Oils (mg kg^{-1})	Heavy metals (mg kg^{-1})			
			Benzene	Toluene	Ethylbenzene	Xylene	Naphthalene	Fluoranthene		As	Cd	Zn	Pb
1st characterisation campaign (1992)	**A3**	1.0 – 1.5	**914**	**748**	50	**501**	**23**	62	n.a.	n.a.	n.a.	n.a.	n.a.
	B1	0.5 – 1.0	**125**	**115**	5	**148**	**2,400**	**1,640**	n.a.	n.a.	n.a.	n.a.	n.a.
	B3	0.0 – 0.5	**1**	1	1	1	**2,500**	**1,400**	n.a.	n.a.	n.a.	n.a.	n.a.
	B5	1.5 – 2.0	**341**	63	11	**174**	0.1	0.2	n.a.	n.a.	n.a.	n.a.	n.a.
	C1*	1.5 – 2.0	**311**	29	14	**119**	16	6.3	n.a.	n.a.	n.a.	n.a.	n.a.
	C2	0.0 – 0.5	**106**	77	7	**168**	**140,000**	**8,600**	n.a.	n.a.	n.a.	n.a.	n.a.
		1.0 – 1.5	**51**	24	4	**34**	**11,610**	**460**	n.a.	n.a.	n.a.	n.a.	n.a.
		1.5 – 2.0	**4,995**	**2,235**	**80**	**1,446**	**7,300**	**3,000**	n.a.	n.a.	n.a.	n.a.	n.a.
	C3	0.0 – 0.5	**987**	**492**	50	**263**	**29**	120	n.a.	n.a.	n.a.	n.a.	n.a.
		1.0 – 1.5	**1,946**	**290**	**577**	**851**	**168**	85	n.a.	n.a.	n.a.	n.a.	n.a.
		1.5 – 2.0	**143,093**	**45,136**	**5,322**	**77,419**	**2,600**	**380**	n.a.	n.a.	n.a.	n.a.	n.a.
	C4	0.5 – 2.0	**3,391**	**3,550**	50	**150**	7.5	0.7	n.a.	n.a.	n.a.	n.a.	n.a.
	D1	1.5 – 2.0	**1**	1	1	1	**360**	9.2	n.a.	n.a.	n.a.	n.a.	n.a.
	D6*	0.0 – 1.0	**130**	1	6	**294**	**7,600**	**21,000**	n.a.	7.1	2.16	181	66
	E6	0.0 – 0.5	**20**	40	1	**91**	**14,000**	**25,000**	n.a.	n.a.	n.a.	n.a.	n.a.
	S2	1.5 – 3.0	**16**	8	5	**64**	**3,800**	**780**	n.a.	n.a.	n.a.	n.a.	n.a.
	S5	1.0 – 2.0	**651**	2	8	**111**	**1,100**	45	n.a.	n.a.	n.a.	n.a.	n.a.
	S7	1.0 – 1.5	**1**	1	1	1	4.7	112	n.a.	n.a.	n.a.	n.a.	n.a.
2nd characterisation campaign (2001)	**101**	0.0 – 0.5	<0.05	<0.05	<0.05	<0.15	1.2	3.71	1,900	36	1.25	163	142
	212*	1.5 – 2.0	**1.41**	0.8	<0.05	0.31	**29.2**	**390**	2,610	51	1.22	427	196
	213*	1.3 – 1.5	**4.1**	20.8	4.96	**124.5**	**13,500**	**5,930**	**51,700**	81.6	**182**	**3,350**	1,090
	216*	0.8 – 1.6	0.45	0.16	<0.05	<0.15	1.21	6.85	3,090	45.6	2.22	309	145
	218*	0.0 – 0.8	0.17	0.21	<0.05	0.17	**39.2**	**662**	4,690	16.6	3.12	396	479
5th characterisation campaign (2005)	**U3**	1.5 – 6.0	**34**	6.4	7	**88**	**1,000**	**1,000**	**10,000**	36	3.7	**1,300**	600
	U4	0.0 – 1.0	**42**	8.7	0.27	10	**70,000**	**1,900**	**37,000**	56	37	1,000	280
		4.0 –5.0	**3,100**	**860**	7.5	**340**	**250**	31	1,200	21	<0.4	34	22
	U16	0.0 – 0.5	**8.5**	4.6	1.5	**85**	**5,600**	**1,200**	**31,000**	<10	0.46	110	0.63
	T2**	2.5 – 3.0	**2,000**	**840**	29	**620**	**9,400**	740	**24,000**	26	13	540	250
		3.0 – 3.5	**22**	0.17	0.4	0.97	**59**	0.59	120	<10	0.76	150	26
	T11**	0.0 – 1.0	**80**	**150**	5.5	**250**	**21,000**	**8,100**	**130,000**	18	4	450	840
	T12**	0.5 – 1.0	**12,000**	**11,000**	**140**	**4,500**	**32,000**	**2,500**	**100,000**	120	**86**	1,100	310

2.4.7.2. Groundwater contamination

Groundwater was sampled and analysed during each characterisation campaign in different piezometers, but there was not a follow-up sampling in the same piezometers through time.
Table 2.3, Table 2.4, and Table 2.5 summarise pollutant concentrations reported from the saturated perched lenses in the backfill layer, and from the upper and middle part of the alluvial aquifer, respectively. Contaminant concentrations of piezometers drilled over the limits of the Flémalle site, in private gardens, are summarised in Table 2.6. The list of pollutant substances analysed is longer than shown in tables, but only the most representative substances are listed.

Table 2.3. Summary of groundwater contamination in the saturated perched lenses in the backfill layer (As: arsenic; Cd: cadmium; Zn: zinc; Pb: lead; n.a.: not analysed; *: observation well presently disappeared, clogged or broken) . Concentrations above the intervention value are represented in bold and grey shadow.

ID	Year	Depth (m)	BTEX (µg L^{-1})				PAHs (µg L^{-1})		Cyanide (µg L^{-1})	Heavy metals (µg L^{-1})			
			Benzene	Toluene	Ethylbenzene	Xylene	Naphthalene	Fluoranthene		As	Cd	Zn	Pb
B1	1991	2.2 – 3.2	**570**	50	50	150	**89**	35	n.a.	n.a.	n.a.	n.a.	n.a.
B4	1991	1.5 – 2.5	0.1	0.15	0.15	0.15	1	1	n.a.	n.a.	n.a.	n.a.	n.a.
C3	1991	1.5 – 2.5	**48,000**	2,600	100	2,000	**5,000**	18	n.a.	n.a.	n.a.	n.a.	n.a.
	1992	1.5 – 2.5	28	28	0.1	2.6	**5,846**	**667**	n.a.	n.a.	n.a.	n.a.	n.a.
D2	1991	2.0 – 3.0	**50,000**	1,500	300	**8,300**	**4,900**	10	n.a.	n.a.	n.a.	n.a.	n.a.
	1992	2.0 – 3.0	26	1.1	0.15	4.1	21	0.1	n.a.	n.a.	n.a.	n.a.	n.a.
S5	1991	1.5 – 2.5	**150,000**	**33,000**	100	**3.800**	**2,000**	10	n.a.	n.a.	n.a.	n.a.	n.a.
	1992	1.5 – 2.5	52	8.4	0.1	2.4	**884**	**773**	n.a.	n.a.	n.a.	n.a.	n.a.
D3	1991	1.0 – 2.0	**7,200**	2,800	100	**3,100**	**1,800**	34	n.a.	n.a.	n.a.	n.a.	n.a.
E2	1991	1.5 – 2.5	**290**	280	50	810	**1,200**	10	n.a.	n.a.	n.a.	n.a.	n.a.
E4	1991	1.2 – 2.2	0.1	0.1	0.1	0.3	1	1	n.a.	n.a.	n.a.	n.a.	n.a.
S1	1991	1.6 – 2.6	**165**	73	35	270	**600**	27	n.a.	n.a.	n.a.	n.a.	n.a.
S3	1991	2.8 – 3.8	**450**	250	350	250	**1,800**	62	n.a.	n.a.	n.a.	n.a.	n.a.

Table 2.4. Summary of groundwater contamination in the upper part of the alluvial aquifer (As: arsenic; Cd: cadmium; Zn: zinc; Pb: lead; n.a.: not analysed; *: observation well presently disappeared, clogged or broken) . Concentrations above the intervention value are represented in bold and grey shadow.

ID	Year	BTEX (µg L^{-1})				PAHs (µg L^{-1})		Mineral Oils (µg L^{-1})	Heavy metals (µg L^{-1})			
		Benzene	Toluene	Ethylbenzene	Xylene	Naphthalene	Fluoranthene		As	Cd	Zn	Pb
A2	1991	0.35	0.5	0.15	0.55	5	9.9	n.a.	n.a.	n.a.	n.a.	n.a.
C1*	1991	**12,000**	1,800	50	1,200	26	7.1	n.a.	n.a.	n.a.	n.a.	n.a.
	1992	20	2.1	0.05	0.65	40	36	n.a.	n.a.	n.a.	n.a.	n.a.
C5	1991	170	2.6	3.9	34	**170**	40	n.a.	n.a.	n.a.	n.a.	n.a.
	1992	0.2	0.15	0.1	0.3	25	156	n.a.	n.a.	n.a.	n.a.	n.a.
	2001	<0.2	<0.2	<0.2	n.a.	**5.43**	0.37	n.a.	8	<1.2	18	<6
	2005	**2,200**	600	2.9	100	**70**	0.31	120	<5	<0.4	14	<5
D1	1991	**560,000**	**77,000**	150	**5,500**	**1,400**	10	n.a.	n.a.	n.a.	n.a.	n.a.
	1992	**360**	60	0.6	11	**632**	0	n.a.	n.a.	n.a.	n.a.	n.a.
	2001	**210,000**	**57,000**	660	**9,400**	**1,400**	3.06	n.a.	7	<1.2	<6	<6
	2005	**230,000**	**45,000**	640	**11,000**	**5,100**	17	2,100	7.7	<0.4	64	<5
D2	1991	**54000**	2,700	300	**12,000**	**3,400**	3.9	n.a.	n.a.	n.a.	n.a.	n.a.
	1992	38	1.8	0.2	5.8	**663**	16	n.a.	n.a.	n.a.	n.a.	n.a.
	2001	**12,000**	1,500	420	**15,200**	**8,140**	118	n.a.	**108**	<1.2	<6	<6
D3	1991	**85,000**	**9,100**	50	**2,700**	**1,400**	10	n.a.	n.a.	n.a.	n.a.	n.a.
	1992	**150**	15	0.15	4.5	**6,421**	0.1	n.a.	n.a.	n.a.	n.a.	n.a.
	2001	**28,000**	**7,800**	190	**3160**	**1,000**	<0.016	n.a.	19	<1.2	<6	<6
	2005	**41,000**	**12,000**	<200	**4,500**	**19,000**	<10	**26,000**	11	<0.4	25	<5
S1	1992	**5,100**	1,100	100	1,300	n.a.	n.a.	n.a.	n.a.	n.a.	n.a.	n.a.
	2001	**1,900**	630	240	1,580	**2,140**	82.7	n.a.	19	<1.2	<6	<6
	2005	**1,000**	500	160	1,100	**11,000**	51	**7,200**	9.1	<0.4	35	34
S2	1992	**15,000**	2,200	100	1,400	**1,200**	39	n.a.	n.a.	n.a.	n.a.	n.a.
	2001	**11,000**	300	370	1,940	**1,040**	112	n.a.	**89**	<1.2	<6	<6
	2005	**8,100**	310	330	2,000	**63,000**	**2,000**	**27,000**	**110**	<0.4	140	**350**
S5	1991	**520,000**	**15,000**	100	2,100	**2,100**	54	n.a.	n.a.	n.a.	n.a.	n.a.
	1992	**380**	11	0.2	3.2	**12,368**	**1,833**	n.a.	n.a.	n.a.	n.a.	n.a.
	2001	**140,000**	680	440	**4,750**	**1,510**	39	n.a.	37	<1.2	<6	7
U4b	2005	**790,000**	**76,000**	190	**5,000**	**2,200**	4.4	2,100	6.7	<0.4	21	<5
U7	2005	**34,000**	**5,900**	<20	530	**250**	<1	320	<5	<0.4	16	<5
U24b	2005	**10,000**	1,300	130	2,000	**13,000**	110	**13,000**	6	<0.4	<10	<5
U25	2005	**2,900**	1,300	85	550	**2,500**	22	**6,600**	<5	<0.4	<10	<5

Table 2.5. Summary of groundwater contamination in the middle part of the alluvial aquifer (As: arsenic; Cd: cadmium; Zn: zinc; Pb: lead; n.a.: not analysed; *: observation well presently disappeared, clogged or broken) . Concentrations above the intervention value are represented in bold and grey shadow.

ID	Year	BTEX (µg L^{-1})				PAHs (µg L^{-1})		Mineral Oils (µg L^{-1})	Heavy metals (µg L^{-1})			
		Benzene	Toluene	Ethylbenzene	Xylene	Naphthalene	Fluoranthene		As	Cd	Zn	Pb
A3	1991	0.3	0.3	0.1	0.25	0.1	0.05	n.a.	n.a.	n.a.	n.a.	n.a.
	2005	**430**	140	n.a.	27	22	0.015	<50	<5.0	<0.4	20	<5.0
C3	1991	**13,000**	400	50	800	**5,000**	18	n.a.	n.a.	n.a.	n.a.	n.a.
	1992	40	0.25	0.1	0.2	**200**	0	n.a.	n.a.	n.a.	n.a.	n.a.
	2001	1.9	<0.2	<0.2	<0.2	1.44	3.33	n.a.	25	<1.2	<6	<6
C3bis	1991/92	**46**	2.6	0.15	1.7	**358**	0.1	n.a.	n.a.	n.a.	n.a.	n.a.
	2005	36	21	n.a.	29	**60**	<0.1	190	10	<0.4	27	<5
C6bis	1992	2.1	0.45	0.05	0.15	0.1	0.1	n.a.	n.a.	n.a.	n.a.	n.a.
	2005	**44**	45	n.a.	52	**230**	<1	260	6.9	<0.4	19	<5
D2bis	1992	17	0.95	0.1	2.2	0.1	0.1	n.a.	n.a.	n.a.	n.a.	n.a.
	2005	**4,100**	650	n.a.	**2,600**	**8,200**	8.6	**38,000**	9.9	<0.4	35	<5
S7	1991	**2,900**	150	50	150	1	5.7	n.a.	n.a.	n.a.	n.a.	n.a.
	1992	1.1	0.05	0.05	0.15	**74**	0.1	n.a.	n.a.	n.a.	n.a.	n.a.
	2001	**6,600**	11	88	58	**75.6**	4.73	n.a.	<5	<1.2	13	<6
	2005	**2,300**	30	n.a.	14	12	2.7	1,100	<5	<0.4	<10	<5
7	1992	1.1	0.05	0.05	0.15	**74**	0.1	n.a.	n.a.	n.a.	n.a.	n.a.
	2005	1.3	0.56	n.a.	3.7	0.74	13	2,400	<5	0.5	80	<5
11	1992	4.8	0.45	0.05	0.35	10	0.1	n.a.	n.a.	n.a.	n.a.	n.a.
	2001	**4,800**	2.2	58	10.4	13.4	3.24	n.a.	7	<1.2	<6	<6
	2005	**1400**	6.9	n.a.	12	15	27	2300	15	<0.4	31	<5
14*	1992	0.7	0.05	0.05	0.15	0.1	0.1	n.a.	n.a.	n.a.	n.a.	n.a.
	2005	260	15	n.a.	33	**1,100**	220	**11,000**	<5	<0.4	15	<5
201	2002	**92,000**	**24,000**	**1,900**	**18,100**	**1,770**	0.89	n.a.	n.a.	n.a.	n.a.	n.a.
	2005	**350,000**	5,300	**1,800**	**1,1000**	**7,800**	n.a.	**11,000**	n.a.	n.a.	n.a.	n.a.
251	2001	0.9	<0.2	<0.2	n.a.	1.5	<0.016	n.a.	11	<1.2	12	<6
	2005	0.41	1.2	n.a.	n.a.	2.4	0.055	<50	6.8	<0.4	38	<5
U3	2005	**850**	31	n.a.	46	**260**	3	640	6.3	<0.4	<1	<5
U5	2005	**600**	350	n.a.	230	**130**	0.14	160	8.4	<0.4	24	<5
U9	2005	**120**	64	n.a.	100	**430**	<1	550	6.7	<0.4	<10	<5
U12	2005	**950**	22	n.a.	220	**6,600**	18	**22,000**	<5	<0.4	43	<5
U21	2005	**110**	0.7	n.a.	n.a.	2.1	0.11	280	11	<0.4	<10	<5

Table 2.6. Summary of groundwater contamination in the upper and middle part of the alluvial aquifer from piezometers drilled over the Flémalle site (As: arsenic; Cd: cadmium; Zn: zinc; Pb: lead; n.a.: not analysed) . Concentrations above the intervention value are represented in bold and grey shadow.

ID	Depth (m)	BTEX (µg L^{-1})				PAHs (µg L^{-1})		Mineral Oils (µg L^{-1})	Heavy metals (µg L^{-1})			
		Benzene	Toluene	Ethylbenzene	Xylene	Naphthalene	Fluoranthene		As	Cd	Zn	Pb
U29	6	**63**	1.8	37	140	**1,500**	21	**6,500**	<5	<0.4	16	<5
	10	**510**	3.5	69	280	**350**	44	**8,200**	<5	1.7	26	<5
U30	6	**90**	1.5	27	62	**860**	9.2	**3,700**	<5	<0.4	18	<5
	10	**170**	0.6	5.1	7.4	2	13	1,700	<5	<0.4	12	<5
U31	7	**660**	<2	7.4	n.a.	14	1	310	<5	<0.4	25	<5
	10	**85**	0.4	2	1.1	23	2.7	780	<5	<0.4	<10	<5
U32	6	5.2	8.5	72	200	**1,100**	19	**9,800**	<5	6.3	71	<5
	9.5	0.53	0.88	11	31	**810**	45	**6,400**	8.5	<0.4	21	<5
U33	5	0.27	1.3	<0.2	0.78	7.5	0.29	220	<5	<0.4	13	<5
	9.5	<0.2	0.31	<0.2	n.a.	0.61	0.11	<50	<5	<0.4	19	<5
U34	6	**410**	32	95	330	<10	<10	**6200**	<5	<0.4	11	<5
	11	**590**	51	170	630	**18,000**	490	**40,000**	8	n.a.	6	n.a.
U35	6	3.3	1.6	3.9	15	**460**	1.1	1,000	<5	<0.4	16	<5
	10	0.48	<0.2	0.82	3.1	**130**	0.33	400	13	<0.4	<10	<5
U36	6	4.5	0.62	21	100	**2,100**	8.9	**4,300**	<5	<0.4	<10	<5
	11	**240**	3.5	63	130	**2,200**	10	**4,800**	<5	<0.4	36	<5
U37	6	0.3	<0.2	<0.2	n.a.	6.1	<0.01	<50	<5	<0.4	19	<5
	9.5	<0.2	<0.2	<0.2	n.a.	1.1	<0.1	<50	10	<0.4	<10	<5

BTEX and PAHs concentrations measured in the saturated perched lenses in the backfill layer are generally high in all sampled piezometers (Table 2.3). Most groundwater samples taken in these piezometers exceed the intervention value (40 μg L^{-1}) for benzene of more than 3 orders of magnitude and all exceed the reference (0.25 μg L^{-1}) and trigger (10 μg L^{-1}) values, respectively. The situation for PAHs components is relatively similar, where most of the piezometers exceed naphthalene and fluoranthene intervention values (410 and 60 μg L^{-1} respectively). Mineral oils and MTEs were not analysed during the sampling campaigns of 1991 and 1992.

A decrease in concentration for BTEX compounds of three orders of magnitude, from 1991 to 1992, is observed in almost all samples. However, this decrease is not observed for the rest of PAHs compounds.

With concentrations up to 560,000 μg L^{-1} of benzene, 77,000 μg L^{-1} of toluene and 15,200 μg L^{-1} of xylene, the upper part of the alluvial aquifer is even more polluted than the saturated perched lenses in the backfill layer (Table 2.4). Concentrations of naphthalene and fluoranthene are two to three orders of magnitude above the intervention value. All samples where mineral oils were analysed, were also reported above the intervention value, defined at 3,000 μg L^{-1}.

Elevated metal trace elements (MTEs) concentrations are locally present in the Flémalle site. The intervention value of As, fixed at 40 μg L^{-1}, is exceeded in two piezometers (D2 and S2), with 108 and 110 μg L^{-1} respectively. Cadmium concentrations do not present important concentrations, while Pb and Zn concentrations are locally above the intervention limit, fixed at 40 and 400 μg L^{-1}, respectively.

Concentrations reported from piezometers screened in the middle part of the alluvial aquifer (Table 2.5) are of the same order of magnitude than those analysed in the upper part of the alluvial aquifer (Table 2.4). BTEX and PAHs compounds are above the intervention value, as well as mineral oils. Figure 2.13 presents the spatial distribution of the main organic contaminants in the alluvial aquifer. MTEs concentrations are likely to be lower than those reported in the upper part of the alluvial aquifer, and concentrations rarely exceed the trigger values, fixed at 5 μg L^{-1} for Cd, 10 μg L^{-1} for As and Pb, and 200 μg L^{-1} Zn.

Generally speaking, although it is observed that pollutant concentrations decrease over time in several piezometers, this is not a general trend. On the contrary, other piezometers are likely to present an inversed trend, with increasing contaminant concentration with time.

Groundwater contamination in the upper and middle part of the alluvial aquifer outside the Flémalle site is significantly lower than inside (Table 2.6). BTEX and PAHs concentrations exceed of one order of magnitude the intervention values. The most significant contamination is related to minerals oils. Soil contamination was not reported during the drilling process of these piezometers. In conjunction with the low contaminant concentrations, it is likely to indicate that the source(s) of contamination was(were) located inside the Flémalle site.

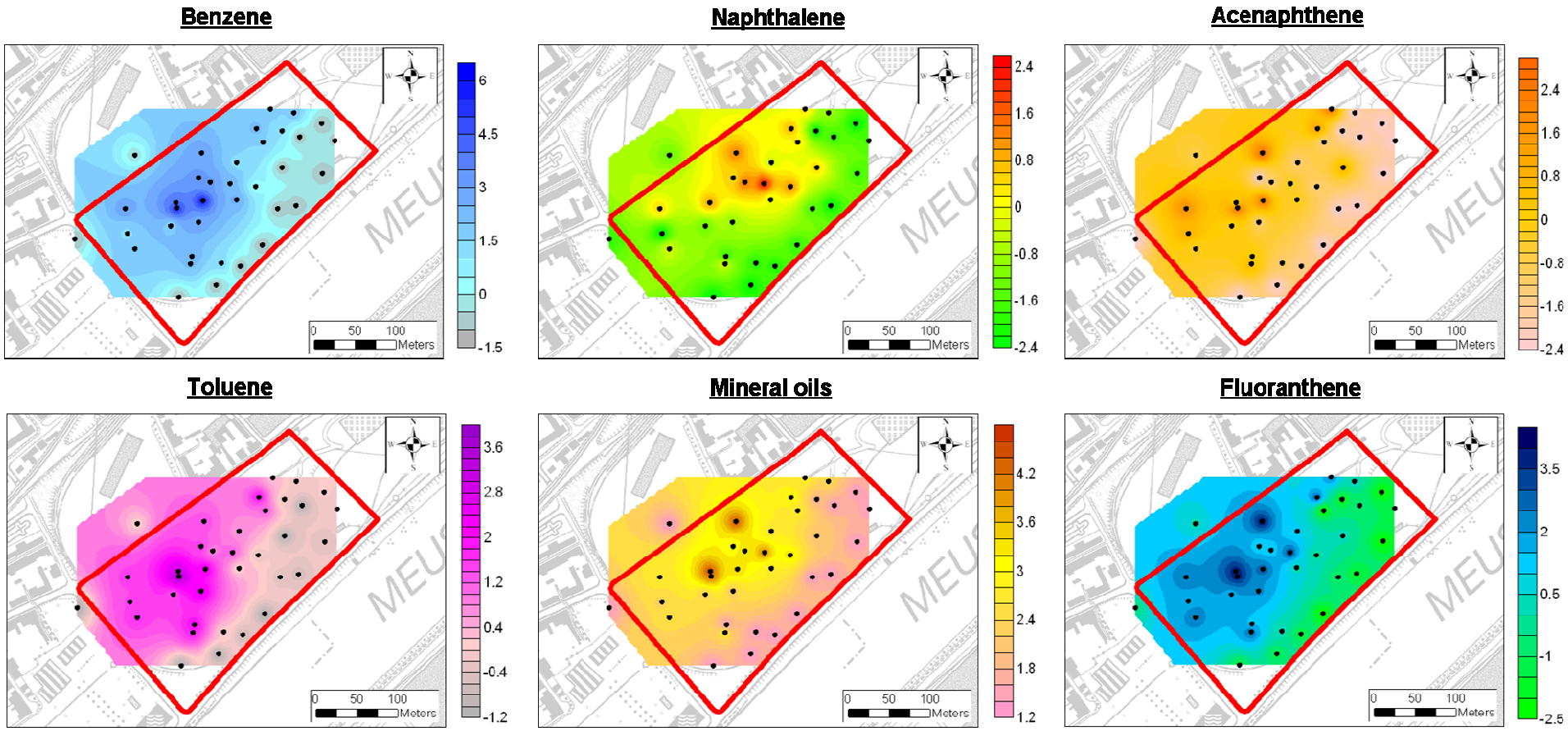

Figure 2.13. Spatial distribution of the main organic pollutants in 2005. Concentrations are expressed in $\log_{10}$ µg L^{-1}. The interpolation method used is the inverse distance weighted. Dots represent sampling points.

2.4.7.3. Possible location of the pollution sources

Considering the present location of the organic pollutants and their spatial distribution presented in Figure 2.13, it is likely that more than one pollution source is active. Detailed examination of old maps has permitted to locate, relatively exactly, different industrial buildings, tanks, reservoirs… which could potentially be associated with the pollution sources. These areas correspond with benzene reservoirs, benzol cleaners and sulphate factories, and they are all located in the "depressed" area of the site (Figure 2.14). Three zones have been identified as potential sources of pollution:

- Zone A. Different subsources of pollution were present, such as benzene and benzol reservoirs, oil tanks…;
- Zone B. Benzene factory;
- Zone C. Benzol cleaners.

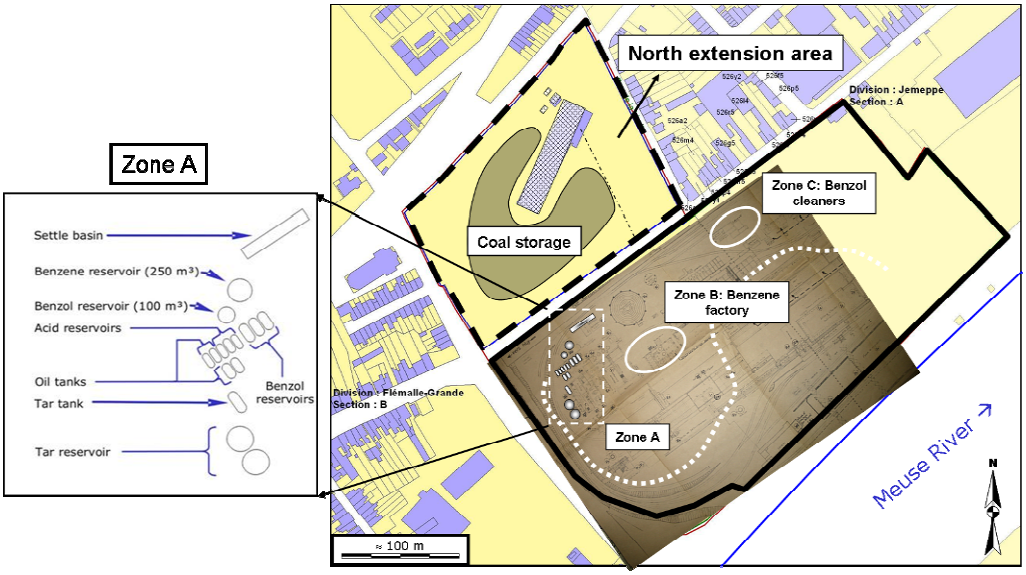

Figure 2.14. Location of the potential sources of pollution.

2.5. Conclusions on chapter 2

As a consequence of former industrial activities related with coke and gas production during the last century, soil and groundwater of the Flémalle site are heavily contaminated by organic (mainly BTEX and PAHs) and inorganic pollutants (As, Cd, Zn and Pb). Organic compounds like benzene, naphthalene and fluoranthene are present in the soil and groundwater at concentration up to 3 to 4 orders of magnitude above the intervention limit. Although concentrations of inorganic pollutants are not so pronounced, their intervention threshold values are locally exceeded, and the aquifer geochemistry can play a key role in their mobilisation/immobilisation.

Particularly regarding groundwater, it is of primary importance to determine which factors will contribute to attenuation or acceleration of contaminant dispersion. Considering that the Meuse River is close to the site, river-aquifer interactions can play an important role on the dispersion of contaminants. At the same time, former studies performed in the Meuse alluvial plain have confirmed that aquifer heterogeneity in determined areas is important.

It is known that biodegradation can take place to reduce the toxicity of organic pollutants if contaminant degrading microorganisms are present and/or hydrogeochemical conditions of the system are favourable. Although biodegradation of organic pollutants at close conditions to the alluvial aquifer of Flémalle have already been proved elsewhere, these processes must be highlighted for the specific case of Flémalle.

It is thus clear that a good characterisation of aquifer heterogeneity, of hydrodynamic and hydrodispersive parameters and of river-aquifer interactions are of primary importance in the Flémalle site. Due to its high solubility and *a priori* elevated mobility, benzene will be on the focus of the attenuation/dispersion characterisation.

2.6. References to chapter 2

Alvarez, P. J. J. & Illman, W. A. (2006). Bioremediation and natural attenuation: process fundamentals and mathematical models. Environmental Science and Technology. John Wiley & Sons. Hoboken, New Jersey, USA. 609 pp.

Azhar, N. G. & Stuckey, D. C. (1994). The influence of chemical structure on the anaerobic catabolism of refractory compounds; a case study of instant coffee wastes. *Water Sci. Technol.* **30**(2): 223-232.

Brouyère, S. (2001). Etude et modélisation du transport et du piégeage des solutés en milieu souterrain variablement saturé (study and modelling of transport and retardation of solutes in variably saturated media). Ph.D thesis. Faculté des Sciences Appliquées. Laboratoire de géologie de l'ingénieur, d'Hydrogéologie et de Prospection géophysique, Université de Liège, Liège (Belgium). 640 pp.

CHST (1984). Cokerill archives. Centre d'Histoire des Sciences et des Techniques. Université de Liège, Belgium. 4 pp.

Dassargues, A. (1994). Paramétrisation et simulation des réservoirs souterrains. Discrétisation du domaine, préparation statistique des données, couplages et non linéarités des paramètres. Ph.D thesis. Faculté des Sciences Appliquées, Université de Liège, Belgium. 313 pp.

De Sousa, C. (2001). Contaminated sites: the Canadian situation in an international context. *J. Environ. Manage.* **62**(2001): 131-154.

DGRNE (2005). Analyse des pressions anthropiques sur les eaux souterraiens. Etat des lieux du District Hydrographique International de la Meuse. Ministère de la Region Wallonne, Direction générale des Ressources naturelles et de l'Environment, Observatoire des Eaux de Surface, Direction des Eaux de Surface, Direction des Eaux Souterraines. 47 pp.

Ertem, M. E. & Özdabak, A. (2005). Energy balance application for Erdemir Coke Plant with thermal camera measurements. *Applied Thermal Engineering* **25**: 423-433.

EU (2000). Directive 2000/60/CE of the European Parliament and of the Council of 23 October 2000 establishing a framework for Community action in the field of water policy. 172 pp.

Ferber, U. & Grimski, D. (2002). Brownfields and redevelopment of urban areas. *Austrian Federal Environment Agency, on behalf of CLARINET*. 132 pp.

Ferraris, J. (1778). Carte de cabinet des Pays-Bas autrichiens. Bruxelles: Pro-Civitate. 12 Cartes. Reimpression de 1778. Vol. 11. 1:25000.

Forth, R. A. & Beaumont, D. (1999). Contaminated groundwater around a former coal carbonisation site - a case history. *International journal of surface mining, reclamation and environment* **13**: 155-158.

Ghose, M. K. (2002). Complete physico-chemical treatment for coke plant effluents. *Water Res.* **36**: 1127-1134.

Haddouchi, B. (1987). Etude géologique et hydrogéologique de la plaine alluviale de la Meuse en Belgique. Ph.D thesis. Faculté des Sciences Appliquées, Université de Liège, Liège (Belgium). 307 pp.

Haerens, B. (2004). Reactive transport modelling of a groundwater contamination from a former coking plant. Ph.D thesis. Faculty of Science, Department of Geography and Geology, Section of Historical Geology, Hydrology and Engineering Geology, Katholieke Universiteit Leuven (KU Leuven), Leuven (Belgium). 243 pp.

Houbotte, A. (1847). Plan général de la partie du cours de la Meuse comprise entre les villages de Chokier et Herstal, destiné à préserver Liège des invasions des eaux et désastres, à améliorer la navigation. Bruxelles: J.B. Blasseau, 1847. 1 plan: n. & b.; 42 x 115 cm. 1:20000.

IGN (1893). Carte géologique nº 134 (planchettes 5-6 de la feuille XLII de la carte topographique), Seraing-Chênée. Institut Geógraphique National. 1:40000.

Jianlong, W., Xiangchum, Q., Libo, W., Yi, Q. & Hegermann, W. (2002). Bioaugmentation as a tool to enhance the removal of refractory compound in coke plant wastewater. *Process biochemistry* **38**: 777-781.

Li, Y. M., Gu, G. W., Zhao, J. F., Yu, H. Q., Qiu, Y. L. & Peng, Y. Z. (2003). Treatment of coke-plant wastewater by biofilm systems for removal of organic compounds and nitrogen. *Chemosphere* **52**: 997-1005.

Melcer, H., Nutt, S., Marvan, I. & Sutton, P. (1984). Combined treatment of coke plant wastewater and blast furnace blowdown water in a coupled biological fluidized system. *J. Water Pollut. Control Fed.* **56**(3): 192-198.

Moutier, M. & Halen, H. (2008). Lessons learned from six years of working with risk-based soil quality standards developed for contaminated land management in Wallonia, Belgium. *In* proceedings of the 10th International conference on soil-water systems ConSoil 2008. Milan, Italy. 319-326 pp.

Myers, R. (2001). Emission Factor Documentation for AP-42. Section 12.2. Coke production. U.S. Environmental Protection Agency. 313 pp.

Peters, V. (1996). Etude hydrogéologique du site de captage d'Amay. Essais de traçage et modélisation du transport de polluant pour la détermination des zones de protection. Faculté des Sciences Appliquées, Université de Liège, Liège. 108 pp.

Prokop, G., Schamann, M. & Edelgaard, I. (2000). Management of contaminated sites in Europe. European Environment Agency (EEA), Copenhagen (Denmark). 171 pp.

Rentier, C. (2002). Méthode stochastique de délimitation des zones de protection autour des captages d'eau. Ph.D thesis. Faculté des Science Appliquées. Departement GEOMAC, Université de Liège, Liège, Belgium. 212 pp.

SPAQuE (2007). Guide pratique d'utilisation des normes pour le sol et l'eau souterraine. Draft-Document de consultation. Société Publique d'Aide à la Qualité de l'Environnement (SPAQuE). 131 pp.

SPAQuE (2007). Site "Cokerie Flémalle" - Phase 2. Bilan historique des activités. *Lg3102-02*. SPAQuE, Département de l'amélioration de la connaissance de sites pollués, Liège, Belgium. 18 pp.

Stamoudis, V. C. & Luthy, R. G. (1980). Determination of biological removal of organic constituents in quench water from high-BTU coal gasification pilot plants. *Water Res.* **14**(8): 1143-1156.

Zhang, M., Tay, J. H., Qian, Y. & Gu, X. S. (1998). Coke plant wastewater treatment by fixed biofilm system for COD and NH_3-N removal. *Water Res.* **32**(2): 519-527.

All truths are easy to understand once they are discovered; the point is to discover them.

Galileo Galilei

Physicist, mathematician, astronomer and philosopher (1564-1642)

3. STATE OF THE ART

3.1. Groundwater – surface water interactions

3.1.1. Groundwater – surface water systems

Surface water bodies (SW), such as rivers, streams, lakes, reservoirs, estuaries and wetlands (Winter *et al.*, 1998), are commonly hydraulically connected to groundwater systems (GW), but their interaction is not always easy to observe and even less to quantify. Traditionally, GW-SW interactions have been ignored in water management and policy making. The increasing concern regarding water resources and environment quality and protection has turn on to consider groundwater and surface water as a single resource. Water supply, quality and degradation of aquatic environments are just a few examples where the study of GW-SW interactions is important.

The interaction between groundwater and a river can be described by three main ways: (1) A river drains water from the aquifer through the riverbed and/or riverbank (known as a gaining river) (Figure 3.1-left); (2) A river looses water to the aquifer through the riverbed and/or riverbank (known as a losing river) (Figure 3.1-right); and (3) A river drains in some reaches and looses in others. While gaining rivers are always connected to the aquifer, losing rivers can be connected or disconnected to the aquifer by an unsaturated zone.

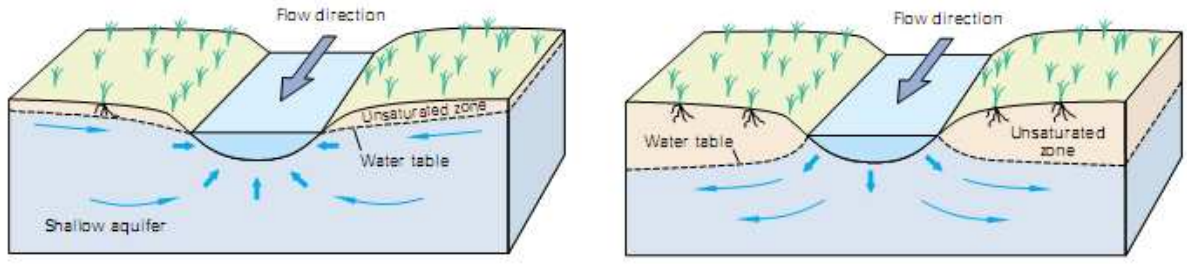

Figure 3.1. Schematic representation of a gaining (left) and a losing (right) river (Winter *et al.*, 1998).

The river can either fully or partially penetrate an unconfined aquifer. The river fully penetrates if its bed lies at or below the lower boundary of the aquifer. Conversely, the river partially penetrates the aquifer when its bed lies above the lower boundary. The flow system behaviour differs from one case to the other. When a river fully penetrates an unconfined aquifer, two cases can be considered: gaining or losing river, according to the groundwater level position with respect to the river water level (Osman and Bruen, 2002).

The spread of contaminants from the river into the aquifer, or from the aquifer into the river, is a problem intimately related to the hydraulics of the river-aquifer system. Fluctuations of groundwater levels in alluvial aquifers related to river water level variations have been noticed by Tabidian *et al.* (1992) and Govindaraju and Koelliker (1994).

Sophocleous (1991) noticed that large groundwater level rises cannot be completely related to rainfall infiltration processes but rather to a pressure-wave propagation through the aquifer as a result of river flooding. He also noticed that aquifers with low storativity and high transmissivity allow the pressure waves to travel rapidly and for long distances from the river. Workman *et al.* (1997) argued that the distance of the flood wave is mainly dependent on the transmissivity and porosity of the aquifer, on the change in the river stage and on the duration of the time rise.

Subsequently, a short overview of direct and indirect techniques used for quantifying groundwater – surface water interactions is presented. Afterwards, analytical and numerical approaches for the study of such environments are exposed. Some of these approaches will be used later in Chapter 5.

3.1.2. Quantification of groundwater – surface water interactions

Most of the studies encountered in the literature concerning the study of groundwater – surface water hydraulics are related to the interaction between alluvial aquifers and relatively small rivers (streams) considered with a mean water depth up to 1 m and a mean width between 3 and 5 m. In these studies, direct access to streambank and streambed sediments is possible, so that *in situ* placement of seepage meters is possible. However, when the river size does not allow direct measurements (as for the Meuse River), one must use indirect methods. The advantage of indirect methods is that they can be applied independently of river size.

A complete review of methods used to measure groundwater – surface water interactions is presented by Kalbus *et al.* (2006). From a practical point of view, three main groups of indirect methods can be listed:

1) methods based on Darcy's law and hydraulic gradient (e.g. Gilmore *et al.*, 1993; Girard *et al.*, 2003; Fritz and Arntzen, 2007; Ha *et al.*, 2007 among others);
2) river gauging at different cross sections over a determined time period (e.g. Cey *et al.*, 1998);
3) tracer studies in the river – aquifer transition zone (e.g. Bencala, 1990; Harvey *et al.*, 1996; Choi *et al.*, 1998; Lambs, 2004 among others), including heat as a tracer.

Fritz and Arntzen (2007) performed continuous monitoring of piezometers located in the hyporheic zone, observing that changes in river stages resulted in fluctuating uranium fluxes in the hyporheic zone. Furthermore, the influx of river water into the unconfined aquifer induced lower uranium concentrations in the aquifer as a result of dilution.

Ha *et al.* (2007) used monitored groundwater levels and river stages to estimate diffusivity (β) [L^2 T^{-1}] and riverbank resistance (α_{LK}) [L] values in a layered aquifer using a floodwave response (method explained in section 3.1.3.2).

A good characterisation of the hydraulic connection between the river and the aquifer requires knowledge of the geology along the river, riverbank conductance, as well as the parameters of the aquifer such as hydraulic transmissivity (T) [L^2 T^{-1}] and storage coefficient (S) [-] or their combined expression, the aquifer diffusivity (β):

$$\beta = \frac{T}{S} \tag{3.1}$$

Aquifer diffusivity is a key parameter in any assessment of the interaction between surface and groundwater, and Knudby and Carrera (2005) argued that hydraulic diffusivity is possibly the best indicator of their hydraulic connection.

Cey *et al*. (1998) combined both, direct and indirect techniques, using upstream and downstream streamflow measurements to account for the net exchanged water between the stream section and the connected aquifer (indirect technique). Mini-piezometers were also placed in the streambed to determine vertical hydraulic gradients beneath the stream (direct technique).

An extensive review of groundwater – surface water exchanges studies using temperature as a tracer is presented by Anderson (2005). Silliman and Booth (1993), Alexander and Cassie (2003), Conant (2004), Kalbus *et al.* (2006), and Keery *et al*. (2007), among others, mentioned heat transport as a robust and relatively unexpensive procedure to estimate exchange fluxes between surface water and aquifer systems and to identify gaining and losing stream reaches.

Although first studies using heat as a tracer in hydrogeology were carried out in the 1960s, a revival of the technique in the 1980s appeared. Nowadays considerable advances have been done related to the technique, often combined to other techniques. Alexander and Caissie (2003) combined the use of temperature as a heat tracer with the use of seepage meters. Conant (2004) combined streambed temperature mapping and geochemical analyses of

interstitial water of the streambed to delineate the pattern of groundwater discharge in a sandy streambed. Kalbus *et al*. (2007) combined streambed temperature and integral pumping tests (IPT method) in the streambank to delineate preferential pathways of groundwater discharge into a stream.

3.1.3. Modelling groundwater – surface water interactions

3.1.3.1. Mathematical description

The seepage rate (Q_{riv}) between an aquifer and an adjacent river is typically represented with a Fourier (or Cauchy or third-type) boundary condition:

$$Q_{riv} = \alpha_R \left(H - h \right) \tag{3.2}$$

where α_R is the river coefficient [L^2 T^{-1}]; H is the river stage elevation [L]; and h is the groundwater head [L].

Prickett and Lonnquist (1971) were the first to introduce the concept of river coefficient used in Equation (3.2) to represent river – aquifer interaction in regional groundwater models based on vertical flows through an aquitard. They suggested that the loss from a river is governed by the low permeability of riverbank deposits.

The approach used in MODFLOW (McDonald and Harbaugh, 1988) to represent river-aquifer interaction is similar to that of Prickett and Lonnquist (1971), and considers that head losses between a river and an aquifer are limited to those across the riverbed/riverbank itself. The river coefficient (river conductance in MODFLOW terminology) for a riverbank is written as follows (Figure 3.2):

$$\alpha_R = \frac{K_s L W}{d} \tag{3.3}$$

where K_s is the hydraulic conductivity of the riverbank material [L T^{-1}], W is the river channel height [L], L is the river reach length [L], and d is the width of the riverbank material [L].

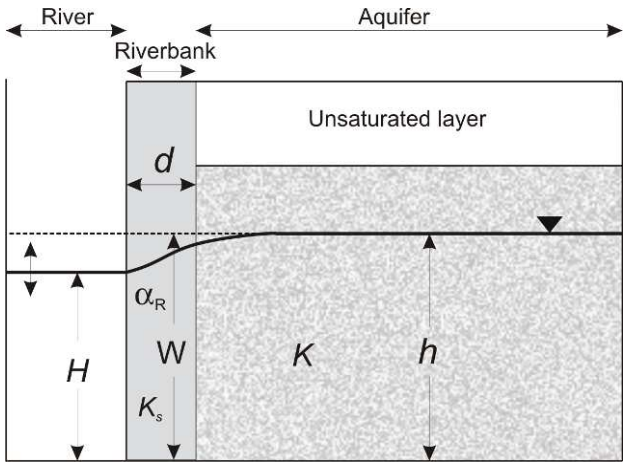

Figure 3.2. Schematisation of the MODFLOW river – aquifer interaction approach (*K* is the horizontal hydraulic conductivity of the aquifer [L T^{-1}]).

For conditions in which semipervious riverbank material is present, Barlow and Moench (1998) used a head-dependent flux boundary condition in their analytical solution (STWT1):

$$\frac{\partial h(x,t)}{\partial x} = -\frac{1}{\alpha_{LK}}\left[h_0 - h(x,t)\right] \tag{3.4}$$

where $\left[h_0 - h(x,t)\right]$ is the change in head across the semipervious riverbank material [L] and a_{LK} is the riverbank leakance (or riverbank resistance) [L], defined as (Figure 3.3):

$$\alpha_{LK} = \frac{Kd}{K_s} \tag{3.5}$$

where K is the aquifer hydraulic conductivity [L T^{-1}] and K_s is the hydraulic conductivity of the riverbank [L T^{-1}].

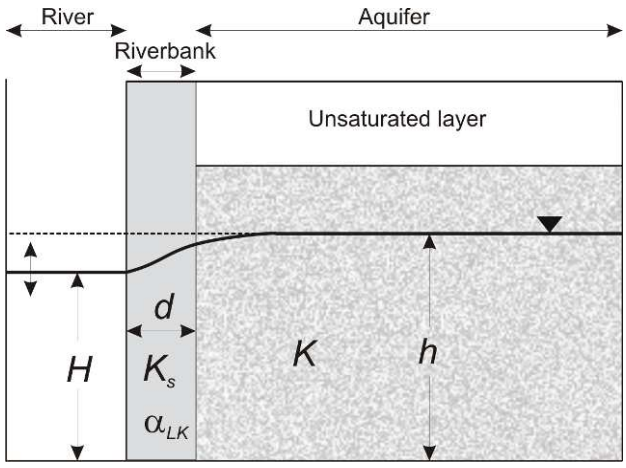

Figure 3.3. Schematisaton of the STWT1 river – aquifer interaction approach.

Hantush (1965) defined the riverbank leakance or riverbank resistance as the effective thickness of aquifer required to cause the same head loss as for the semipervious riverbank. Moench *et al.* (1974) showed that this parameter improve substantially the simulation of streamflow hydrographs.The riverbank leakance (or riverbank resistance) is a parameter that account not only for the increased resistance to flow at the riverbank caused by the semipervious riverbank material but also for the penetration of the river (Barlow *et al.*, 2000).
Both MODFLOW and STWT1 approaches will be used in Chapter 5.
Whatever all subtilities in these definitions, they all come more or less to the classical expression of a Fourier (Cauchy, third type) boundary condition as expressed in Equation (3.2).

3.1.3.2. Analytical modelling

There are three main approaches to analytically model aquifer - river interactions and estimate riverbank and aquifer hydraulic properties:

1) analytical solutions derived for confined aquifers and used for unconfined aquifers under several assumptions (methods based in the linear/non-linear Boussinesq equation);
2) floodwave approach;
3) step-response approach.

The transient groundwater flow equation is a non-linear partial differential equation, known as the non-linear ***Boussinesq equation***. Applied to unconfined aquifers, three main assumptions are considered: (1) specific yield can replace storativity; (2) changes in the

height of the groundwater table are small in comparison with the saturated thickness of the aquifer; and hence (3) saturated thickness of the aquifer can be assumed as remaining constant. Thus, the Boussinesq equation for a one dimensional semi-infinite unconfined aquifer can be written as follows:

$$\frac{\partial h}{\partial t} = \frac{K}{S_y}\frac{\partial}{\partial x}\left(h\frac{\partial h}{\partial x}\right) \tag{3.6}$$

where S_y is the specific yield coefficient [-] and t is the time [T].

The hydraulics of a river-stage system can be studied with the solution of the Boussinesq equation subject to a non-linear free-surface boundary condition, and time-dependent river boundary conditions. Solution to this equation is not easy because it is usually subject to a set of boundary conditions, among which the most difficult to handle is the free-surface boundary condition (Serrano, 1995). Although linearisation of the Boussinesq equation with the Dupuit assumption has been used (e.g. Govindaraju and Koelliker, 1994; Workman *et al.*, 1997; Manglik *et al.*, 2004; Pulido-Velázquez *et al.*, 2006, among others), Serrano and Workman (1998) noticed that the use of the linearised Boussinesq equation may not be an accurate approach because in cases of high fluctuations on river stage, transmissivity is strongly correlated to the hydraulic head. Using decomposition methods, approximated solutions of the non-linear Boussinesq equation are possible (Serrano and Workman, 1998; Srivastava *et al.*, 2006).

The ***floodwave approach*** consists in analysing the response of the aquifer to the river stage variation, calculating the aquifer diffusivity (Jha *et al.*, 2004). This method has been applied by Govindaraju and Koelliker (1994), Serrano and Workman (1998), Workman *et al.* (1997), Pulido-Velázquez *et al.* (2006), Srivastava *et al.* (2006), among others.

Although the floodwave response method is a priori designed for confined aquifers, it can also be used for unconfined aquifers if, instead of the main assumptions mentioned before for the use of the Boussinesq equation, one more assumption is met: the aquifer saturated thickness is considered a function of the height of the water table (Jha *et al.*, 2004; Ha *et al.*, 2007). However, the main drawback is that the aquifer diffusivity is a time-invariant parameter, which is not true for unconfined aquifers. The saturated thickness of an unconfined aquifer can change considerably during the passage of floodwave and, hence, the aquifer diffusivity. This was the main argument of Jha *et al.* (2004) to explain their relatively poor matching of recession limbs between observed and calculated well hydrographs. Other

authors that have used the floodwave approach are Singh *et al*. (2002) and Ha *et al*. (2007), among others.

The ***step-response approach*** focuses on unconfined aquifers where groundwater flow is considered as two-dimensional (perpendicular to the river in a vertical plane). This approach consists in the use of the method of convolution (or superposition), which leads to an effective simulation of the groundwater table due to river stage fluctuations. This effective simulation is due to the consideration of a 2D flow, which makes this technique closer to reality than precedents. This approach has been used by van de Giesen *et al.* (1994), Higgins (1980), Neuman (1981), and Moench and Barlow (2000), among others. This technique, being used in Chapter 5, is briefly presented here.

The approach is based on the governing partial differential equation of transient groundwater flow in a saturated, homogeneous, slightly compressible, and anisotropic aquifer. This equation, derived from Darcy's law and the law of mass conservation, is written in two dimensions as follows:

$$K_x \frac{\partial^2 h}{\partial x^2} + K_z \frac{\partial^2 h}{\partial z^2} = S \frac{\partial h}{\partial t} + q \tag{3.7}$$

where K_x and K_z are the horizontal and vertical hydraulic conductivity of the aquifer, respectively [L T^{-1}], S is the aquifer storage coefficient [-], q is a volumetric flow rate to or from the aquifer per unit volume of aquifer [T^{-1}], and x an z are horizontal and vertical coordinate directions, respectively [L].

Analytical solutions are derived for the condition of an instantaneous step change of the water level in the river relative to the water level in the adjacent aquifer. Such solutions are referred to as unit-step responses of the aquifer. Unit-step response solutions are dimensionless groundwater head functions that describe the ratio of the change of groundwater head in the aquifer at a given location (x, z) and at time t to an instantaneous step change of water level in the river:

$$H_D(x,z,t) = \frac{H_i - H(x,z,t)}{c} \tag{3.8}$$

where $H_D(x,z,t)$ is the dimensionless unit-step response solution [-]; c is the instantaneous step change in river water level ($H_i - H_0$) [L]; H_i is the initial water level of the river-aquifer

system [L], and H_0 is the river water level after the step change [L]. Solutions to the Equation (3.7) are derived in the Laplace space, and constitute the basis of the superposition (or convolution) methodology.

Euqation (3.7) takes into account both, step rise or fall in the river water level or in the aquifer. The unique difference between these two stresses is the direction of seepage at the river-aquifer boundary. A rise in river water level usually results in surface water recharge to the aquifer, and a rise in the groundwater level usually results in groundwater discharge (seepage) to the river.

Since boundary values are considered as linear, individual responses of hydraulic heads due to step changes in water level of the river are summed by use of a convolution integral, which relates a time series of step changes (system input stresses) to a time series of groundwater head changes (system output responses):

$$h(x,z,t) = H_i + \int_0^t F'(\tau) H_D(x,z,t-\tau)\, d\tau \tag{3.9}$$

where F'(τ) is the time rate of change of the system stress [L T^{-1}] (it can be either, change in river water level or groundwater level due to recharge or evapotranspiration) and τ is the time variable of integration (delay time) [T]. Because the use of the convolution integral assumes linearity in systems, changes in groundwater heads must be relatively small in comparison with the aquifer thickness (Barlow and Moench, 1998).

Seepage rates between the river and the aquifer are determined with the convolution method, from the head gradient at the river-aquifer boundary ($x = x_o$), according to Darcy's law:

$$Q_{riv}(t) = \frac{Kb}{x_0} \int_0^t F'(\tau) \frac{\partial H_D(x_0, z, t-\tau)}{\partial x_D}\, d\tau \tag{3.10}$$

where b is the saturated thickness of the aquifer [L], x_D is the dimensionless distance x/x_o [-]; and x_o is the distance from the middle of the river to the river-aquifer boundary [L]. It is assumed that seepage is negative when flow is from the river to the aquifer and positive when water is flowing from the aquifer to the river.

Complete implementation of the convolution method to the analytical solutions for time-varying inputs can be found in Barlow and Moench (1998). DeSimone and Barlow (1999),

Barlow *et al.* (2000) and Moench and Barlow (2000) applied these analytical solutions to hypothetical confined, unconfined and leaky aquifers with satisfactory results. This approach will be used in Chapter 5.

3.1.3.3. Numerical modelling

Numerical models have also been used to explore river – aquifer interactions. Sophocleous *et al*. (1995) studied stream depletion due to pumping in a nearby aquifer using a numerical model. Wroblicky *et al*. (1998) used MODFLOW (McDonald and Harbaugh, 1984) to simulate near-stream flow systems and estimate the planimetric areal dimensions of lateral hyporheic zones. Osman and Bruen (2002) suggested a technique to incorporate the mechanism of stream – aquifer seepage into MODFLOW (Harbaugh and McDonald, 1996a; 1996b) for partially penetrating streams.

Nemeth and Solo-Gabriele (2003) incorporated the reach transmissivity approach to a regional numerical model, in order to couple groundwater and surface water models by calculating seepage between them.

Peterson and Connely (2004) employed the Subsurface Transport Over Multiple Phases (STOMP) (White and Oostrom, 2000), to calculate flow direction and velocity in hourly increment using hydraulic head data from wells and an adjacent river.

Fleckenstein *et al.* (2006), in regard of the ecological importance of low flows in rivers, used numerical simulations to study the influence of the alluvial hydrofacies heterogeneity over river seepage and low flows.

3.2. Pollutant fate and transport into saturated subsurface media

3.2.1. Sources of groundwater contamination

Sources of contamination can be divided into two main groups according to their origin: point sources and diffuse contamination. Point sources are sources of pollution that can be traced back to a single location. Examples of point sources of groundwater contamination are: storage tanks, septic systems, hazardous waste sites, landfills, and brownfields. The Flémalle site falls into the last category.

Because the main problem in the Flémalle site is the dispersion/attenuation of organic pollutants, a brief overview on pollutant transport in porous aquifers is given hereafter, with special attention to benzene biodegradation processes and original techniques applied to the Flémalle site to quantify the biodegradation rate constant.

3.2.2. Pollutant transport in porous media

Migration of dissolved pollutants in groundwater is mainly controlled by *advection* and *hydrodynamic dispersion* (combined contaminant transport mechanisms of *mechanical dispersion* and *molecular diffusion*). At the same time, pollutants are often delayed and/or trapped, which results in a longer transit time through the porous media (retardation) and attenuation. The partial differential equation describing the transient fate and transport of solute contaminants in groundwater in 3D, can be written as follows:

$$\frac{\partial(\theta C)}{\partial t} + \rho_b \frac{\partial \overline{C}}{\partial t} = \frac{\partial}{\partial x_i}\left(\theta D_{ij} \frac{\partial C}{\partial x_j}\right) - \frac{\partial}{\partial x_i}(\theta v C) + q_s C_s - q_s^{'} C - \lambda_1 \theta C - \lambda_2 \rho_b \overline{C} \tag{3.11}$$

where θ is the porosity of the aquifer [-]; C is the dissolved concentration of contaminant species [M L^{-3}]; $\overline{C}$ is the concentration of contaminant species sorbed on the subsurface solids [M M^{-1}]; ρ_b is the bulk density of the subsurface medium [M L^{-3}]; $D_{i,j}$ is the hydrodynamic dispersion coefficient tensor [L^2 T^{-1}]; v is the effective water velocity [L T^{-1}]; q_s is the volumetric flow rate per unit volume of aquifer representing fluid sources and sinks [T^{-1}]; C_s is the concentration of the source or sink flux for the contaminant species [M L^{-3}]; $q_s^{'} = \partial\theta/\partial t$ is the rate of change in transient groundwater storage [T^{-1}]; λ_1 is the first-order reaction rate for the dissolved phase [T^{-1}]; and λ_2 is the first-order reaction rate for the sorbed (solid) phase [T^{-1}].

Equation (3.11) is essentially a mass balance statement, that is, the change in the mass storage at any given time is equal to the difference in the mass inflow and outflow due to dispersion, advection, sink/source, and chemical reaction.

The term $\partial(\theta v C)/\partial x_i$ in Equation (3.11) corresponds to the advection term, which describes the transport of miscible contaminants at the same velocity as groundwater. In aquifers (i.e. porous media with a high hydraulic conductivity), this term usually dominates over other terms. Assessment of this dominance degree can be provided by the Peclet number (P_e), defined as:

$$P_e = \frac{|v| l}{D} \tag{3.12}$$

where l is the characteristic length between one point to another, typically taken as the grid cell width [L], and D is the dispersion [L^2 T^{-1}].

Dispersion mechanism in porous media refers to the spreading of contaminants over a larger zone of the porous media than would be predicted solely from advection. Dispersion is the sum of two processes, *mechanical dispersion* and *molecular diffusion*. The first one is the result of deviations of actual velocities and flow paths within the Representative Elementary Volume (REV) from the average groundwater velocity, while the second corresponds to contaminant spreading caused by concentration gradients. In aquifers, molecular diffusion is often negligible in comparison with mechanical dispersion, therefore hydrodynamic dispersion is hence typically set equal to mechanical dispersion.

The dispersion tensor, D_{ij}, for an isotropic porous medium, is defined in the following component terms:

$$D_{xx} = \alpha_L \frac{\nu_x^2}{|\nu|} + \alpha_T \frac{\nu_y^2}{|\nu|} + \alpha_T \frac{\nu_y^2}{|\nu|} + D^* \tag{3.13}$$

$$D_{yy} = \alpha_L \frac{\nu_y^2}{|\nu|} + \alpha_T \frac{\nu_x^2}{|\nu|} + \alpha_T \frac{\nu_z^2}{|\nu|} + D^* \tag{3.14}$$

$$D_{zz} = \alpha_L \frac{\nu_z^2}{|\nu|} + \alpha_T \frac{\nu_x^2}{|\nu|} + \alpha_T \frac{\nu_y^2}{|\nu|} + D^* \tag{3.15}$$

$$D_{xy} = D_{yx} = (\alpha_L - \alpha_T) \frac{\nu_x \nu_y}{|\nu|} \tag{3.16}$$

$$D_{xz} = D_{zx} = (\alpha_L - \alpha_T) \frac{\nu_x \nu_z}{|\nu|} \tag{3.17}$$

$$D_{yz} = D_{zy} = (\alpha_L - \alpha_T) \frac{\nu_y \nu_z}{|\nu|} \tag{3.18}$$

where D_{xx}, D_{yy} and D_{zz} are the principal components of the dispersion tensor [L^2 T^{-1}]; D_{xy}, D_{xz}, D_{yx}, D_{yz}, D_{zx} and D_{zy} are the cross terms of the dispersion tensor [L^2 T^{-1}], α_L is the longitudinal dispersivity [L], α_T is the transverse dispersivity [L], D^* is the effective molecular diffusion coefficient [-], ν_x, ν_y, and ν_z are the components of the Darcy flux along the x, y and z axes [L T^{-1}], and $|\nu| = \sqrt{\nu_x^2 + \nu_y^2 + \nu_z^2}$ is the magnitude of the Darcy flux vector [L T^{-1}].

Both, advection and dispersion are affected by physical properties such as the pore size, tortuosity and friction in pore throat in the aquifer medium (Figure 3.4).

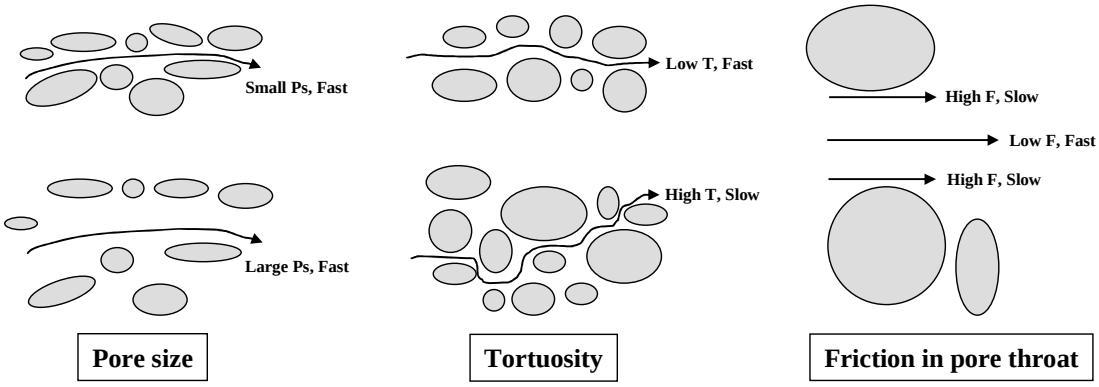

Figure 3.4. Physical processes causing dispersion at microscopic scale (Wiedemeier *et al.*, 1998).

Retardation effects can be divided into two major categories (Brouyère *et al.*, 2000):

1. chemical retardation, including all chemical reactions that occurs between the solute and the porous media (sorption – desorption, cation exchange);
2. physical retardation or dual-porosity effect.

Sorption refers to the mass transfer process between the contaminants dissolved in groundwater (aqueous phase) and the contaminants sorbed on the porous medium (solid phase). It is often assumed that equilibrium conditions exist between the aqueous-phase and the solid-phase concentrations and that the sorption reaction is fast enough, relative to groundwater velocity, to be treated numerically as instantaneous. In this case, different types of equilibrium-controlled sorption isotherms are proposed in the literature (linear, Freundlich, and Langmuir). The simplest relation expresses a linear sorption isotherm, which considers that the sorbed concentration is directly proportional to the solute concentration:

$$\overline{C} = K_d C \tag{3.19}$$

where K_d is the distribution coefficient [L^3 M^{-1}]. In this case, the retardation factor (R_{fc}) is given by:

$$R_{fc} = 1 + \frac{\rho_b}{\theta}\frac{\partial \overline{C}}{\partial C} = 1 + \frac{\rho_b}{\theta} K_d \tag{3.20}$$

Physical retardation processes affect all the solutes transported into the porous media. In fact, physical retardation mainly depends on the heterogeneity degree of the aquifer, which is randomly distributed (Herr *et al.*, 1989), while chemical retardation processes are specific for each solute.

The dual-porosity concept, introduced by Coats and Smith (1964), considers two domains of porosity, mobile porosity and immobile (or much less mobile) porosity. In the case of a gravel aquifer, immobile water is assumed to represent the less pervious silty to clay lenses and layers present in the alluvial deposits, while the mobile water is associated with the most pervious (sand to gravel) horizons (Käss, 1998; Brouyère, 2001). Advection and dispersion are assumed to take place only in the mobile zone, while adsorption-desorption and degradation can take place in either zone, although not necessarily at the same rate. Diffusion of solutes between both mobile and immobile water connects the two domains (Jaynes *et al.*, 1995).

The transport equation in a one-dimensional unsaturated flow of a conservative non-sorbing solute in a soil containing mobile and immobile water can be written as follows:

$$\theta_m \frac{\partial C_m}{\partial t} + \theta_{im} \frac{\partial C_{im}}{\partial t} = \theta_m D \frac{\partial^2 C_m}{\partial x^2} - v_D \frac{\partial C_m}{\partial x} \tag{3.21}$$

where θ_m is the effective (mobile) porosity [-], θ_{im} is the immobile porosity [-] (both related as $\theta = \theta_m + \theta_{im}$, the total porosity), C_m and C_{im} are the solute concentration in the mobile and immobile domains [M L^{-3}], t is time and D is the dispersion [L^2 T^{-1}], only active in the mobile domain, and v_D is the Darcy flux [L T^{-1}]. Exchange between mobile and immobile porosity can be expressed as:

$$\theta_{im} \frac{\partial C_{im}}{\partial t} = \alpha \left(C_m - C_{im} \right) \tag{3.22}$$

where α is the first-order transfer coefficient between mobile and immobile water [T^{-1}]. If the solute is non-conservative, a linear decay constant (λ [T^{-1}]) can be added in the right hand of the equation, obtaining:

$$\theta_{im}\frac{\partial C_{im}}{\partial t} = -\lambda\theta_{im}C_{im} + \alpha\left(C_m - C_{im}\right) \tag{3.23}$$

If sorption is considered for solute transport in a dual-domain system, Equation (3.21) is written as follows:

$$\theta_m\frac{\partial C_m}{\partial t} + f\rho_b\frac{\partial \overline{C}_m}{\partial t} + \theta_{im}\frac{\partial C_{im}}{\partial t} + (1-f)\rho_b\frac{\partial \overline{C}_{im}}{\partial t} = \theta_m D\frac{\partial^2 C_m}{\partial x^2} - v_D\frac{\partial C_m}{\partial x} \tag{3.24}$$

where f is the fraction of sorption in contact with the mobile phase ($p = 1 - f$, where p is the fraction of sorption in contact with the immobile phase). It is usually accepted that f is equal to θ_m/θ (Zheng and Wang, 1999).

Dual-porosity has been largely studied in unsaturated subsurface system to simulate preferential movement of water and solutes (Gerke and van Genuchten, 1993a; Zurmühl and Durner, 1996) and to evaluate the transfer term, α, between one domain to another (Gerke and van Genuchten, 1993b), among others.

The use of a dual-porosity concept in the saturated subsurface has been traditionally used in models developed for fractured aquifers (Bottrell *et al.*, 2000; Cornaton and Perrochet, 2002; Pili *et al.*, 2004; Brouyère, 2005; Samardzioska and Popov, 2005; Brouyère, 2006). In unfractured porous media, such as sandy and gravel aquifers with randomly distributed heterogeneity, this approach is much less frequently used. Herr *et al.* (1989) used the dual-porosity approach in mass transport studies carried out in laboratory, while Brouyère (2001) used the concept of dual-porosity to calibrate a solute transport model to measured breakthrough curves (BTCs) from radially converging tracer tests carried out in a gravel aquifer. Kim and Corapcioglu (2002) used the dual-porosity model to explain the pollutant transfer in a riverbank filtration.

3.2.3. Natural attenuation

The concept of "natural attenuation" covers all natural physical, chemical and biological processes that help to reduce the mass of dissolved contaminants in a groundwater plume, such as dispersion, sorption, volatilisation, biological and chemical degradation (Nyer and Duffin, 1997; Wiedemeier *et al.*, 1999; Kao and Wang, 2000; Zamfirescu and Grathwohl, 2001). In practice, natural attenuation processes are also referred by several other terms, such

as intrinsic remediation, intrinsic bioremediation, natural restoration, or passive bioremediation. Natural attenuation processes, such as biodegradation, can often be dominant factors in the fate and transport of contaminants (Wiedemeier *et al.*, 1998).

Natural attenuation offers large benefits to owners and managers of contaminated sites, but often raises strong objections from those who live and work near a site where long-term risks are concerned. Natural attenuation is sometimes viewed with scepticism by activists and environmentalists, assimilating natural attenuation as a "do nothing" strategy that allows site owners and regulators to "walk away" from a site, transferring all the risk to those who live and work nearby.

Main advantages associated to natural attenuation processes for cleanup of contaminated sites are:

- in situ destruction of contaminants and smaller volume of remediation wastes;
- potential of application to all contaminated site, or part of it, in function of the site conditions and remediation objectives;
- possibility to be used with, or as follow-up to, other remedial measures;
- lower remediation costs compared to active remediation techniques.

Obviously, some disadvantages are also associated to natural attenuation processes for cleanup contaminated sites:

- toxicity and/or mobility of transformation products may exceed that of the parent compounds;
- longer time frame is required to achieve remediation objectives, compared to active remediation measures;
- favourable conditions for natural attenuation may change over time, resulting in possible adverse impact for remedial effectiveness;
- requirement of extensive monitoring for a long period.

Whereas microorganisms in soil and aquifer are able to eliminate or minimise the risk of organic pollutants, this is not the case for inorganic pollutants. However, under certain conditions (e.g., through sorption or oxidation-reduction (= redox) reactions), effective reduction of dissolved and/or toxic forms of inorganic contaminants in groundwater can be achieved (USEPA, 1997). Both, metals and non-metals may be attenuated by sorption reactions such as precipitation, adsorption on the surfaces of soil minerals, absorption into the

matrix of soil mineral, or partitioning into organic matter. Redox reactions can transform the valence states of some inorganic contaminants to less soluble and thus less mobile forms or less toxic forms (e.g. hexavalent chromium to trivalent chromium).

3.2.3.1. Biodegradation

Biodegradation is often the most important attenuation mechanism for dissolved organic contaminants in groundwater. Biodegradation can be defined as biotransformation of an organic compound's structure by breaking molecular bonds. It occurs only when conditions in a polluted medium are conductive to the growth of specific degraders and the functioning of their enzymes (Alvarez and Illman, 2006).

Mineralisation is a form of biodegradation that results in conversion of an organic molecule into its inorganic constituents (e.g. CO_2, CH_4, H_2O, SO_4^{2-}, and PO_4^{3-}) or mineral salts. The responsible organisms typically benefit from mineralisation reactions, i.e. they gain energy, which might serve for microbial growth (it is to note that under anoxic environment, bacteria often cannot gain enough energy from contaminant degradation to "grow", just to "survive"). Aromatic and aliphatic hydrocarbons and chlorinated solvents are examples of common pollutants that can be mineralised. Biodegradation can lead to a *detoxification*, where products resulted from the original compounds are less problematic. This is the example of the oxidation of alkanes in contaminated sites with petroleum products, where alkane is transformed into a primary alcohol. Nevertheless, there are some noteworthy exceptions where a pollutant is transformed to a product of greater toxicity, like the reductive dechlorination of the solvent tetrachloroethylene (TCE) to the end-product vynil chloride (VC) under anoxic conditions.

3.2.3.2. BTEX biodegradation

Benzene, with a high solubility of 1.78 g l^{-1} (Alvarez and Illman, 2006), is the most soluble petroleum hydrocarbon. Since TEX compounds all degrade naturally in groundwater systems, the scientific community is divided regarding oxic and/or anoxic conditions to degrade benzene.

BTEX degradation occurs in both, aerobic and anaerobic media, although it is generally accepted that the process occurs more rapidly under oxic conditions. Aerobic biodegradation of BTEX compounds have been demonstrated by numerous authors (e.g. Swindoll *et al.*, 1988; Ridgway *et al.*, 1990; Pruden *et al.*, 2003; Reinhard *et al.*, 2005, among others). However, Lu *et al.* (1999) stated that in laboratory experiments, anaerobic degradation was

responsible of 70% of total BTEX degradation. Indeed, laboratory and field tests typically produce relatively different results. The attenuation rates estimated by laboratory techniques can be one or two orders of magnitude greater than the field rates (Hunt *et al.*, 1997).

During the cellular respiration of bacteria, a chain of oxidation – reduction couples takes places, whereby energy is extracted via stepwise oxidation (removal of electron) of the substrate molecules. Terminal electron acceptors (EAs) are the compounds that provide a "sink" for the electrons expelled at the end of the chain of reactions. In oxic conditions dissolved oxygen (O_2) is the EA, while in absence of oxygen (anoxic conditions), a number of less oxidised compounds may be used. The typical chain of TEAs include, NO_3^-, Fe(III), SO_4^{2-} and CO_2, in the mentioned order. Benzene biodegradation has been reported with all these electron acceptors (Lovley, 2000).

Benzene degradation under denitrifying and Fe(III)-reducing conditions was observed by Nales *et al.* (1998) and Durant *et al.* (1999). Lovley *et al.* (1995), Phelps *et al.* (1996) and Reinhard *et al.* (1997), among others, demonstrated that sulphate-reducing conditions were also suitable to degrade benzene. Methanogenic conditions were also demonstred as favourable for benzene degradation (Kazumi *et al.*, 1997; Heider *et al.*, 1999). When no other electron acceptors remain than CO_2, it is suggested that benzene might be degraded to CO_2 and methane (Grbic-Galic and Vogel, 1987; Kazumi *et al.*, 1997; Weiner and Lovley, 1998).

Aquifer geochemical footprints can be indicative of natural attenuation of BTEX compounds. These footprints are (some of them, observed in the Flémalle site, will be presented in Chapter 5):

- decrease of electron acceptors (mainly O_2, NO_3^-, Fe (III), and SO_4^{2-}). In particular, one should look for O_2, NO_3^-, and SO_4^{2-} levels below background in the core of the plume;
- generation of the products of acceptor reductions (such as Fe(II) and CH_4). Fe(II) and CH_4 should be highest in the core of the plume;
- presence of organic acids that are known intermediate products of petroleum hydrocarbon degradation;
- an increased concentration of dissolved inorganic carbon (CO_2) and a characteristic change in the alkalinity;
- decrease of BTEX concentrations over time and distance.

Under natural conditions, aquifers are poor in organic carbon and therefore mostly oxic. When organic contaminants are present, they become the major carbon source, resulting in reducing conditions. Therefore, reducing conditions of an aquifer can be also viewed as an indication of biodegradation. Kao and Wang (2001) found a decline in Eh in plume area (-211 mV) compared to those of the background area (329 mV), reflecting the change from oxidising to reducing conditions, suggesting BTEX biodegradation processes.

Aquifer heterogeneity has also been considered in some studies of BTEX biodegradation (e.g. MacQuarrie *et al.*, 1989; Lu *et al.*, 1999; Lee *et al.*, 2001; Uçankus and Ünlü, 2008, among others).

3.2.3.3. On the new trends of indicators of organic compounds biodegradation

Physical transport processes such as advection, dispersion, or sorption, do not leave chemical signatures that can be analysed. On the contrary, biodegradation often causes a substancial kinetic isotope effect. Several biochemical reactions result in carbon isotope fractionation and molecules containing the lighter ^{12}C-isotope are used preferentially. The consequence of this is that $^{13}C/^{12}C$ isotope ratio of the substrate's residual fraction is enriched in ^{13}C. This is the basis of stable isotope analysis to prove biodegradation. The isotopic fractionation technique was proposed as a candidate technique for the assessment of intrinsic bioremediation of petroleum hydrocarbon in contaminated sites (e.g. Ahad *et al.*, 2000; Spence *et al.*, 2001; Ward *et al.*, 2001, among others). This technique was applied in the Flémalle site by CHYN, an AquaTerra partner, and their results are used in this work. In consequence, a short overview of this technique is presented.

Carbon isotope ratios are given in delta notation as $\delta^{13}C$ [‰] from an international standard, the VPDB standard (Vienna Pee Dee Belemnite, a limestone fossil of *Belemnitella americana* from the geologic formation Pee Dee in South Carolina):

$$\delta^{13}C = \left(\frac{{}^{13}C/{}^{12}C_s}{{}^{13}C/{}^{12}C_{std}} - 1 \right) \times 1000 = \left(R_s / R_{std} - 1 \right) \times 1000 \qquad (3.25)$$

where R_s is the ratio of the heavy isotope to the light isotope ($^{13}C/^{12}C$) of the sample, and R_{std} is the corresponding ratio of the standard. A negative δ indicates that the sample under study is depleted in the less common isotope with respect to the standard. A positive δ indicates a sample in which the less common isotope is in greater abundance compared to the isotopic standard, so an enrichment in ^{13}C.

Changes in isotope signatures over time as absolute differences in $\Delta\delta^{13}C$ are given by Equation (3.26):

$$\Delta\delta^{13}C = \varepsilon \times \ln \kappa \tag{3.26}$$

where ε is the enrichment factor [-] and κ is the fraction of the substrate remaining in the sample [-] at time t [T]. Changes in isotope ratios can also be regarded over distance. The approximation usually done consists in approximate t via distance, x [L], and groundwater effective velocity, v [L T^{-1}] (de Weert *et al.*, 2007; Morasch *et al.*, 2007b):

$$t = \Delta x / v \tag{3.27}$$

This technique is fully presented and applied by Richnow *et al*. (2003), Meckenstock *et al.* (2004), Mckelvie *et al.* (2005) and Fischer *et al.* (2007), among others, obtaining clear indications of *in situ* biodegradation.

The biodegradation rate coefficient, λ_B [T^{-1}], describes the rate at which a contaminant is being degraded. This degradation rate is usually approximated by a first-order decay regime with respect to the contaminant concentration, C [M L^{-1}]:

$$\lambda_B = -\frac{v}{\Delta x} \ln\left(\frac{C_{(x)}}{C_0}\right) \tag{3.28}$$

Recently, in the scope of the AquaTerra project, Morasch *et al.* (2007a) applied this technique in the Flémalle site to investigate the intrinsic biodegradation potential under in situ-like conditions, obtaining a mean degradation rate equal to 0.017/d, assuming a mean groundwater flow velocity of 1.04×10^{-5} m s^{-1}.

Furthermore, Morasch et al. (2007a) used a new method based on the addition of ^{13}C-labeled contaminants in microcosms and the subsequent analysis of ^{13}C-CO_2 generated during biodegradation was used in laboratory. To calculate benzene degradation rates, Morasch *et al.* (2007a) used the general first-order approximation of Equation (3.28) with the simplified Rayleigh equation (Equation (3.26)) (Rayleigh, 1896):

$$\lambda_B = -\frac{\Delta\delta^{13}C}{\varepsilon \times t} \tag{3.29}$$

Morasch *et al.* (2007a) concluded that benzene, naphthalene and acenaphthene degradation in the alluvial sediments of the Flémalle site was evident in both aerobic and anaerobic microcosms amended with ^{13}C-labeled substrates. They obtained a relatively good agreement between degradation rate constants for anaerobic benzene degradation in microcosm experiments and by the field approach, suggesting that stable isotope-based methods might be useful and appropriate for the quantification of *in situ* contaminant degradation. The average first-order biodegradation rates were 0.12/d and 0.06/d for microcosms with aquifer material from Flémalle under oxic and anoxic conditions, respectively.

3.2.3.4. Effect of groundwater table fluctuations on organic pollutant biodegradation

Water table elevation and capillary fringe in unconfined aquifers are likely to change over time for different reasons (rainfall, changes in surface water elevation adjacent to the aquifer…). Water table fluctuations affect the spatial distribution of dissolved pollutants within an aquifer, particularly in the vertical direction (Dobson *et al.*, 2007). As water table drops, dissolved pollutants migrate downwards leaving behind a residual fraction in the unsaturated zone. A subsequent rise leads to the reverse process. But it also leads to entrapment of pollutants and air below the water table (Lenhard, 1992; Lenhard *et al.*, 1993). This air provides an additional source of oxygen for biodegradation processes (Fry *et al.*, 1997).

Besides performing laboratory experiments to study the effects of trapped gas on the hydraulic conductivity of the porous medium, Fry *et al.* (1997) presents a complete review of soil science literature on trapped gas due to water table fluctuations, mainly performed in laboratory.

Sinke *et al.* (1998) performed column experiments to evaluate the effect of a changing redox environment introduced by a fluctuating water table on the transport and transformation of representative volatile pollutants, toluene and 4-nitrobenzoate. Williams and Oostrom (2000) used the STOMP model to simulate observed water table fluctuations and dissolved oxygen (DO) concentrations. Dobson *et al.* (2007) performed laboratory tests to examine the effect of water table fluctuation over LNAPL distribution, dissolution and biodegradation compared to a non-fluctuating reference system.

3.3. Inverse modelling in hydrogeology

3.3.1. The objective function

The parameter estimation problem deals with the concept of identifying the "best" set of model parameters. The comparison of simulated and observed values is accomplished quantitatively using an *objective function*. Parameter values that produce the best fit between both simulated and observed values are defined as those that produce the smallest value of the objective function.

Using hydraulic heads and flows data as observations, the weighted least-squares objective function, *Φ(u)*, can be expressed as (Hill and Tiedeman, 2007):

$$\Phi(u) = \sum_{i=1}^{NH} \omega_{h_i} \left[h_i^{obs} - h_i^{sim}(u) \right]^2 + \sum_{j=1}^{NQ} \omega_{q_j} \left[q_j^{obs} - q_j^{sim}(u) \right]^2 \tag{3.30}$$

where *u* is a vector containing values of each of the parameters being estimated; *NH* is the number of hydraulic-head observations; *NQ* is the number of flow observations; h_i^{obs} is the *i*th observed hydraulic head being matched by the regression; $h_i^{sim}(u)$ is the simulated hydraulic head that corresponds to the *i*th observed hydraulic head; q_j^{obs} is the *j*th observed flow being matched by the regression; $q_j^{sim}(u)$ is the simulated flow that corresponds to the *j*th observed flow; ω_{h_i} is the weight for the *i*th head observation; and ω_{q_j} is the weight for the *j*th flow observation.

For *NH* and *NQ*, multiple observations at the same location are each included. Using ξ to indicate a generic contribution of any kind and *ω* to indicate its weight, the objective function is more commonly expressed as:

$$\Phi(u) = \sum_{i=1}^{ND} \omega_i \left[\xi_i^{obs} - \xi_i^{sim}(u) \right]^2 = \sum_{i=1}^{ND} \omega_i e_i^2 \tag{3.31}$$

where *ND* is the number of observations; ξ_i^{obs} is the *i*th observation value being matched by the regression; $\xi_i^{sim}(u)$ is the simulated equivalent, defined as the simulated value that

corresponds to ξ_i^{obs} ; ω_i is the weight for the *i*th contribution to the objective function; e_i is the *i*th weighted residual, equal to $\left[\xi_i^{obs} - \xi_i^{sim}(u)\right]$.

3.3.2. Calibration in groundwater modelling

The most important step during groundwater modelling tasks is the calibration, because reliability of the model results and predictions will depend of its quality. In the next sections, emphasis is given on the calibration processes and techniques used to calibrate a model.

While observations are generally limited in number, model inputs that need to be estimated are often distributed spatially and/or temporally, so that the number of parameter values could be infinite. This is a great discrepancy, and one of the major challenges. *Parameterisation*, or spatial parameter definition, allows a limited number of parameter values to define model inputs throughout the spatial domain and time of interest. Parameterisation is thus the process of defining hydraulic properties with a limited number of model parameters (unknowns to be found during the inversion process), obtaining faithful matches between observed and computed data (Carrera *et al.* 2005).

Determination of reliable parameters can frequently be an ill-posed problem (Zechner and Frielingsdorf, 2004). Ill-posedness is influenced by *non-uniqueness* and *instability* of the solution (Yeh, 1986; Carrera and Neuman, 1986b; McLaughlin and Townley, 1996). *Instability* mainly implies large values for some model parameters due to unbounded fluctuations, which causes also large “jumps” in the value of the hydraulic properties over short distances (Alcolea *et al.*, 2006). In other words, instability refers to large fluctuations of parameter values during the calibration caused by small measurement errors. Different combinations of parameters values leading to similar simulation results, is known as *non-uniqueness*.

Different possibilities to overcome ill-posed problems are available. A suggested approach, is to incorporate regulating prior statistics based on field measurements (Carrera and Neuman, 1986b). An approach that has gained adepts these last years consists in constraining the model calibration process including other field measurements in addition to groundwater heads. Fluxes at aquifer boundaries (Poeter and Hill, 1997; Beckers and Frind, 2001) and groundwater solute concentration (Strecker and Chu, 1986; Keidser and Rosbjerg, 1991; Medina and Carrera, 1996) have been demonstrated to reduce parameter correlation to identify model parameters.

Calibration can be accomplished manually or automatically. Although reliable results can be obtained by manual "trial and error", it can be a tedious procedure, and is often criticised for its subjectivity in delineating zones of homogeneous hydraulic conductivity (*K*). On the contrary, automatic calibration is accomplished by formal methods that attempt to estimate parameter values given a mathematical model of system processes and a set of relevant observations. These methods are called *inverse methods*, which derivate to the worldwide accepted "inverse model problem" to design the automated calibration process.

Two contrasted automatic techniques of parameterisation are presented here, both used subsequently in Chapter 5. One is maybe the more systematically used from the beginning of groundwater modelling (*zonation*), while the other one, *pilot points*, rely on a geostatictical basis which makes it an original and functional technique.

3.3.2.1. Zonation

Although this is the typical idea that one has about "trial and error" method as referred above, it is a technique that can be also used in an automatic way. The model is divided into subareas on the basis of geological features or other evidences, and then using parameter estimation software, hydraulic conductivity values are assigned to these zones. The main advantage of this technique is its flexibility to accommodate geological information. However, the procedure is quite unsatisfying, and it becomes usually clear, as the calibration process progresses, that areas assigned with the same geology do not necessarily possess uniform hydraulic properties. Based on that, the modeller is inevitably tempted to introduce more zones into the model domain, estimating thus more parameters to obtain a good fit between model outcomes and field measurements (Doherty, 2003). As more and more zones are added to the model to accommodate heterogeneity, the calibration process becomes more time-consuming and a tedious task with less reliability on the results.

3.3.2.2. Pilot points

Originally devised by de Marsily *et al.* (1984), pilot points has become a method of parameter determination or parameterisation very popular in inverse modelling (LaVenue *et al.*, 1995; RamaRao *et al.*, 1995; Vesselinov *et al.*, 2001; Doherty, 2003; Hernández *et al.*, 2003; Alcolea *et al.*, 2006), becoming the standard for non-linear geostatistical inversion.

The basis of this methodology is to characterise the hydraulic property distribution by assigning values to a set of points distributed throughout the model domain. The values at the pilot points are the hydraulic properties unknown of the model, and the assignment of

parameters to pilot points is done so as to minimise discrepancies between model outputs and field measurements (small objective function). These parameters are subsequently interpolated to the model grid, resulting in a smoothed variation of the hydraulic property over the model.

Parameterisation methods typically express aquifer properties as linear combinations of the unknown model parameters to be estimated. Using pilot points, parameterisation is done following the next equation (Carrera *et al.*, 2005):

$$K(x) = \sum_{i=1}^{\dim(g_0)} \eta_i^{g_0}(x)\, g_{0i} + \sum_{j=1}^{N} \eta_j^{PP}(x)\, g_j \tag{3.32}$$

where K is the hydraulic property; g are the unknown values of the hydraulic property K; g_o are the initial values (if known) of the hydraulic property K; N is the number of unknown values of the hydraulic property K; and $\eta_i^{g_0}$ and η_i^{PP} are the interpolation weights for the initial values (if known) and pilot points, respectively.

Although there is no universal methodology about the required and optimal number and location of the pilot points (M.C. Hill, personal communication during *UCODE_2005 and PEST: universal inversion code for automated calibration*, 13-15 September'07, Copenhagen), Doherty (2003) noticed that pilot points should be placed literally throughout the model domain, with increased spatial density in areas of suspected heterogeneity, and where measurement density is higher. The more pilot points are used in the parameterisation process, the more likely they will be suitably located to describe heterogeneity that may exist within the model domain. Moreover, a large number of pilot points implies that the interpolation process has a low influence in parameter averaging around the model area, and the less matter do the location of the pilot points. This was the justification of Moore and Doherty (2006), who considered that a number of 104 pilot points was enough to ensure that the conclusions drawn of their research was minimally affected by pilot point induced parameter averaging.

However, *numerical instability* can occur when trying to estimate too many parameters. This fact was reported as an important drawback by Cooley (2000) and Cooley and Hill (2000), what they called *overparameterisation*. This drawback leads also to *instability*. This constraint can be eliminated through a *regularisation process*. RamaRao *et al.* (1995) and Gómez-Hernández *et al.* (1997) used upper and lower bounds on the model parameters to

avoid the unbounded fluctuations. It seems however that this approach causes the solution to fluctuate between those arbitrary bounds.

Because instability is due to overparameterisation of the model, a second tactic to avoid instability consists in reducing the number of parameters. In this way, several solutions are proposed. In a first instance, RamaRao *et al.* (1995) propose to start calibration with a single point and add pilot points at the end of each iteration. As mentioned before, placement of the pilot points is subjective and user dependant. Lavenue and Pickens (1992) propose to locate new pilot points accordingly to their ability in reducing the value of the objective function. This is measured by sensitivity coefficients. However, this leads out to other problems: (1) the accuracy to identify heterogeneity is decreased; (2) it is critical to use a good geostatistical characterisation (which is often not possible due to the poor number of data available); and (3) sensitivity of the problem to the location of pilot points arises again. Certes and de Marsily (1991) propose to use knowledge of the aquifer geology and of risk zones as well as location of the piezometers used for the fitting of the model.

Several authors have applied the pilot points approach in their numerical modelling works in the last two decades (e.g. Certes and de Marsily, 1991; LaVenue *et al.*, 1995; RamaRao *et al.*, 1995; Vesselinov *et al.*, 2001; Doherty, 2003; Hernández *et al.*, 2003; Kowalsky *et al.*, 2004; Wood *et al.*, 2005; Wylie and Doherty, 2005; Moore and Doherty, 2006, among others).

3.4. References to chapter 3

Ahad, J. M. E., Sherwood Lollar, B., Edwards, E. A., Slater, G. F. & Sleep, B. E. (2000). Carbon isotope fractionation during anaerobic biodegradation of toluene: implications for intrinsic bioremediation. *Environ. Sci. Technol.* **34**: 892-896.

Alcolea, A., Carrera, J. & Medina, A. (2006). Pilot points method incorporating prior information for solving the groundwater flow inverse problem. *Adv. Water Resour.* **29**: 1678-1689.

Alexander, M. D. & Caissie, D. (2003). Variability and comparison of hyporheic water temperatures and seepage fluxes in a small Atlantic salmon stream. *Ground Water* **41**(1): 72-82.

Alvarez, P. J. J. & Illman, W. A. (2006). Bioremediation and natural attenuation: process fundamentals and mathematical models. Environmental Science and Technology. John Wiley & Sons. Hoboken, New Jersey, USA. 609 pp.

Anderson, M. (2005). Heat as a ground water tracer. *Ground Water* **43**(6): 951-968.

Barlow, P. M., DeSimone, L. A. & Moench, A. F. (2000). Aquifer response to stream-stage and recharge variations. II. Convolution method and applications. *J. Hydrol.* **230**: 211-229.

Barlow, P. M. & Moench, A. F. (1998). Analytical solutions and computer programs for hydraulic interactions of stream-aquifer systems. *US Geol. Survey Open File Report 98-415A*. USGS, Marlborough, Massachusetts, USA. 99 pp.

Beckers, J. & Frind, E. O. (2001). Simulating groundwater flow and runoff for the Oro Moraine aquifer system. Part II. Automated calibration and mass balance calculations. *J. Hydrol.* **243**: 73-90.

Bencala, K. E. (1990). Characterization of transport in an acidic and metal-rich mountain stream based on a lithium tracer injection and simulations of transient storage. *Water Resour. Res.* **26**(5): 989-1000.

Bottrell, S. H., Moncaster, S. J., Tellam, J., H., Lloyd, J. W., Fisher, Q. J. & Newton, R. J. (2000). Controls on bacterial sulphate reduction in a dual porosity aquifer system: the Lincolnshire Limestone aquifer, England. *Chemical Geology* **169**: 461 - 470.

Brouyère, S. (2001). Etude et modélisation du transport et du piégeage des solutés en milieu souterrain variablement saturé (study and modelling of transport and retardation of solutes in variably saturated media). Ph.D thesis. Faculté des Sciences Appliquées. Laboratoire de géologie de l'ingénieur, d'Hydrogéologie et de Prospection géophysique, Université de Liège, Liège (Belgium). 640 pp.

Brouyère, S. (2005). Solute contaminant transport in variably saturated dual-porosity/dual permeability chalk: field tracer experiments and modelling. *Reactive transport in soil and groundwater processes and models*: doi 10.1007/b138022.

Brouyère, S. (2006). Modelling the migration of contaminants through variably saturated dual-porosity, dual-permeability chalk. *J. Contam. Hydrol.* **82**: 195-219.

Brouyère, S., Dassargues, A., Therrien, R. & Sudicky, E. A. (2000). Modelling of dual porosity media: comparison of different techniques and evaluation of the impact on plume transport simulations. *In* Proceedings of the Calibration and Reliability in Groundwater Modelling, ModelCARE'99. Zürich, Switzerland. 22-27 pp.

Carrera, J., Alcolea, A., Medina, A., Hidalgo, J. & Slooten, L. J. (2005). Inverse problem in hydrogeology. *Hydrogeology Journal* **13**: 206-222.

Carrera, J. & Neuman, S. P. (1986b). Estimation of aquifer parameters under transient and steady-state conditions. 2. Uniqueness, stability and solution algorithms. *Water Resour. Res.* **22**(2): 211-227.

Certes, C. & de Marsily, G. (1991). Application of the pilot points method to the identification of aquifer transmissivities. *Adv. Water Resour.* **14**(5): 284-300.

Cey, E. E., Rudolph, D. L., Parkin, G. W. & Aravena, R. (1998). Quantifying groundwater discharge to a small perennial stream in southern Ontario, Canada. *J. Hydrol.* **210**: 21-37.

Choi, J., Hulseapple, S. M., Conklin, M. H. & Harvey, J. W. (1998). Modeling CO_2 degassing and pH in a stream-aquifer system. *J. Hydrol.* **209**: 297-310.

Coats, K. H. & Smith, B. D. (1964). Dead-end pore volume and dispersion in porous media. *Soc. Petrol. Engng. J.* **4**: 73-84.

Conant, B. J. (2004). Delineating and quantifying ground water discharge zones using streambed temperatures. *Ground Water* **42**(2): 243-257.

Cooley, R. L. (2000). An analysis of the pilot point methodology for automated calibration of an ensemble of conditionally simulated transmissivity fields. *Water Resour. Res.* **36**(4): 1159-1163.

Cooley, R. L. & Hill, M. C. (2000). Comment on RamaRao *et al.* (1995) and Lavenue *et al.* (1995). *Water Resour. Res.* **36**(9): 2795-2797.

Cornaton, F. & Perrochet, P. (2002). Analytical 1D dual-porosity equivalent solutions to 3D discrete single-continuum models. Application to karstic spring hydrograph modelling. *J. Hydrol.* **262**: 165-176.

de Marsily, G., Lavedan, G., Boucher, M. & Fasanino, G. (1984). Interpretation of interference tests in a well field using geostatistical techniques to fit the permeability distribution in a reservoir model. *In* Proceedings of Geostatistics for natural resources characterization. Verly *et al.* (ed.). D. Reidel Pub. Co. **Part 2**. 831-849 pp.

de Weert, J., van Eekert, M., Janniche, G. S., Morasch, B., Albrechtsen, H.-J., Schraa, G. & Langenhoff, A. (2007). Second new results of biodegradation of the selected compounds under various conditions (2nd report on a sequence of 4). *Deliverable BGC5.9*. AquaTerra (Integrated Project FP6 no. 505428). 37 pp.

DeSimone, L. A. & Barlow, P. M. (1999). Use of computer programs STLK1 and STWT1 for analysis of stream-aquifer hydraulic interaction. *Water Resources Investigations Report 98-4212*. US Geological Survey, Marlborough, Massachusetts, USA. 61 pp.

Dobson, R., Schroth, M. H. & Zeyer, J. (2007). Effect of water-table fluctuation on dissolution and biodegradation of a multi-component, light nonaqueous-phase liquid. *J. Contam. Hydrol.* **94**: 235-248.

Doherty, J. (2003). Ground water model calibration using pilot points and regularization. *Ground Water* **41**(2): 170-177.

Durant, L. P. W., D'Adamo, P. C. & Bouwer, E. J. (1999). Aromatic hydrocarbon biodegradation with mixtures of O_2 and NO_3^- as electron acceptors. *Environmental Engineering Science* **16**: 487 - 500.

Fischer, A., Theuerkorn, K., Stelzer, N., Gehre, M., Thullner, M. & Richnow, H. H. (2007). Applicability of stable isotope fractionation analysis for the characterization of benzene biodegradation in a BTEX-contaminated aquifer. *Environ. Sci. Technol.* **41**: 3689-3696.

Fleckenstein, J. H., Niswonger, R. G. & Fogg, G. E. (2006). River-aquifer interactions, geologic heterogeneity, and low flow management. *Ground Water* **44**(6): 837-852.

Fritz, B. G. & Arntzen, E. V. (2007). Effect of rapidly changing river stage of uranium flux through the hyporheic zone. *Ground Water* **45**(6): 753-760.

Fry, V. A., Selker, J. S. & Gorelick, S. M. (1997). Experimental investigations for trapping oxygen gas in saturated porous media for in situ bioremediation. *Water Resour. Res.* **33**(12): 2687-2696.

Gerke, H. H. & van Genuchten, M. T. (1993a). A dual-porosity model for simulating the preferential movement of water and solutes in structured porous media. *Water Resour. Res.* **29**(2): 305-319.

Gerke, H. H. & van Genuchten, M. T. (1993b). Evaluation of a first-order water transfer term for variably saturated dual-porosity flow models. *Water Resour. Res.* **29**(4): 1225-1238.

Gilmore, T. J., Borghese, J. V. & Newcomer, D. R. (1993). Effects of river stage and waste discharges on the unconfined aquifer, Wasington. *Ground Water Monit. Rem.* **13**: 130-138.

Girard, P., da Silva, C. J. & Abdo, M. (2003). River-groundwater interactions in the Brazilian Pantanal. The case of the Cuiabá River. *J. Hydrol.* **283**: 57-66.

Gómez Hernández, J. J., Sahuquillo, A. & Capilla, J. E. (1997). Stochastic simulation of transmissivity fields conditional to both transmissivity and piezometric data- I.Theory. *J. Hydrol.* **203**: 162-174.

Govindaraju, R. S. & Koelliker, J. K. (1994). Applicability of linearized Boussinesq equation for modeling bank storage under uncertain aquifer parameters. *J. Hydrol.* **157**: 349-366.

Grbic-Galic, D. & Vogel, T. M. (1987). Transformation of toluene and benzene by mixed methanogenic cultures. *Appl. Environ. Microbiology* **53**(2): 254-260.

Ha, K., Koh, D.-C., Yum, B.-W. & Lee, K.-K. (2007). Estimation of layered diffusivity and river resistance using flood wave response model. *J. Hydrol.* **337**: 284-293.

Hantush, M. S. (1965). Wells near streams with semi-pervious beds. *J. Geophy. Res.* **10**(12): 2829 - 2838.

Harbaugh, A. W. & McDonald, M. G. (1996a). User's documentation for MODFLOW'96, an update to the U.S. Geological Survey Modular Finite Difference Ground-Water Flow Model. *Open-File Report 96-485*. U.S. Geological Survey, Reston, Virginia. 63 pp.

Harbaugh, A. W. & McDonald, M. G. (1996b). Programmeer's documentation for MODFLOW-96, an update to the U.S. Geological Survey modular finite-difference ground-water flow model. *Open-File Report 96-483*. US Geological Survey. 220 pp.

Harvey, J. W., Wagner, B. J. & Bencala, K. E. (1996). Evaluating the reliability of the stream tracer approach to characterize stream-subsurface exchange. *Water Resour. Res.* **32**(8): 2441-2451.

Heider, J., Spormann, A. M., Beller, H. R. & Widdel, F. (1999). Anaerobic bacterial metabolism of hydrocarbons. *FEMS Microbiol. Ecol.* **22**: 459-473.

Hernández, A. F., Neuman, S. P., Guadagnini, A. & Carrera, J. (2003). Conditioning mean steady state flow on hydraulic head and conductivity through geostatistical inversion. *Stochas. Env. Res. Risk Assess.* **17**(5): 329-338.

Herr, M., Schäfer, G. & Spitz, K. (1989). Experimental studies of mass transport in porous media with local heterogeneities. *J. Contam. Hydrol.* **4**: 127-137.

Higgins, D. T. (1980). Unsteady drawdown in 2-D water table aquifer. *American Society of Civil Engineers, Journal of the Irrigation and Drainage Division* **106**(IR3): 237-251.

Hill, M. C. & Tiedeman, C. R. (2007). Effective groundwater model calibration. With Analysis of data, sensitivities, predictions and uncertainty. John Wiley & Sons. New Jersey. 455 pp.

Hunt, M. J., Shafer, M. B., Barlaz, M. A. & Borden, R. C. (1997). Anaerobic biodegradation of alkylbenzenes in aquifer material under methanogenic and iron-reducing conditions. *Bioremediation J.* **1**: 53-64.

Jaynes, D. B., Logsdon, S. D. & Horton, R. (1995). Field method for measuring mobile/immobile water content and solute transfer rate coefficient. *Soil Sci. Soc. Am. J.* **59**: 352-356.

Jha, M. K., Jayalekshmi, K., Machiwal, D., Kamii, Y. & Chikamori, K. (2004). Determination of hydraulic parameters of an unconfined alluvial aquifer by the floodwave-response technique. *Hydrogeology Journal* **12**: 628-642.

Kalbus, E., Reisntorf, F. & Schirmer, M. (2006). Measuring methods for groundwater - surface water interactions: a review. *Hydrol. Earth Syst. Sci.* **10**: 873-887.

Kalbus, E., Schmidt, C., Bayer-Raich, M., Leschik, S., Reinstorf, F., Balcke, G. U. & Schirmer, M. (2007). New methodology to investigate potential contaminant fluxes at the stream - aquifer interface by combining integral pumping tests and streambed temperatures. *Environ. Pollut.* **148**: 808-816.

Kao, C. M. & Wang, C. C. (2000). Control of BTEX migration by intrinsic bioremediation at a gasoline spill site. *Water Res.* **34**(13): 3413-3423.

Kao, C. M. & Wang, Y. S. (2001). Field investigation of the natural attenuation and intrinsic biodegradation rates at an underground storage tank site. *Environ. Geol.* **40**(4-5): 622-631.

Käss, W. (1998). Tracing technique in geohydrology. A.A.Balkema P.O.Box 1675, 3000 BR Rotterdam, Netherlands. 581 pp.

Kazumi, J., Caldwell, M. E., Suflita, J. M., Lovley, D. R. & Young, L. Y. (1997). Anaerobic degradation of benzene in diverse anoxic environements. *Environ. Sci. Technol.* **31**(3): 813-818.

Keery, J., Binley, A., Cook, N. & Smith, J. W. N. (2007). Temporal and spatial variability of groundwater - surface water fluxes: development and application of an analytical method using temperature time series. *J. Hydrol.* **336**(1-2): 1-16.

Keidser, A. & Rosbjerg, D. (1991). A comparison of four inverse approaches to groundwater flow and transport parameter identification. *Water Resour. Res.* **27**(9): 2219-2232.

Kim, S.-B. & Corapcioglu, M. Y. (2002). Contaminant transport in dual porosity media with dissolved organic matter and bacteria present as mobile colloids. *J. Contam. Hydrol.* **59**: 267-289.

Knudby, C. & Carrera, J. (2005). On the relationship between indicators of geostatistical, flow and transport connectivity. *Adv. Water Res.* **28**(4): 405-421.

Kowalsky, M. B., Finsterle, S. & Rubin, Y. (2004). Estimating flow parameter distributions using ground-penetrating radar and hydrological measurements during transient flow in the vadose zone. *Adv. Water Res.* **27**: 583-599.

Lambs, L. (2004). Interactions between groundwater and surface water at river banks and the confluence of rivers. *J. Hydrol.* **288**: 312-326.

LaVenue, A. M. & Pickens, J. F. (1992). Application of a coupled adjoint sensitivity and kriging approach to calibrate a groundwater flow model. *Water Resour. Res.* **28**(6): 1543-1569.

LaVenue, A. M., RamaRao, B. S., de Marsily, G. & Marietta, M. G. (1995). Pilot point methodology for automated of an ensemble of conditionally simulated transmissivity fields 2. Application. *Water Resour. Res.* **31**(3): 495-516.

Lee, J.-Y., Cheon, J.-Y., Lee, K.-K., Lee, S.-Y. & Lee, M.-H. (2001). Factors affecting the distribution of hydrocarbon contaminants and hydrogeochemical parameters in a shallow sand aquifer. *J. Contam. Hydrol.* **50**: 139-158.

Lenhard, R. J. (1992). Measurement and modeling of three-phase saturation-pressure hysteresis. *J. Contam. Hydrol.* **9**: 243-269.

Lenhard, R. J., Johnson, T. G. & Parker, J. C. (1993). Experimental observations of nonaqueous-phase liquid subsurface movement. *J. Contam. Hydrol.* **12**: 79-101.

Lovley, D. R. (2000). Anaerobic benzene degradation. *Biodegradation* **11**(2-3): 107-116.

Lovley, D. R., Coates, J. D., Woodward, J. C. & Phillips, E. J. P. (1995). Benzene oxidation coupled to sulfate reduction. *Appl. Environ. Microbiology* **61**(3): 953-958.

Lu, G., Clement, T. P., Zheng, C. & Wiedemeier, T. H. (1999). Natural attenuation of BTEX compounds: model development and field-scale application. *Ground Water* **27**(5): 707-717.

MacQuarrie, K. T. B., Sudicky, E. A. & Frind, E. O. (1989). Simulation of biodegradable organic contaminants in groundwater, 1. Numerical formulation in principal directions. *Water Resour. Res.* **26**(2): 207-222.

Manglik, A., Rai, S. N. & Singh, V. S. (2004). Modelling of aquifer response to time varying recharge and pumping from multiple basins and wells. *J. Hydrol.* **292**: 23-29.

McDonald, M. G. & Harbaugh, A. W. (1984). A modular three-dimensional finite-difference groundwater flow model. *Open-File Report 83-875*. US Geological Survey. 528 pp.

McDonald, M. G. & Harbaugh, A. W. (1988). A modular three-dimensional finite-difference ground-water flow model. *Techniques of Water-Resources Investigations, book 6, chapter A1*. US Geological Survey. 586 pp.

McKelvie, J. R., Lindstrom, J. E., Beller, H. R., Richmond, S. A. & Sherwood Lollar, B. (2005). Analysis of anaerobic BTX biodegradation in a subartic aquifer using isotopes and benzylsuccinates. *J. Contam. Hydrol.* **81**: 167-186.

McLaughlin, D. & Townley, L. R. (1996). A reassessment of the groundwater inverse problem. *Water Resour. Res.* **32**(5): 1131-1161.

Meckenstock, R. U., Morasch, B., Griebler, C. & Richnow, H. H. (2004). Stable isotope fractionation analysis as a tool to monitor biodegradation in contaminated aquifers. *J. Contam. Hydrol.* **75**: 215-255.

Medina, A. & Carrera, J. (1996). Coupled estimation of flow and solute transport parameters. *Water Resour. Res.* **32**(10): 3063-3076.

Moench, A. F. & Barlow, P. M. (2000). Aquifer response to stream-stage and recharge variations. I. Analytical step-response functions. *J. Hydrol.* **230**(3-4): 192-210.

Moench, A. F., Sauer, V. B. & Jennings, M. E. (1974). Modification of routed streamflow by channel loss and base flow. *Water Resour. Res.* **10**(5): 963-968.

Moore, C. & Doherty, J. (2006). The cost of uniqueness in groundwater model calibration. *Adv. Water Resour.* **29**: 605-623.

Morasch, B., Höhener, P. & Hunkeler, D. (2007a). Evidence for in situ degradation of mono- and polyaromatic hydrocarbons in alluvial sediments baed on microcosm experiments with ^{13}C-labeled contaminants. *Environ. Pollut.* **148**(3): 739-748.

Morasch, B., Höhener, P., Hunkeler, D. & Langenhoff, A. (2007b). Quantitative evaluation of biodegradation at the BASIN site of Flémalle. *Report BGC5.10*. AquaTerra (Integrated Project FP6 no. 505428). 15 pp.

Nales, M., Butler, B. J. & Edwards, E. A. (1998). Anaerobic benzene degradation: a microcosm survey. *Bioremediation J.* **2**: 125-144.

Nemeth, M. S. & Solo-Gabriele, H. M. (2003). Evaluation of the use of reach transmissivity to quantify exchange between groundwater and surface water. *J. Hydrol*. **274**: 145-159.

Neuman, S. P. (1981). Delayed drainage in a stream-aquifer system. *American Society of Civil Engineers, Journal of the Irrigation and Drainage Division* **107**(IR4): 407-410.

Nyer, E. K. & Duffin, M. E. (1997). The state of art of bioremediation. *Ground Water Monit. Rem.* **17**(2): 64-69.

Osman, Y. Z. & Bruen, M. P. (2002). Modelling stream-aquifer seepage in an alluvial aquifer: an improved loosing-stream package for MODFLOW. *J. Hydrol.* **264**: 69-86.

Peterson, R. E. & Connelly, M. P. (2004). Water movement in the zone of interaction between groundwater and the Columbia River, Hanford site, Washington. *Journal of Hydraulic Research* **42**(Extra Issue): 53-58.

Phelps, C. D., Kazumi, J. & Young, L. Y. (1996). Anaerobic degradation of benzene in BTX mixtures dependent of sulfate reduction. *FEMS Microbiology Letters* **145**: 433-437.

Pili, É., Perrier, F. & Richon, P. (2004). Dual porosity mechanism for transient groundwater and gas anomalies induced by external forcing. *Earth Planet. Sci. Lett.* **227**: 473-480.

Poeter, E. P. & Hill, M. C. (1997). Inverse models: a necessary next step in ground-water modeling. *Ground Water* **35**(2): 250-260.

Prickett, T. A. & Lonnquist, C. G. (1971). Selected digital computer techniques for groundwater resources evaluation. *Bull. No. 55*. Illinois State Water Surveypp.

Pruden, A., Sedran, M. A., Suidan, M. T. & Venosa, A. D. (2003). Biodegradation of MTBE and BTEX in an aerobic fluidized-bed reactor. *Water Sci. Technol.* **47**(9): 123-128.

Pulido-Velázquez, D., Sahuquillo, A. & Andreu, J. (2006). A two-step explicit solution of the Boussinesq equation for efficient simulation of unconfined aquifers in conjunctive-use models. *Water Resour. Res.* **42**(W05423): doi:10.1029/2005WR004473.

RamaRao, B. S., LaVenue, A. M., de Marsily, G. & Marietta, M. G. (1995). Pilot point methodology for automated calibration of an ensemble of conditionally simulated transmissivity fields. 1.Theory and computational experiments. *Water Resour. Res.* **31**(3): 475-493.

Rayleigh, J. W. S. (1896). Theoretical considerations respecting the separation of gases by diffusion and similar processes. *Philos. Mag.* **42**: 493-498.

Reinhard, M., Hopkins, G. D., Steinle-Darling, E. & LeBron, C. A. (2005). In situ biotransformation of BTEX compounds under methanogenic conditions. *Ground Water Monit. Rem.* **25**(4): 50-59.

Reinhard, M., Shang, S., Kitanidis, P. K., Orwin, E., Hopkins, G. D. & LeBron, C. A. (1997). In situ BTEX biotransformation under enhanced nitrate- and sulfate-reducing conditions. *Environ. Sci. Technol.* **31**(3): 28-36.

Richnow, H. H., Annweiler, E., Michaelis, W. & Meckenstock, R. U. (2003). Microbial in situ degradation of aromatic hydrocarbons in a contaminated aquifer monitored by carbon isotope fractionation. *J. Contam. Hydrol.* **65**: 101-120.

Ridgway, H. F., Safarik, J., Phipps, D., Carl, P. & Clark, D. K. (1990). Identification and catabolic activity of well-derived gasoline-degrading bacteria from a contaminated aquifer. *Appl. Environ. Microbiology* **56**(11): 3565-3575.

Samardzioska, T. & Popov, V. (2005). Numerical comparison of the equivalent continuum, non-homogeneous and dual porosity models for flow and transport in fractured porous media. *Adv. Water Res.* **28**: 235 - 255.

Serrano, S. E. (1995). Analytical solutions of the nonlinear groundwater flow equation in unconfined aquifers and the effect of heterogeneity. *Water Resour. Res.* **31**(11): 2733-2742.

Serrano, S. E. & Workman, S. R. (1998). Modeling transient stream/aquifer interaction with the non-linear Boussinesq equation and its analytical solution. *J. Hydrol.* **206**: 245-255.

Silliman, S. E. & Booth, D. F. (1993). Analysis of time-series measurements of sediment temperature for indentification of gaining *vs*. losing portions of Juday Creek, Indiana. *J. Hydrol.* **146**: 131-148.

Singh, S. K., Mishra, G. C., Swamee, P. K. & Ojha, C. S. P. (2002). Aquifer diffusivity and stream resistance from varying stream stage. *J. Irrig. Drain. Eng.* **128**(1): 1108-1118.

Sinke, A. J. C., Dury, O. & Zobrist, J. (1998). Effects of fluctuating water table: column study on redox dynamics and fate of some organic pollutants. *J. Contam. Hydrol.* **33**: 231-246.

Sophocleous, M. A. (1991). Stream-floodwave propagation through the Great Bend alluvial aquifer, Kansas: field measurements and numerical simulations. *J. Hydrol.* **124**: 207-228.

Sophocleous, M. A., Koussis, A., Martin, J. L. & Perkins, S. P. (1995). Evaluation of simplified stream-aquifer depletion models for water rights administration. *Ground Water* **33**(4): 579-588.

Spence, M. J., Bottrell, S. H., Higgo, J. J. W., Harrison, I. & Fallick, A. E. (2001). Denitrification and phenol degradation in a contaminated aquifer. *J. Contam. Hydrol.* **53**: 305-318.

Srivastava, K., Serrano, S. E. & Workman, S. R. (2006). Stochastic modeling of transient stream-aquifer interaction with the nonlinear Boussinesq equation. *J. Hydrol.* **328**: 538-547.

Strecker, E. W. & Chu, W. (1986). Parameter identification of a groundwater contaminant transport model. *Ground Water* **24**(1): 56-62.

Swindoll, C. M., Aelioni, A. M. & Pfaender, F. K. (1988). Influence of inorganic and organic nutrients of aerobic biodegradation and on the adaption response of subsurface microbial community. *Appl. Environ. Microbiology* **54**(1): 212-227.

Tabidian, M. A., Pederson, D. & Tabidian, P. A. (1992). A paleovalley aquifer system and its interaction with the Big Blue River of Nebraska during a major flood. *In* The Future Availability of Ground Water Resources. W.L. Lyke R.C. Borden (ed.). American Water Resources Association. 165-172 pp.

Uçankus, T. & Ünlü, K. (2008). The effect of aquifer heterogeneity on natural attenuation rate of BTEX. *Environ. Geol.* **54**: 759-776.

USEPA (1997). Use of monitored natural attenuation superfund, RCRA corrective action, underground storage tank sites. OSWER directive no. 9200.4-17. 34 pp.

van de Giesen, N. C., Parlange, J.-Y. & Steenhuis, T. S. (1994). Transient flow to open drains: comparison of linearized solutions with and without the Dupuit assumption. *Water Resour. Res.* **30**(11): 3033-3039.

Vesselinov, V. V., Neuman, S. P. & Illman, W. A. (2001). Three dimensional numerical inversion of pneumatic cross-hole tests in unsaturated fractured tuff 2. Equivalent parameters, high-resolution stochastic imaging and scale effects. *Water Resour. Res.* **37**(12): 3019-3041.

Ward, J. A. M., Ahad, J. M. E., Lacrampe-Couloume, G., Salter, G. E., Edwards, E. A. & Sherwood Lollar, B. (2001). Hydrogen isotope fractionation during methanogenic degradation of toluene: potential for direct verification of bioremediation. *Environ. Sci. Technol.* **34**: 4577-4581.

Weiner, J. M. & Lovley, D. R. (1998). Rapid benzene degradation in methanogenic sediments from a petroleum-contaminated aquifer. *Appl. Environ. Microbiology* **64**(5): 1937-1939.

White, M. D. & Oostrom, M. (2000). STOMP. Subsurface Transport Over Multiple Phases. Version 2.0 Theory guide. *PNNL-12030 UC-2010*. U.S. Department of Energy, Richland, Washington 99352. 182 pp.

Wiedemeier, T. H., Rifai, H. S., Newell, C. J. & Wilson, J. T. (1999). Natural attenuation of fuels and chorinated solvents in the subsurface. Wiley. New York. 617 pp.

Wiedemeier, T. H., Swanson, M. A., Moutoux, D. E., Gordon, E. K., Wilson, J. T., Wilson, B. H., Kampbell, D. H., Haas, P. E., Miller, R. N., Hansen, J. E. & Chapelle, F. H. (1998). Technical protocol for evaluating natural attenuation of chlorinated solvents in ground water. *EPA/600/R-98/128*. United States Environmental Protection Agency, Washington DC, USA. 78 pp.

Williams, M. D. & Oostrom, M. (2000). Oxygenation of anoxic water in a fluctuating water table system: an experimental and numerical study. *J. Hydrol.* **230**: 70-85.

Winter, T. C., Harvey, J. W., Franke, O. L. & Alley, W. M. (1998). Ground water and surface water. A single resource. *U.S. Geological Survey Circular 1139*. U.S. Geological Survey, Denver, Colorado, USA. 79 pp.

Wood, T. R., Helm-Clark, C., M., Huang, H., Magnuson, S., McLing, T., Orr, B., Roddy, M., Rohe, M. J., Plummer, M. A. & Podgorney, R. (2005). Operable unit 10-08. Summary report of the subregional-scale two dimensional aquifer model. *ICP/EXT-05-00979*. US Department of Energy, Idaho Falls, Idaho (USA). 180 pp.

Workman, S. R., Serrano, S. E. & Liberty, K. (1997). Development and application of an analytical model of stream/aquifer interaction. *J. Hydrol.* **200**: 149-163.

Wroblicky, G. J., Campana, M. E., Valett, H. M. & Dahm, C. N. (1998). Seasonal variation in surface-subsurface water exchange and lateral hyporheic area of two stream-aquifer systems. *Water Resour. Res.* **34**(3): 317-328.

Wylie, A. & Doherty, J. (2005). Eastern snake plain aquifer model calibration report. *DDM-008*. Idaho Water Resources, University of Idaho. 19 pp.

Yeh, W. W.-G. (1986). Review of parameter identification procedures in groundwater hydrology: The inverse problem. *Water Resour. Res.* **22**(2): 95-108.

Zamfirescu, D. & Grathwohl, P. (2001). Occurrence and attenuation of specific organic compounds in the groundwater plume at a former gasworks site. *J. Contam. Hydrol.* **53**: 407-427.

Zechner, E. & Frielingsdorf, W. J. (2004). Evaluating the use of canal seepage and solute concentration observations for aquifer parameter estimation. *J. Hydrol.* **289**: 62-77.

Zheng, C. & Wang, P. P. (1999). MT3DMS: a modular three-dimensional multispecies transport model for simulation of advection, dispersion, and chemical reactions of contaminants in groundwater systems; documentation and user's guide. *Contract Report SERDP-99-1*. U.S. Army Engineer Research and Development Center, Vicksburg, Massachussests (USA). 202 pp.

Zurmühl, T. & Durner, W. (1996). Modeling transient water and solute transport in a biporous soil. *Water Resour. Res.* **32**(4): 819-829.

Knowledge is like money: the more he gets,
the more he craves.
Josh Billings
Humorist and lecturer (1815-1885)

4. MONITORING AND FIELD WORKS

4.1. Objectives

Three main priorities were highlighted to be studied in the Flémalle site at the end of Chapter 2: (1) the need to know whether a river - aquifer interaction exists; (2) characterisation of the alluvial aquifer heterogeneity; and (3) determination of groundwater fluxes discharging to the Meuse River. Monitoring and field works described in the present Chapter 4 were performed with the scope to supply the enough data to achieve these priorities.

Collected data such as rainfall and Meuse River level fluctuations are described. Monitoring and field works performed (pumping, injection and tracer tests) are described, interpreted and results analysed.

Overall data obtained from monitoring and field tests will be subsequently used in the development of analytical and numerical modelling approaches, in Chapter 5.

4.2. Data mining and monitoring

4.2.1. Precipitation data

Rainfall is measured by the Ministry of Equipments and Transport (MET) of the Walloon Region at meteorological stations situated in Bierset and Sart Tilman, at respective distances of 4.4 km North-West and 6 km South-East from the Flémalle site, located uphill against it. Data are monitored on an hourly basis at both stations. All these data have been obtained regularly from the beginning of 2005. In addition, at 2 km upstream of the Flémalle site, daily rainfall values are also recorded at the level of the Ivoz-Ramet dam. Although cumulative rainfall are not significantly different, the “meteorological station” of Ivoz-Ramet has been considered as more representative for the Flémalle site because it is closer to it and it is also located in the alluvial plain, at a very similar altitude. Cumulative rainfall for hydrologic years 2005-06 and 2006-07, and daily rainfall for the same periods, is presented in Figure 4.1.

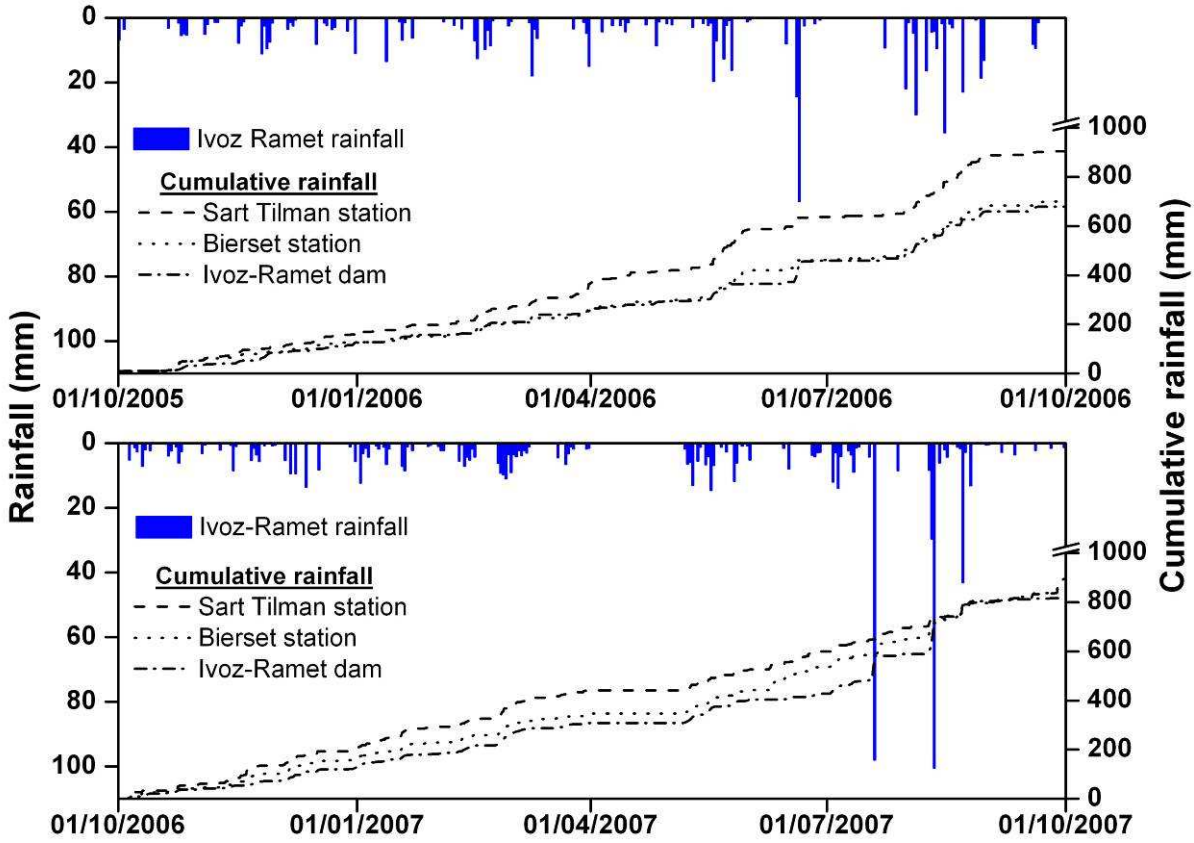

Figure 4.1. Cumulative rainfall at meteorological stations of Bierset, Sart Tilman and Ivoz-Ramet dam and daily rainfall at Ivoz-Ramet dam, for the hydrologic years 2005-06 (above) and 2006-07 (below).

4.2.2. Data on the Meuse River

In the opposite river bank, in front of the Flémalle site, there is a hydroelectric plant (SPE-TGV) where temperature, surface water level and discharge of the Meuse River are monitored continuously. Hourly data have been obtained from 1st January 2005 to 10th January 2008. Figure 4.2 shows river water levels and river discharge for the mentioned period.

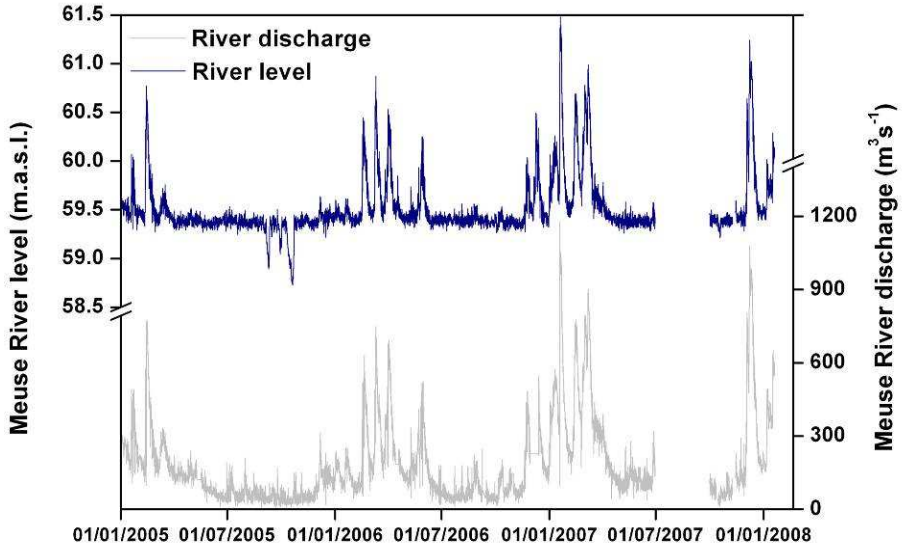

Figure 4.2. Hourly records of the Meuse River water level and discharge in front of the Flémalle site, for years 2005, 2006 and 2007.

Due to dam operations, the mean surface water level in the Meuse River is relatively constant, varying of a few centimetres around 59.4 meters a.s.l. (above sea level). However, when the discharge rate becomes significantly high, the river water level can increase up to 2 m.

As pointed out by Gilmore *et al.* (1993), seasonal river stage fluctuations are likely to influence the hydraulic gradient of the unconfined aquifer near the river. Indeed, seasonal variations of the Meuse River water level were observed during the studied period, with low river levels during June and July, and high river water levels during February and April (Figure 4.2).

4.2.3. Groundwater head monitoring

4.2.3.1. Monthly groundwater head monitoring

From February 2005 to December 2006 groundwater monitoring campaigns were performed approximately each two months. During this period, 14 monitoring campaigns were done: 9 in 2005 and 5 in 2006.

This monitoring has confirmed that the main groundwater flow direction is South-East oriented (Figure 4.3), which means that, in normal conditions, the alluvial aquifer discharges into the Meuse River. Monitoring campaigns of groundwater levels have also indicated that the alluvial aquifer is characterised by a low hydraulic gradient, with a mean value of 0.3%, with maximum values on the East part (0.45%) to minimum values on the South-West area (0.15%).

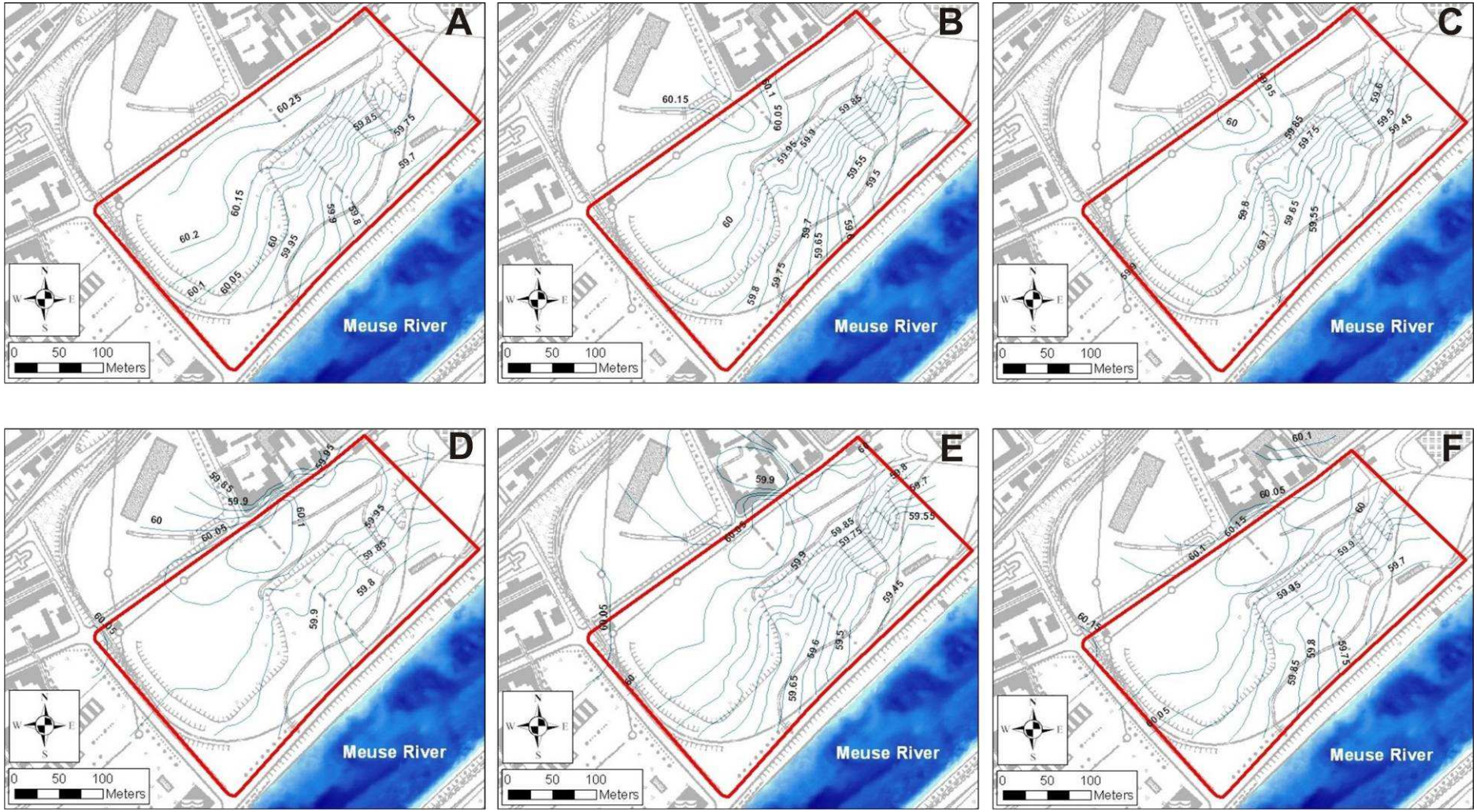

Figure 4.3. Piezometric maps corresponding to monthly groundwater head monitoring campaigns of March 2005 (A); May 2005 (B); July 2005 (C); February 2006 (D); April 2006 (E) and, December 2006 (F).

4.2.3.2. Automatic groundwater head monitoring

Several wells were selected for continuous monitoring of piezometric levels with the idea to have a good spatial cover of observation wells monitored, during more than 2 years, using Level TROLL® pressiometric probes with automatic data acquisition. Details of observation wells monitored are summarised in Table 4.1.

Table 4.1. Characteristics of wells monitored with Level TROLL® pressiometric probes.

Well ID	Depth (m)	Diameter (m)	Screen depth (m)	Distance from the river (m)	Monitored period (days)
U5	11.5	0.1	9.5 – 11.5	113.9	598
U3	10.0	0.1	6.0 – 10.0	207.1	514
P3	15.0	0.15	10.5 – 14.5	26.1	385
U8	7.0	0.05	6.0 – 7.0	80.4	171
U15	14.2	0.1	11.2 -14.2	31.6	85
U23	12.0	0.1	10.0 – 12.0	124.4	29
P5	15.3	0.15	10.0 – 15.0	45.7	31
Pz12	13.7	0.05	Unknown	136.4	31
U17	14.2	0.1	12.2 – 14.2	38.7	35
U31	9.5	0.1	7.5 – 9.5	188.1	35
P1	18.2	0.15	12.5 – 16.7	62.4	34
C6bis	14.6	0.05	Unknown	156.0	34
U19	13.8	0.1	11.8 – 13.8	61.5	43
U33	9.5	0.1	7.5 – 9.5	223.8	43
P4	15.5	0.15	9.5 – 15.0	24.6	42
U12	11.0	0.1	8.0 – 11.0	181.2	35

Two wells (U5 and U3) were monitored for almost the whole 2 year period. At the same time, 2 other pressiometric probes were placed successively in 14 other piezometers for more limited periods of a few weeks, trying, as much as possible, to select monitoring points located along groundwater flow lines, at different distances from the Meuse River (Figure 4.4).

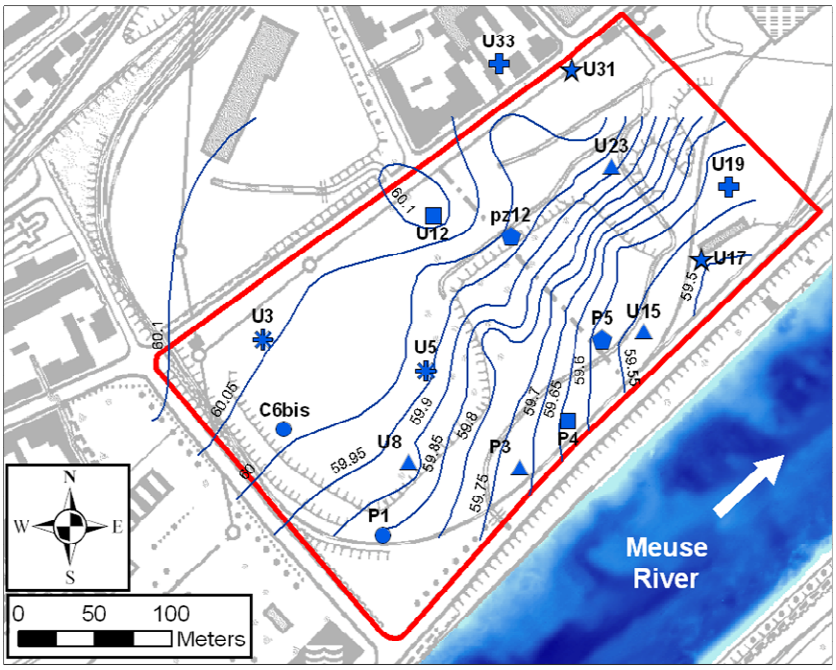

Figure 4.4 Location of observation wells monitored with Level TROLL® pressiometric probes.

Results of the detailed groundwater monitoring campaign are presented in Figure 4.5 to Figure 4.7[5]. Meuse river stages and rainfall are also presented to highlight the possible relation between groundwater and surface water systems and/or groundwater and rainfall. Groundwater level hydrographs corresponding to observation wells located near the river, such as P3 or U17 (Figure 4.5A and Figure 4.6A, respectively) are very similar to the hydrograph corresponding to the Meuse River. For observation wells located far from the river, the hydrograph is smoothed and groundwater level peaks are less important and delayed in time respect to those of the Meuse River (Figure 4.5B, Figure 4.6B and Figure 4.7A-B). This is due to the attenuation of the "floodwave" propagation into the aquifer.

Groundwater table level is higher than river water level, thus causing discharge to the river in regular conditions. Nevertheless, during high river stages, the hydraulic gradient between the aquifer and the river can be reversed with a temporal recharge of the alluvial aquifer by surface water. This change may significantly affect travel times and paths of contaminants in the system, particularly near the river (Gilmore *et al.*, 1993).

[5] Figures corresponding to the other monitored observation wells are presented in Annex 1.

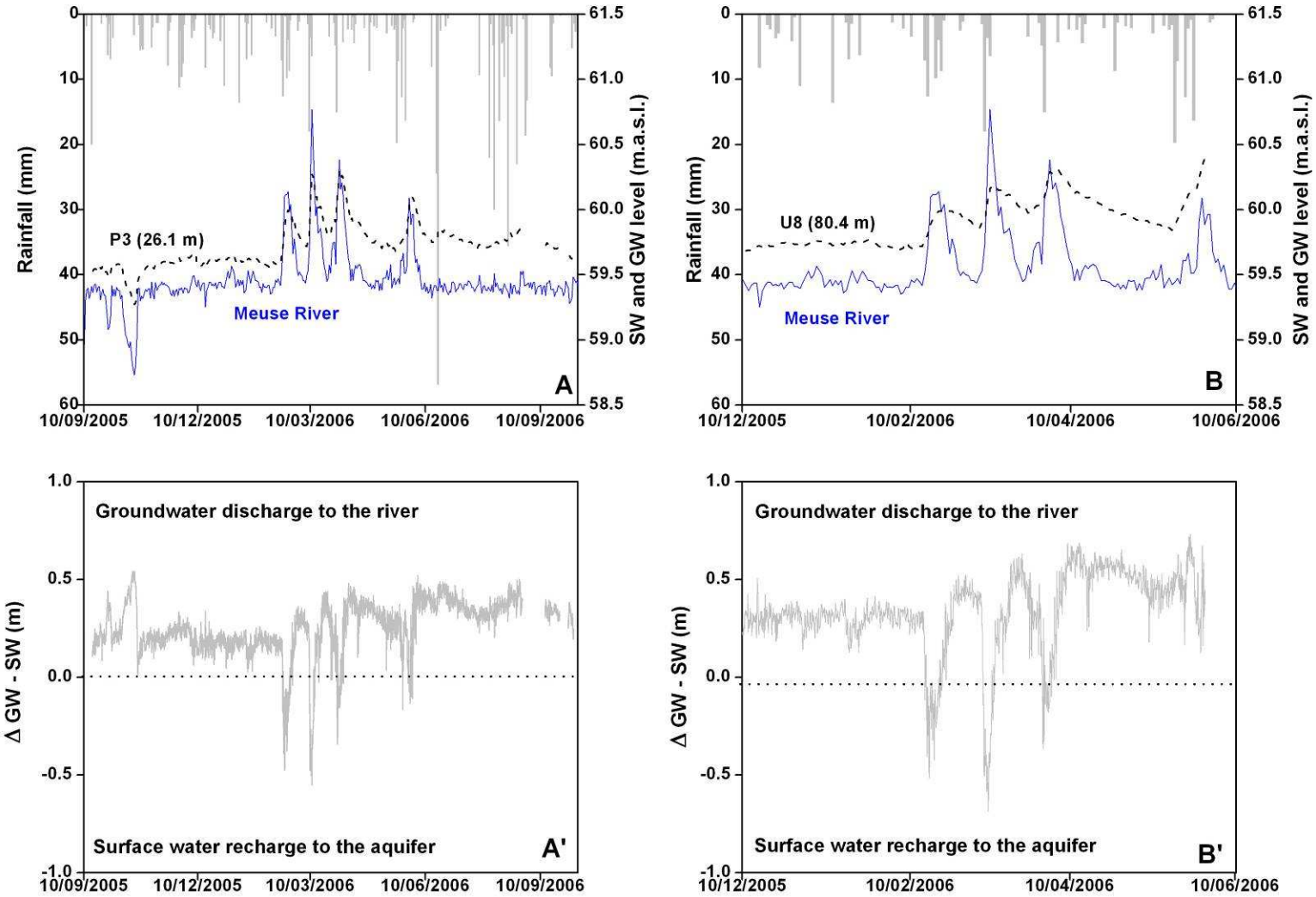

Figure 4.5. Daily groundwater (GW) and Meuse River levels (SW) , and rainfall (Ivoz-Ramet dam), for observation wells P3 (A) and U8 (B). Difference between groundwater and Meuse River levels (Δ GW – SW), calculated with hourly data, is also presented (A' and B', respectively).

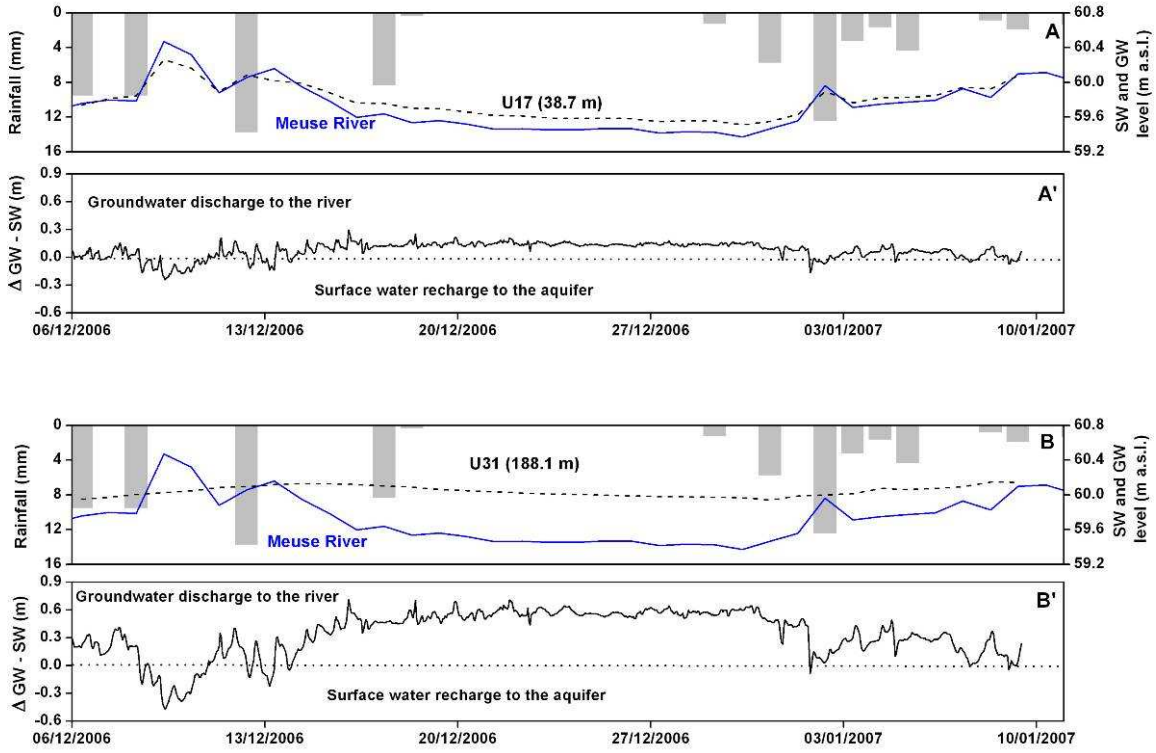

Figure 4.6. Daily groundwater (GW) and Meuse River levels (SW), and rainfall (Ivoz-Ramet dam), for observation wells U17 (A) and U31 (B). Difference between groundwater and Meuse River levels (Δ GW – SW), calculated with hourly data, is also presented (A' and B', respectively).

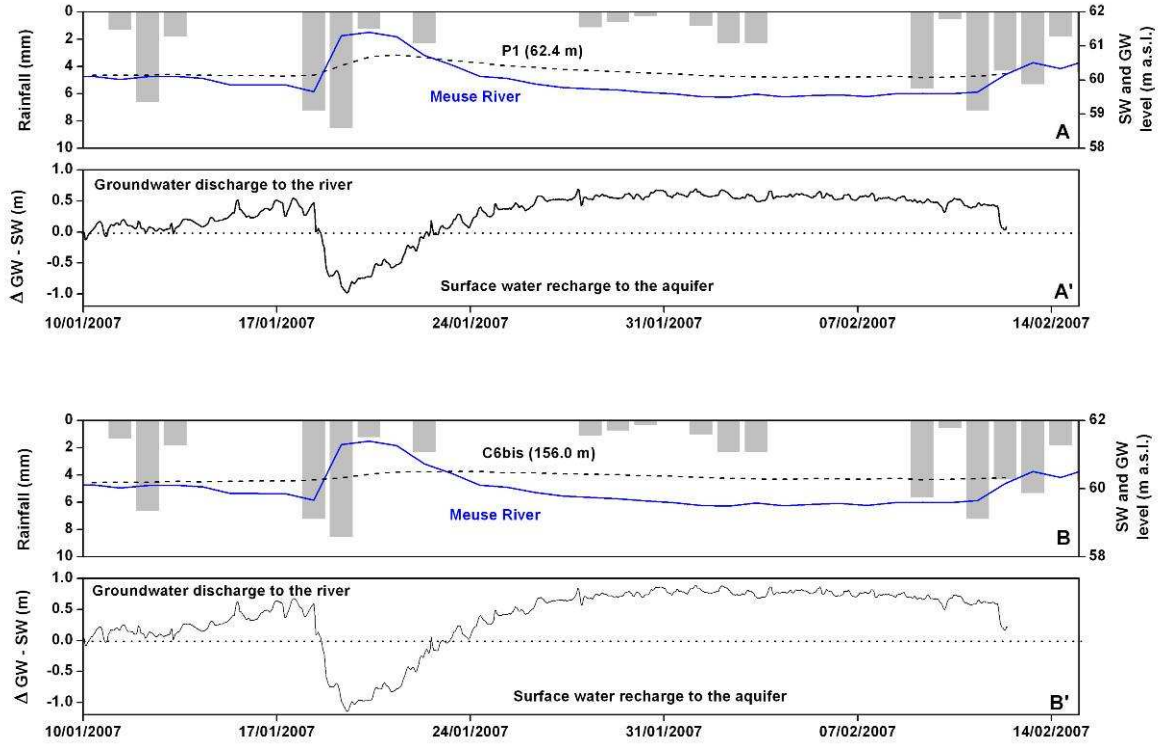

Figure 4.7. Daily groundwater (GW) and Meuse River levels (SW), and rainfall (Ivoz-Ramet dam), for observation wells P1 (A) and C6bis (B). Difference between groundwater and Meuse River levels (Δ GW – SW), calculated with hourly data, is also presented (A' and B', respectively).

4.2.4. Groundwater temperature monitoring

In Chapter 2, it was mentioned the use of heat as a tracer to point out the interaction between a river and an adjacent aquifer.

The range of Meuse River water temperatures reflect seasonal temperature fluctuations from 5ºC during the winter season, up to 28ºC during the summer season. The same seasonal variation in air temperatures[6] is observed, varying from -10ºC during winter season, up to 35ºC in summer (Figure 4.8A). On the contrary, an inversed situation is observed in the river water level, with maximum river water levels during winter season (period of minimum temperatures) and minimum river water levels the rest of the year (when river water and air reach the maximum temperature values) (Figure 4.8B).

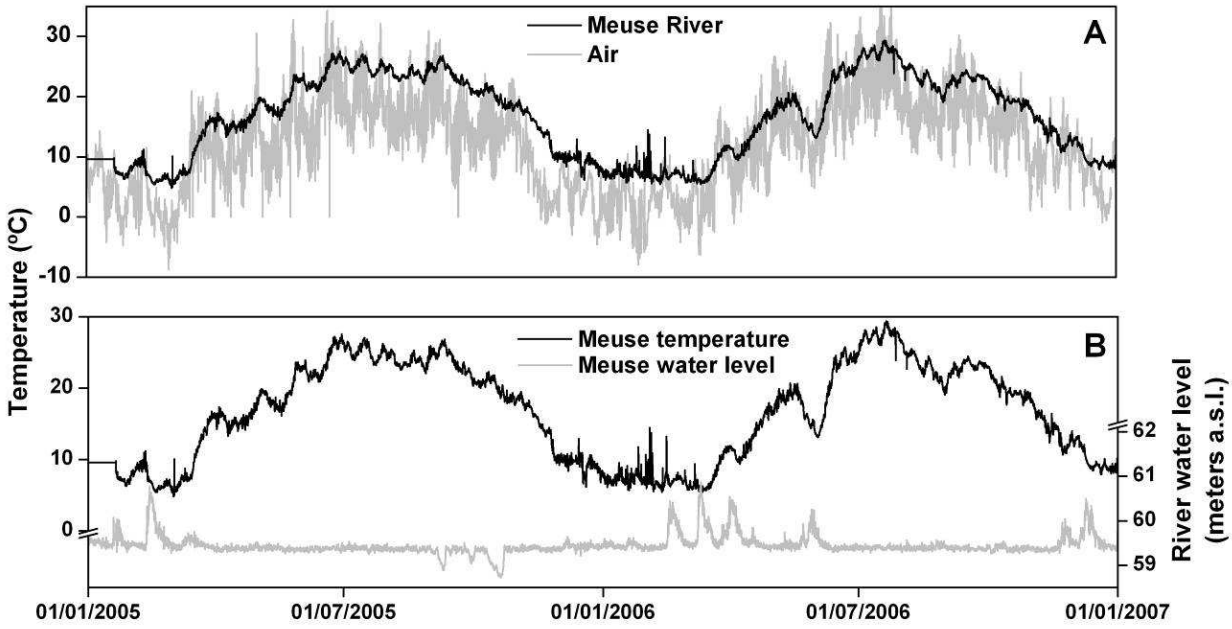

Figure 4.8. Meuse River level and temperature for years 2005 and 2006.

Several Level TROLL® probes used for monitoring groundwater head were also able to measure temperature. When comparing Meuse River and air temperatures with groundwater temperatures monitored for a relatively long period in three observation wells (U3, U5 and U8), it is observed that groundwater temperature presents a periodic, annual trend in inverse proportion to that observed in surface water and in the air (Figure 4.9). Maximal groundwater

[6] Air temperature measured at 3 m height from the soil surface, at the air quality station TMSG01-Jemeppe-Seraing (10 km downstream of the Flémalle site) (http://fluidmach.fpms.ac.be/WebAirQuality3/Accueil.aspx)

temperatures are observed during the winter and minimal temperatures during the summer. This seasonal time-lag of difference between air and groundwater temperature is often observed in shallow aquifers (Lee and Hahn, 2006). The inversed trend observed in the groundwater temperature could also be explained by the time that surface water infiltrating to the alluvial aquifer in the upstream dam takes to arrive at the Flémalle site. However, this hypothesis should be further studied to be confirmed. The seasonal amplitude variation of groundwater temperatures is around 1 degree.

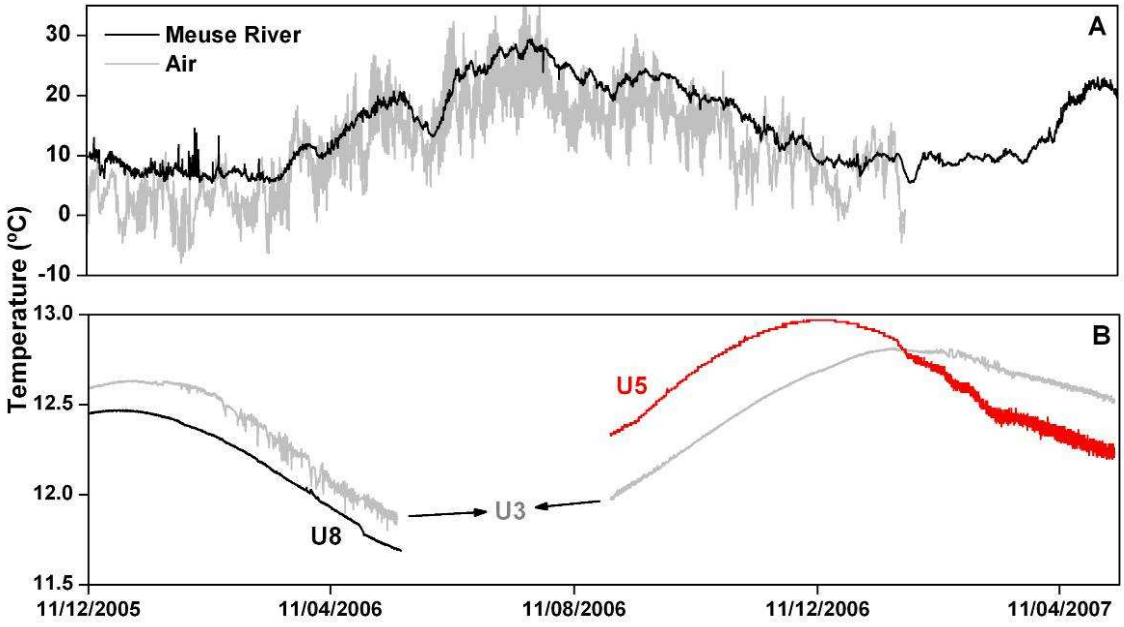

Figure 4.9. Meuse River and air temperature (A); groundwater temperature at three different observation wells (B).

Concomitantly to this annual trend, local variations of groundwater temperature are observed when the hydraulic gradient is inversed due to an increase of river water level. Figure 4.10, presents local decreases of groundwater temperature in observation well U15 caused by inversion of the groundwater gradient in the interface river – aquifer. This well is located at a distance of 31.6 m from the Meuse River.

The sudden decrease of groundwater temperature in well U15, at the moment of hydraulic gradient inversion, can be related with the entrance of colder surface water from the river to the aquifer.

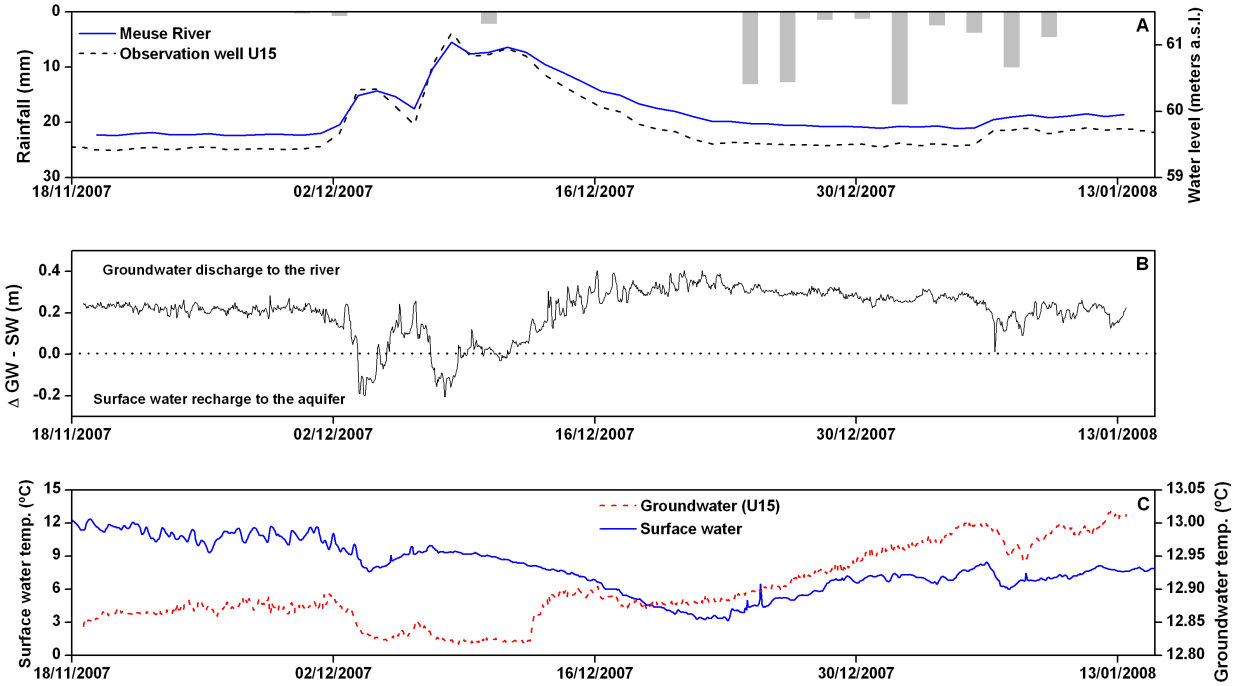

Figure 4.10. Meuse River and groundwater levels in observation well U15 (A); difference between groundwater and Meuse River levels (Δ GW – SW) (B); and Meuse River and groundwater temperature in U15 (C).

On the contrary, groundwater temperature in observation well P1 (62.4 m from the Meuse River) was monitored at the same time that the Meuse River level increased up to 2 meters from its regular level. Even if an important inversion of the hydraulic gradient was produced, no changes were observed in the seasonal trend of the groundwater (Figure 4.11). The distance of the well to the Meuse River can be responsible of this absence of effect. However, considering the magnitude of the surface water level increase and the inversion of hydraulic gradient it seems that the zone corresponding to observation well P1 is not a preferential path for surface water intrusion into the aquifer. On the contrary, the zone where near the well U15 seems to present a better connection with the river.

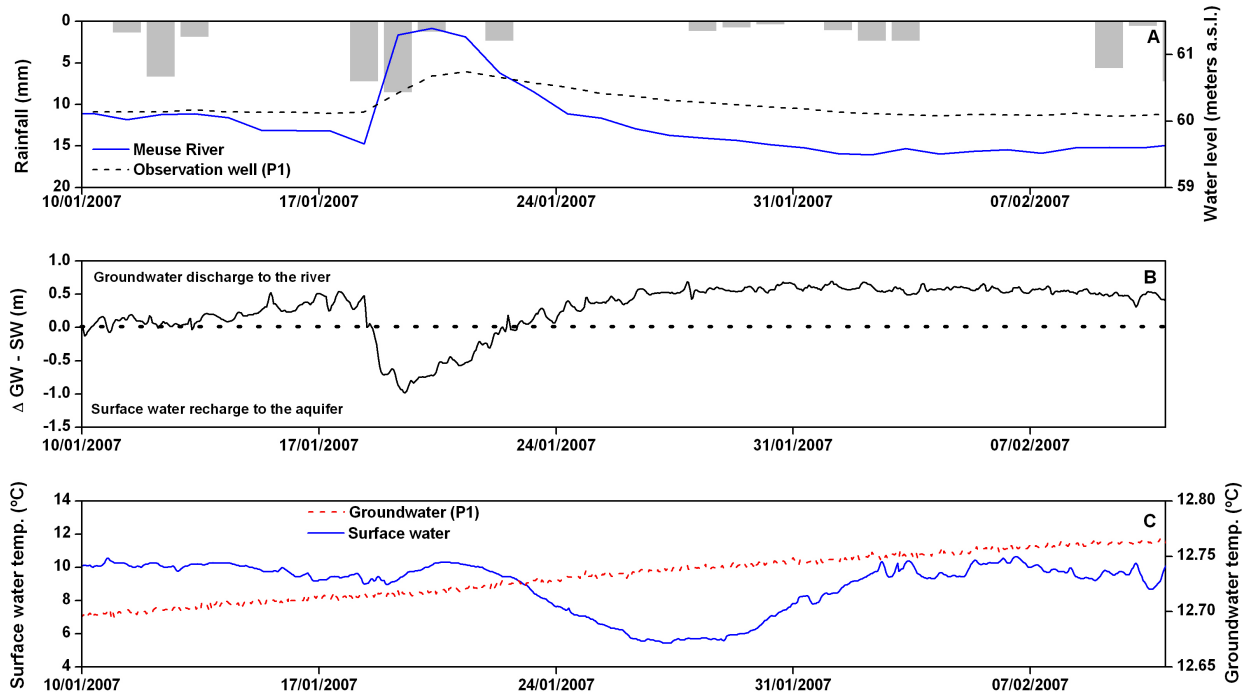

Figure 4.11. Meuse River and groundwater levels in observation well P1 (A); difference between groundwater and Meuse River levels (Δ GW – SW) (B); and Meuse River and groundwater temperature in P1 (C).

The analysis of groundwater temperatures leads to three main conclusions:

1. An increase of surface water levels beyond 60 m a.s.l. cause inversion of the groundwater gradient, susceptible to produce an entrance of surface water to the aquifer;
2. The entrance of surface water to the aquifer, which occurs mainly during the winter, cause a decrease of the groundwater temperature (increases in groundwater temperature due to the entrance of warmer surface water was not observed, because no inversion of the groundwater gradient was reported during the summer);
3. As distance to the Meuse River increase, the change in groundwater temperature due to surface water is attenuated. Furthermore, changes in groundwater temperature lead out to delimitate zones potentially better connected to the river.

4.2.5. Analysis of monitored data

Analysis of monitored data has been performed applying several time series analysis techniques. These techniques consider rainfall and/or surface water as inputs of the system (aquifer) and piezometric head as outputs. Its application to time series analysis has been extensively used (i.e. Padilla and Pulido-Bosch, 1995; Larocque *et al.*, 1998; Massei *et al.*, 2006; Panagopoulos and Lambrakis, 2006, among others). The analysis of time series such as river heads and discharges, piezometric levels, chemical data… provides valuable information of hydrodynamic characteristics of the aquifer. In the Flémalle site, the study of time series analysis was performed in order to establish the delay between the input (river levels and/or rainfall) and output (groundwater levels) of the system.

Cross-correlation analysis have been performed with the TEMPO® software (Pinault, 2001) from BRGM, designed to treat and model hydrogeological and hydrogeochemical time series. The cross-correlation coefficient (*r(k)*) between river levels (or rainfall) and groundwater levels is calculated as follows:

$$r_{xy}(k) = \frac{\sum_{t=1}^{n-k}\left[(x_t - \mu_x)(y_{t+k} - \mu_y)\right]}{\sigma_x \sigma_y} \tag{4.1}$$

where x_t and y_{t+k} are single events at time t and $t+k$ of time series X and Y; k is the time lag; n is the total number of records; μ_x and μ_y are the mean of time series X and Y respectively; and σ_x and σ_y are the standard deviations of respective time series.

4.2.5.1. Cross-correlation analysis between Meuse River water levels and groundwater levels

Cross-correlation functions were calculated between Meuse River and groundwater levels using hourly monitored data and considering the Meuse River as an input in the system. Results are summarised in Table 4.2 and some cross-correlation functions obtained are presented in Figure 4.12. As expected, the cross-correlation function present a maximum of longer amplitude and smaller time lag for wells located close to the Meuse River (i.e. wells P5 and U15) as compared to wells located further away (i.e. wells C6bis and U23).

Table 4.2. Summary of cross-correlation and regression analysis results.

Observation well ID	Distance to Meuse River (m)	Meuse River		Rainfall (Ivoz-Ramet dam)	
		Cross-correlation		Cross-correlation	
		r(k)	delay (h)	r(k)	delay (h)
U5	113.9	0.698	79	0.123	216
U3	207.1	0.736	106	**0.105**	264
P3	26.1	0.824	20	0.140	96
U8	80.4	0.659	26	0.247	120
U15	31.6	0.883	0.5	0.290	120
U23	124.4	**0.325**	169	0.218	24
P5	45.7	0.969	1.0	0.262	48
Pz12	136.4	0.742	46	0.217	216
U17	38.7	0.982	0.5	0.361	96
U31	188.1	0.672	77	0.411	144
P1	62.4	0.895	21	0.353	48
C6bis	156.0	0.588	56	0.171	216
U19	61.5	**0.984**	0.5	**0.662**	144
U33	223.8	0.508	66	0.441	192
P4	24.6	0.858	0.5	0.162	108
U12	181.2	0.432	45	0.137	108

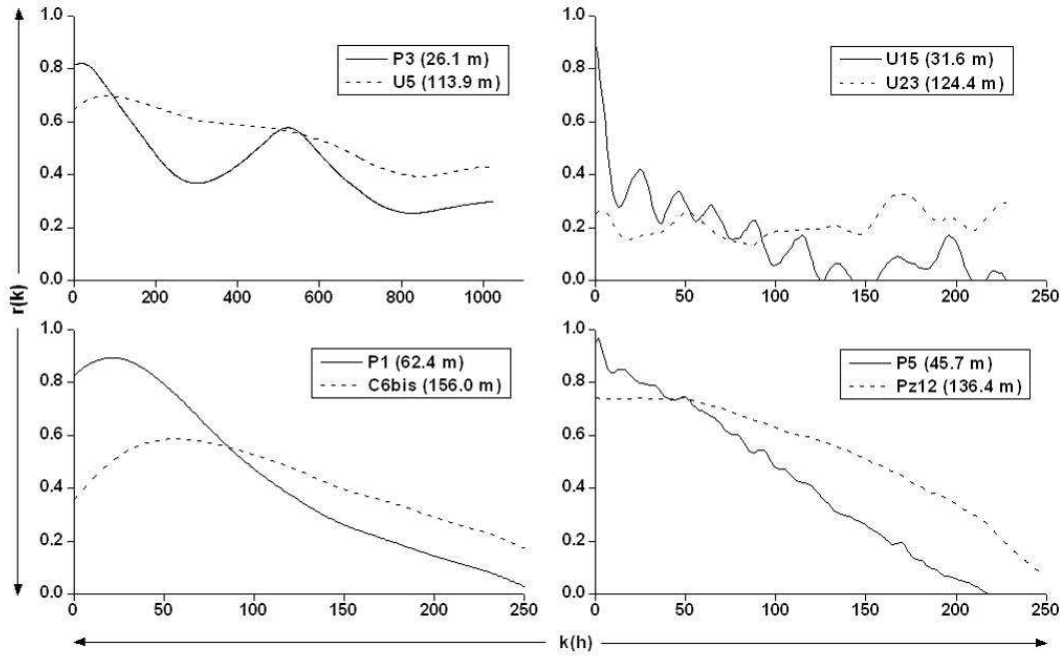

Figure 4.12. Cross-correlation functions between river-stage and groundwater level at different observation wells. Distance of observation wells to the Meuse River is showed in brackets.

Based on Table 4.2 and Figure 4.13, one can notice that, unsurprisingly, the time delay increases with the distance. Based on the theory (Workman *et al.*, 1997; Serrano and Workman, 1998; Hogarth *et al.*, 1999; Srivastava *et al.*, 2006) the delay should be a function of the aquifer diffusivity (β).

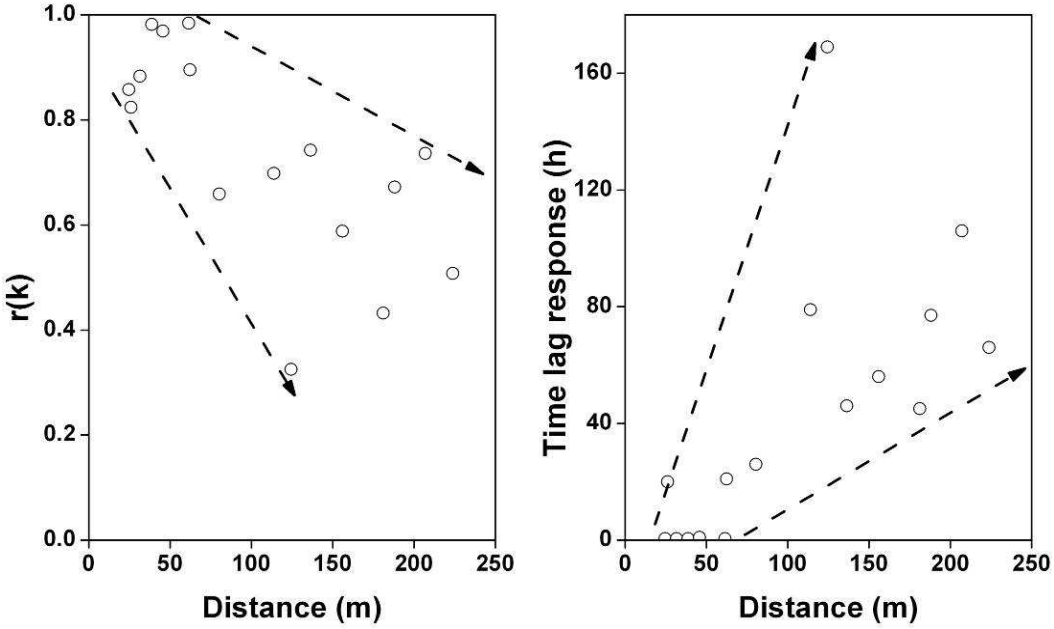

Figure 4.13. Relation between distance to the river and cross-correlation coefficient ($r(k)$) (left); and time lag response ($k(h)$) (right).

4.2.5.2. Cross-correlation analysis between rainfall and groundwater levels

Cross-correlation functions were also calculated between rainfall (input) and groundwater levels (output) in different observation wells. Cross-correlation functions are presented in Figure 4.14 and cross-correlation results and time lags are summarised in Table 4.2.

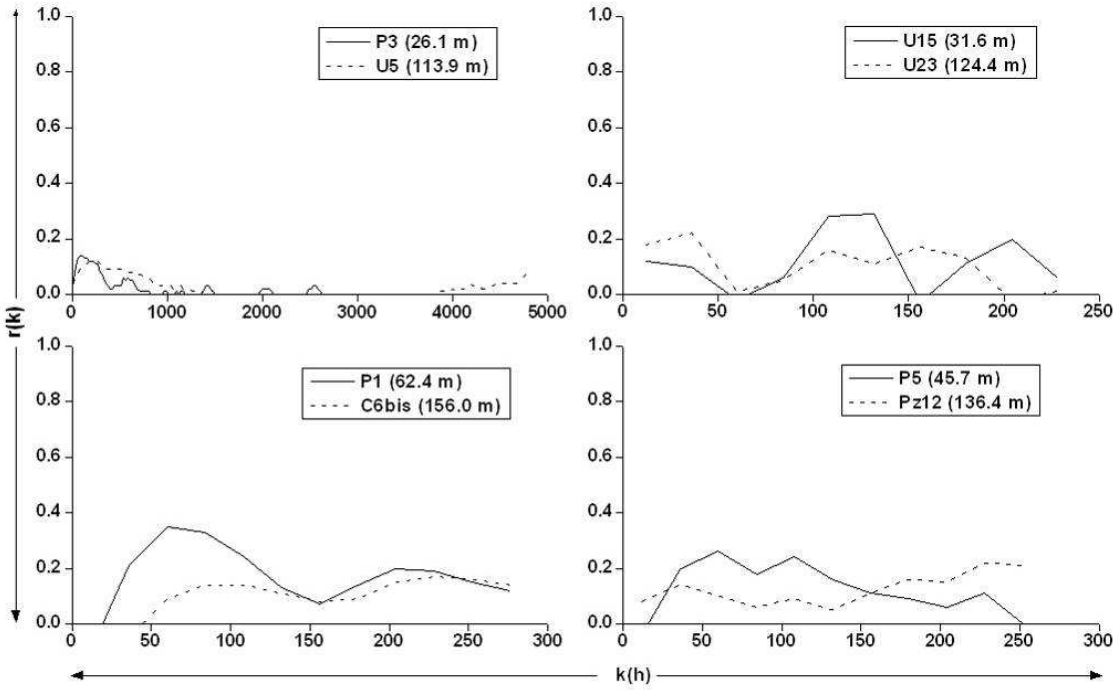

Figure 4.14. Cross-correlation functions between rainfall and groundwater levels at different observation wells.

As compared to cross-correlations coefficients observed between river water and groundwater levels (as high as 0.8 to 0.9), the maximum correlation between rainfall and groundwater levels is significantly lower (maximum of 0.3). This indicates that rainfall and direct groundwater recharge do not play a significant influence on the dynamics of groundwater levels in the alluvial aquifer in Flémalle.

4.2.6. Conclusions on data mining and monitoring

The continuous monitoring of river water level and temperature, groundwater level and temperature and daily rainfall has enabled to assess that the dynamics of groundwater levels depends mainly on river – stage variations.

Any change in the surface water level produces a pressure wave that propagates into the aquifer with an amplitude that is progressively attenuated as distance from the river increases. Practically speaking, this also confirms that the riverbank is not impervious and the exchange between groundwater in the alluvial aquifer and the Meuse River does occur.

In Chapter 5, these data will be further used and processed to develop an analytical model (STWT1) of groundwater – surface water interactions, and a numerical model (MODFLOW) of groundwater flow and contaminant transport.

4.3. Pumping tests

All deep wells in the site have diameters of 2" (~5 cm) and 4" (~10 cm), except for 6 wells (P1, P2, P3, P4, P5 and P6) close to the Meuse River, with a diameter of 6" (~15 cm). Pumping tests were carried out in these 6 wells in order to have the possibility to pump at a sufficient rate to produce measurable drawdowns in the aquifer. During each pumping test, between 6 and 10 observation wells were monitored at different distances and depths (Table 4.3) (Figure 4.15).

Table 4.3 Pumping and observation wells used during the pumping tests

Pumping test type	Date	Pumping well	Observation wells
Constant rate	17.05.2006	P4	1, 2, 6, P2, P3, P5, U10, U11, U14, U15
	28.05.2005	P5	1, 2, 6, 7, P3, P4, U5, U14, U15
Step-wise	31.05.2006	P1	A4p, A5, B4p, B5p, B6p, P2, U9
	30.05.2006	P2	A2p, A3, A4p, P1, P4, U10
	19.05.2006	P3	A2p, A3, P1, P2, P4, P5, U5, U8, U9, U10
	02.06.2006	P6	8, P5, U15, U16, U17, U19

Step-wise pumping tests at different discharge rates were performed in wells P1, P2, P3 and P6. Constant rate pumping tests were performed in wells P4 and P5 (Figure 4.15). Pumping tests were performed using an immersed pump Grundfos SQ35-5, the monitoring of groundwater levels being performed either manually or using pressiometric Level TROLL® probes.

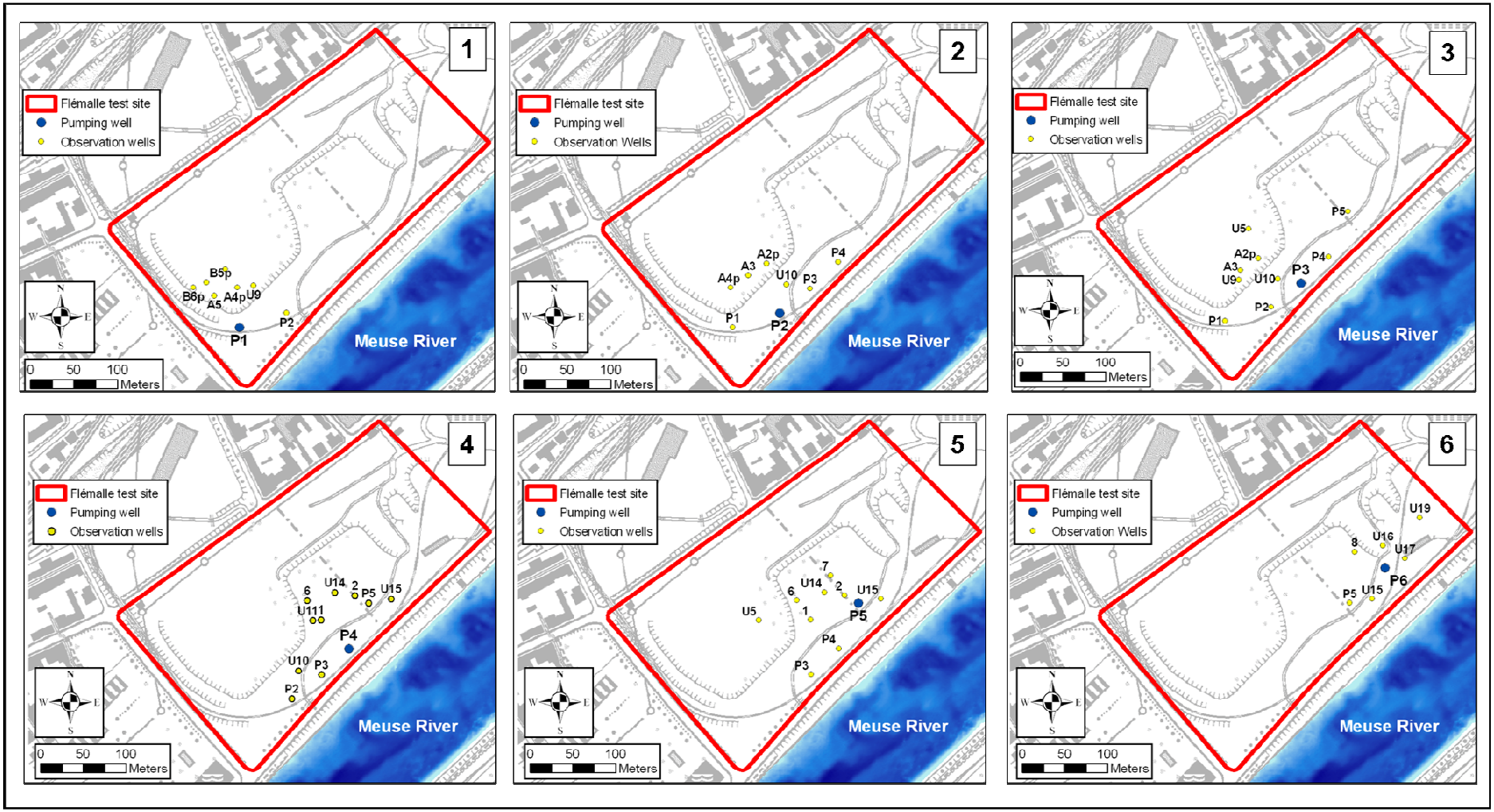

Figure 4.15. Location of pumping and observation wells during the pumping test campaign.

4.3.1. Interpretation methods

Interpretation of the pumping tests was performed, in a first instance, without taking into account the influence of the Meuse River.

Hydraulic conductivity values corresponding to drawdown and recovery periods of constant rate pumping tests, and recovery period of step-wise pumping tests were calculated using the Theis-Jacob method. Although this method is designed for confined aquifers, it can be applied for unconfined aquifers if drawdowns observed in monitoring wells are not greater than 15% of the saturated aquifer height, which is observed in most of the monitoring wells. The Theis-Jacob equation to be used for the drawdown period is written as follows:

$$\Delta h = \frac{0.183 Q_p}{T} \log\left(\frac{2.25T}{x^2 S}\right) + \frac{0.183 Q_p}{T} \log t \qquad (4.2)$$

where Δh is the drawdown [L]; Q_p is the pumping rate [L^3 T^{-1}]; T is the aquifer transmissivity [L T^{-1}]; x is the distance between the pumping and observation well [L]; S is the aquifer storage coefficient [-]; and t is the time [T]. The equation used for the recovery period is:

$$\Delta h_{rec} = \frac{0.183 Q_p}{T} \log\left(\frac{t}{t'}\right) \qquad (4.3)$$

where Δh_{rec} is the drawdown during the recovery period [L]; and t' is the time since the cessation of pumping [T].

Drawdown period corresponding to the step-wise period was calculated using the Dupuit's and the Birsoy - Summer methods. The Dupuit's method, designed for unconfined aquifers, is based on the following equation:

$$h^2 - h_0^2 = \frac{0.73 Q_p}{K} \log R_{\mathrm{inf}} - \frac{0.73 Q_p}{K} \log x \qquad (4.4)$$

where h and h_0 are the groundwater head before the pumping tests and after groundwater level stabilisation [L]; and R_{inf} is the radius of influence [L].

The Birsoy-Summer's method is an analytical solution for the drawdown response in a confined aquifer pumped step-wise at different discharge rates. For the drawdown in the aquifer at time *t* during the nth pumping discharge, the following equation is used:

$$\Delta h = \frac{0.183 Q_{p(n)}}{T} \log\left[\left(\frac{2.25T}{x^2 S}\right)\chi_{t(n)}\left(t-t_n\right)\right] \tag{4.5}$$

where

$$\chi_{t(n)}\left(t-t_n\right) = \sum_{i=1}^{n}\left(t-t_i\right)^{\Delta Q_{p(i)}/Q_{p(n)}} = \left(t-t_1\right)^{\Delta Q_{p(1)}/Q_{p(n)}} \times \left(t-t_2\right)^{\Delta Q_{p(2)}/Q_{p(n)}} \times \ldots \times \left(t-t_n\right)^{\Delta Q_{p(n)}/Q_{p(n)}} \tag{4.6}$$

where $\Delta Q_{p(i)} = Q_{p(i)} - Q_{p(i-1)}$ is the discharge increment beginning at time t_i [L^3 T^{-1}].

These methods were only applied to drawdowns and/or recoveries observed in observation wells. Drawdowns measured in pumping wells were not considered in the interpretation in order to avoid problems related to possible head losses.

4.3.2. Pumping test at well P1

Five steps at increasing pumping rates (3.4, 5.7, 13.5, 16.4 and 21.0 m^3 h^{-1}) during 3 h were performed in well P1. 7 observation wells were monitored manually (A4p, B4p and B5p) or using pressiometric probes (A5, B6p, P2, and U9). Groundwater level stabilisation was almost achieved at each pumping step excepting in the last step. Maximum drawdown monitored in observation wells was around 16 cm in observation well P2, located at 56.1 meters from the pumping well. Drawdowns in the rest of piezometers were between 4 and 12 cm, depending on the distance to the pumping well.

Measured drawdowns and the corresponding *K* values of pumping test at well P4 are presented in Figure 4.16 and in Table 4.4, respectively.

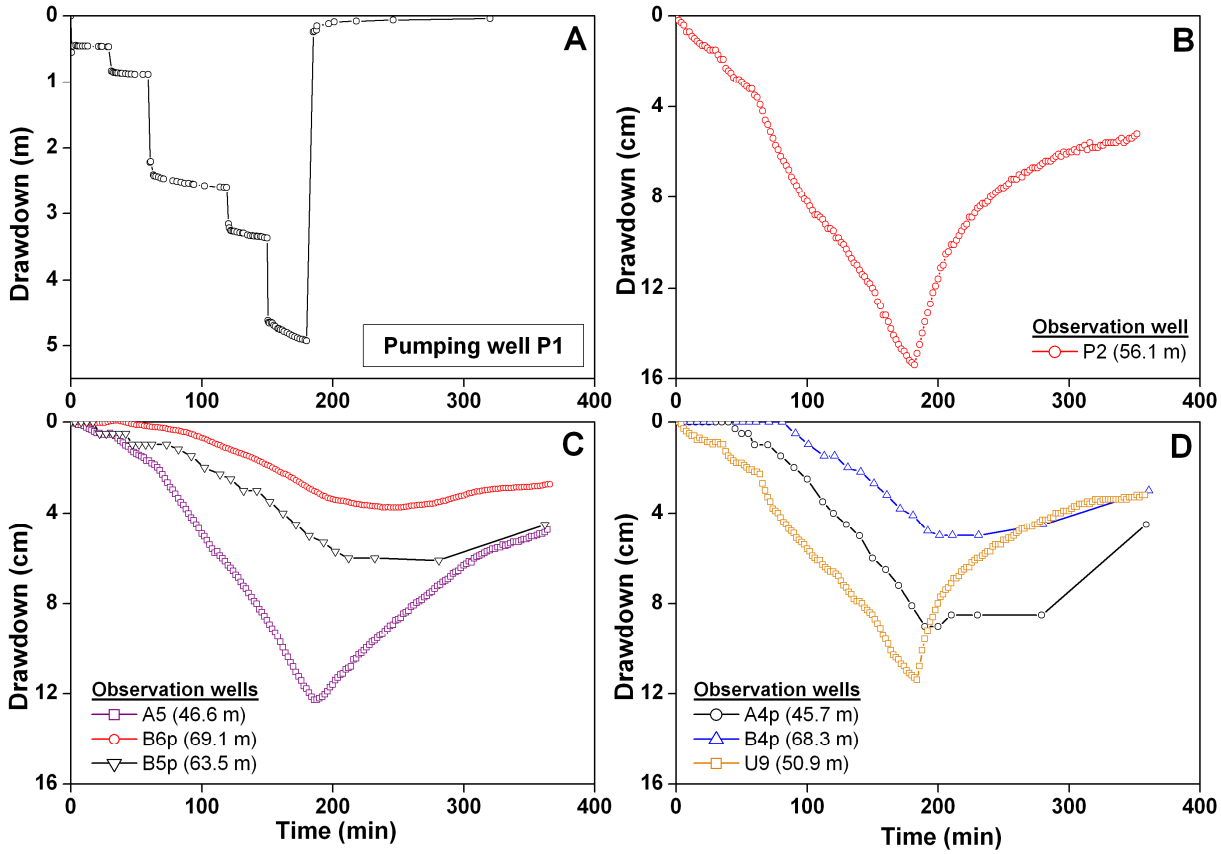

Figure 4.16. Drawdown curves of the pumping test performed at well P1 (A) and corresponding observation wells (B, C and D).

Table 4.4 Hydraulic conductivity values obtained after interpretation (Dupuit and Birsoy-Summer's for the drawdown period and Theis-Jacob for the recovery period) of pumping test at well P1 (Q_p = pumping rate; R_{inf} = radius of influence; K = hydraulic conductivity)

Pumping well P1 (Dupuit interpretation)										
Pumping step	**Q_p (m^3 h^{-1})**	**Time step (h)**	**R_{inf} (m)**	**Drawdown K (m s^{-1})**						
				P2 (56.1 m)	**U9 (50.9 m)**	**A5 (46.6 m)**	**A4p (45.7 m)**	**B4p (68.3 m)**	**B5p (63.4 m)**	**B6p (69.1 m)**
1	3.4	0.5	58.9	2.75×10^{-4}	8.11×10^{-4}	3.58×10^{-3}	--	--	1.26×10^{-3}	--
2	5.7	0.5	61.4	3.45×10^{-4}	9.38×10^{-4}	2.39×10^{-3}	4.83×10^{-3}	4.06×10^{-4}	2.11×10^{-3}	6.58×10^{-4}
3	13.5	1.0	60.9	2.73×10^{-4}	6.58×10^{-4}	1.50×10^{-3}	3.84×10^{-3}	3.21×10^{-4}	1.67×10^{-3}	1.56×10^{-3}
4	16.4	0.5	61.9	7.98×10^{-4}	1.85×10^{-3}	3.49×10^{-3}	7.05×10^{-3}	4.88×10^{-4}	3.05×10^{-3}	5.93×10^{-4}
5	21.0	0.5	60.6	7.54×10^{-4}	1.68×10^{-3}	3.61×10^{-3}	8.68×10^{-3}	5.37×10^{-4}	2.61×10^{-3}	5.69×10^{-4}
Recovery (Theis-Jacob)	--	--	--	4.68×10^{-3}	1.1×10^{-2}	6.12×10^{-3}	3.46×10^{-2}	1.27×10^{-2}	1.73×10^{-2}	1.78×10^{-2}
Pumping well P1 (Birsoy-Summer's interpretation)										
1	3.4	0.5	--	6.10×10^{-3}	2.01×10^{-2}	2.63×10^{-2}	--	--	--	8.50×10^{-2}
2	5.7	0.5	--	6.30×10^{-3}	1.36×10^{-2}	1.65×10^{-2}	--	--	--	5.45×10^{-2}
3	13.5	1.0	--	5.22×10^{-3}	1.44×10^{-2}	1.20×10^{-2}	1.52×10^{-2}	1.43×10^{-2}	1.75×10^{-2}	3.02×10^{-2}
4	16.4	0.5	--	6.42×10^{-3}	1.41×10^{-2}	1.01×10^{-2}	1.05×10^{-2}	4.33×10^{-2}	1.04×10^{-2}	3.69×10^{-2}
5	21.0	0.5	--	6.68×10^{-3}	1.36×10^{-2}	1.08×10^{-2}	1.14×10^{-2}	3.91×10^{-2}	1.12×10^{-2}	3.49×10^{-2}

4.3.3. Pumping test at well P2

Two steps at increasing pumping rates (2.9 and 6.1 $m^3 h^{-1}$) during 2.5 hours were performed in well P2. A total of 7 observation wells were monitored manually (A2p, A3 and A4p) or using pressiometric probes (P1, P3, P4 and U10). Groundwater level stabilisation was almost achieved in each pumping step. The maximum drawdown observed was of 15 cm in well U10, located at 34.1 meters from pumping well.

Measured drawdowns and the corresponding *K* values of pumping test at well P4 are presented in Figure 4.17 and in Table 4.5, respectively.

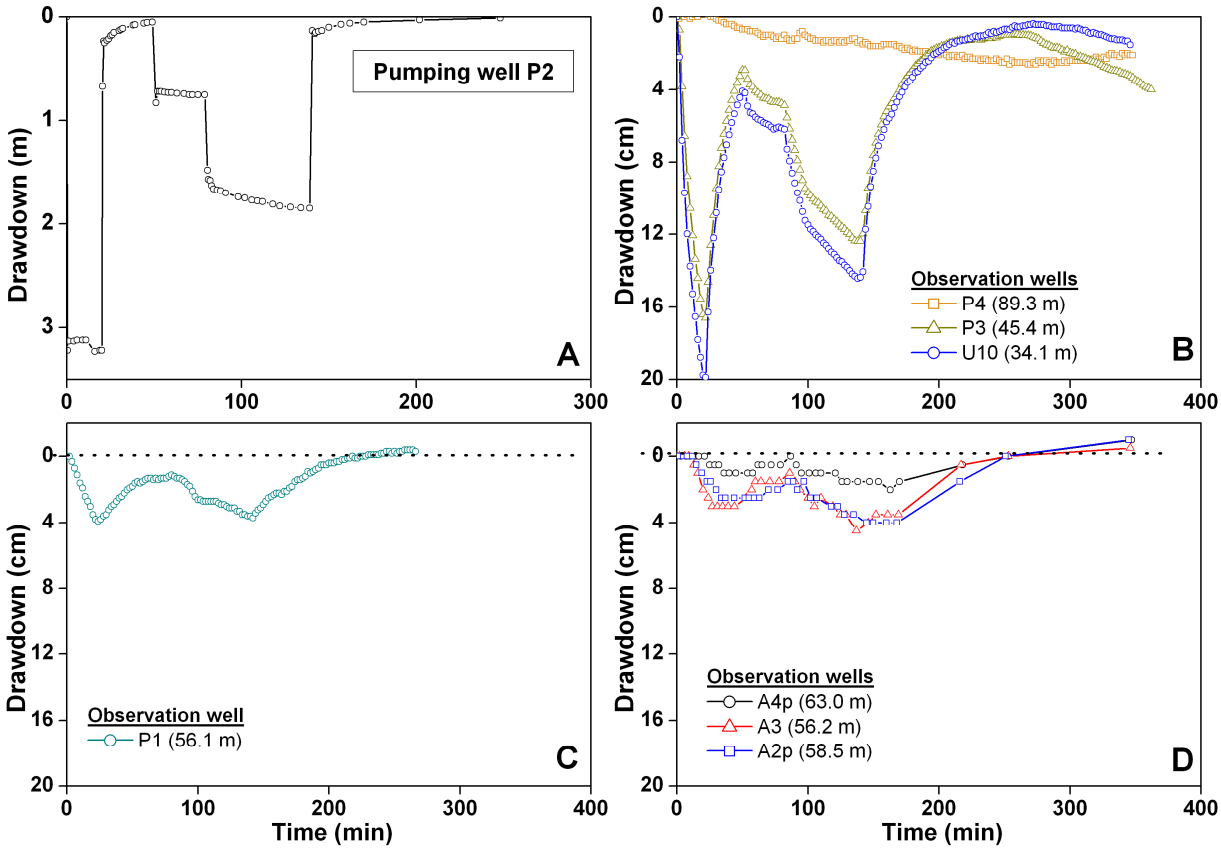

Figure 4.17. Drawdown curves of the pumping test performed at well P2 (A) and corresponding observation wells (B, C and D).

Table 4.5 Hydraulic conductivity values obtained after interpretation (Dupuit and Birsoy-Summer's for the drawdown period and Theis-Jacob for the recovery period) of pumping test at well P2 (Q_p = pumping rate; R_{inf} = radius of influence; K = hydraulic conductivity)

Pumping well P2 (Dupuit interpretation)										
Step pumping	**Q_p (m^3 h^{-1})**	**Time step (h)**	**R_{inf} (m)**	**Drawdown K (m s^{-1})**						
				P1 (56.1 m)	**P4 (88.9 m)**	**P3 (45.4 m)**	**U10 (34.1 m)**	**A4p (63.0 m)**	**A3 (56.2 m)**	**A2p (58.5 m)**
1	2.9	0.5	55.8	7.45×10^{-6}	--	3.70×10^{-5}	1.82×10^{-5}	1.47×10^{-5}	1.33×10^{-5}	1.95×10^{-5}
2	6.1	1.0	52.2	1.52×10^{-5}	--	6.68×10^{-5}	3.64×10^{-5}	3.07×10^{-5}	2.69×10^{-5}	4.05×10^{-5}
Recovery (Theis-Jacob)	--	--	--	3.8×10^{-3}	--	1.61×10^{-4}	2.76×10^{-3}	7.69×10^{-3}	7.22×10^{-3}	3.31×10^{-3}
Pumping well P2 (Birsoy-Summer's interpretation)										
1	--	0.5	--	--	--	1.20×10^{-3}	1.20×10^{-3}	--	--	--
2	--	1.0	--	6.02×10^{-4}	1.88×10^{-3}	1.29×10^{-4}	3.64×10^{-4}	--	2.84×10^{-4}	3.38×10^{-4}

4.3.4. Pumping test at well P3

At well P3, three steps during 2.5 h were performed at increasing pumping rates (14.5, 17.5 and 21.7 m^3 h^{-1}, respectively). 10 observation wells were monitored manually (A2p, A3, U5, U8 and U9) or using pressiometric probes (P1, P2, P4, P5 and U10).

Groundwater level stabilisation was reached at each pumping step. Observed drawdowns were not always proportional to the distance from the pumping well, reflecting again the important spatial heterogeneity in the alluvial aquifer. For example, in observation well U5, located at 110.2 meters, a maximum drawdown of 12 cm was monitored, while in observation P4, located at 44.3 meters from the pumping well, a very small drawdown of 2 cm could be observed. For P4, this can be also explained by a possible influence of the Meuse River, being this one the nearest well to the river.

Measured drawdowns and the corresponding *K* values of pumping test at well P4 are presented in Figure 4.18 and in Table 4.6, respectively.

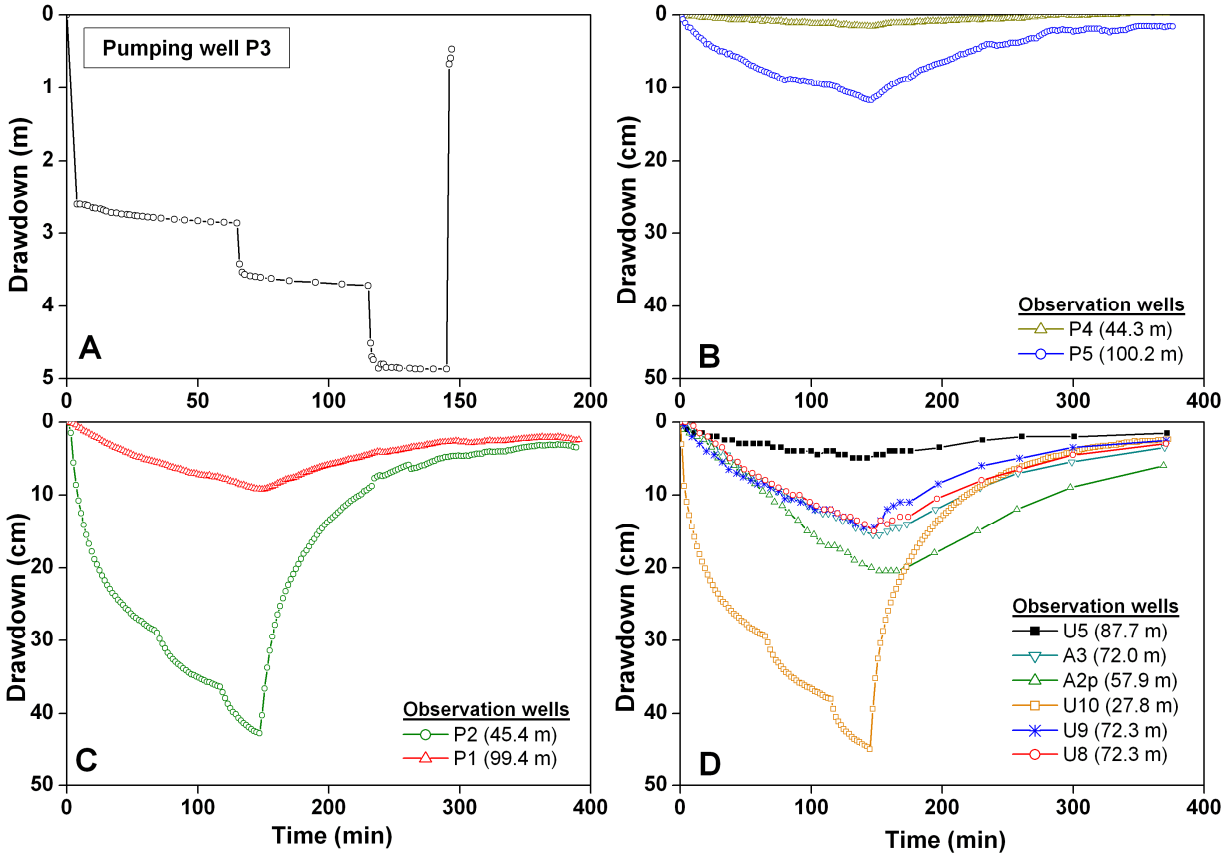

Figure 4.18. Drawdown curves of the pumping test performed at well P3 (A) and corresponding observation wells (B, C and D).

Table 4.6 Hydraulic conductivity values obtained after interpretation (Dupuit and Birsoy-Summer's for the drawdown period and Theis-Jacob for the recovery period) of pumping test at well P3 (Q_p = pumping rate; R_{inf} = radius of influence; K = hydraulic conductivity)

Pumping well P3 (Dupuit interpretation)												
Pumping step	**Q_p ($m^3 h^{-1}$)**	**Time step (h)**	**R_{inf} (m)**	**Drawdown K ($m s^{-1}$)**									
				P2 (45.4 m)	**P1 (99.4 m)**	**P4 (44.3 m)**	**P5 (100.3 m)**	**U10 (27.8 m)**	**U8 (72.3 m)**	**U5 (87.7 m)**	**U9 (72.3 m)**	**A3 (72.0 m)**	**A2p (58.3 m)**
1	14.5	1.1	83.7	3.32×10^{-4}	3.54×10^{-4}	1.31×10^{-2}	3.26×10^{-4}	5.17×10^{-4}	1.98×10^{-3}	1.17×10^{-3}	6.66×10^{-4}	9.76×10^{-4}	2.70×10^{-3}
2	17.5	0.8	126.5	1.38×10^{-3}	8.66×10^{-4}	2.27×10^{-2}	1.28×10^{-3}	2.08×10^{-3}	5.02×10^{-3}	4.35×10^{-3}	2.02×10^{-3}	2.18×10^{-3}	4.43×10^{-3}
3	21.7	0.5	104.6	2.13×10^{-3}	1.42×10^{-3}	3.49×10^{-2}	1.43×10^{-3}	3.18×10^{-3}	2.78×10^{-3}	5.35×10^{-3}	3.49×10^{-3}	4.04×10^{-3}	1.20×10^{-2}
Recovery (Theis-Jacob)	--	--	--	1.68×10^{-3}	1.96×10^{-3}	2.29×10^{-2}	1.23×10^{-3}	3.41×10^{-3}	1.03×10^{-2}	3.56×10^{-2}	8.64×10^{-3}	1.18×10^{-2}	2.83×10^{-3}
Pumping well P3 (Birsoy-Summer's interpretation)													
1	14.5	1.1	--	8.36×10^{-4}	2.59×10^{-3}	1.74×10^{-2}	2.22×10^{-3}	4.74×10^{-3}	1.35×10^{-2}	3.86×10^{-2}	9.06×10^{-3}	1.40×10^{-2}	6.86×10^{-3}
2	17.5	0.8	--	1.28×10^{-3}	3.53×10^{-3}	1.76×10^{-2}	4.64×10^{-3}	5.95×10^{-3}	1.98×10^{-2}	3.27×10^{-2}	1.22×10^{-2}	2.02×10^{-2}	5.87×10^{-3}
3	21.7	0.5	--	1.18×10^{-3}	4.65×10^{-3}	1.59×10^{-2}	3.01×10^{-3}	6.64×10^{-3}	3.48×10^{-2}	3.62×10^{-2}	1.40×10^{-2}	2.85×10^{-2}	1.21×10^{-2}

4.3.5. Pumping test at well P4

A pumping test at a constant rate of 30.9 m^3 h^{-1} was performed in well P4. 10 observation wells were monitored manually (1, 2, 6, U11 and U14) or using pressiometric probes (P2, P3, P5, U10 and U15). Stabilisation of the groundwater level was not really achieved after 3 h of pumping. A maximum drawdown of 7 cm was observed in well U15, located at 76.6 m of P4. Measured drawdowns and the corresponding *K* values of pumping test at well P4 are presented in Figure 4.19 and in Table 4.7, respectively.

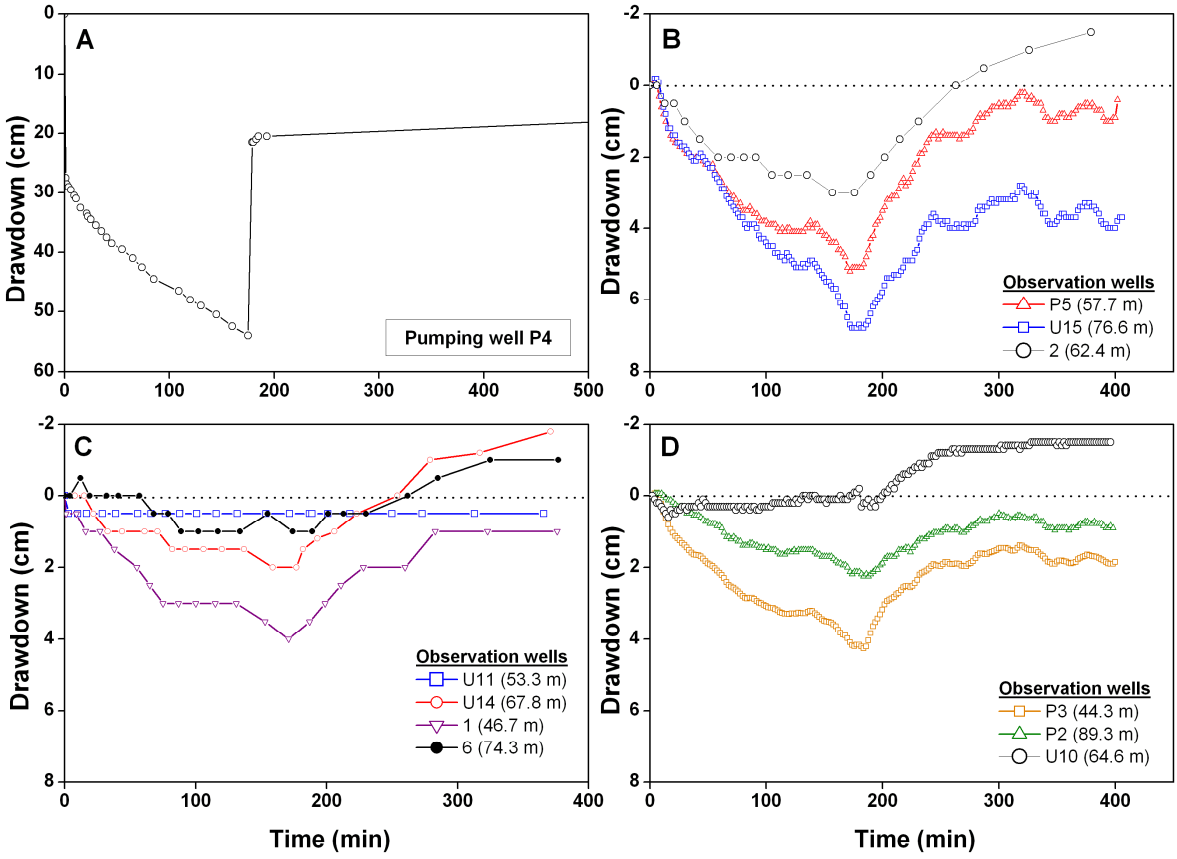

Figure 4.19. Drawdown curves of the pumping test performed at well P4 (A) and corresponding observation wells (B, C and D).

Table 4.7. Hydraulic conductivity values obtained after interpretation of the pumping test at well P4 (Q_p: pumping rate; K: aquifer hydraulic conductivity; S: aquifer storage coefficient)

Q_p ($m^3\ h^{-1}$)	Observation well	Distance to pumping well (m)	Maximum drawdown (cm)	K ($m\ s^{-1}$)		S (-)
				Drawdown period	Recovery period	
30.9	P3	44.3	4.2	1.59×10^{-2}	1.54×10^{-2}	0.03
	1	46.7	4.0	4.50×10^{-2}	4.08×10^{-2}	0.06
	U11	53.3	0.5	--	--	--
	P5	57.7	5.2	6.54×10^{-3}	7.52×10^{-3}	0.02
	2	62.4	3.0	5.17×10^{-2}	2.43×10^{-2}	0.05
	U10	64.6	1.0	--	--	--
	U14	67.8	2.0	--	--	--
	6	74.3	1.0	3.19×10^{-2}	3.21×10^{-2}	--
	U15	76.6	6.8	8.67×10^{-3}	1.27×10^{-2}	0.01
	P2	89.3	2.2	1.73×10^{-2}	1.83×10^{-2}	0.05

4.3.6. Pumping test at well P5

A pumping test at a constant rate of 5.5 $m^3\ h^{-1}$ was performed in well P5, reduced later to 4.8 $m^3\ h^{-1}$ in order to achieve stabilisation of the groundwater level. 9 observation wells were monitored using pressiometric probes (1, 2, 6, P3, P4, P5, U5, U14 and U15). The duration of the pumping test was of 23.5 h. A maximum drawdown of 30 cm was observed in well 2, located at 18.1 meters of P5. It is worth noticing that at well P4, located at 57.7 meters from P5, the measured drawdown was the same (8 cm) that the drawdown observed at well U5, located at 118.2. This reflects again the spatial heterogeneity of the alluvial aquifer.

Most of the monitoring wells presented a “rebound” effect of groundwater level during the recovery period, consisting in a temporally increase of groundwater level higher than the initial level and a slow stabilisation to the initial level. This is explained by the variation of groundwater levels related to river stage variations in the Meuse River.

Measured drawdowns at observation wells and estimated K values are presented in Figure 4.20 and in Table 4.8, respectively.

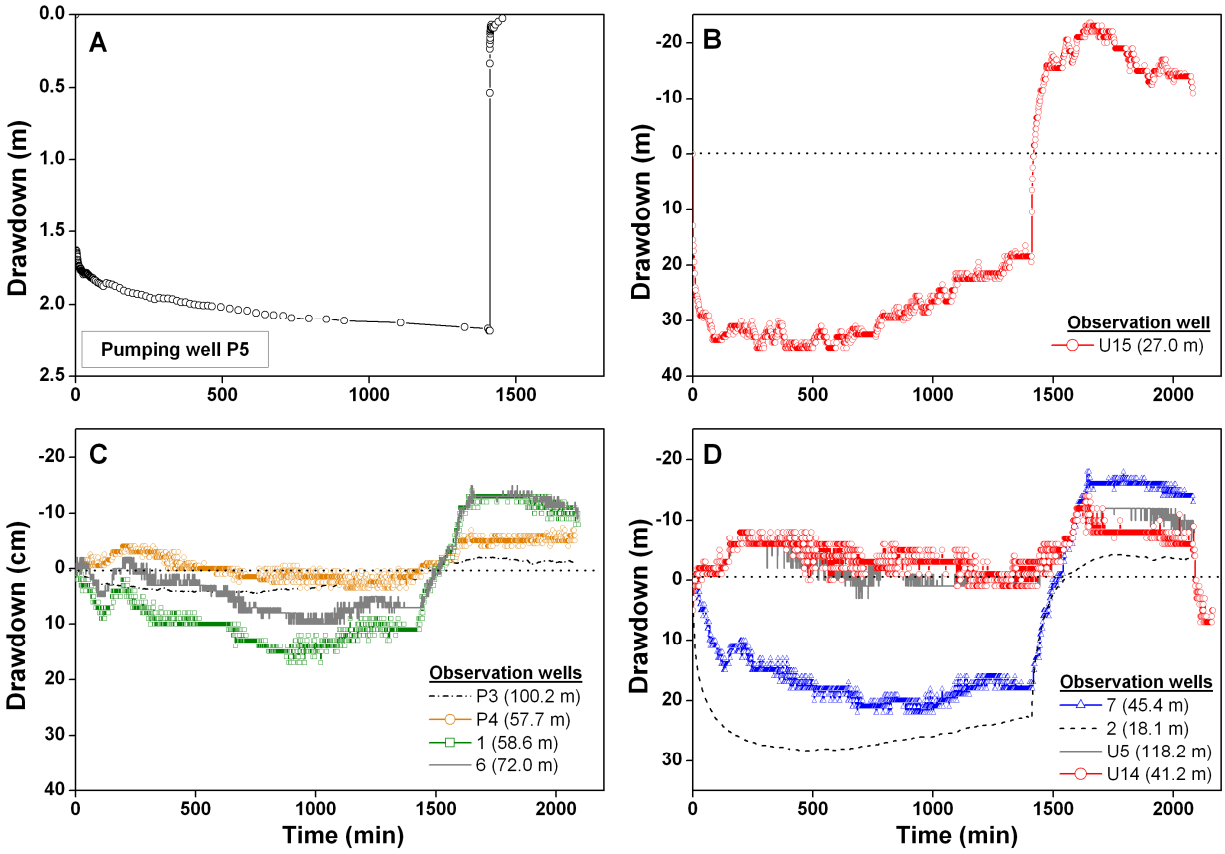

Figure 4.20. Drawdown curves of the pumping test performed at well P5 (A) and corresponding observation wells (B, C and D).

Table 4.8 Hydraulic conductivity values obtained after interpretation of the pumping test at well P5 (Q_p = pumping rate; K = hydraulic conductivity; S = aquifer storage coefficient)

Q_p (m^3 h^{-1})	Observation well	Distance to pumping well (m)	Maximum drawdown (cm)	K (m s^{-1})		S (-)
				Drawdown period	Recovery period	
5.5 to 4.8	2	18.1	28.3	1.83×10^{-3}	1.45×10^{-3}	0.0014
	U15	27.0	35.0	1.86×10^{-3}	1.63×10^{-3}	--
	U14	41.2	1.0	--	--	--
	7	45.4	22.0	2.19×10^{-3}	1.26×10^{-3}	0.0024
	P4	57.7	4.0	--	--	--
	1	58.6	17.0	2.70×10^{-3}	1.37×10^{-3}	0.0059
	6	72.0	10.0	9.04×10^{-4}	1.44×10^{-3}	0.025
	P3	100.2	4.4	6.36×10^{-3}	6.16×10^{-3}	0.0026
	U5	118.2	8.0	--	--	--

4.3.7. Pumping test at well P6

At well P6, three steps during 3.4 h were performed at increasing pumping rates (10.5, 13.2 and 21.5 $m^3 h^{-1}$). 6 observation wells were monitored manually (U16, U17 and U19) or using pressiometric probes (8, P5 and U15).

Groundwater level stabilisation was achieved at each pumping step. Maximum drawdown in monitored wells was of 80 cm, observed in well U17, located at 24.7 meters of P6, while wells located farther, like P5 and U19, at 58.5 and 71.4 meters respectively, maximum drawdowns of 20 cm were observed. A rebound effect was also observed in all the monitoring wells during the recovery period, as occurred also during the recovery period of pumping test at well P5.

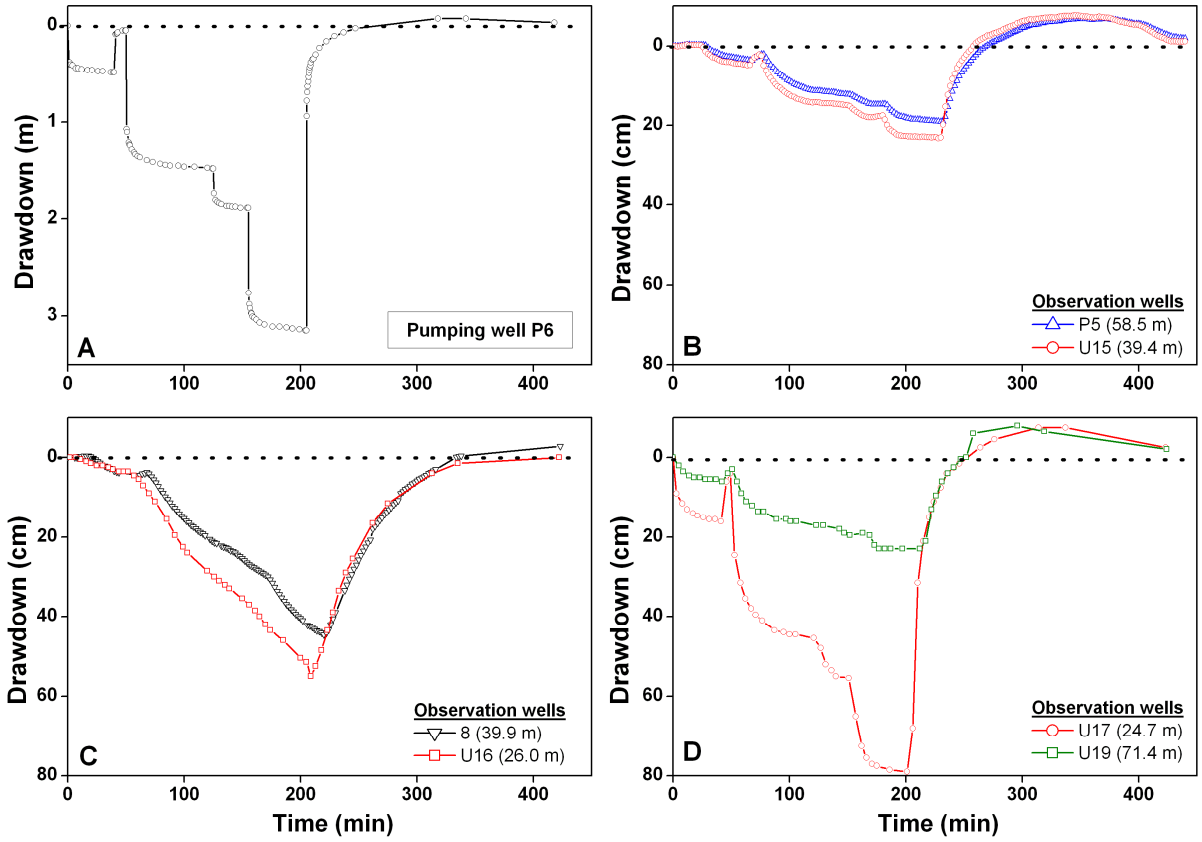

Figure 4.21. Drawdown curves of the pumping test performed at well P6 (A) and corresponding observation wells (B, C and D).

Table 4.9 Hydraulic conductivity values obtained after interpretation (Dupuit and Birsoy-Summer's for the drawdown period and Theis-Jacob for the recovery period) of pumping step test at well P6 (Q_p = pumping rate; R_{inf} = radius of influence; K = hydraulic conductivity)

Pumping well P6 (Dupuit interpretation)									
Step pumping	**Q_p (m^3 h^{-1})**	**Time step (h)**	**R_{inf} (m)**	**Drawdown K (m s^{-1})**					
				P5 (58.1 m)	**U15 (39.6 m)**	**U16 (25.6 m)**	**U17 (26.5 m)**	**U19 (71.6 m)**	**8 (39.9 m)**
1	10.5	1.25	84.2	2.48×10^{-4}	5.01×10^{-4}	1.95×10^{-3}	4.91×10^{-4}	1.03×10-4	6.71×10^{-4}
2	13.2	0.5	126.5	1.18×10^{-3}	2.52×10^{-3}	1.13×10^{-2}	6.29×10^{-4}	5.86×10-4	2.81×10^{-3}
3	21.5	0.8	104.6	1.03×10^{-3}	1.92×10^{-3}	8.30×10^{-3}	1.28×10^{-3}	6.84×10-4	1.93×10^{-3}
Recovery (Theis-Jacob)	--	--	--	6.30×10^{-4}	1.35×10^{-3}	1.03×10^{-3}	7.70×10^{-4}	1.43×10-3	4.31×10^{-4}
Pumping well P6 (Birsoy-Summer's interpretation)									
1	10.5	1.25	--	2.52×10^{-4}	4.63×10^{-4}	2.83×10^{-4}	3.35×10^{-4}	6.48×10^{-4}	1.71×10^{-4}
2	13.2	0.5	--	2.74×10^{-4}	3.74×10^{-4}	6.82×10^{-4}	2.94×10^{-4}	4.96×10^{-4}	2.15×10^{-4}
3	21.5	0.8	--	5.86×10^{-4}	7.67×10^{-4}	8.23×10^{-4}	5.03×10^{-4}	6.53×10^{-4}	2.72×10^{-4}

4.3.8. First conclusions drawn from the pumping tests

4.3.8.1. Influence of the Meuse River

Because the Meuse River is likely to have an influence on the pumping test results, further interpretations of the pumping tests were performed considering the river equivalent to a constant piezometric level. This correction to the Dupuit analytical solution, called the Dietz method (image well method), takes into account the effect of the river by considering a virtual injection well or (image well) on the opposite side from the river, at the same distance as between the pumping well and the river. The image well has a prescribed injection rate equal to the pumping rate of the real well. The results of the Dietz method are generally considered as more representative than those obtained with the classical Dupuit interpretations because the interpretation takes into account the presence of the river, which acts as a prescribed piezometric level boundary condition. This methodology was evaluated with data from constant rate pumping test performed in well P4 (Table 4.10).

Table 4.10 Comparison of *K* values in pumping test at well P4, wih the classical Theis-Jacob interpretation and the Dietz method (*K*: hydraulic conductivity).

Pumping well P4	*K* (m s^{-1})		
	Theis-Jacob		Dietz
	Drawdown period	Recovery period	
P3	1.59×10^{-2}	1.54×10^{-2}	3.46×10^{-3}
P5	6.54×10^{-3}	7.52×10^{-3}	2.92×10^{-3}
P2	1.73×10^{-2}	1.83×10^{-2}	3.15×10^{-3}
U15	8.67×10^{-3}	1.27×10^{-2}	1.26×10^{-3}
1	4.50×10^{-2}	4.08×10^{-2}	4.84×10^{-3}
2	5.17×10^{-2}	2.43×10^{-2}	4.91×10^{-3}

As expected, hydraulic conductivity values obtained with this interpretation framework are lower, around one order of magnitude, than those obtained with the classical Theis-Jacob interpretation.

The pumping well P4 is the closest to the Meuse River (24.6 m) and it is where the maximum pumping rate was possible (30.9 m^3 h^{-1}), at the same time as monitored drawdowns were very low, sometimes not measurable in most of the observation wells around. When well P4 was used as an observation well during pumping tests performed in other wells, measured drawdowns were often too low to perform a reliable interpretation (see interpretation results from pumping tests in wells P5 and P2 -Table 4.8 and Table 4.5-, or even in well P3 -Table

4.6-, where hydraulic conductivity values are significantly high in comparison with obtained in surrounding observation wells). This fact seems to evidence that the well P4 is strongly influenced by the proximity of the river, which keeps its piezometric level relatively invariable. This fact is translated by an apparent higher value of hydraulic conductivity when the river is not considered during pumping test interpretations.

The influence of the Meuse River to the aquifer hydrodynamics is also clearly visible on the drawdown curves, in the form of rebound effects observed during most recovery phases of the tests.

4.3.8.2. Spatial heterogeneity of the alluvial gravels

Hydraulic conductivity values estimated from pumping tests are lower than expected for an alluvial aquifer, ranging from 1×10^{-5} to 1×10^{-3} m s^{-1}. The spatial distribution of these values and differences in monitored drawdowns in function of the distance and direction, seem to indicate that the heterogeneity of the hydraulic conductivity field plays an important role on the hydrodynamics of the alluvial aquifer.

Adjusted *K* values obtained at a same observation well can differ of 1 order of magnitude according to the pumping test location. Table 4.11 presents a comparison of hydraulic conductivity values for a same observation well obtained from pumping tests performed at different wells. Comparing the *K* values corresponding to the recovery period (K_{rec}), differences of one order of magnitude for a same observation well are obtained (i.e. observation wells 1, 6, P3 and P5). This is mainly due to differences of the hydraulic conductivity between the pumping and observation well from one location to another, evidencing an important spatial heterogeneity of the hydraulic conductivity in the alluvial aquifer. This draws the conclusion that the modelling approach considered in Chapter 5 will have to be able to take explicitly into account the spatial variability of the hydraulic conductivity field.

Table 4.11. Comparison of *K* values at a same observation well, obtained from pumping tests at different wells (K_{draw}: hydraulic conductivity corresponding to the drawdown period; K_{rec}: hydraulic conducitivity corresponding to the recovery period).

Observation well	Pumping well	Distance (m)	Maximum drawdown (cm)	K_{draw} (m s^{-1})	K_{rec} (m s^{-1})
2	P4	62.4	3.0	5.17×10^{-2}	2.43×10^{-2}
	P5	18.1	28.3	1.83×10^{-3}	1.45×10^{-3}
U15	P4	76.6	6.8	8.67×10^{-3}	1.27×10^{-2}
	P5	27.0	35.0	1.86×10^{-3}	1.63×10^{-3}
	P6	39.6	23.4	3.74×10^{-4} – 2.52×10^{-3}	1.35×10^{-3}
6	P4	74.3	1.0	3.19×10^{-2}	3.21×10^{-2}
	P5	72.0	10.0	9.04×10^{-4}	1.44×10^{-3}
1	P4	46.7	4.0	4.50×10^{-2}	4.08×10^{-2}
	P5	58.6	17.0	2.70×10^{-3}	1.37×10^{-3}
P3	P4	44.3	4.2	1.59×10^{-2}	1.54×10^{-2}
	P5	100.3	4.4	6.36×10^{-3}	6.16×10^{-3}
P5	P3	100.3	5.2	3.26×10^{-4} – 4.64×10^{-3}	1.23×10^{-3}
	P4	57.7	5.1	6.54×10^{-3}	7.52×10^{-3}
	P6	58.1	19.4	2.48×10^{-4} – 1.18×10^{-3}	6.3×10^{-4}
A3	P2	56.2	4.5	1.82×10^{-5} – 1.29×10^{-4}	7.22×10^{-3}
	P3	72.0	15.5	9.76×10^{-4} – 2.85×10^{-2}	1.18×10^{-2}

4.4. Slug tests

In the most contaminated zone of the site, pumping tests could not be performed for two main reasons: (1) difficulties in managing the pumped polluted groundwater; and (2) the diameters of the wells were too small to perform pumping tests at a sufficient pumping rate to create measurable drawdowns. In order to obtain hydraulic conductivity values in these zones, slug permeability tests were carried out as an alternative.

The slug test consists in producing an instantaneous change in groundwater level in the well, usually by injecting rapidly an important volume of water in the well, and to monitor subsequently the rate at which the groundwater level returns to its initial state. The slug test has two main advantages. First, no water is extracted. Second, because water is injected, there are no head losses that might bias the interpretation afterwards. However, there is an important drawback: the permeability measurement is very local and its representativity is limited. Figure 4.22 shows the location of the wells where slug tests were carried out (U2, U3, U4, U5 and U12) and the well used for pumping water (P1) for injection.

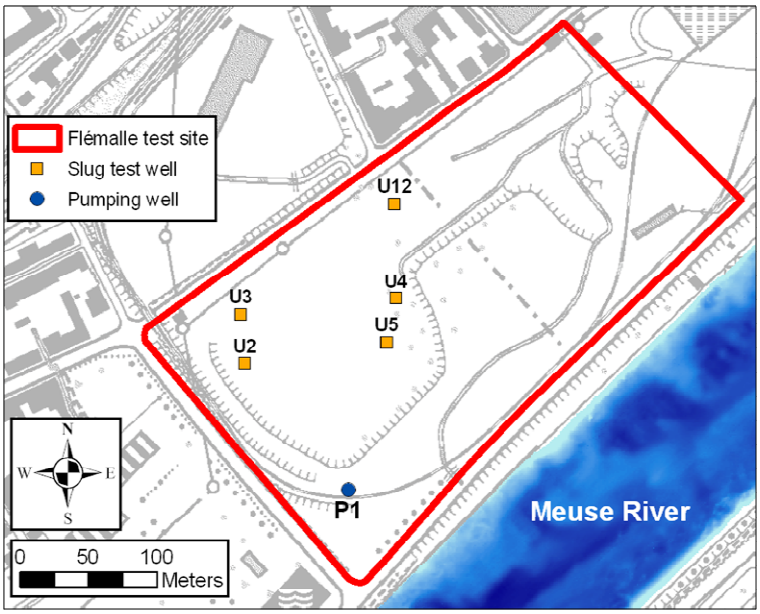

Figure 4.22. Location of wells used to perform slug tests.

Slug test interpretation was performed using the Bouwer and Rice method (Bouwer and Rice, 1976; Bouwer, 1989). The Bouwer and Rice equation is written as follows (Fetter, 2001):

$$K = \frac{r_w^2 \ln\left(R_e / r_{gp}\right)}{2e_{scr}} \frac{1}{t} \ln\left(\frac{h_0}{h_t}\right) \tag{4.7}$$

where K is the aquifer hydraulic conductivity [L T^{-1}]; r_w is the radius of the well casing [L]; r_{gp} is the radius of the gravel pack [L]; e_{scr} is the screen length of the well through which water can enter [L]; h_0 is the groundwater level in the well at initial time [L]; h_t is the groundwater level at time t [L]. Because there is no way to know exactly what could be the value of R_e for a given well, Bouwer and Rice (1976) presented a method for estimating the dimensionless ratio $\ln\left(R_e / r_{gp}\right)$, as follows:

$$\ln \frac{R_e}{r_{gp}} = \left[\frac{1.1}{\ln\left(L_w / r_{gp}\right)} + \frac{A + B \ln\left[\left(h - L_w\right) / r_{gp}\right]}{e_{scr} / r_{gp}} \right]^{-1} \tag{4.8}$$

where L_w is equal to b for fully penetrating wells and < b for partially penetrating wells (Figure 4.23); and A and B are dimensionless numbers that can be found from a theoretical diagram in Bouwer (1989).

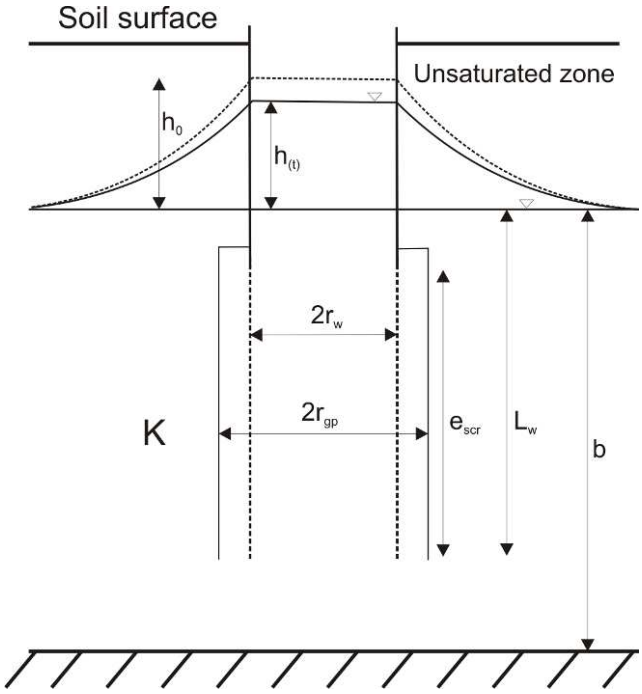

Figure 4.23. Geometry and symbols for a slug test on a partially penetrating well.

Hydraulic conductivities estimated using the presented Bouwer and Rice method are listed in Table 4.12.

Table 4.12. Hydraulic conductivity values obtained from slug tests experiments.

	U2	U3	U4	U5	U12
***K* (m s^{-1})**	8.38×10^{-6}	1.00×10^{-4}	5.60×10^{-4}	6.23×10^{-5}	3.99×10^{-4}

Although their very local representation, slug tests performed in the central zone of the Flémalle site confirms the low hydraulic conductivity values obtained in the pumping test experiments, with hydraulic conductivity values from 8.38×10^{-6} to 5.6×10^{-4} m s^{-1}.

4.5. Tracer experiments

Two tracer test campaigns with contrasted objectives were carried out in the Flémalle test site. The first one consisted in a radially converging flow tracer test aiming at identifying and quantifying hydrodispersive processes in the alluvial aquifer. The second tracer experiment consisted in performing single-well tracer tests using the Finite Volume Point Dilution Method (FVPDM) (Brouyère *et al.*, 2008). This second campaign of tracer experiments was performed with the goal of quantifying groundwater fluxes close to the Meuse River.

4.5.1. Radially converging flow tracer experiments

4.5.1.1. Experimental setup

Two injection phases were carried out between August - September 2005 (Phase I) and between December 2005 – February 2006 (Phase II). Injection wells were chosen as a function of the distance and position with regards to the recovery well (P5) (Figure 4.24). Table 4.13 summarises the main characteristics of the injections.

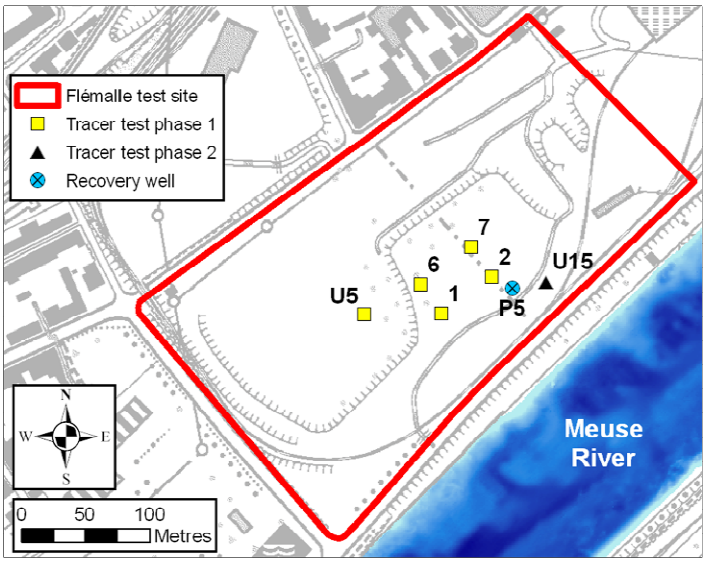

Figure 4.24. Location of the injection and recovery wells for the radially converging flow tracer experiments (Phases I and II).

Salt and fluorescent (dyes) tracers were used in both Phase I and II. Nitrate, lithium and iodide were used as salt tracers; eosin yellowish[7], naphtionate[8], uranine[9] and sulforhodamine B[10] were used as dye tracers.

An immersed pump Grundfos SQ35-5 was used to pump at well P5. The pumping rate (Q_{mean} = 3.5 m^3 h^{-1}) was held constant as much as possible, except small variations (mainly during the Phase I and beginning of the Phase II) to avoid drying out the well during river level decreases (Figure 4.25).

Table 4.13. Radially converging flow tracer tests: synthesis of the results. Q_p is the pumping rate during the tracer experiment; M_{inj} is the injected mass of tracer, T_{min} is the time of the first tracer arrival; V_{max} is the maximum velocity; T_{mod} is the modal arrival time of the tracer; V_{mod} is the modal velocity; R_{rec} is the recovered mass of tracer at the end of the monitoring; and T_{rec} is the duration of sampling/monitoring processes.

Phase	Well ID	Dist. (m)	Tracer	Q_p (m^3 h^{-1})	M_{inj} (kg)	T_{min} (h)	V_{max} (m h^{-1})	T_{mod} (h)	V_{mod} (m h^{-1})	R_{rec} (%)	T_{rec} (d)
Ph. I	Pz2	18.06	Nitrate (NO_3^-)	4.2 to 3	12.16	Not detected					
			Sulforhodamine B	4.2 to 3	0.10	Not detected					
	Pz1	58.06	Lithium (Li^+)	4.2 to 3	1.39	Not detected					
	Pz6	71.96	Iodide (I^-)	4.2 to 3	3.82	Not detected					
	Pz7	45.37	Naphtionate	4.2 to 3	1.00	Not detected					
	U5	118.19	Uranine	4.2 to 3	0.20	Not detected					
Ph. II	U15	27.00	Eosin yellowish	5.2 to 2.15	1.00	11.8	2.29	44.8	0.60	78.28	35.0
			Naphtionate	2.14	0.01	39.8	0.68	148.3	0.18	44.09	22.0
			Sulforhodamine B	2.14	0.01	43.8	0.62	-	-	0.80	34.5
			Uranine	2.14	0.01	43.8	0.62	219.3	0.12	16.69	32.5
			Lithium (Li^+)	2.08	0.60	48.6	0.55	144.6	0.19	31.77	25.7
			Iodide (I^-)	2.08	0.76	35.6	0.76	108.6	0.25	61.57	25.7

[7] Eosin yellowish. Chemical formula $C_{20}H_6Br_4Na_2O_5$ Main extinction wavelength: 516 nm
[8] Naphtionate (Sodium-naphtionate). Chemical formula $C_{10}H_8NNaO_3S$ Main extinction wavelength: 320 nm
[9] Uranine. Chemical formula $C_{20}H_{10}Na_2O_5$ Main extinction wavelength: 491 nm
[10] Sulforhodamine B. Chemical formula $C_{27}H_{29}N_2NaO_7S_2$ Main extinction wavelength: 564 nm

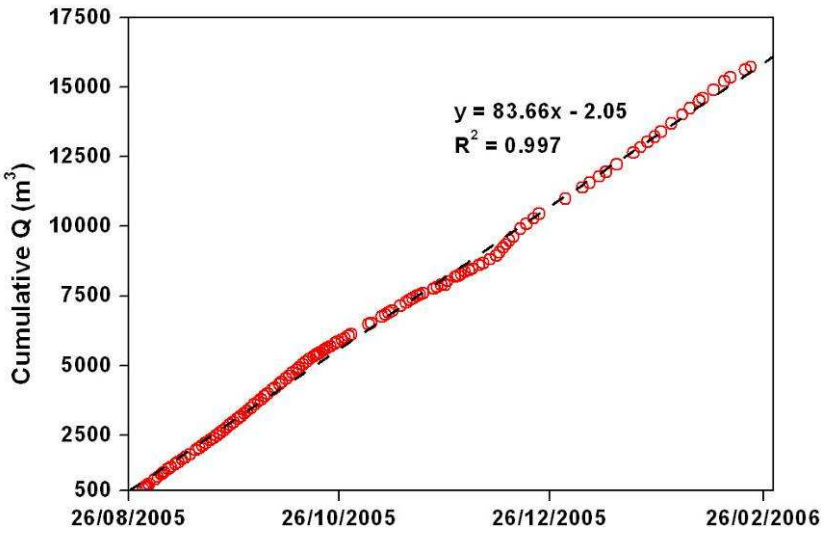

Figure 4.25. Radially converging flow tracer tests: cumulative groundwater pumped in P5 during the radially converging flow tracer tests.

Groundwater samples were taken, at predetermined time-interval, from the pumped groundwater using an automatic sampler ISCO 6700 (Figure 4.26).

Figure 4.26. Radially converging flow tracer tests: experimental setup. Pumping device (left); automatic sampler (right).

4.5.1.2. Tracer tests results

Tracers injected during Phase I were never detected at the recovery well (sampling duration: 3 months). Because of that, it was decided to inject between the recovery well and the Meuse River, in observation well U15, in order to check if the pumping well P5 was preferentially draining water from the Meuse River rather than from the aquifer. Eosin yellowish was injected in U15 on 13th December, resulting in a relatively fast breakthrough of the tracer at

the recovery well. The large recovery factor, approximatively 80%, confirms that most of the groundwater pumped at P5 comes from the Meuse River. Afterwards, between December'05 - February'06, tracers previously injected during the Phase I were also injected at U15 in order to check if non-conservative behaviours were likely to explain the non detection of these tracers during Phase I. The resulting breakthrough curves, presented in Figure 4.27, indicate that the non-conservative processes such as sorption or degradation cannot explain completely the fact that tracers injected during Phase I were never detected at the recovery well. Further explanations will be given based on the numerical modelling results in Chapter 5.

Primary conclusions can be drawn from Table 4.13 and Figure 4.27. The eosin yellowish breakthrough curve shows earlier breakthrough and modal time because the pumping rate at P5 was higher (Q_{mean} = 5.0 m^3 h^{-1}) during this experiment than during the subsequent one (Q_{mean} = 2.1 m^3 h^{-1}). The pumping rate had to be reduced progressively to avoid drying the pumping well. The tracer tests performed with naphtionate, sulforhodamine B, uranine, lithium and iodide show contrasting breakthrough curves, with different travel times, concentrations and tailing, reflecting the specific properties of each tracer.

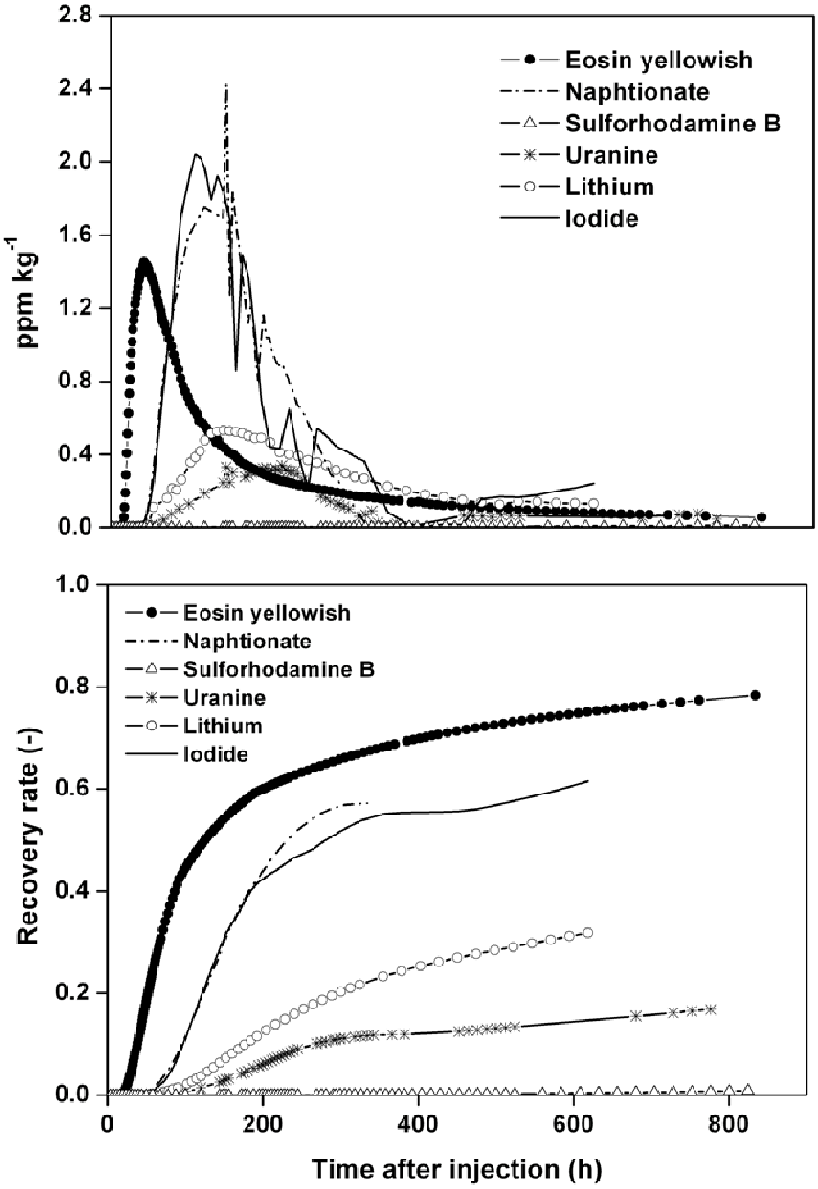

Figure 4.27. Radially converging flow tracer tests: breakthrough curves and corresponding recovery rates for tracers injected during Phase II (December'05 - February'06).

4.5.1.3. First interpretations of tracer experiments

Preliminary interpretation of the tracer test results was performed using the software CATTI (Sauty *et al.*, 1992). CATTI allows solving analytically or semi-analytically different models for transport of solutes in groundwater, including radially converging flow advection-dispersion transport equation. Breakthrough curves were modelled by adjusting the first arrival time and the modal time, playing on the effective porosity (θ_m) and the longitudinal dispersivity (α_L). For easier comparison, calculated concentrations were fitted to observed

concentrations by normalising the breakthrough curves according to the maximal concentration. A more detailed calibration on the whole breakthrough curve is not possible using CATTI, as physico-chemical retardation processes cannot be considered.

Results of this modelling are presented in Figure 4.28, and adjusted hydrodispersive parameters (effective porosity and longitudinal dispersivity) are listed in Table 4.14. With all the caution required with such simplified analytical solutions, one can already derive the following first conclusions:

- The adjusted values of effective porosity of the alluvial aquifer are somehow lower than expected. As an example, Brouyère (2001) found values ranging between 3.7 and 8.5 % at Hermalle-sous-Argenteau, in the alluvial plain of the Meuse River, North from Liège (Belgium). However, one has to remember that the analytical solution assumes a radially symmetric distribution of groundwater fluxes and effective velocities. This condition is probably not met here: the tracer experiments have clearly shown that P5 is essentially fed by water coming from the Meuse. It is thus likely that the hypothesis of homogeneity leads to strong underestimation of groundwater fluxes between U15 and P5, which has to be compensated by defining an "apparent" low effective porosity;
- The longitudinal dispersion coefficient is low, as expected for gravel deposits.

Table 4.14. Radially converging flow tracer tests: hydrodispersive parameters (θ_m –effective porosity- and α_L –longitudinal dispersivity-) obtained from CATTI simulations.

	Eosin yellowish	Naphtionate	Uranine	Lithium	Iodide
θ_m (%)	1.6	1.5	2.9	2.0	1.7
α_L (m)	1.8	1.4	3.4	1.4	1.6

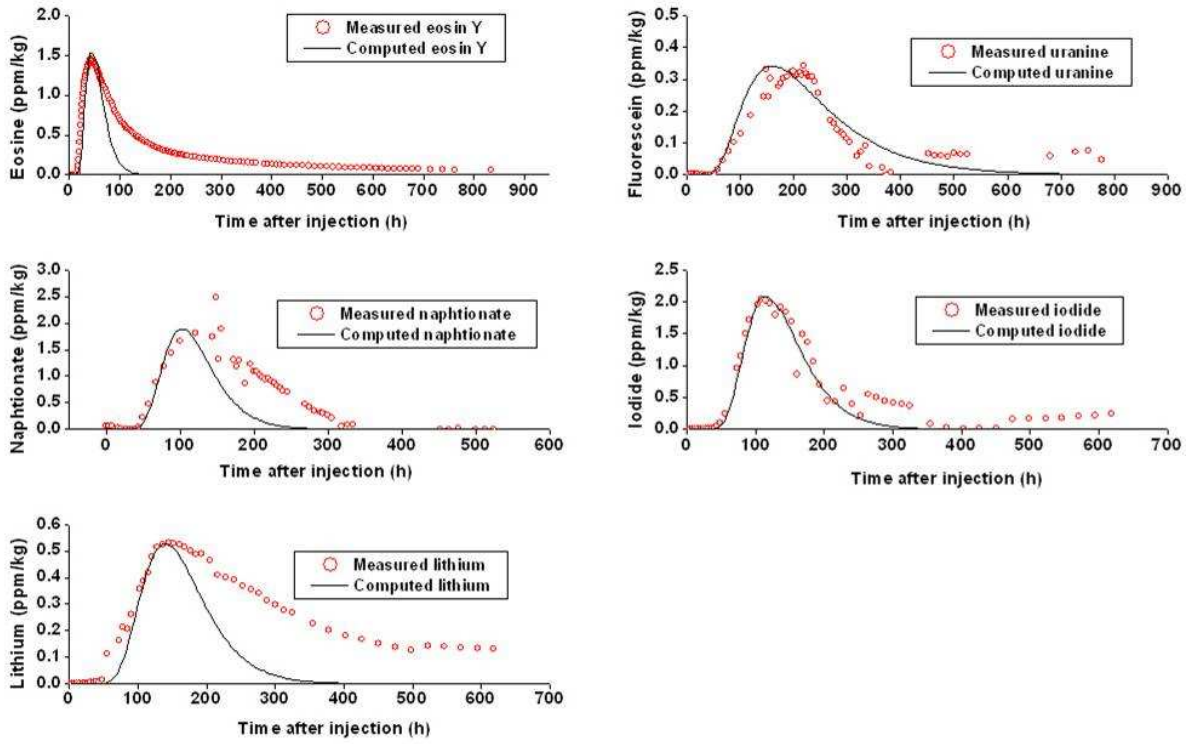

Figure 4.28. Radially converging flow tracer tests: first interpretation using CATTI (Sauty *et al.*, 1992).

A more advanced calibration of breakthrough curves corresponding to the radially converging flow tracer tests, using MODFLOW and MT3DMS, will be presented in Chapter 5.

4.5.2. Single well tracer experiments (the Finite Volume Point Dilution Method – FVPDM)

Previous results have shown that a precise evaluation of groundwater fluxes near the Meuse River is essential. To obtain direct estimates of Darcy fluxes, 4 single well tracer experiments were performed in different available observation wells. To do so, the new Finite Volume Point Dilution Method (FVPDM) was used. All details on the physical, mathematic and experimental background of the method can be found in Brouyère *et al*. (2008).

The FVPDM generalises the single-well point dilution method to the case of finite volumes of tracer fluid and water flush. Figure 4.29 and Figure 4.30 show the basic experimental devices and their layout in the field.

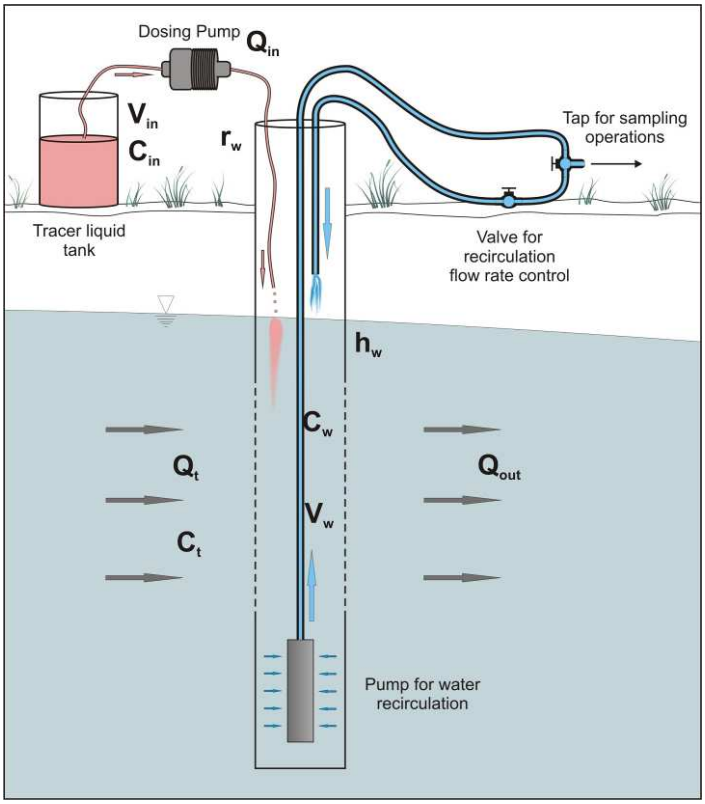

Figure 4.29. FVPDM: schematic experimental design. Q_{in}: injection flow rate [L^3 T^{-1}]; V_{in}: volume of injected fluid [L^3]; C_{in}: concentration in the injected fluid [M L^{-3}]; r_w: radius of the injection well [L]; h_w: height of the water column in the well bore [L]; Q_t: transit flow rate intercepted by the well screens [L^3 T^{-1}]; C_t: tracer concentration in the transit flux intercepted by the well [M L^{-3}]; C_w: tracer concentration in the injection well [M L^{-3}]; V_w: volume of water in the injection well [L^3]; Q_{out}: flow rate leaving the well through the screens [L^3 T^{-1}] (Brouyère *et al.*, 2008).

Figure 4.30. FVPDM: experimental design in the field during realisation of the experiment in well P3. (1) Tracer liquid tank; (2) Dosing pump; (3) Valve for control of the recirculation flow rate; (4) Tap for sampling operations; (5) Injection well (modified from Brouyère *et al.*, 2008).

According to Figure 4.29 and Figure 4.30, during the experiments performed in the Flémalle site, the tracer solution was continuously mixed using an automatic mixing device placed in the top of the barrel storage. The tracer was injected using a peristaltic pump EASYDOS 3.4 for injection rates lower than 3.4 l h^{-1} or a dosing pump MAGDOS LT17 for injection rates up to 40 l h^{-1}. Groundwater circulation was performed in the injection well in order to homogenise the tracer concentration in the well, as well as to obtain representative groundwater samples for tracer concentration measurement at the injection well. This task was accomplished using an immersed pump Grundfos SQ1-35, with a circulation rate ranging between 0.3 and 1 m^3 h^{-1}.

4.5.2.1. Mathematical basis

Brouyère *et al.* (2005) obtained the following analytical solution for calculating the concentration evolution in the injection well:

$$C_w(t) = \frac{Q_{in}C_{in} - \left(Q_{in}C_{in} - Q_{out}C_{w,0}\right)\exp\left(-\frac{Q_{out}}{V_w}\left(t - t_o\right)\right)}{Q_{out}} \tag{4.9}$$

with,

$$Q_{out} = Q_{in} + Q_t^{in} \tag{4.10}$$

where $V_w = \pi r_w^2 h_w$ is the volume of water in the injection well [L^3], where r_w is the radius of the injection well [L] and h_w is the height of the water column in the injection well [L]; C_w, C_{in} and C_w^0 in are tracer concentrations in the well, in the injection water, and in the injection well, respectively, at time t_0 [M L^{-3}]; Q_{in} is the injection rate [L^3 T^{-1}]; Q_t^{in} is the rate of water intercepted by the well at the screen level (transit flow rate) [L^3 T^{-1}]; Q_{out} is the flow rate that leaves the well through the screens, carrying tracer at concentration C_w [L^3 T^{-1}]. The superscript "in" in the transit flow rate Q_t^{in} indicates the fact that this flow rate dynamically depends on the injection rate Q_{in}.

The physical process behind the FVPDM is dilution by mixing of the different flow rate components (Q_{in} and Q_t^{in}), which is similar to the standard dilution technique commonly used in hydrogeology on calculate flow rates in streams (Gilman, 1977a, 1977b; Ruehl *et al.*, 2006).

The FVPDM is, however, more complex than the dilution technique because the relationship between the injection flow rate Q_{in} and the transit flow rate Q_t^{in} in non-linear, as it depends on the flow patterns around the injections well and on the well geometry. As explained by Brouyère (2003), the transit flow rate Q_t^{in} is maximum when the injection rate is equal to zero and in progressively decreases as the injection rate increases. For a critical value of the injection rate $Q_{in} = Q_{cr}$, the transit flow rate Q_t^{in} is exactly zero. Above the critical injection rate, only injection water leaves the well screen (Figure 4.31). This implies that the FVPDM should be performed with a tracer injection rate which is less than a critical injection rate (Q_{cr}) above which the transit flow rate crossing the screens of the injection well could not be determined because it would be cancelled. The key for developing the FVPDM is thus to accurately express the dependency of Q_t^{in} on Q_{in} and to evaluate as accurately as possible the critical injection rate (Q_{cr}).

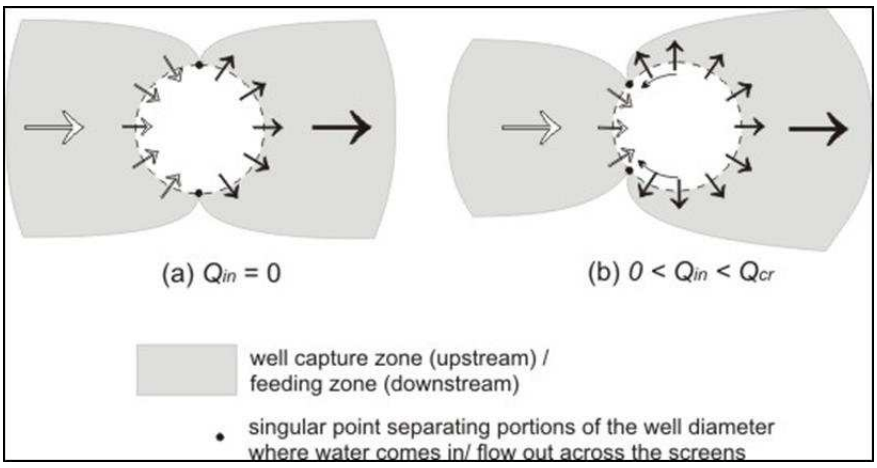

Figure 4.31. FVPDM: flow patterns around the injection well (a) in natural flow conditions, (b) modified by the injection of water in the well and radial coordinate system used to calculate the components of Darcy flux at the vicinity of the injection well (Brouyère *et al.*, 2008).

Finally, the expression for the transit flow rate is given by:

$$Q_t^{in} = Q_{out} - Q_{in} = 2r_w e_{scr} v_{ap} \sin\left(\arccos Q_{in}^*\right) - \frac{Q_{in}}{2\pi}\left(2\arccos Q_{in}^*\right) \quad (4.11)$$

where $Q_{in}^* = Q_{in}/Q_{cr}$; e_{scr} is the screen length of the well [L]; and v_{ap} is the apparent Darcy flux [L T^{-1}].

4.5.2.2. The FVPDM as performed in the field (experimental conditions)

The objective of the study and the conditions prevailing in the field are the main constraining factors for dimensioning the tracer experiments. However, based on the theory, it is possible to propose a very structured methodology for dimensioning the experiment prior to going to the field. This is summarised in the form of a flowchart in Figure 4.32.

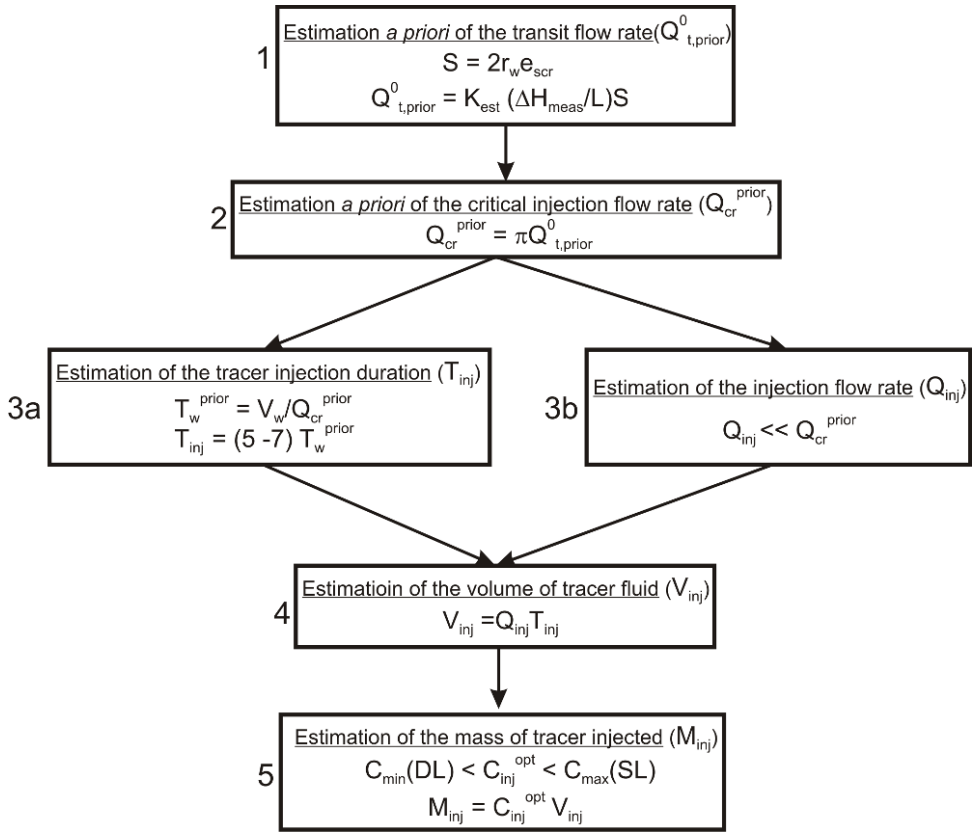

Figure 4.32. FVPDM: flowchart for an optimal design of the FVPDM injection profiles (Brouyère *et al.*, 2008).

As already mentioned, an essential condition for the FVPDM to be valid is that the injection rate should be less than the critical injection rate (Q_{inj}^{*}<1). If that condition is not met, the tracer concentration in the injection well (C_w) would become equal to the tracer concentration of the injected water (C_{inj}) and the monitored evolution of concentration in the well have no meaning anymore.

The first step in setting up the experiment is thus to estimate a priori the critical injection rate Q_{cr} by applying Darcy's law with previously estimated hydraulic conductivity and hydraulic gradient (Figure 4.32, step 1). Values of hydraulic conductivity and hydraulic gradient were obtained from pumping tests results and from groundwater levels measured in the vicinity of the injection well, respectively.

When the critical injection rate Q_{cr} is estimated from Q_t (Figure 4.32, step 2), one can define the injection profile (Q_{inj}, V_{inj}, T_{inj}, C_{inj}) as follows. Theoretically, a single injection step at a constant rate Q_{inj} is sufficient to obtain a concentration evolution that is useful for the FVPDM interpretation. However, we decide to perform various injection steps with increasing and decreasing injection rates, the idea being to check that the relationship between Q_t^{inj} and Q_{inj} remains valid for different values of Q_{inj}. It is also expected that the resulting multi-step concentration evolution can provide a more reliable estimation of Darcy fluxes. Using increasing injection rates reduces also the risk of injecting the tracer at a rate that is larger than the critical injection rate.

Knowing Q_{cr} and V_w, one can estimate T_w and then T_{inj} (Figure 4.32, step 3a). At the same time, the prior estimate of Q_{cr} allows one to define an optimal value of Q_{inj}, as low as possible as compared to Q_{cr} (Figure 4.32, step 3b). Having defined Q_{inj} and T_{inj} allows then to determine the volume of tracer fluid V_{inj} (Figure 4.32, step 4).

The quantity of tracer has to be defined so as to have concentrations in the injection fluid (C_{inj}) and in the injection well (C_w) that are higher than the detection limit ($C_{inj}>C_{DL}$), to be easily detected and monitored, but still low enough to avoid adverse problems such as saturation of monitoring devices or density effects ($C_{inj} < C_{SL}$). So, the final step consists in defining the quantity of tracer M_{inj} such that concentrations in the injection fluid C_{inj} and in the injection well C_w, are within this acceptable interval (Figure 4.32, step 5). During the experiment, "real-time" measurements of the electrical conductivity or the fluorescence is recommended to monitor continuously and in "real-time" the concentration evolution, as well as to check that the injection rate remains lower than the critical injection rate ($Q_{inj} < Q_{cr}$).

During the experiment, the tracer solution was continuously mixed using an automatic mixing device placed in the top of the barrel storage. The tracer was injected using a peristaltic pump EASYDOS 3.4 for injection rates lower than 3.4 l h^{-1} or a dosing pump MAGDOS LT17 for injection rates up to 40 l h^{-1}. Groundwater circulation was performed in the injection well in order to homogenise the tracer concentration in the well, as well as to obtain representative groundwater samples for tracer concentration measurement at the injection well. This task was accomplished using an immersed pump Grundfos SQ1-35, with a circulation rate ranging between 0.3 and 1 m^3 h^{-1}.

4.5.2.3. FVPDM: description of the injections in the Flémalle site

Four wells (P1, P3, P4 and U15), located at distances ranging from 25 to 62 meters from the Meuse River, were selected to perform this tracer technique Figure 4.33.

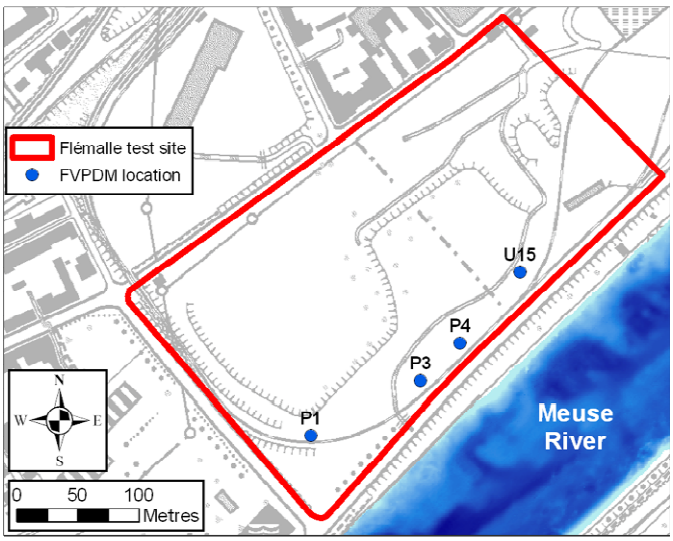

Figure 4.33. FVPDM: location of wells used to perform FVPDM experiments.

Tracer solutions were stored in 500 l barrels (Figure 4.30). The volume of tracer fluid and the injection durations were determined to optimise the chances of reaching the stabilisation of concentration in the injection well for each injection step, as explained in Figure 4.32. Tracers were continuously injected and monitored in each well during several days. Bromide was injected in well U15 using two steps of increasing injection rate followed by one step with a decreased injection rate; iodide was injected in well P4 using four steps of increasing injections rates; sulforhodamine B was used in well P3 performing two steps of increasing injection rate; and uranine was injected in well P1 using two steps of increasing injection rate. Characteristics of each injection are summarised in Table 4.15.

Table 4.15 FVPDM: characteristics of wells used during injections and experimental set-up characteristics of tracer injections.

		U15				P4					P3			P1		
Borehole depth (m)		14.2				15.5					15.0			18.2		
Water column h_w (m)		6.66				7.32					7.03			10.11		
Well radius r_w (m)		0.05				0.075					0.075			0.075		
Water well volume V_w (m^3)		0.05				0.13					0.12			0.18		
Screen length e_{scr} (m)		3.0				5.5					4.0			4.25		
K_{mean} (pumping test) (m s^{-1})		3.3×10^{-3}				1.1×10^{-3}					4.0×10^{-4}			2.7×10^{-4}		
Estimated $\underline{V}_D$ (m s^{-1})		1.1×10^{-5}				4.8×10^{-6}					9.8×10^{-7}			5.6×10^{-7}		
Estimated Q_{cr} (m^3 s^{-1})		1.1×10^{-5} (39.6 l h^{-1})				1.3×10^{-5} (46.8 l h^{-1})					1.9×10^{-6} (6.84 l h^{-1})			1.1×10^{-6} (3.96 l h^{-1})		
Tracer		Br^-				I^-					Sluforhodamine B			Uranine		
Total M_{inj} (kg)		2.69				2.77					4.45×10^{-5}			4.25×10^{-5}		
Total V_{inj} (m^3)		0.46				0.98					0.50			0.50		
C_{inj} (ppm)		5818				2775					0.088			0.085		
Q_{rec} (m^3 h^{-1})		0.3				3.0					1.0			0.3		
Injection parameters	**Injection step**	*1*	*2*	*3*	***Total***	*1*	*2*	*3*	*4*	***Total***	*1*	*2*	***Total***	*1*	*2*	***Total***
	Q_{inj} (l h^{-1})	9.3	32.9	20.3		1.5	5.4	19.2	39.4		1.7	22.8		10.5	20.1	
	Time (h)	3.00	9.58	5.92	**18.50**	23.4	12.62	20.73	12.30	**69.05**	29.37	19.83	**49.20**	19.08	14.92	**34.00**
	Volume (m^3)	0.028	0.315	0.120	**0.463**	0.035	0.068	0.398	0.485	**0.986**	0.050	0.450	**0.500**	0.200	0.300	**0.500**
	Tracer mass (kg)	0.16	1.83	0.70	**2.69**	0.10	0.19	1.12	1.36	**2.77**	4.4×10^{-6}	4.0×10^{-5}	**4.4×10^{-5}**	1.7×10^{-5}	2.5×10^{-5}	**4.2×10^{-5}**

4.5.2.4. FVPDM: tracer monitoring and sampling

With saline tracers (iodide and bromide), the time evolution of concentration was continuously monitored by measuring the electrical conductivity with a YSI 600 XLM probe in the circulation water (compared to the electrical conductivity measured in the injection fluid). With fluorescent tracers, a field fluorimeter GGUN-FL30 #1370 was used to monitor the evolution of concentration during the experiment. During each experiment, samples were also taken using an ISCO 6700 automatic sampler and manually (control samples) in order to be analyzed in the laboratory. Groundwater level and temperature were also continuously monitored in the injection wells (every 2 minutes) using a pressiometric Level TROLL® probe.

4.5.2.5. FVPDM: modelling of groundwater sampling results

Concentration evolutions in the injection wells during and after the tracer injections, together with water levels monitored in the injection well and in the Meuse River are presented in Figure 4.34. Most often, the various injection steps were clearly identifiable, but the monitored concentrations in the injection wells hardly reached stability. River stage variations generate indirectly local changes in the hydraulic gradients in the aquifer and thus changes in groundwater fluxes close to the injection wells. This phenomenon was observed during most of the injection experiments. During the transient phase of the evolution of concentration in the injection well, at the beginning of each tracer injection step, the influence of the changes in groundwater fluxes is not as visible because it overlaps with the normal rise of concentration. On the contrary, when the tracer concentration has stabilised in the injection well, changes in groundwater fluxes induce variations in the tracer concentration in the well. This perturbation is clearly visible when looking at the concomitant changes in water levels in the Meuse River and the anomalies in concentration monitored in the injections wells. In Figure 4.34A and in the second injection step of the Figure 4.34B, the observed decreases in Meuse water levels are systematically associated with decreases in concentrations in the well because the hydraulic gradient and Darcy fluxes are increased in the vicinity of the injection well. On the contrary, during the stabilised phase of the second step of bromide injection in well U15 (Figure 4.34C), an increase in tracer concentration is observed, corresponding to a rise in water level in the Meuse because the hydraulic gradient and Darcy fluxes are reduced close to U15.

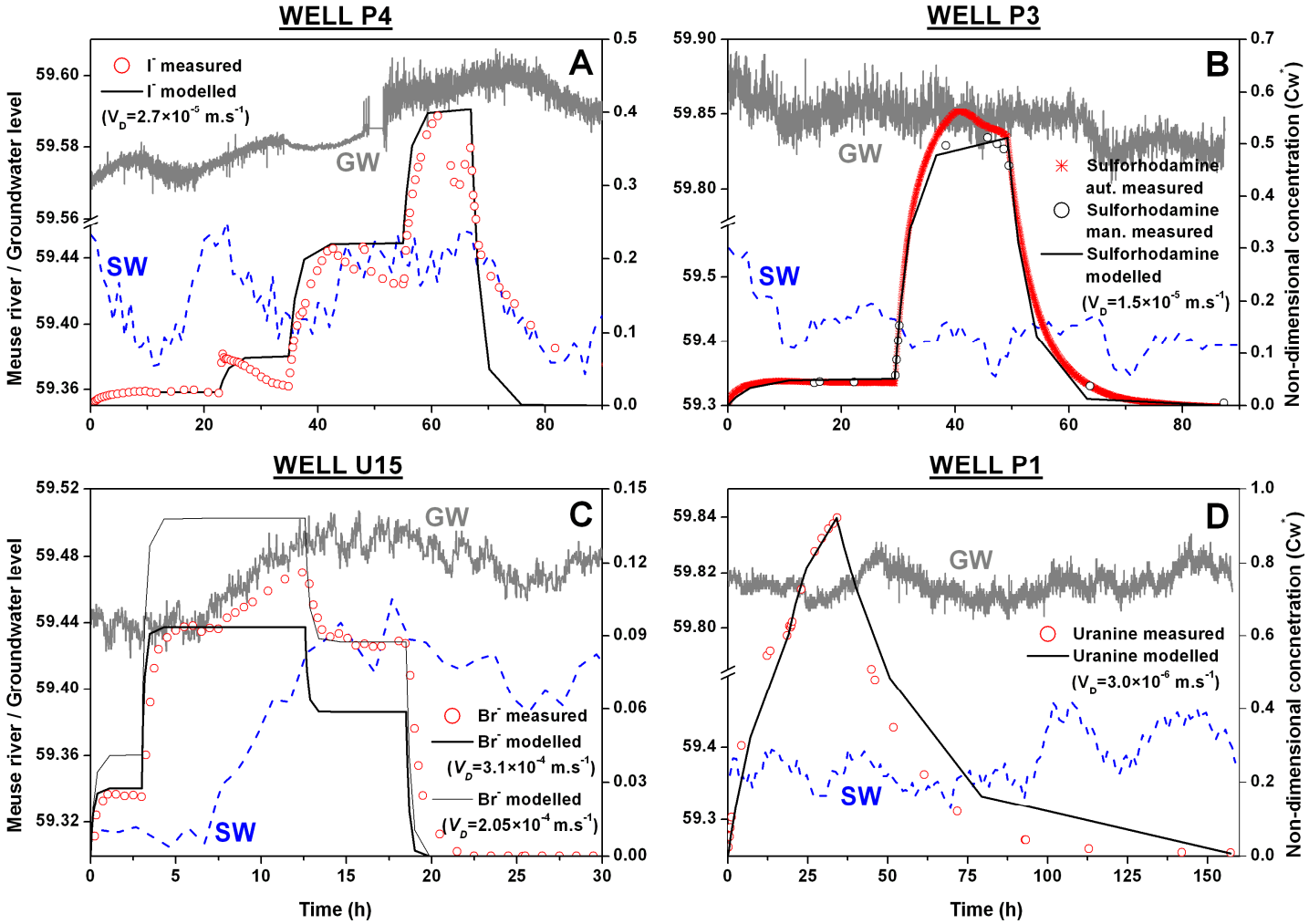

Figure 4.34 FVPDM: comparison between concentration evolutions monitored and modelled, and representation of the Meuse River (SW) and groundwater (GW) levels.

The non-dimensional tracer concentration in the well (C_w^*) is obtained performing C_W / C_{inj} .

4.5.2.6. FVPDM: modelling results

Using Equation (4.9), calculated evolutions of concentrations were fitted to the monitored ones by modifying the apparent Darcy flux ν_{ap} (Figure 4.34). All other terms appearing in the mentioned equation were defined based on the experimental conditions (Q_{inj}, C_{inj}, V_w…). Results are summarised in Table 4.16. Considering that the influences of changes in water levels in the Meuse River was not taken into account directly in the interpretation, one can consider that tracer concentration evolutions calculated with the analytical solution are very close to the measured ones. As explained before, for the injection performed in well U15, the strong deviation of concentration observed during injection in step 2 is related to a rise of about 15 cm in the Meuse water level during the FVPDM experiment. For a Darcy flux of 3.1×10^{-4} m s^{-1}, the first injection step and the beginning of the second step are well reproduced, but not the third for which the calculated concentration is too low. These results are consistent with the fact that the rise in Meuse water level has reduced the gradient and thus Darcy fluxes in the alluvial aquifer near the river bank. The third step was adjusted separately, using a lower Darcy flux equal to 2.05×10^{-4} m s^{-1}.

Table 4.16 FVPDM: results of the single-well tracer test performed in the Flémalle site

	U15	**P4**	**P3**	**P1**
Darcy's flow ν_D (m s^{-1})	$2.05 – 3.1\times10^{-4}$	2.7×10^{-5}	1.5×10^{-5}	3.0×10^{-6}
Groundwater flow Q_t^0 (m^3 s^{-1})	$6.15 – 9.30\times10^{-5}$ (221.4 – 334.8 l h^{-1})	2.23×10^{-5} (80.2 l h^{-1})	9.60×10^{-6} (34.56 l h^{-1})	1.91×10^{-6} (6.9 l h^{-1})
Critical injection flow rate Q_{cr} (m^3 s^{-1})	$1.93\times10^{-4} – 2.92\times10^{-4}$ (694.8 – 1051.2 l h^{-1})	7×10^{-5} (251.9 l h^{-1})	3.02×10^{-5} (108.7 l h^{-1})	6.02×10^{-6} (21.6 l h^{-1})

The estimated Darcy fluxes are similar in P3 and P4, on the order of 2×10^{-5} m s^{-1} while in the vicinity of well P1, they are 10 times lower, around 3×10^{-6} m s^{-1}. In the vicinity of well U15, the estimated Darcy flux is approximatively 10 times higher of those in P3 and P4, of the order of 2×10^{-4} m s^{-1}. This seems to indicate a zone of higher hydraulic conductivity in the vicinity of U15.

Two main results must be highlighted specifically for the FVPDM:

1. Darcy fluxes change continuously in time because of frequent changes in the difference of head between the river and its alluvial aquifer;
2. Estimates of Darcy fluxes seem to indicate changes in the heterogeneity of the hydraulic conductivity field of the alluvial aquifer, from higher values in the surroundings of well U15 to lower values in the neighbourhood of well P1.

4.5.3. Conclusions to tracer experiments

Generally speaking, conclusions related to tracer tests performed in the Flémalle site can be summarised in three main points:

1. Tracer experiments performed in the Flémalle site have provided very useful information on the hydrodynamics and on hydrodispersive processes in the alluvial aquifer. First estimates are available for the effective porosity (θ_m = 1.5 – 2.9%) and longitudinal dispersivity (α_L = 1.4 – 3.4 m) of the alluvial deposits, based on modelling the radially converging flow tracer tests using a semi-analytical solution;
2. The tracer experiments have also provided further evidence on the importance and dynamics of the groundwater – surface water interaction and on the heterogeneity of the hydraulic conductivity;
3. The specific behaviour of tracers used during the first radially converging flow tracer test performed in the site cannot fully explain the non-observation of these tracers during this phase. Again, the heterogeneity of the flow field has to be examined as a complementary explanation to this surprisingly results. This will be further studied using the MODFLOW – MT3DMS numerical modelling in Chapter 5.

Specifically for the FVPDM, it must to be stated that this technique provide a control of injection conditions together with complementary information on groundwater flows in the vicinity of the injection well. The interpretation can take advantage of both the rising and the stabilised part of the concentration evolutions in the injection well.

As a consequence of its high sensitivity to experimental conditions, the FVPDM is a well candidate technique for studying and monitoring changes in Darcy fluxes and groundwater flows in transient conditions, such as changes in hydraulic gradients, with potential applications in monitoring the dynamics of groundwater – surface water interactions in the hyporheic zone. To do so, one needs to continuously inject a tracer at a very low rate and to monitor the temporal changes in concentration in the injection.

4.6. Conclusions to chapter 4

Before performing the monitoring and field experiments, knowledge on hydrodynamics in the alluvial aquifer of the Flémalle site was reduced to an idea of groundwater flow directions, known to be from the aquifer to the river. Nothing was known about river – aquifer interactions and the spatial aquifer heterogeneity. The numerous wells available from precedent characterisation campaigns (presented in Chapter 2) were very useful to perform monitoring and field experiments, which aimed to obtain a relatively complete idea of the interactions between the river and the aquifer, of the spatial heterogeneity of the hydraulic conductivity field, of groundwater fluxes discharging to the river and first estimates of the main hydrodynamic and hydrodispersive parameters governing the flow and transport of dissolved solutes in the alluvial aquifer.

Table 4.17 presents a summary of the main results obtained after 2 years of monitoring and field experiments. All the data obtained will serve to perform, in a first instance, an analytical groundwater flow model, and subsequently, a numerical groundwater flow and transport model of the Flémalle site, which will deserve to determine which processes are responsible of migration and/or attenuation of the organic pollutants dissolved in groundwater.

Table 4.17. Summary of the main results issued from monitoring and field experiments.

Groundwater – surface water interaction	
Groundwater flux direction	• From the aquifer to the river under regular conditions (*H* ~ 59.4 m a.s.l.)
Dynamics of the river – aquifer interface	• Hydraulic gradient inversed when *H* increases over 60 m a.s.l.; • Darcy flux continuously varying due to river fluctuations (demonstrated with FVPDM results); • Surface water flows into the aquifer when important inversions of the hydraulic gradient are produced (observed using temperature as a tracer). However, this seems to be restricted to the firsts meters of the alluvial aquifer; • Areas of good connection between the river and the aquifer, as well as preferential paths of surface water flowing into the aquifer are highlighted using data analysis and groundwater temperature, respectively.
Hydrodynamic & hydrodispersive parameters of the alluvial aquifer	
Groundwater head	• Groundwater head variations are mainly explained by river fluctuations (80%); • Rainfall has a reduced impact in groundwater levels (20%);
Spatial heterogeneity of the hydraulic conductivity field	• Values ranging between 1×10^{-5} and 1×10^{-3} m s^{-1}; • High spatial variability of the hydraulic conductivity field (observed from pumping and tracer tests).
Hydrodispersive parameters	• Low values of effective porosity (1.5 – 2.9 %); • Low values of longitudinal dispersivity (1.4 – 3.4 m); • Still to explain factors determining the absence of tracer recovering during Phase I.

As mentioned in Chapter 2, a former river channel of the Meuse River (and its associated island, named Corbeaux Island) is located near to or in the Flémalle site. At present, the location of this channel can be precisely located thanks to SPAQuE (2007). Its location is presented in Figure 4.35, together with groundwater heads corresponding to the monthly monitoring campaign of April 2006.

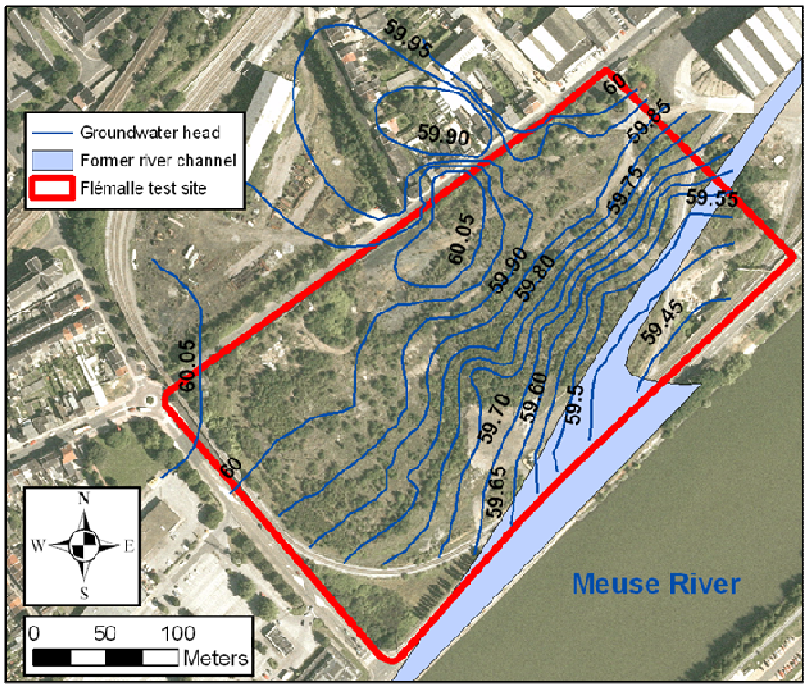

Figure 4.35. Location of the former channel associated with the past morphology of the Meuse River. Piezometric map corresponds to monthly monitoring campaign of April 2006.

In addition, Figure 4.36 shows the former river channel together with observation wells used during pumping tests, and radially converging flow and FVPDM tracer tests.

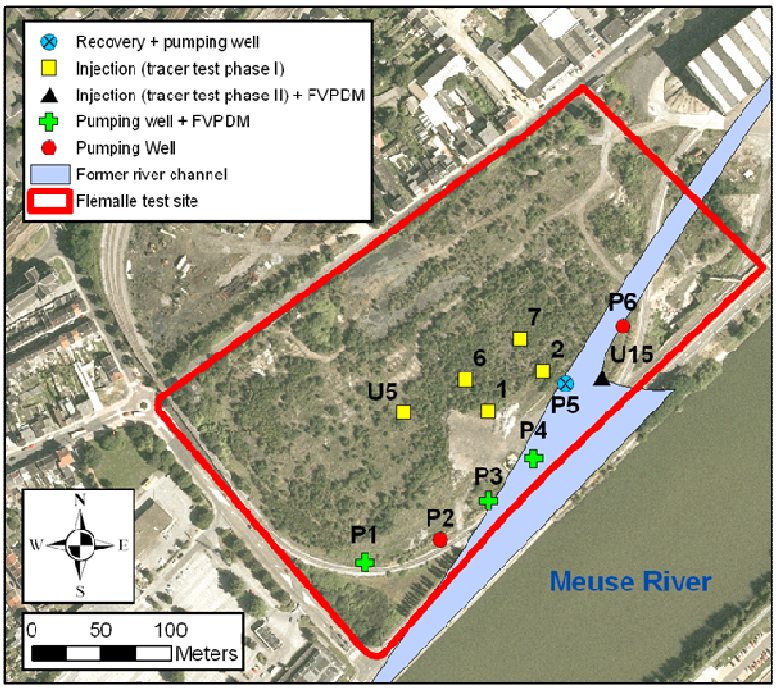

Figure 4.36. Location of the former channel associated with the past morphology of the Meuse River. Reference observation wells used in pumping and tracer experiments are depicted.

The actual role of the old river channel must be investigated with regard to the non arrival of tracers injected in Phase I. This hypothesis will be discussed in Chapter 5, where tracer tests will be numerically modelled.

4.7. References to chapter 4

Bouwer, H. (1989). The Bouwer and Rice slug tests-An update. *Ground Water* **27**(3): 304-309.

Bouwer, H. & Rice, R. C. (1976). A slug test method for determining hydraulic conductivity of unconfined aquifers with completely or partially penetrating wells. *Water Resour. Res.* **12**(3): 423-428.

Brouyère, S. (2001). Etude et modélisation du transport et du piégeage des solutés en milieu souterrain variablement saturé (study and modelling of transport and retardation of solutes in variably saturated media). Ph.D thesis. Faculté des Sciences Appliquées. Laboratoire de géologie de l'ingénieur, d'Hydrogéologie et de Prospection géophysique, Université de Liège, Liège (Belgium). 640 pp.

Brouyère, S. (2003). Modeling tracer injection and well-aquifer interactions: a new mathematical and numerical approach. *Water Resour. Res.* **39**(3): doi:10.1029/2002WR001813.

Brouyère, S., Batlle-Aguilar, J., Goderniaux, P. & Dassargues, A. (2008). A new tracer technique for monitoring groundwater fluxes: the Finite Volume Point Dilution Method. *J. Contam. Hydrol.* **95**: 121-140.

Brouyère, S., Carabin, G. & Dassargues, A. (2005). Influence of injection conditions on field tracer experiments. *Ground Water* **43**(3): 389-400.

Fetter, C. W. (2001). Applied hydrogeology. Prentice-Hall, Inc. Upper Saddle River, New Jersey (USA). 691 pp.

Gilman, K. (1977a). Dilution gauging on the recession limb: 1. Constant rate injection method. *Hydrol. Sci. Bull.* **22**(3): 353 - 369.

Gilman, K. (1977b). Dilution gauging on the recession limb: 2. The integration method. *Hydrol. Sci. Bull.* **22**(4): 469 - 481.

Gilmore, T. J., Borghese, J. V. & Newcomer, D. R. (1993). Effects of river stage and waste discharges on the unconfined aquifer, Wasington. *Ground Water Monit. Rem.* **13**: 130-138.

Hogarth, W. L., Parlange, J.-Y., Parlange, M. B. & Lockington, D. (1999). Approximate analytical solution of the Boussinesq equation with numerical validation. *Water Resour. Res.* **35**(10): 3193-3197.

Larocque, M., Mangin, A., Razack, M. & Banton, O. (1998). Contribution of correlation and spectral analyses to the regional study of a large karst aquifer (Charente, France). *J. Hydrol.* **205**: 217-231.

Lee, J.-Y. & Hahn, J.-S. (2006). Characterization of groundwater temperature obtained fromthe Korean national groundwater monitoring stations: implications for heat pumps. *J. Hydrol.* **329**: 514-526.

Massei, N., Dupont, J. P., Mahler, B. J., Laignel, B., Fournier, M., Valdes, D. & Ogier, S. (2006). Investigating transport properties and turbidity dynamics of a karst aquifer using correlation, spectral, and wavelet analyses. *J. Hydrol.* **329**: 244-257.

Padilla, A. & Pulido-Bosch, A. (1995). Study of hydrographs of karstic aquifers by means of correlation and cross-spectral analysis. *J. Hydrol.* **168**: 73-89.

Panagopoulos, G. & Lambrakis, N. (2006). The contribution of time series analysis to the study of the hydrodynamic characteristics of the karst systems: Application on two typical karst aquifers of Greece (Trifilia, Almyros Crete). *J. Hydrol.* **329**: 368-376.

Pinault, J.-L. (2001). Manuel utilisateur de TEMPO. Logiciel de traitement et de modélisation des séries temporelles en hydrogéologie et en hydrogéochimie. *RP-51459-FR*. BRGM, Orléans, France. 233 pp.

Ruehl, C., Fisher, A. T., Hatch, C., Los Huertos, M., Stemler, G. & Shennan, C. (2006). Differential gauging and tracer tests resolve seepage fluxes in a strongly-losing stream. *J. Hydrol.* **330**: 235-248.

Sauty, J.-P., Kinzelbach, W. & Voss, A. (1992). CATTI: computer aided tracer test interpretation, program documentation. BRGM, Orléans, FRANCE. 64 pp.

Serrano, S. E. & Workman, S. R. (1998). Modeling transient stream/aquifer interaction with the non-linear Boussinesq equation and its analytical solution. *J. Hydrol.* **206**: 245-255.

SPAQuE (2007). Site "Cokerie Flémalle" - Phase 2. Bilan historique des activités. *Lg3102-02*. SPAQuE, Département de l'amélioration de la connaissance de sites pollués, Liège, Belgium. 18 pp.

Srivastava, K., Serrano, S. E. & Workman, S. R. (2006). Stochastic modeling of transient stream-aquifer interaction with the nonlinear Boussinesq equation. *J. Hydrol.* **328**: 538-547.

Workman, S. R., Serrano, S. E. & Liberty, K. (1997). Development and application of an analytical model of stream/aquifer interaction. *J. Hydrol.* **200**: 149-163.

Calibration task doesn't end when you decide to finish; it really finishes when there is no more time to spend on it.

Pascal Goderniaux

FNRS Belgium & Ph.D candidate in Hydrogeology Unit, University of Liège, during "one of the several days that we spent in front of the computer...waiting for good calibration results" (winter 2008).

5. GROUNDWATER FLOW AND TRANSPORT MODELLING

5.1. The need for groundwater modelling

Groundwater modelling allows bringing all available data together into a logical holistic picture on a quantitative basis. It has become indispensable in answering questions regularly posed by stakeholders regarding groundwater quality at a certain point of compliance or how a contaminant plume may evolve over time.

Two approaches are used here: analytical and numerical modelling.

Main objectives of the analytical modelling are:

- To provide a better understanding of the system groundwater – surface water;
- To obtain first estimates of hydrodynamic parameters of the alluvial aquifer;
- To get an idea of the order of magnitude of the riverbank hydraulic conductivity.

Subsequently, the numerical groundwater flow and transport model should aim to consider the spatial heterogeneity of the alluvial aquifer. Main objectives of this model are:

- To provide a better evaluation of the hydrodynamic and hydrodispersive properties, considering explicitly the spatial heterogeneity of the alluvial aquifer in order to reproduce groundwater head variations;
- To be able to run scenarios of contaminant dispersion in the alluvial aquifer and towards the Meuse River as a support for risk assessment of contaminants present in the alluvial aquifer.

5.2. Analytical modelling

Using monitored time series of water levels in the river and in the aquifer, the computer program STWT1 (Barlow and Moench, 1998) was used to evaluate the hydrodynamic properties of the alluvial aquifer and of the aquifer-river interface and to estimate water flow rates across the river-aquifer interface, considering groundwater flow conditions and water river level fluctuations.

5.2.1. Conceptual model

The conceptual model of the system is presented in Figure 5.1. R_{ch} is the recharge rate of the aquifer [L T^{-1}]; K is the horizontal hydraulic conductivity of the aquifer [L T^{-1}]; K_y is the ratio of vertical to horizontal hydraulic conductivity [-]; d is the width of the semipervious riverbank material [L]; S_y is the specific yield coefficient [-]; b is the mean saturated thickness of the aquifer [L]; β is the aquifer diffusivity (i.e. ratio of transmissivity to storage coefficient)

[L^2 T^{-1}]; α_{LK} is the river leakance or river resistance [L] (defined in Chapter 3, Equation (3.5)); and h is the groundwater head [L].

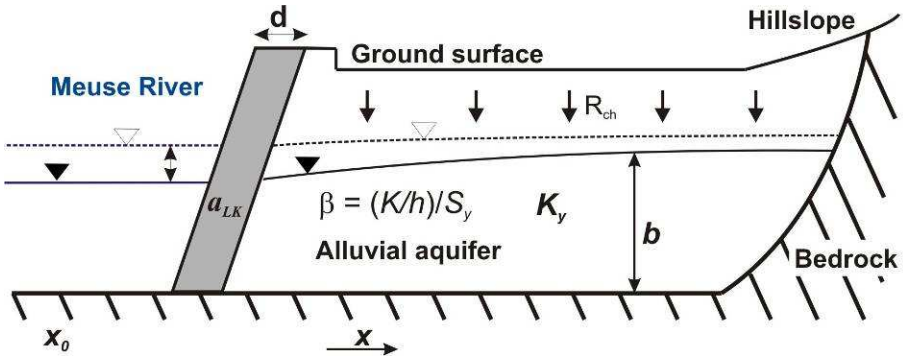

Figure 5.1. Conceptual model of the analytical groundwater - surface water system modelled (orthogonal transect or slide). Not at scale.

Additionally to the assumption of horizontal flow in the aquifer, other simplifying assumptions are considered in the use of analytical solution (Barlow and Moench, 1998):

- The aquifer is homogeneous, isotropic, and of uniform thickness;
- The lower boundary of the aquifer is horizontal and impermeable;
- Hydraulic properties of the aquifer do not change with time;
- The aquifer material and groundwater are slightly compressible;
- The river fully penetrates the aquifer;
- The semipervious riverbank material has negligible water storage capacity;
- The river water level is at the same elevation as groundwater everywhere in the aquifer. This means that at $t = 0$ the river water level is suddenly lowered or raised to a new position.

The aquifer is modelled as a finite-width water-table with semipervious riverbank material. The aquifer mean saturated thickness (b) is set equal to 8 m, and the width of the orthogonal transect to the Meuse river considered for groundwater modelling at observation wells is set equal to 1 m (analysis performed per unit length of river – aquifer interface).

Modelled groundwater heads are adjusted to measured ones by playing on the hydraulic conductivity of the semipervious riverbank material (K_s) for adjusting the mean groundwater level and on the diffusivity (β) for adjusting the amplitude of groundwater variations (distance of influence in the aquifer of changes in river stages).

5.2.2. Discretisation of convolution relations

The analytical solutions derived and implemented by STWT1 are mathematical models of river-aquifer hydraulic interaction. Governing equations and convolution relations used to relate time series of river stage changes (system input stresses) to time series of groundwater head changes (system output responses) were exposed in Chapter 3.

For the implementation in the STWT1 program, the integrals appearing in Equation (3.9) and Equation (3.10) are discretised as follows:

$$h(x, z, j) = h_i + \sum_{k=2}^{J} F'(k-1)\, H_D(x, z, j-k+1)\, \Delta t \tag{5.1}$$

and

$$Q_{riv}(j) = \frac{Kb}{x_0} \sum_{k=2}^{J} F'(k-1) \frac{\partial H_D(x_0, z, j-k+1)}{\partial x_D} \Delta t \tag{5.2}$$

where j is the upper limit of time integration [-]; k is the time variable of integration (time step number) [-]; Δt is the time step size [T]; and $F'(k-1)$ is the time rate of change of the system input [L T^{-1}].

The program requires an approximation of input hydrographs of river-stage into a time series of discrete time steps of length Δt. The time rate of change of the system input for each time step is calculated by:

$$F'(k-1) = \frac{F(k) - F(k-1)}{\Delta t} \tag{5.3}$$

where $F(k-1)$ and $F(k)$ are the system inputs (river stage and/or recharge) at time steps $k-1$ and k, respectively. The accuracy of the convolution method, and therefore of the program, is improved by use of smaller, i.e. hourly, time steps (Barlow *et al.*, 2000).

5.2.3. Analytical modelling for the Flémalle test site

5.2.3.1. Calibration of monitored groundwater heads

Observation wells where the analytical solution was applied are those where groundwater level fluctuations were monitored using pressiometric Level TROLL® probes (Chapter 4). Figure 5.2 presents monitored wells used for analytical modelling calibration.

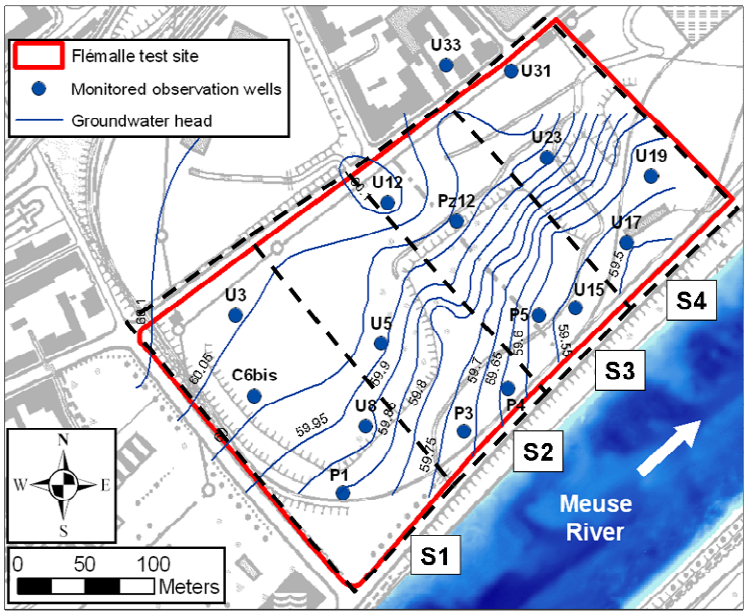

Figure 5.2. Location of 16 observation wells monitored with pressiometric probes Level TROLL®. Piezometric lines correspond to the monthly groundwater survey campaign performed in June 2005. S1, S2, S3 and S4 correspond to sections or "slides" in which the Flémalle site was divided for applying the analytical solution.

Table 5.1, presents the modelled periods, corresponding rainfall measured at the Ivoz-Ramet dam (*Rf*) and the estimated groundwater recharge (R_{GW}), as well as the parameters resulting from the calibration based on groundwater heads monitored in the 16 observation wells. The comparison between modelled and monitored groundwater heads is presented in the form of coefficients of determination (R^2). For the observation wells where a long period of time was monitored (P3, U5, U3 and U8), shorter monitoring periods were first fitted independently before addressing the entire monitored period.

Representative hydrographs of modelled groundwater heads at observation wells P3 and U5, both located in the *slide* S2, are presented in Figure 5.3 and Figure 5.4, as well as the resulting calculated mean seepage rates across the aquifer – river interface. The main objective of these

figures is to show and evaluate modelling results for observation wells located at different distances from the river.

The hydraulic conductivity values resulting from the calibration range between 2.5×10^{-4} and 1.6×10^{-3} m s^{-1}, in good agreement with hydraulic conductivity values obtained from the pumping tests. Specific yield values range between 0.03 and 0.16. The mean hydraulic conductivity of the riverbank material is 3×10^{-5} m s^{-1}, lower than the mean hydraulic conductivity of the aquifer.

The results obtained using the analytical solution constitute first estimates and it is likely that the aquifer heterogeneity is higher and distributed along two (x, y) or even three (x, y, z) spatial dimensions. The resulting hydraulic property values can however be viewed as good estimates and basis for more complex modelling scenarios.

The STWT1 analytical solution considers positive seepage flowing from the aquifer to the river and negative seepage from the river to the aquifer. This sign convention will be used further in Chapter 5.

Table 5.1. Hydraulic properties of the aquifer and riverbank and calibration parameters used in the analytical model (*Rf* = measured rainfall at Ivoz-Ramet dam during the modelled period [L]; *x* = distance to observation well from river-aquifer interface [L]; *d* = width of the semipervious riverbank [L]; *b* = saturated thickness of the aquifer [L]; *K* = horizontal hydraulic conductivity of the aquifer [L T^{-1}]; K_y = ratio of vertical to horizontal hydraulic conductivity [-];S_y = storage yield coefficient [-]; α_{LK} = streambank leakance [L]; K_s = hydraulic conductivity of the semipervious riverbank [L T^{-1}]; R_{GW} = groundwater recharge [L]; R^2 = coefficient of determination between observed and calculated groundwater heads).

Well ID	Modelled period	*Rf* (mm)	x (m)	Calibration parameters						R^2
				K (m s^{-1})	K_y (-)	S_y (-)	α_{LK} (m)	K_s (m s^{-1})	R_{GW} (mm)	
P3 (I)	25.01.2006 – 22.02.2006	50.1	26.1	2.50×10^{-4}	1.0×10^{-2}	0.16	40	1.88×10^{-5}	7.46	**0.995**
P3 (II)	05.02.2006 – 05.05.2006	137.7		2.50×10^{-4}	1.0×10^{-2}	0.15	40	1.88×10^{-5}	24.88	0.983
P3	16.09.2005 – 13.09.2006	688.6		2.50×10^{-4}	1.0×10^{-2}	0.16	40	1.88×10^{-5}	41.7	0.932
U5 (I)	25.01.2006 – 22.02.2006	50.1	113.9	3.05×10^{-4}	1.0×10^{-2}	0.14	40	2.29×10^{-5}	6.52	0.964
U5 (II)	05.02.2006 – 05.05.2006	137.7		3.05×10^{-4}	1.0×10^{-2}	0.12	40	2.29×10^{-5}	20.4	0.982
U5	16.09.2005 – 08.05.2007	1003.7		3.05×10^{-4}	1.0×10^{-2}	0.13	40	2.29×10^{-5}	56.02	0.849
U3 (I)	25.01.2006 – 22.02.2006	50.1	207.1	3.30×10^{-4}	4.8×10^{-3}	0.12	30	3.30×10^{-5}	5.59	0.868
U3 (II)	05.02.2006 – 05.05.2006	137.7		3.30×10^{-4}	3.5×10^{-3}	0.09	30	3.30×10^{-5}	19.22	0.970
U3 (III)	10.12.2005 – 16.05.2006	209.5		4.72×10^{-4}	4.8×10^{-3}	0.09	30	3.30×10^{-5}	22.04	0.959
U3 (IV)	19.11.2006 – 08.05.2007	261.3		4.72×10^{-4}	4.8×10^{-3}	0.09	30	3.30×10^{-5}	18.36	0.978
U3	10.12.2005 – 08.05.2007	900.1		3.30×10^{-4}	3.5×10^{-3}	0.09	30	3.30×10^{-5}	40.94	0.840
U8 (I)	25.01.2006 – 22.02.2006	50.1	90.4	3.05×10^{-4}	1.0×10^{-2}	0.15	40	2.29×10^{-5}	6.99	0.967
U8 (II)	05.02.2006 – 05.05.2006	137.7		2.77×10^{-4}	1.0×10^{-2}	0.11	30	2.77×10^{-5}	20.78	0.979
U8	10.12.2005 – 17.05.2006	211.1		2.77×10^{-4}	1.0×10^{-2}	0.12	30	2.77×10^{-5}	35.52	0.952
U15	06.10.2006 – 04.11.2006	36.92	31.6	1.42×10^{-3}	8.0×10^{-4}	0.10	40	1.07×10^{-4}	1.15	0.830
U23	06.10.2006 – 04.11.2006	36.92	124.4	5.83×10^{-4}	3.0×10^{-3}	0.10	40	4.37×10^{-5}	3.50	**0.234**
P5	04.11.2006 – 05.12.2006	46.0	45.7	6.11×10^{-4}	1.0×10^{-3}	0.12	40	4.58×10^{-5}	4.44	0.972
12	04.11.2006 – 05.12.2006	46.0	156.4	6.11×10^{-4}	6.0×10^{-3}	0.12	40	4.58×10^{-5}	3.99	0.911
U17	05.12.2006 – 09.01.2007	62.9	38.7	1.61×10^{-3}	8.0×10^{-4}	0.06	40	1.21×10^{-4}	4.08	0.992
U31	05.12.2006 – 09.01.2007	62.9	188.1	6.67×10^{-4}	7.0×10^{-3}	0.08	40	5.00×10^{-5}	14.45	0.966
P1	09.01.2006 – 12.02.2007	56.1	62.4	3.30×10^{-4}	8.0×10^{-3}	0.12	30	3.30×10^{-5}	22.89	0.981
C6bis	09.01.2006 – 12.02.2007	56.1	156.0	4.17×10^{-4}	8.0×10^{-3}	0.11	30	4.17×10^{-5}	22.99	0.929
U19	12.02.2007 – 27.03.2007	98.9	61.5	1.61×10^{-3}	8.0×10^{-4}	0.04	40	1.21×10^{-4}	8.22	0.976
U33	12.02.2007 – 27.03.2007	98.9	223.8	1.19×10^{-3}	1.0×10^{-3}	0.05	40	8.93×10^{-5}	22.80	0.879
P4	27.03.2007 – 08.05.2007	11.7	24.6	1.58×10^{-3}	1.0×10^{-2}	0.09	40	3.54×10^{-5}	0	0.942
U12	05.10.2007 – 08.11.2007	65.3	221.2	2.50×10^{-4}	1.0×10^{-3}	0.03	40	1.88×10^{-5}	0	0.794

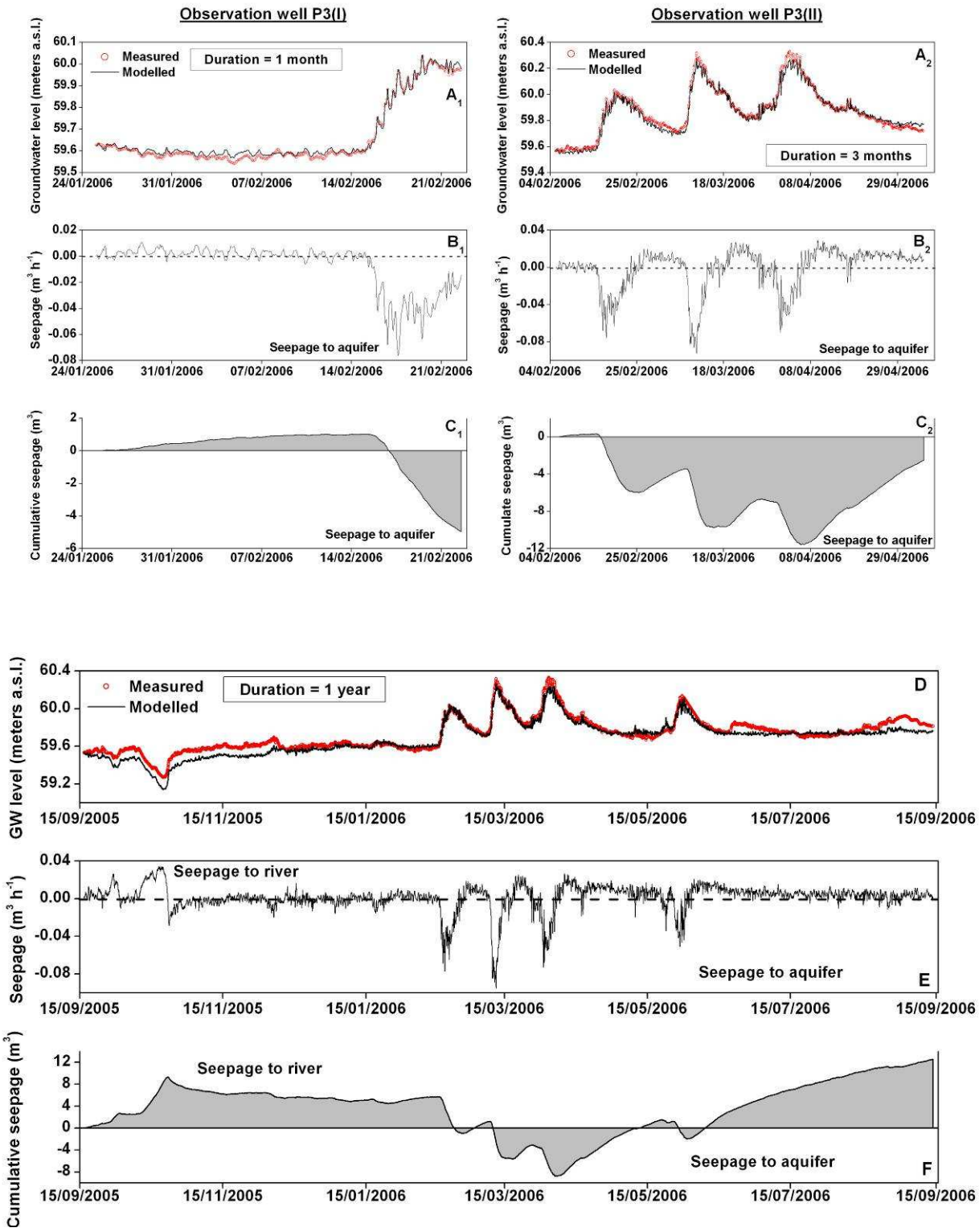

Figure 5.3. Measured and modelled groundwater head and corresponding calculated seepage and cumulative seepage for observation well P3 (distance: 26.1 m).

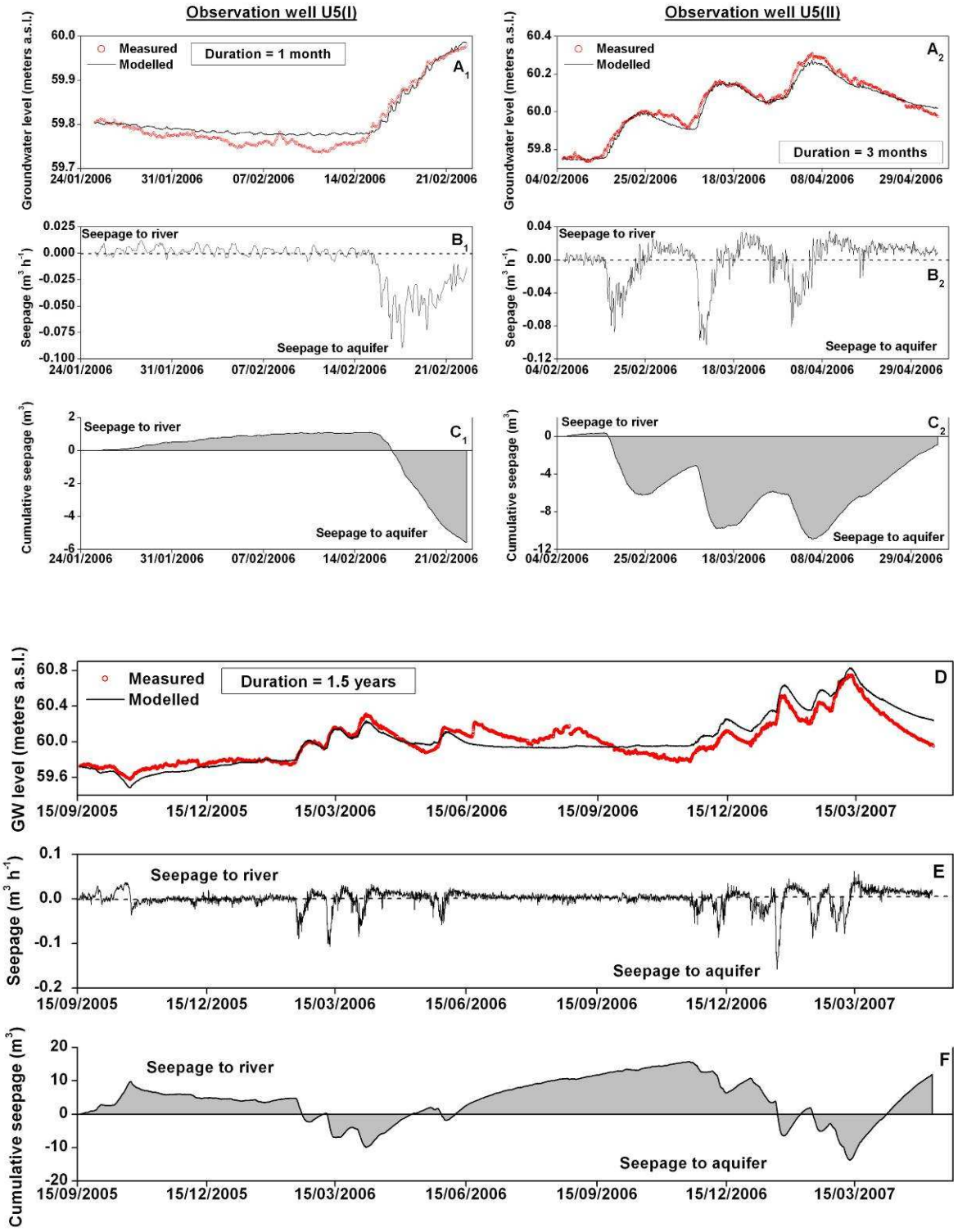

Figure 5.4. Measured and modelled groundwater head and corresponding calculated seepage and cumulative seepage for observation well U5 (distance: 113.9 m).

As shown by the different examples presented in Figure 5.3 and Figure 5.4, a very good adjustment can generally be obtained, with coefficient of determination from 0.849 to 0.995. Generally speaking, the adjustment is better in two cases:

1. when shorter calibration periods are considered (e.g. Figure 5.3A_1-A_2 as compared to Figure 5.3D);
2. for wells located closer to the Meuse River (e.g. Figure 5.3D as compared to Figure 5.4D).

When a well is located close to the river, its dynamics is more strongly related to that of the river (as discussed in Chapter 4). At the same time, if shorter periods of time are considered for the calibration procedure, matching between observed and measured groundwater levels is much better. On the contrary, if a long period of time is considered for the calibration procedure, it is likely that factors other than changes in river stage are likely to change, such as rainfall. It becomes difficult to consider the time changes in all influencing factors, and a *mean* calibration can only be obtained. For example, between June and September 2006 groundwater heads increased while river water levels remained constant (Figure 5.3D and Figure 5.4D). This fact is due to high rainfall (as recorded at the Ivoz-Ramet dam station, 2-km upstream of the Flémalle site). Fortunately, the derived information (seepage rate and cumulative seepage rates) do not seem to be very affected by discrepancies in the calibration (i.e. Figure 5.3B_2, Figure 5.3C_2 compared to Figure 5.3E, or even Figure 5.4B_2, Figure 5.4C_2 compared to Figure 5.4E, where seepage and cumulative seepage rates are of the same order of magnitude, respectively).

Modelling results can also be observed concomitantly at wells located at different distances along transects (*slides*) oriented along the mean groundwater flow direction. Modelling results for observation wells located in *slides* S1, S3 and S4 are presented in Figure 5.5, Figure 5.6, and Figure 5.7. Results are presented for a single monitoring period, and hydrographs corresponding to observation wells in the same transect are presented one next to the other to facilitate comparison of modelling results.

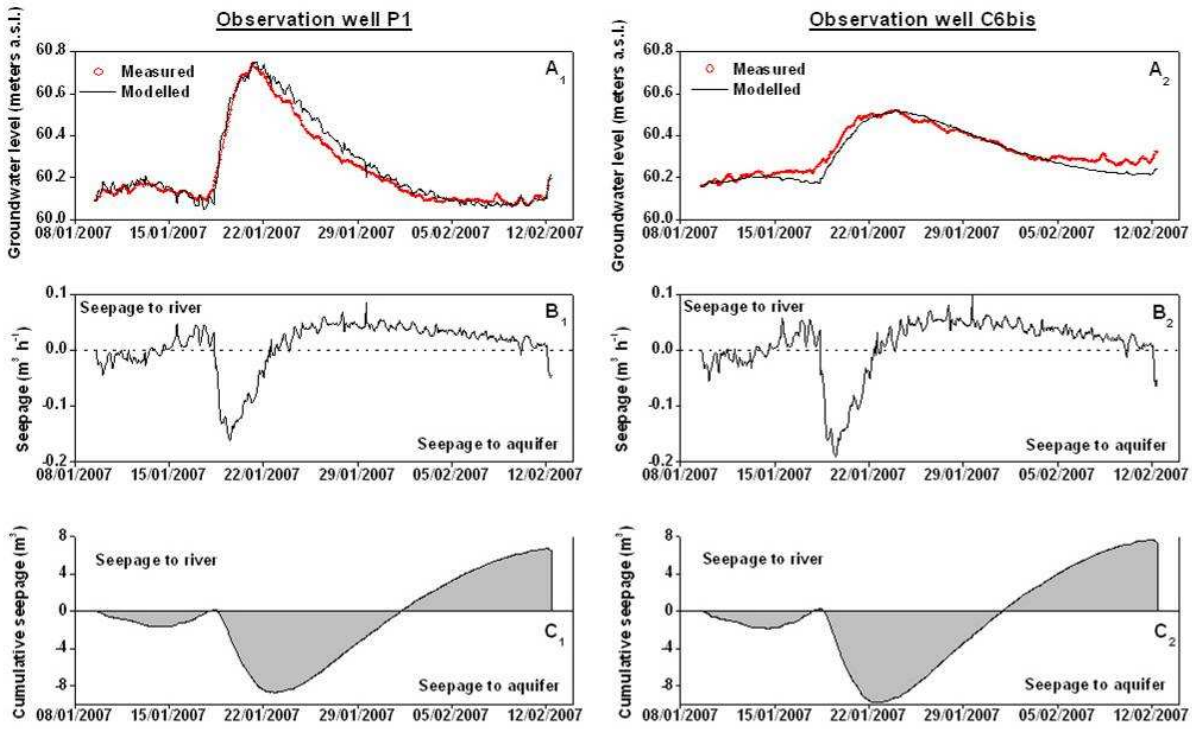

Figure 5.5. Measured and modelled groundwater head and corresponding calculated seepage and cumulative seepage for observation wells P1 and C6bis, located in S1 (distance: 62.4 and 156.0 m respectively).

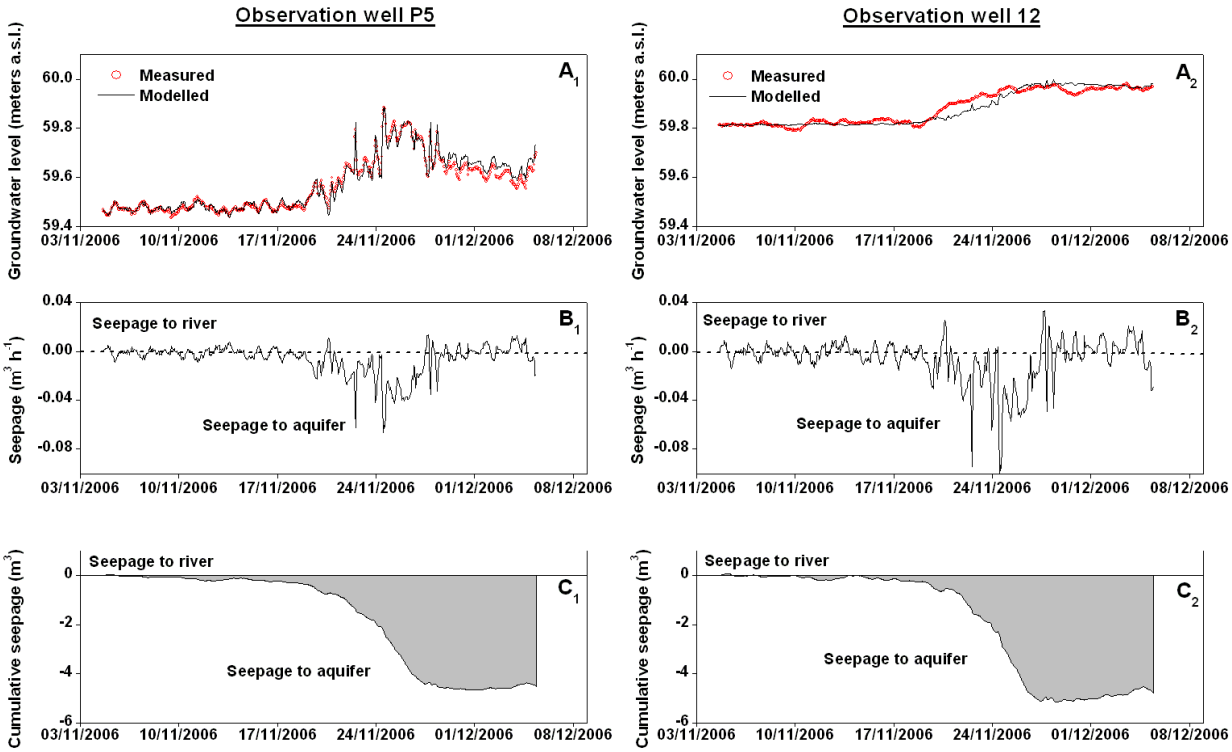

Figure 5.6. Measured and modelled groundwater head and corresponding calculated seepage and cumulative seepage for observation wells P5 and 12, located in S3 (distance: 45.7 and 136.4 m respectively).

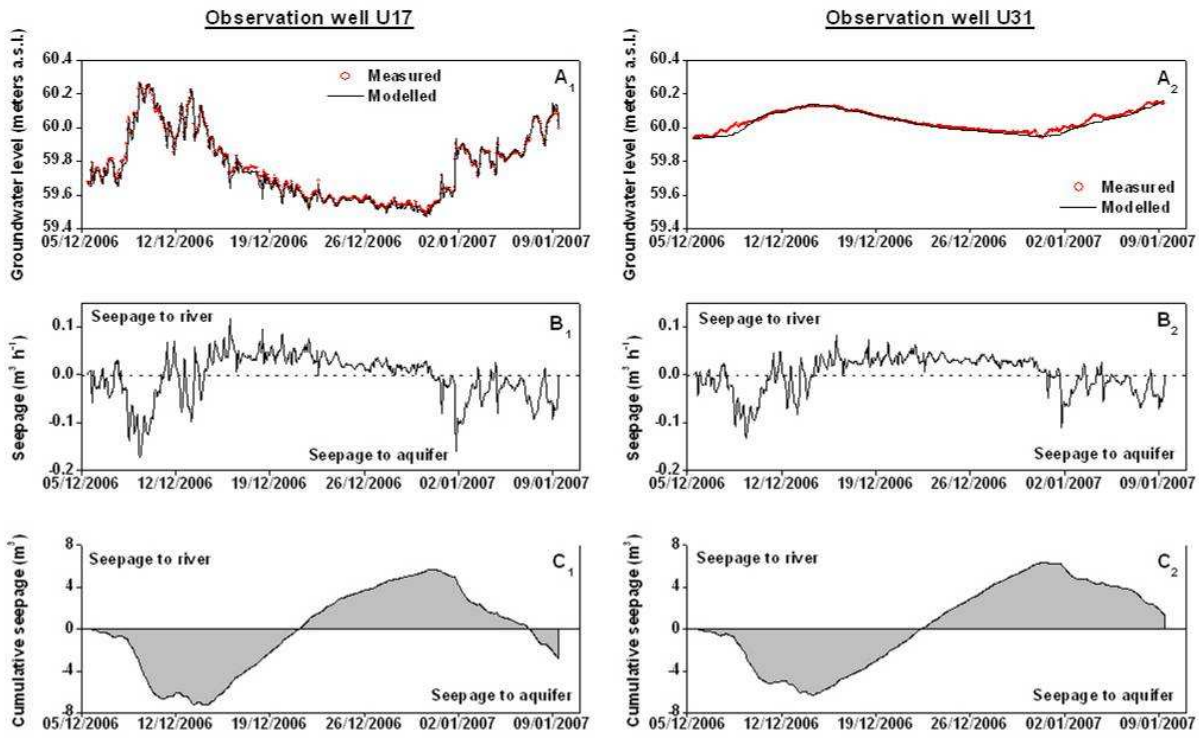

Figure 5.7. Measured and modelled groundwater head and corresponding calculated seepage and cumulative seepage for observation wells U17 and U31, located in S3 (distance: 38.7 and 188.1 m, respectively).

As already mentioned, monitored groundwater heads in observation wells located near the Meuse River fit better than those for observation wells located at a longer distance from the river (Figure 5.5A_1 and A_2, Figure 5.6A_1 and A_2, and Figure 5.7A_1 and A_2). This is due to the attenuation of the wave pressure transmitted by the river stage variations, which contributes to smoothness and delay of the river peak fluctuation. However, despite the differences in calibrating groundwater levels at shorter and longer distances from the Meuse River, the predicted seepage and cumulative seepage rates are very similar, as can be observed in Figure 5.5B_1 and B_2 (seepage rate), in Figure 5.5C_1 and C_2 (cumulative seepage rate), and in Figure 5.6B_1 and B_2 (seepage rate), and Figure 5.6C_1 and C_2 (cumulative seepage rate), or even in Figure 5.7B_1 and B_2 (seepage rate) and Figure 5.7C_1 and C_2 (cumulative seepage rate).

5.2.3.2. Quantification of seepage rates and Darcy fluxes

An interesting capability of the analytical model is its capability to compute seepage rates between the aquifer and the river, and their direction, at the river – aquifer interface. A diminution of seepage rate or change in its direction is likely to occur when there is a decrease or an inversion of the hydraulic gradient between the river and the aquifer due to a change of water level in the river.

As an example, an inversion of gradient is observed in observation well P1 in January 2007 (Figure 5.5B$_1$). During that event, the water level in the Meuse River rose of about 1.5 m (data not shown), resulting in an increase of the groundwater level at P1 of ± 0.6 m. During this period, the analytical solution allows one to calculate the inversion of seepage rate across the aquifer – river interface, with a surface water flow rate of up to 0.15 m^3 h^{-1} per m of riverbank.

Transient Darcy fluxes (v_D) in the river – aquifer interface for the hydraulic year 2005-06 were calculated considering the four different *slides* presented in Figure 5.2. Mean hydrodynamic parameters corresponding to observation wells located in each slide were used (Table 5.1). The evolution of Darcy fluxes are presented in Figure 5.8.

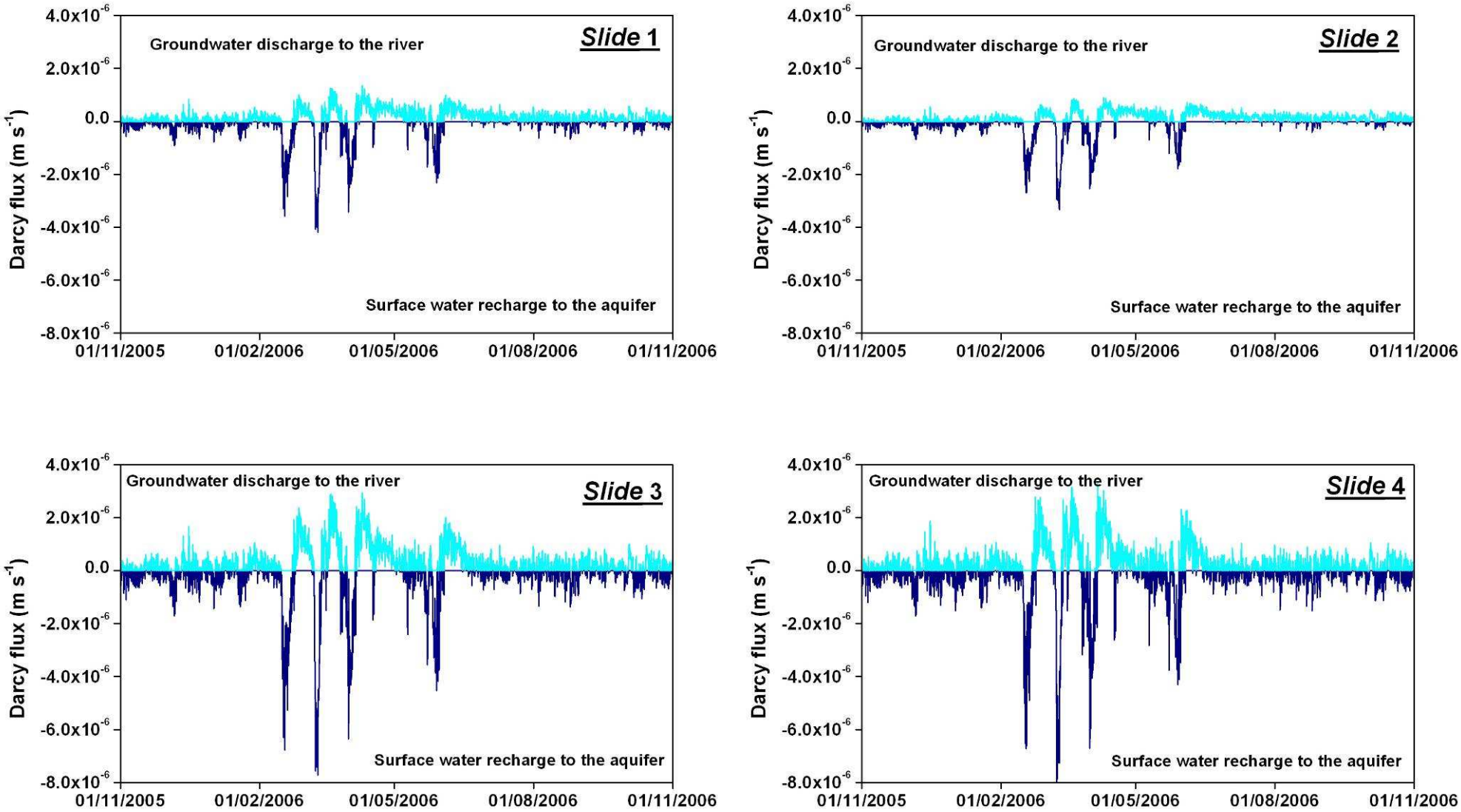

Figure 5.8. Transient Darcy fluxes calculated with the analytical model.

Maximum and mean Darcy fluxes presented in Figure 5.8 are summarised in Table 5.2.

Table 5.2. Summary of calculated Darcy fluxes at the river-aquifer interface using the analytical model.

	Darcy flux discharge to the river (m s^{-1})		Darcy flux recharge to the aquifer (m s^{-1})	
	Maximum	**Mean**	**Maximum**	**Mean**
***Slide* 1**	4.19×10^{-6}	4.25×10^{-7}	-1.36×10^{-6}	-2.65×10^{-7}
***Slide* 2**	9.12×10^{-7}	2.10×10^{-7}	-3.33×10^{-6}	-3.68×10^{-7}
***Slide* 3**	2.94×10^{-6}	5.18×10^{-7}	-7.72×10^{-6}	-7.23×10^{-7}
***Slide* 4**	3.35×10^{-7}	5.13×10^{-7}	-8.14×10^{-6}	-6.60×10^{-7}

Mean Darcy fluxes discharging to the river range between 2.10×10^{-7} and 5.18×10^{-7} m s^{-1}, while maximum values are up to 4.19×10^{-6}. A similar situation but of inversed sign was found for Darcy fluxes recharging the aquifer, with mean values between -2.65×10^{-7} and -7.23×10^{-7} m s^{-1}, and maximum values up to -8.14×10^{-6}. This confirms the high influence of transient conditions of the river – aquifer interactions. This situation is likely to have important consequences for the dispersion of dissolved contaminants in the aquifer.

Analytically computed Darcy fluxes will be subsequently compared to those obtained from the numerical modelling approach.

5.2.4. Conclusions on analytical modelling

First estimates of aquifer hydraulic conductivities, specific yield, recharge and riverbank hydraulic conductivity were obtained by modelling analytically the alluvial aquifer of the former Flémalle coke plant. Even if the analytical solution assumes that the aquifer is homogeneous along each slide, it turns out to be robust and efficient in reproducing the dynamics of piezometric levels. Furthermore, it allows obtaining very useful information on the hydrodynamics of the alluvial aquifer and riverbank (estimates of K, S_y and K_s), as well as seepage rates (Q_{riv}) across the river – aquifer interface including their dynamics with time.

5.3. Numerical modelling

Although analytical modelling supplies reliable and valuable results concerning hydrodynamic aquifer properties and groundwater flow budgets, numerical modelling allows for advanced data analysis, including more flexibility in the spatial heterogeneity of the alluvial deposits and aquifer boundaries.

A numerical groundwater flow and transport model has been developed for the Flémalle test site using MODFLOW 2000 (Harbaugh *et al.*, 2000) and MT3DMS (Zheng and Wang, 1999) under the GMS v6.5 (Environmental Modeling Systems, Inc.) environment.

MT3DMS is an extended version of MT3D (Zheng, 1990) that can simulate transport of multiple contaminant species at one time, as well as simulate radioactive decay and biodegradation. Solute transport computations are based on the flow field calculated with MODFLOW.

5.3.1. Groundwater flow modelling

5.3.1.1. Conceptual model and boundary conditions

Although the site of concern is restricted to the brownfield of 400 m length and 200 m width, the limits of the modelled zone have been extended to a larger part of the alluvial plain in order to fit with more “natural” boundary conditions and to avoid the influence of prescribed boundary conditions on the modelling results obtained in the site (Figure 5.9).

Upstream along the Meuse River (SW boundary), the model was extended up to the Ivoz-Ramet dam where a difference of 3 m in the Meuse River water level is produced by the dam, inducing a lateral “bypass” of water through the alluvial plain. At this boundary, piezometric levels are prescribed at a level equal to the water level in the Meuse River upstream of the dam, to account for the possible “bypass” of surface water. Downstream along the Meuse River (NE boundary), the model is extended to 1 km downstream of the Flémalle site. At this boundary, piezometric levels are prescribed because there is no reason to think that no flow may occur there. Laterally (NW boundary), the modelled area is extended to the limit between the alluvial plain and the shaly bedrock. Because of the large difference in hydraulic conductivity between the shaly bedrock and the alluvial deposits, a no-flow boundary condition was assumed. At the boundary between the Meuse River and the alluvial aquifer (SE boundary), a third type (Fourier) boundary condition is assumed, similarly to the analytical solution, to account for the riverbank effect.

Unfortunately, piezometric data are not available outside the Flémalle cokery site to adjust groundwater head values, thus regional conditions were assessed in order to optimise groundwater head values inside the local site, without regarding what happens outside.

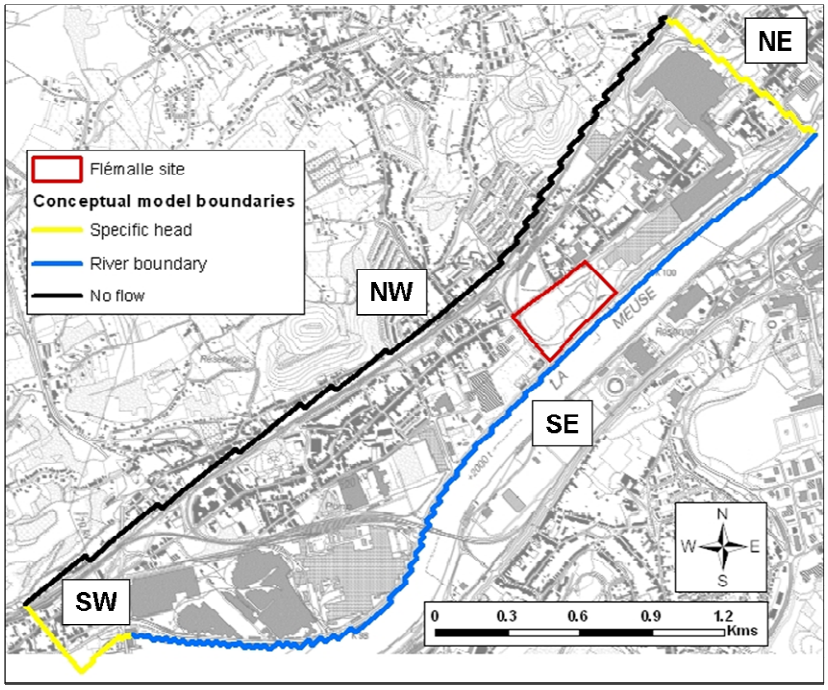

Figure 5.9. Illustration of the regional and local modelling zone, and main features considered in the conceptual model.

5.3.1.2. Finite difference discretisation

The modelled domain is made of a single layer subdivided horizontally into 204 columns and 88 rows with variable grid refinement from 5m × 5m inside the Flémalle site to 25m × 25m at the limits of the modelled domain, with a total number of 17952 active cells. The top of the model is considered as the soil surface topography. The bottom of the model is considered at the top of the shale bedrock, hydrogeologically considered as impermeable. Because the depth of the bedrock is not perfectly known, it was interpolated from point estimates coming from boreholes information.

As mentioned in Chapter 2, the Flémalle site is characterised by a backfill layer above the alluvial aquifer, with a variable thickness between 2 and 5 meters and composed of a large variety of materials (waste materials from former building, ashes…). Because of the presence of silty lenses in this layer, perched lenses of water are present seasonally. However, they cannot really be considered as an aquifer, because there is no gradient for groundwater

flowing. Further, during summer - autumn season, these perched lenses are dry and they have been disregarded.

The upper part of the aquifer is characterised by a mixing of silt-sand small gravel dimensions, which confers to the aquifer semi-unconfined conditions. However, because this situation is only met from place to place in the field, the alluvial aquifer has been considered as unconfined.

Finally, because it is a 2D groundwater model, only horizontal heterogeneity is considered, taking into account depth-average conditions for the vertical heterogeneity.

5.3.1.3. Calibration approach: zonation and pilot points

As mentioned before, the regional model deserves the objective of excluding boundary conditions from the zone of interest in the model, i.e. the brownfield, and to distribute piezometric levels and groundwater fluxes as naturally as possible at the boundaries of the brownfield. In other words, the regional scale is not supposed to provide an accurate representation of the regional piezometry and aquifer heterogeneity, but only to provide natural boundary conditions at the limits of the brownfield. On the contrary, in the brownfield, it is required to obtain a representation, as accurate as possible, of the heterogeneity of the gravels and of the piezometry, which are two of the most determinant factors for the fate of contaminant present there. The model calibration was performed using a two-scale approach: classical zonation for the regional model combined to pilot points (de Marsily *et al.*, 1984) distributed throughout the area corresponding to the Flémalle brownfield. The pilot points provide an efficient parameterisation method for setting into evidence and considering in the calculation, the heterogeneity of the alluvial deposits and thus the consequence on groundwater flow and contaminant transport in the test site. The zonation approach used at regional scale offers enough flexibility to adjust piezometric levels around the site without introducing overparameterisation, provided that the number of zones defined remains as small as possible.

Hydraulic conductivity values at the pilot points are optimised so as to minimise discrepancies between observed and calculated groundwater levels. Optimised hydraulic conductivity values are interpolated to the entire zone, giving an appropriate heterogeneity image of the aquifer. In the absence of geostatistical data describing the spatial distribution of the hydraulic conductivity data, the interpolation method of *inverse to the distance weighted* has been used. Parameterisation is accomplished through optimisation using PEST (Parameter Estimation; Doherty, 2003), available also in the GMS software.

Three different subdivisions of the model domain were considered in the zonation approach: 4, 3 and 2 zones (not shown). Although the best match between observed and modelled groundwater heads was for the scheme corresponding to 3 zones, the final scheme retained was the one considering 2 zones, one of them corresponding to the brownfield in which a total of 82 pilot points were defined (Figure 5.10). The small differences between observed and modelled groundwater heads and the lack of information to consider different zones outside the brownfield were the reasons of this choice.

Based on the hydraulic conductivity values obtained from the pumping tests, upper and lower bounds of *K* values for the pilot points are fixed at 1×10^{-5} and 5×10^{-2} m s^{-1}, with an initial value of 1×10^{-3} m s^{-1}.

The calibration was performed in two main steps described hereafter: first an initial steady state calibration aiming at obtaining acceptable fit of the piezometric heads; second, transient simulations aiming at better reproducing the dynamics of groundwater levels and groundwater fluxes and the spatial heterogeneity of the alluvial deposits.

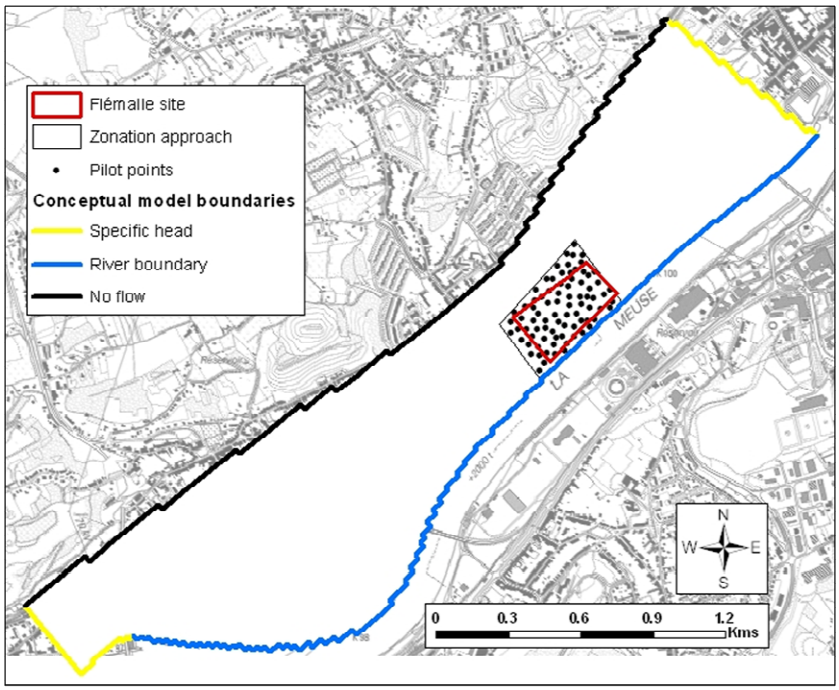

Figure 5.10. Delimitation of the 2 zones and the 82 pilot points (inside the zone corresponding to the Flémalle site) used in the combined zonation - pilot point approach with automatic inverse modelling.

5.3.1.4. Steady state calibration

The initial steady state calibration was performed with the zonation approach only using successively the 14 monthly campaigns performed between February 2005 and December 2006, together with monthly mean groundwater recharges. Depending on the monthly piezometric campaign, between 52 and 86 piezometric measurements were used to accomplish the steady state calibration. Simulated *vs.* modelled groundwater head values, corresponding to overall 14 campaigns are presented in Figure 5.11. The regression coefficient showed is the best match between observed and modelled groundwater heads under steady state conditions, corresponding to the campaign carried out in March 2005. This simulation will serve as starting point for the subsequent transient calibration.

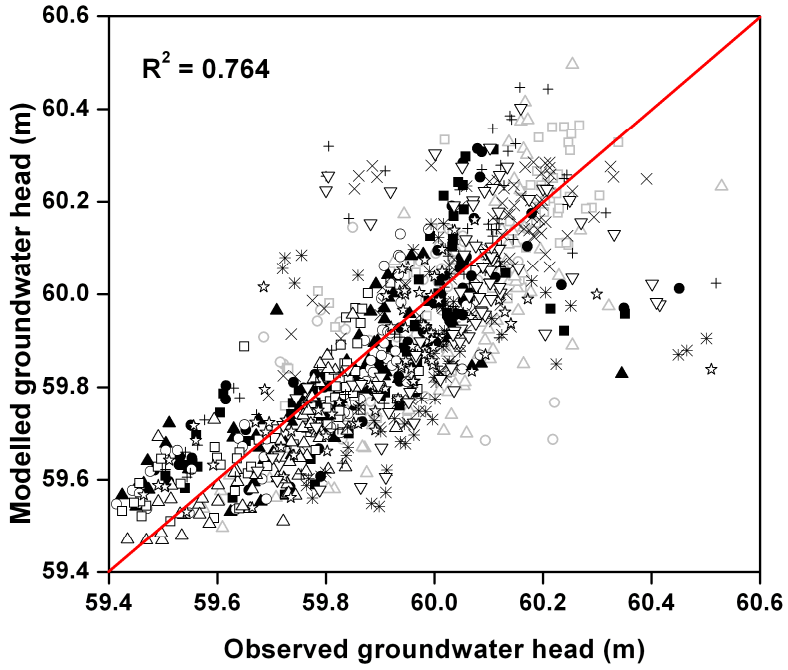

Figure 5.11. Observed vs. modelled groundwater head of the steady state calibration of 09.03.2005.

5.3.1.5. Transient calibration

Monitored groundwater levels obtained from the automatic monitoring campaign performed from 2005 to 2007 were used for the transient calibration. Most of the observation wells depicted in Figure 5.2 were used to accomplish this task. However, instead of hourly data, daily data were used, in order to avoid memory crashes due to the huge quantity of data (more than 25,000 water level values are available for some monitored wells). To do so, datasets were resampled to account for daily data, using finally 1,865 groundwater head observations for the transient calibration. The same procedure was done for river data.

As mentioned before, the hydraulic conductivity zone corresponding to the Flémalle site was replaced by 82 pilot points. Initial *K* values for the 2 zones correspond to those of the steady state calibration, and upper and lower bounds for these zones are the same as for the pilot points.

Groundwater recharge is not directly measurable, and indirect methods, mainly based on water balance and Darcy's law, are quite inaccurate. Recharge estimation becomes even more inaccurate in urbanised areas, because these environments are highly heterogeneous in terms of land use, subsoil characteristics and other factors, which influences all hydrological processes. Urban surfaces, such as road pavements or parking slots, are not impervious, as shown by Ragab *et al.* (2003), who observed that 6 - 9% of total annual rainfall recharges the aquifer, and that 21 – 24% evaporates. Consistent results where found by Grimmond and Oke (1991; 2002), Berthier *et al.* (2006) and Dupond *et al*. (2006), who considered evapotranspiration to be a major component of the water budget within urban areas.

According to Ragab *et al*. (2003), and considering that recharge rate in analytical modelling was around 10% of the annual rainfall at the Ivoz-Ramet dam station, this ratio was considered to define the groundwater recharge into the numerical model, based on daily rainfall data. A "warm-up" period of 5 months before the first observed data was used to reach the natural equilibrium of the system.

5.3.1.6. Results of transient calibration

Transient calibration of the groundwater flow model has resulted in a detailed spatial distribution of the hydraulic conductivity (Figure 5.12). It is evident that the heterogeneity of the alluvial aquifer is important in the Flémalle site, with hydraulic conductivity values ranging from 1×10^{-5} m s^{-1} to 5×10^{-3} m s^{-1}, with a predominant mean value of 1×10^{-4} m s^{-1} around the site. These values are consistent with those estimated from pumping tests.

The spatial distribution of the hydraulic conductivity is very similar for the three scenarios considered (4, 3 and 2 zones). As already mentioned, the final scheme retained was the one consisting in 2 zones. Matching between measured and modelled groundwater heads is very similar for the three schemes, but we do not dispose of evidences to consider different zones outside the brownfield. Moreover, the scheme with 3 zones present the highest *K* values, which is in lesser good agreement with results of pumping tests performed.

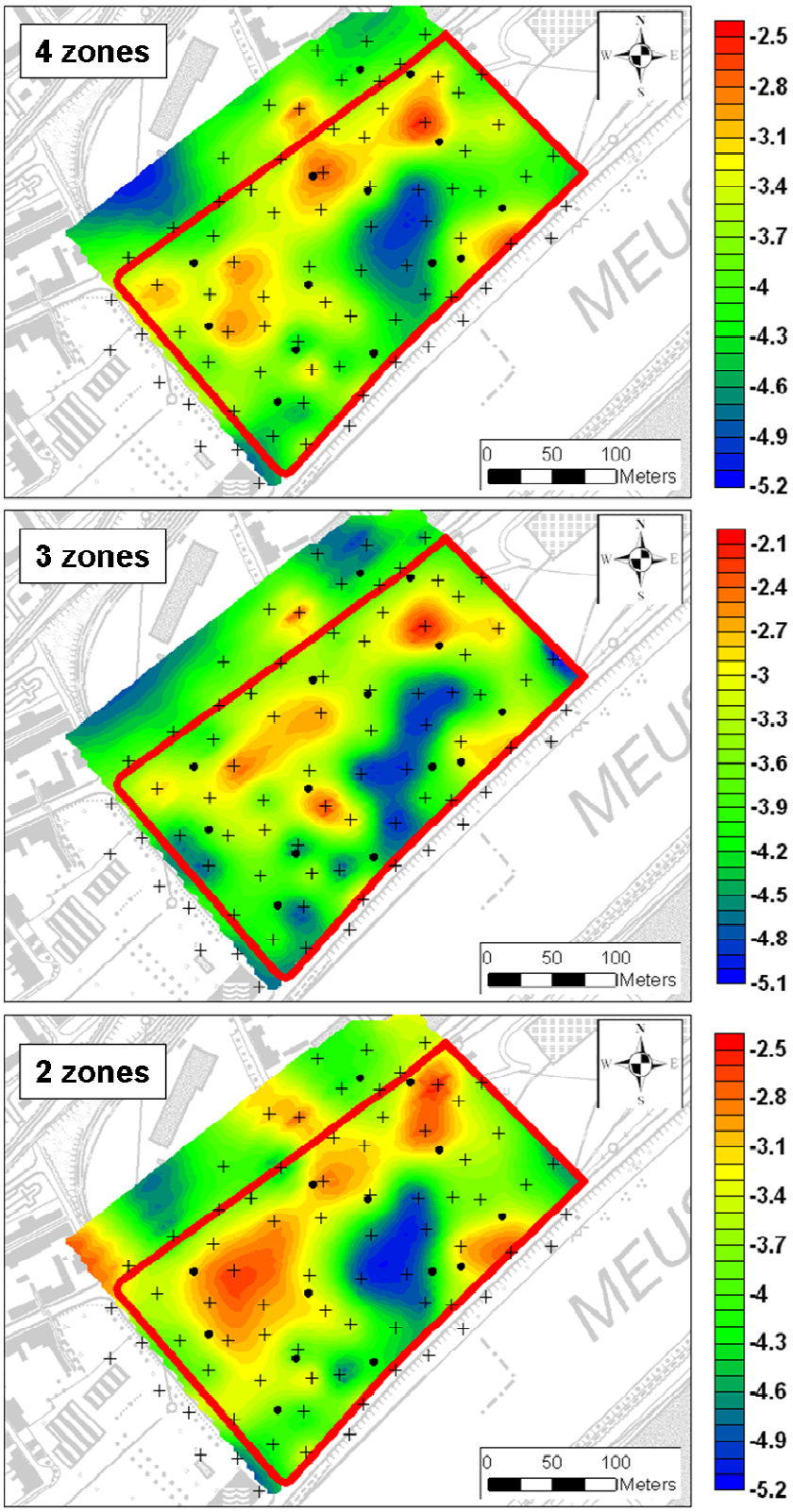

Figure 5.12. Spatial distribution of the log *K* in the Flémalle test site resulting from the pilot point transient calibration of piezometric levels obtained using the Meuse as a stress factor. Crosses indicate location of pilot points; dots indicate location of monitoring wells used in the calibration process.

Figure 5.13 presents the observed *vs*. modelled groundwater heads, which states the quality of matching of the calibration. Groundwater heads are located in the diagonal line, indicating the good fit of the modelled groundwater heads. Although the spatial subdivision retained was the one consisting in 2 zones, observed *vs*. modelled groundwater heads with 4 and 3 zones are also presented in Figure 5.13 for comparison.

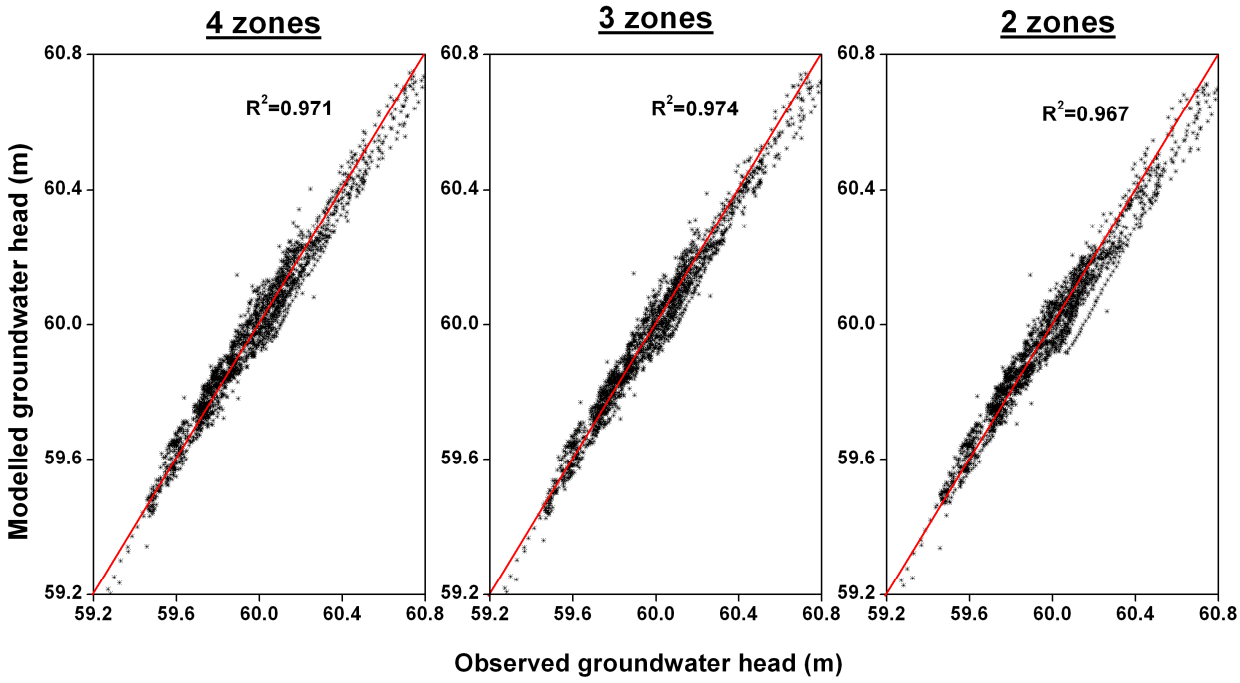

Figure 5.13. Observed *vs.* modelled groundwater heads.

Hydrographs of the observed and modelled groundwater heads are presented in pairs of observation wells, located in the same orthogonal transect to the river at two different distances from the river, near and far respectively. For those pairs, vertical scale is the same for a better comparison. Figure 5.14 presents results for two long series monitored, one year and one year and half for observation wells P3 and U5, respectively.

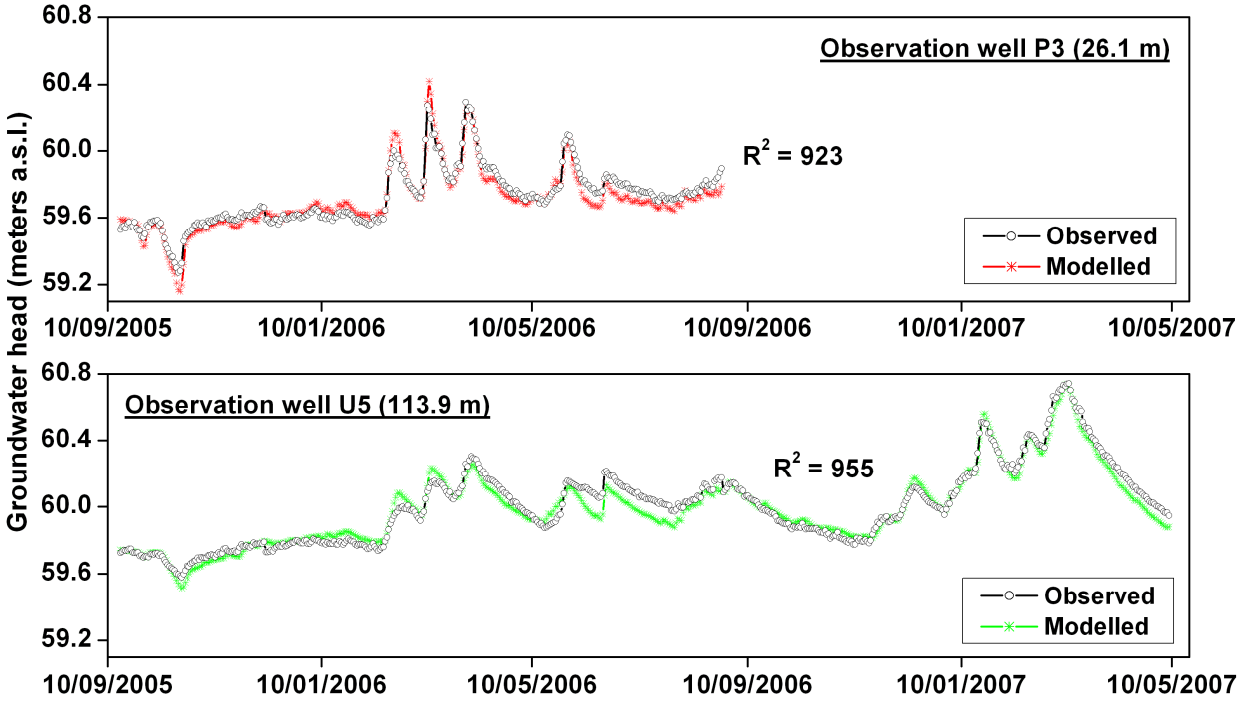

Figure 5.14. Observed and modelled groundwater heads in observation wells P3 and U5.

Shorter monitored periods are presented in Figure 5.15 and Figure 5.16. Observed and modelled groundwater heads are in a good agreement, corroborating the good model fit.

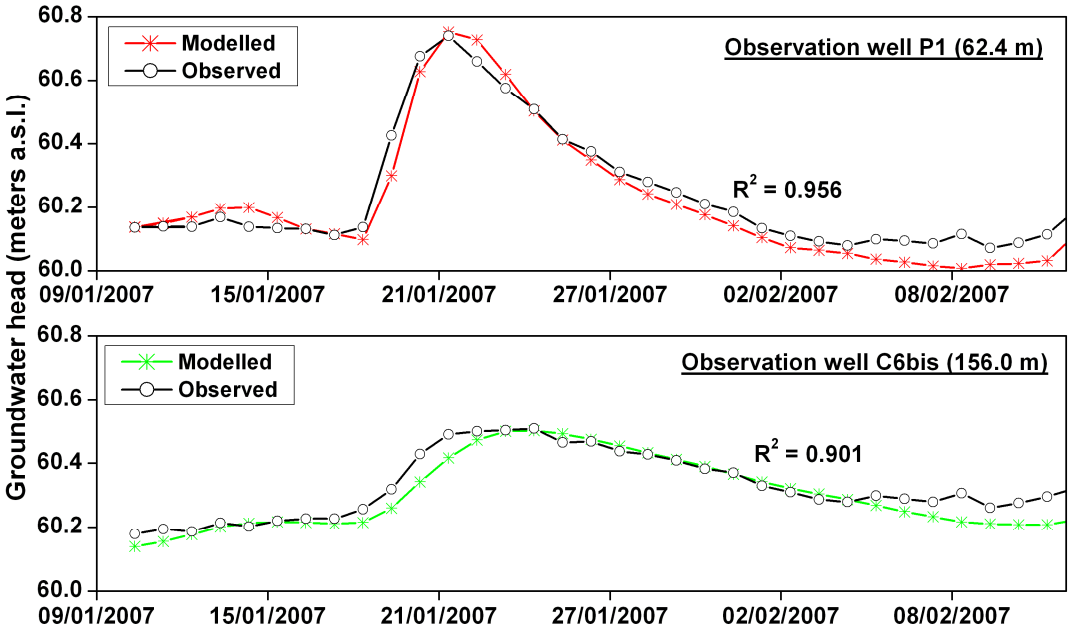

Figure 5.15. Observed and modelled groundwater heads in observation wells P1 and C6bis.

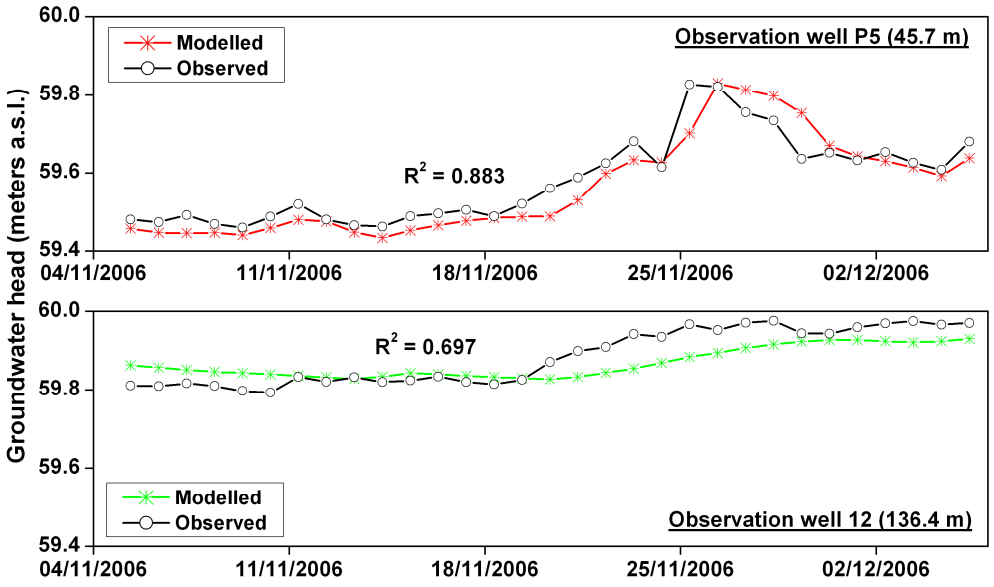

Figure 5.16. Observed and modelled groundwater heads in observation wells P5 and 12.

5.3.1.7. Riverbank hydraulic conductivity and transient Darcy flux

The hydraulic conductivity value of the riverbank (K_s) used in the numerical model is of 6.74×10^{-4} m s^{-1}, in relatively good agreement with the range of values from the analytical model, i.e. 1.88×10^{-5} to 1.07×10^{-4} m s^{-1} (Table 5.1).

Transient Darcy fluxes estimated at the river-aquifer interface, for the hydrologic year 2005-06, are presented in Figure 5.17.

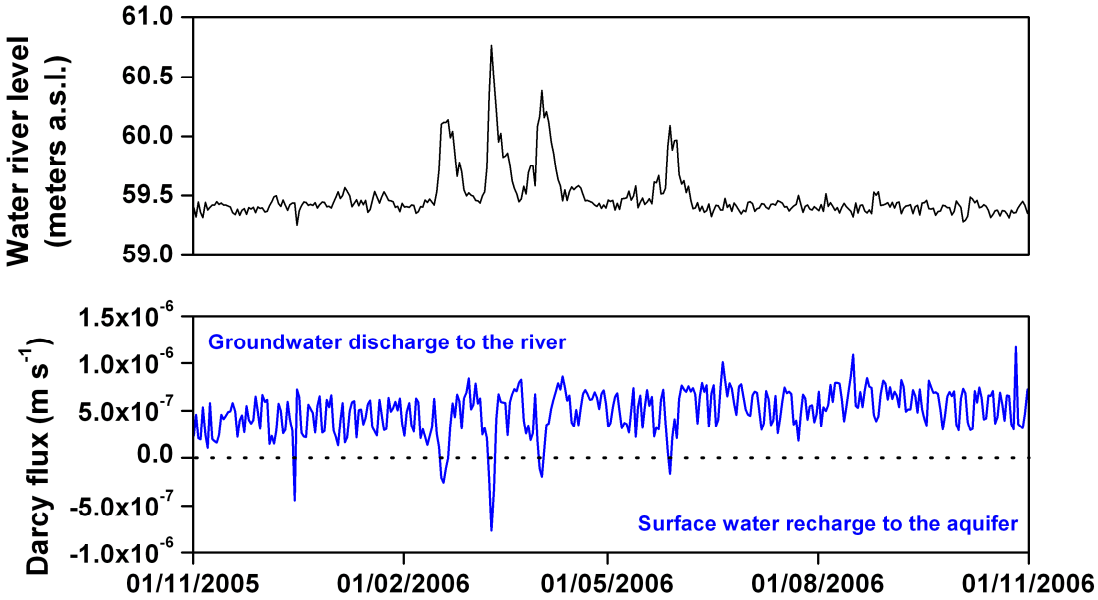

Figure 5.17. Meuse River level fluctuations and Darcy flux variations in the river – aquifer interface in front of the Flémalle site for the hydrologic year 2005-06.

In regular conditions, when the Meuse River level is around 59.4 meters a.s.l., the Darcy flux is positive, flowing from the aquifer to the river. However, the hydraulic gradient decrease when Meuse River level increase of some centimetres, and it is temporarily inversed when river water level increase beyond 59.9 meters a.s.l., with maximum negative Darcy fluxes observed during winter and spring months, period of the year when the river level can increase up to 61.0 meters a.s.l. This confirms again that Darcy flux changes continuously in the Flémalle site, mainly caused by hydraulic gradient changes related to river water level fluctuations. As already mentioned, this fact is likely to have a capital influence on dissolved contaminant transport in the aquifer, and will be subsequently discussed.

Table 5.3 gives a summary of Darcy fluxes calculated with the analytical and numerical approaches. Fluxes are in a good agreement, although interesting differences are worth to be noted. Darcy fluxes from the aquifer to the river calculated with MODFLOW are similar to those calculated with the analytical model. On the contrary, Darcy fluxes from the river to the aquifer calculated with MODFLOW are lesser important than those calculated with the analytically. This could be mainly due to: (1) the "regional" scale of the numerical model, aiming to accounts for upstream groundwater coming from the Ivoz-Ramet dam, while the analytical model only considers rainfall as recharge; (2) the assumption of the analytical model that the initial river water level is set at the same as the groundwater level (however, this fact should have only effect at the beginning of the simulated period); (3) the analytical model used hourly data for river fluctuations, while the numerical model used daily river fluctuations; doing so, small increases of river water level in the analytical model are translated in an inversion of the hydraulic gradient, while in reality, it contributes only to decrease but not to inverse the hydraulic gradient, as calculated with the numerical model. This contributes to a difference of one order of magnitude in the total volume per year of groundwater flowing from the aquifer to the river in front of the Flémalle brownfield, estimated at 4.8×10^{4} m^3 and 1.7×10^{3} m^3 with the numerical and analytical model, respectively.

Table 5.3. Comparison of calculated Darcy fluxes at the river-aquifer interface using analytical and numerical models.

	Darcy flux discharging into the river ($m\ s^{-1}$)		Darcy flux recharging the aquifer ($m\ s^{-1}$)	
	Maximum	**Mean**	**Maximum**	**Mean**
MODFLOW	1.2×10^{-6}	5.1×10^{-7}	-7.7×10^{-7}	-4.1×10^{-8}
STWT1	2.2×10^{-6}	4.0×10^{-7}	-8.1×10^{-6}	-6.0×10^{-7}

The groundwater flow model has also been used to calculate local Darcy fluxes at the grid cells where observation wells used for the FVPDM are located. Estimated Darcy fluxes using three approaches, the FVPDM, the MODFLOW and the Darcy's law equation, are presented in Table 5.4.

Table 5.4. Comparison of Darcy flux estimates in the observation wells where the FVPDM was performed.

Well ID	Darcy flux ($m\ s^{-1}$)			
	FVPDM	**MODFLOW**	**Darcy's law (estimated *K* values from pumping tests)**	**Darcy's law (estimated *K* values from MODFLOW)**
P1	3.0×10^{-6}	2.9×10^{-7}	5.6×10^{-7}	8.5×10^{-8}
P3	1.5×10^{-5}	8.0×10^{-7}	9.8×10^{-7}	2.1×10^{-7}
P4	2.7×10^{-5}	2.0×10^{-7}	4.8×10^{-6}	1.2×10^{-7}
U15	3.0×10^{-4}	4.4×10^{-7}	1.1×10^{-5}	2.3×10^{-6}

Darcy fluxes calculated with the numerical model are from 1 to 3 orders of magnitude lower than those obtained with the FVPDM. As already argued by Batlle-Aguilar and Brouyère (2007), the FVPDM provides a point estimate of Darcy fluxes, with limited integration of aquifer heterogeneity around the tested well and with a possible influence of flow field distortion in the vicinity of the injection well bore (Brouyère, 2003). On the contrary, the numerical model integrates an important area comprised from 2 km upstream and downstream of the Flémalle site and, moreover, is a 2D simplification of the reality. Darcy's law, from its side, is the most simple approach to estimating groundwater fluxes but it can be subject to important errors (Devlin and McElwee, 2007), and it is only valid at the scale of the distance between the observation wells used to calculate the hydraulic gradient or at the scale of the pumping test used to determine the hydraulic conductivity. Unfortunately, since this was the first time that the FVPDM was applied in the field, no examples exist in the literature to compare these results with others obtained in similar conditions.

The discrepancies observed do not invalidate the Darcy flux estimation from the FVPDM. Because of its very local scale of application, is an important technique to estimate in a detailed way Darcy fluxes for remediation techniques, such as reactive barriers, because their feasibility and efficiency mainly depend on the local magnitude of groundwater and contaminant fluxes in the aquifer. Moreover, as shown in Chapter 4, it is an efficient technique to detect small changes in Darcy fluxes.

5.3.2. Calibration of the contaminant transport model using tracer tests results

Developing a transport model responds to the objective of evaluating the pollutants fate in the alluvial aquifer and the risk of contaminant dispersion offsite.

As described in Chapter 2, there are many different kinds of contaminants in the Flémalle site (BTEX, PAHs, mineral oils,…). In the scope of this work, it has been decided to focus on benzene for several reasons:

- the contaminant sources are relatively well known (position and strength);
- benzene is a very common groundwater contaminant, encountered at very high concentrations in the Flémalle site and that causes much more worries as compared to others also present in the alluvial aquifer of Flémalle, due to its high solubility (1.78 g L^{-1}, Alvarez and Illman, 2006);
- in the scope of the AquaTerra project, CHYN (Centre for Hydrogeology of Universitvy of Neuchâtel, Switzerland. Daniel Hunkeler & Barbara Morasch) have studied, at field and laboratory scale, the biodegradation potential for benzene in Flémalle (Morasch *et al.*, 2007a; Morasch *et al.*, 2007b).

The transport model, performed with MT3DMS (Zheng and Wang, 1999), was calibrated using radially converging flow tracer tests performed in the field (previously described in Chapter 4).

5.3.2.1. Boundary conditions and spatial discretisation for tracer tests modelling

The basis of the transport model is the groundwater flow model described previously. A submodel is used with dimensions of 316 × 260 m. The model domain is subdivided in 183 columns and 159 rows, with variable grid refinement 0.5m × 0.5m in the vicinity of the recovery and injection wells to 5m × 5m in the limits of the model, with a total of 29,097 active cells.

At the boundary between the Meuse River and the alluvial aquifer (SE boundary), a third type (Fourier) boundary condition is assumed, as done for the groundwater flow model. On the NE, NW and SW boundaries, piezometric levels are prescribed. However, instead of considering these boundaries as constant value groundwater heads, time-varying piezometric levels are considered as computed by the regional groundwater flow model for the period corresponding to the tracer test. Taking into account that groundwater heads in the aquifer are strongly influenced by river level variations, this assumption is much more conforming to reality.

5.3.2.2. Calibration of tracer tests

Among the 6 different tracers used during the tracer tests (eosin yellowish, naphtionate, uranine and sulforhodamine B as dye tracers, and iodide and lithium as salt tracers), iodide and eosin yellowish are known as the most conservative (Käss, 1998; Brouyère, 2001). Both, iodide and eosin yellowish have been considered as reference tracer tests and thus used for calibration of the transport model. However, the other tracer tests have also been modelled afterwards to try to explain the non-arrivals and to identify their specific properties in the alluvial aquifer.

The procedure used to calibrate the tracer tests is as follows:

- In a first step, the model is calibrated to reproduce T_{min} and T_{mod} (time of the first and modal arrival –concentration peak- of the tracer, respectively), which depend directly of advection and dispersion processes.
- Secondly, physical retardation processes are considered, using a generalised dual-domain (dual-porosity) model, as proposed and applied by Brouyère (2001) at Hermalle-sous-Argenteau (downstream of Liège), to account for concentration peak-attenuation and tailing.
- Finally theoretical sorption values for the benzene transport were also considered.

The advection dispersion equation (ADE), considering mobile immobile water effect (MIM) and sorption, has been used in transport modelling. This equation has been presented in Chapter 3, Equation (3.24). Corresponding hydrodispersive parameters used for transport calibration are summarised in Table 5.5.

Each tracer test has been calibrated independently from the others. Doing so provides a range of adjusted hydrodispersive parameters (mobile porosity -θ_m-, immobile porosity -θ_{im}-, longitudinal dispersivity -α_L-) rather than single values with which the calibration of every single tracer test would be apparently less accurate.

Calibration results for the reference tracers (iodide and eosin yellowish) are presented in Figure 5.18 and Figure 5.19 respectively. Modelling results for the other tracers used in Phase II are presented in Figure 5.20. The advection term has been solved using the explicit finite difference method.

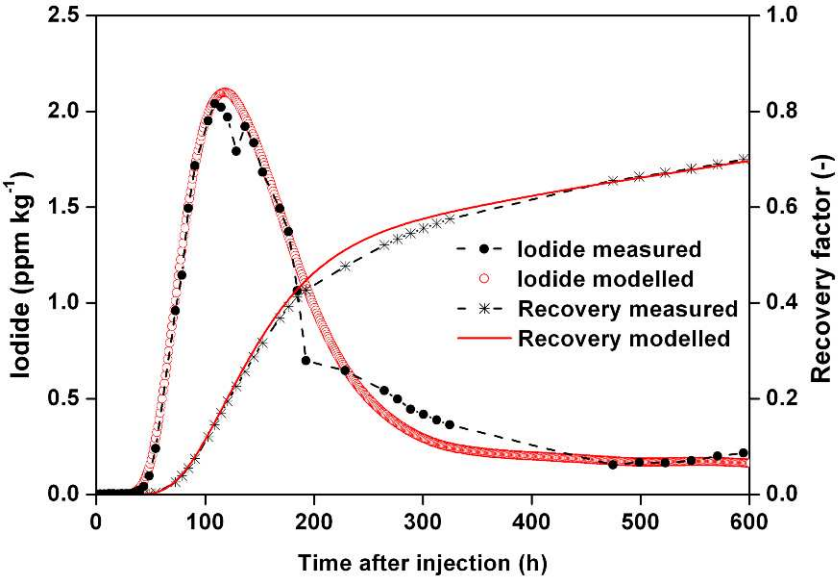

Figure 5.18. Comparison of measured and modelled breakthrough curves for the iodide tracer test (Phase II).

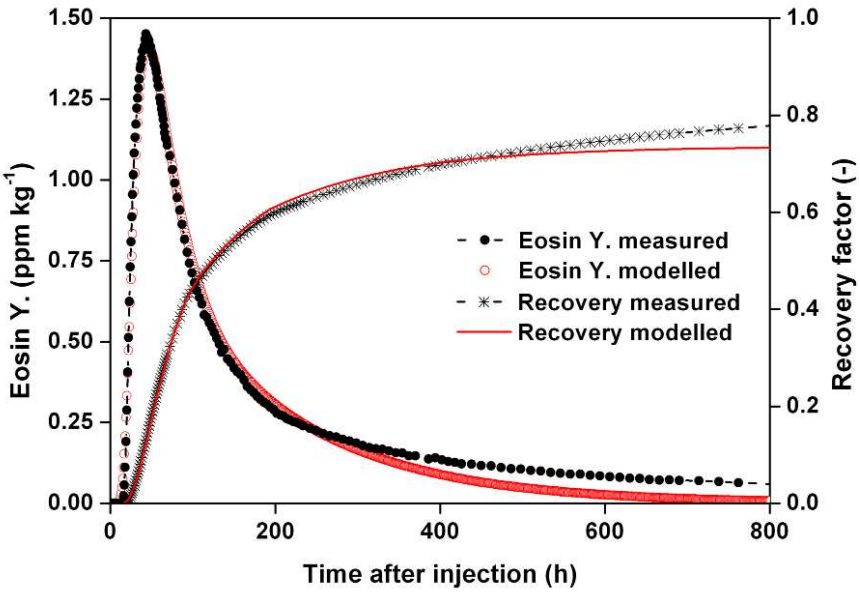

Figure 5.19. Comparison of measured and modelled breakthrough curves for the eosin yellowish tracer test (Phase II).

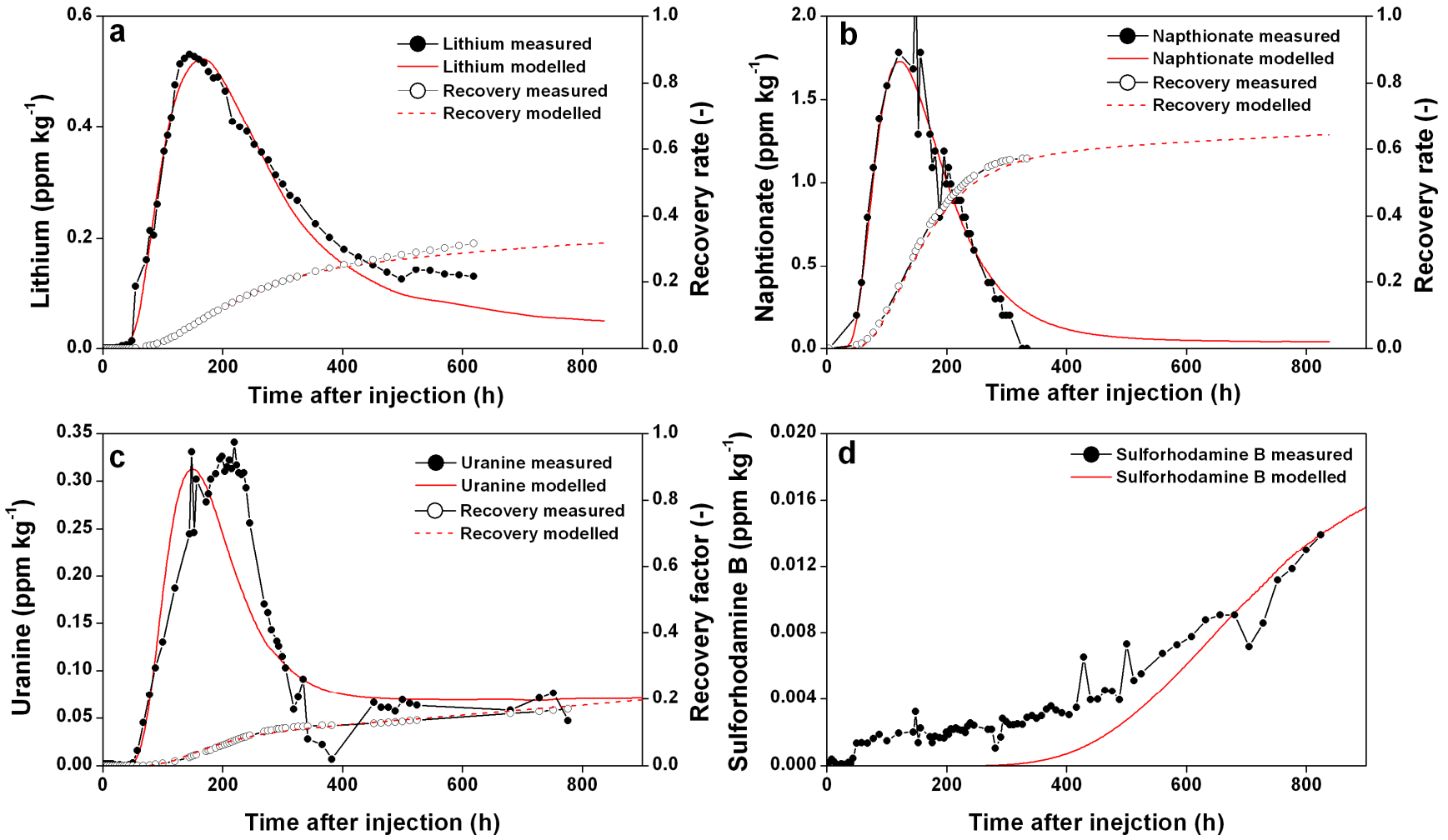

Figure 5.20. Comparison of measured and modelled breakthrough curves for lithium (a), naphtionate (b), uranine (c) and sulforhodamine B (d), corresponding to tracer test Phase II.

Table 5.5. Hydrodispersive parameters used for tracer tests calibration (θ_m: mobile porosity; θ_{im}: immobile porosity; α_L: longitudinal dispersivity; α: first-order transfer between mobile and immobile water; K_d: distribution coefficient between sorbed and dissolved phases; p: fraction of sorption in contact with the immobile phase). Bulk density - ρ_b - is set equal to 2,000 kg m^{-3}.

	θ_m (-)	θ_{im} (-)	α_L (m)	α (s^{-1})	K_d (m^3 kg^{-1})	p (-)
Iodide	0.041	0.10	1.4	4.50×10^{-8}	-	-
Eosin yellowish	0.060	0.05	3.0	1.60×10^{-7}	-	-
Lithium	0.068	0.70	4.5	1.05×10^{-7}	1.0×10^{-4}	0.91
Uranine	0.050	0.70	2.0	2.10×10^{-7}	1.0×10^{-4}	0.93
Sulforhodamine B	0.03	0.70	3.0	3.00×10^{-7}	7.6×10^{-3}	0.96
Naphtionate	0.047	0.10	2.2	2.10×10^{-8}	-	-

In general, tracer recoveries were well adjusted to those measured for the entire of tracers injected during the Phase II. Hydrodispersive parameters obtained through calibration of each tracer test independently of each other are in a good agreement, with relatively low values of effective porosity and longitudinal dispersivity. The immobile porosity is not negligible, confirming once more the high heterogeneity of the Flémalle alluvial aquifer. Although Brouyère (2001) required considering first-order degradation process to model naphtionate, this consideration was not needed here, the hydrodispersive parameters used for naphtionate being almost the same as of the reference tracers, iodide and eosin yellowish.

From the results of Brouyère (2001) in Hermalle-sous-Argenteau, it appears that, in the alluvial deposits of the Meuse River, sorption sites are preferentially located in the immobile water. To account for this retardation effect in the immobile water, the fraction of sorption in contact with the immobile domain (p) has been set between 0.91 and 0.96. However, into the GMS environment it is not possible to directly handle this value. Consequently, the immobile porosity for these tracers was increased in order to obtain higher values of p, following Equation (5.4):

$$p = 1 - \frac{\theta_m}{\theta_m + \theta_{im}} \tag{5.4}$$

where θ_m is the mobile porosity and θ_{im} is the immobile porosity.

Sulforhodamine B was modelled using a higher K_d than that used for lithium and uranine, with results relatively good considering the very low concentrations recovered. Low recovery of sulforhodamine B, compared with recoveries of dye tracers injected at the same time (naphtionate and uranine), and the elevated K_d value needed, can be justified by the high affinity of sulforhodamine B to be sorbed in silty - clay materials.

Even thought no recoveries for tracers injected during the Phase I were measured, they have been modelled for a period of 4 months (~3000 h) (sampling operations were done continuously during 3 months after tracer injection) using corresponding hydrodispersive parameters arising from tracer test calibration of Phase II. Modelled breakthrough curves are presented in Figure 5.21.

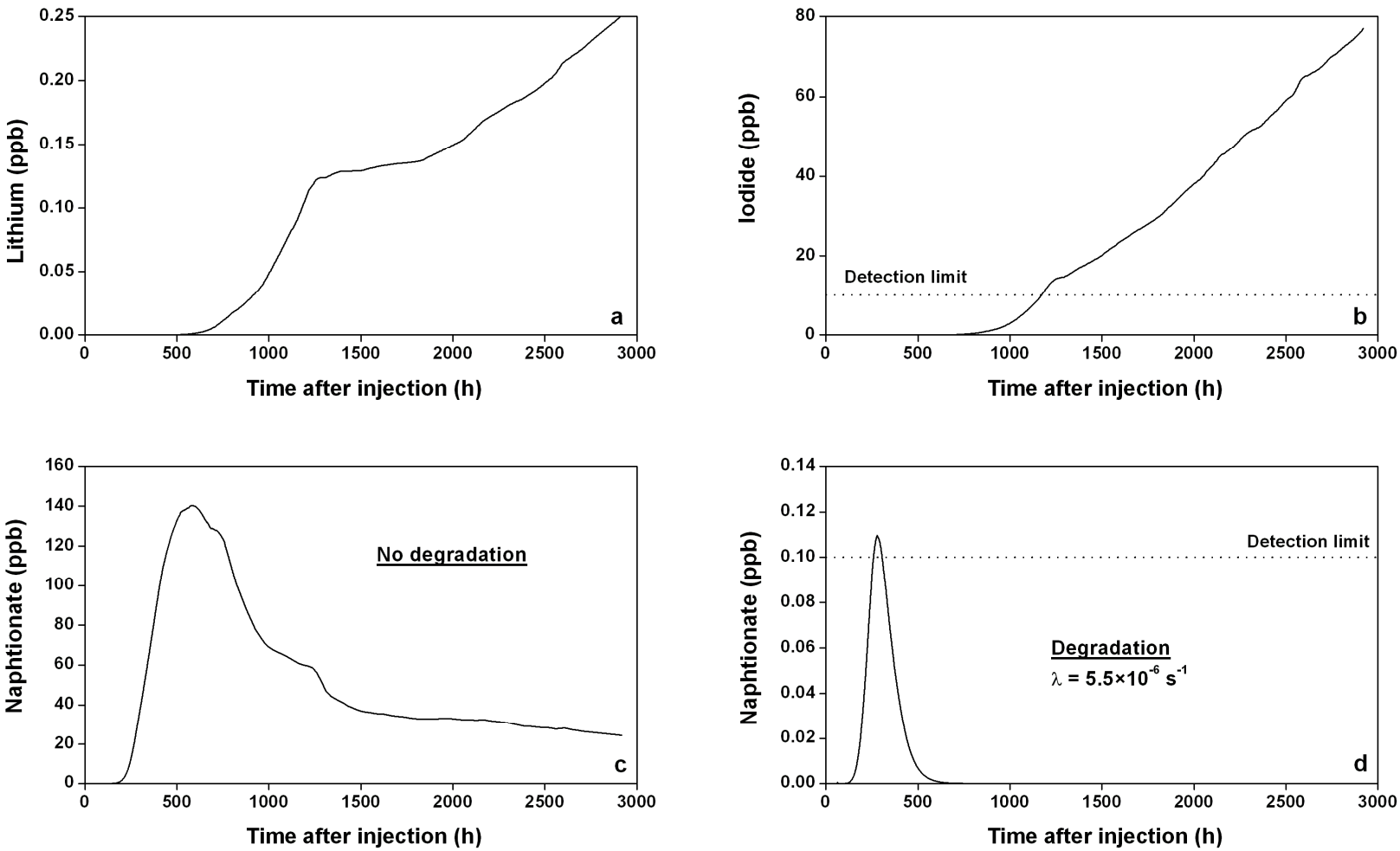

Figure 5.21. Modelled breakthrough curves for lithium (a), iodide (b), and naphtionate, without considering degradation (c) and considering degradation (d), all them corresponding to tracer test Phase I.

Modelling results of uranine confirm the non-arrival in the recovery well. Indeed, the groundwater flow model predicts that the injection well (U5), located at more than 100 m upstream of the recovery well (P5), is located close to, but outside, the limit of P5 capture zone.

The absence of lithium in the recovery well has been highlighted with the model (Figure 5.21a). Modelling results indicate that, although lithium might have arrived at the recovery well, the concentration reached after 4 months is just lightly above of 0.25 ppb, while the laboratory detection limit is equal to 5 ppb.

The laboratory detection limit of iodide is equal to 10 ppb. This concentration is predicted for the model to be exceeded after 50 days at the recovery well (Figure 5.21b). This was not the case and its arrival was never observed.

Naphtionate has been modelled, in a first instance, without considering degradation, as done before in modelling this tracer in Phase II. Doing so, with a detection limit of 0.1 ppb, naphtionate should be observed after 10 days (Figure 5.21c). However, this was not the case since napthionate was never detected during the 3 months of continuous sampling. Naphtionate has also been modelled considering the degradation ($\lambda = 5.5\times10^{-6}$ s^{-1}) found by Brouyère (2001) in Hermalle-sous-Argenteau (Figure 5.21d). In this case, the maximum concentration of napthionate observed in the recovery well is 0.11 ppb, almost equal to the detection limit.

The low hydraulic conductivity area between the recovery and the injection wells, does not explain the non-detection of tracers in Phase I, since this spatial heterogeneity is taken into account in the groundwater transport model (Figure 5.22a). However, there is one fact not considered in the groundwater transport model: geochemical conditions of the aquifer. Injection wells used in Phase I are located in a zone where negative Eh conditions prevail (Figure 5.22b). These conditions could possibly enhance the degradation, retention or sorption of the tracers. This fact, combined with other specific geochemical conditions related to the presence of organic pollutants near the injection wells in Phase I, could partly contribute to explain the absence of tracer recovery.

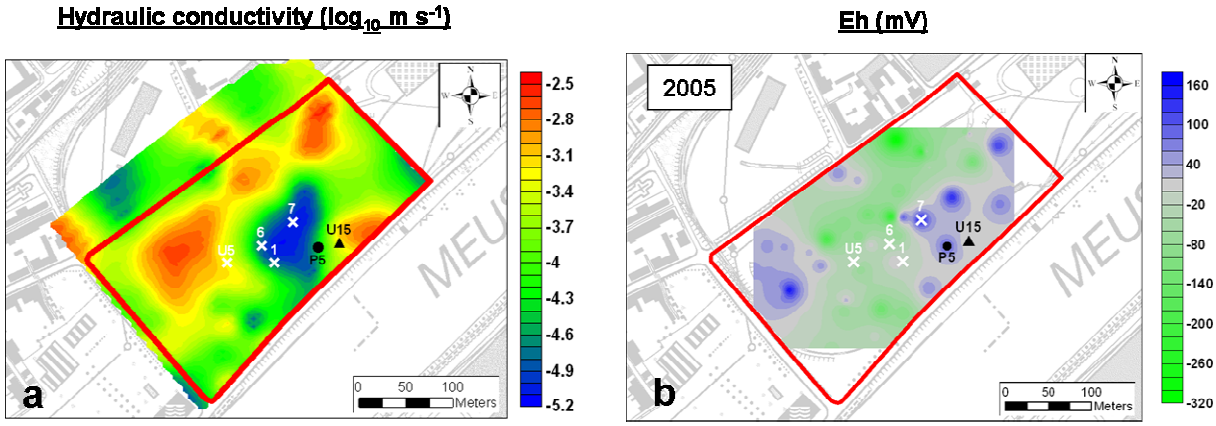

Figure 5.22. Location of injection wells in Phase I (crosses), injection well in Phase II (triangle) and recovery well (dot), with hydraulic conductivity field (a) and Eh conditions (b).

5.3.3. Modelling benzene transport in the alluvial aquifer

5.3.3.1. Evidences of benzene biodegradation (footprints)

Up to now, benzene has never been observed in the part of the Flémalle site directly adjacent to the Meuse River, while important concentrations have been analyzed in various sampled wells in the centre of the site (Chapter 2). The objective in modelling benzene transport dissolved in groundwater is to understand why benzene has not been encountered already in the border of the Meuse River and to see if biodegradation processes could be at the origin of this fact. Indeed, CHYN, as AquaTerra partner, performed a study in the Flémalle site with the objective to highlight biodegradation processes and to calculate degradation rates constants (Morasch *et al.*, 2007a; Morasch *et al.*, 2007b). They concluded that biodegradation rate is a reality in the Flémalle site, calculating microcosm and field degradation constants.

Although 5 characterisation campaigns were performed in Flémalle site, there has been no continuous monitoring of benzene concentrations, and, unfortunately, only local (in time and space) analyses are available at some wells. The most important sampling campaign for benzene was performed in 2005, the results of which are presented in Figure 5.23.

Benzene biodegradation is an oxidation-reduction process, resulting in the oxidation of the electron donor compounds (ED), which is benzene, and the concomitant reduction of an electron acceptor (EA). Common EAs in groundwater, listed in the expected sequence of use which is established based on the Gibb's free energy of the redox reactions, are: dissolved oxygen (O_2), nitrate (NO_3^-), Fe(III) or Mn(III), sulphate (SO_4^{2-}), and carbon dioxide (CO_2). Field evidences of benzene degradation that one could expect are the decrease of EA concentrations and increase of Fe(II) and methane (CH_4), and turnover to negative Eh values.

The stoichiometry of different benzene degradation processes can be described by the following set biochemical reactions, listed in the expected sequence of occurrence (Lu *et al.*, 1999):

$$C_6H_6 + 7.5O_2 \rightarrow 6CO_2 + 3H_2O \quad (5.5)$$

$$6NO_3^- + 6H^+ + C_6H_6 \rightarrow 6CO_2 + 6H_2O + 3N_2 \quad (5.6)$$

$$30Fe(OH)_3 + 6H^+ + C_6H_6 \rightarrow 6CO_2 + 78H_2O + 30Fe^{2+} \quad (5.7)$$

$$3.75SO_4^{2-} + 7.5H^+ + C_6H_6 \rightarrow 6CO_2 + 3H_2O + 3.75H_2S \quad (5.8)$$

$$C_6H_6 + 4.5H_2O \rightarrow 2.25CO_2 + 3.75CH_4 \quad (5.9)$$

As beforementioned, one can notice in this sequence that dissolved oxygen is depleted, followed by a depletion of nitrate, Fe^{3+} and sulphate. At the same time, concentrations of CO_2, Fe^{2+} and CH_4 increase.

Taking into account the scarcity of former groundwater sampling campaigns and analysis, Eh, nitrate and sulphate concentrations are presented in Figure 5.23. No methane analyses have ever been performed on the site, and measurements of dissolved oxygen in 2005 showed that the central part of Flémalle site is almost under anoxic conditions or at least very low O_2 concentrations (1-2 mg L^{-1}). Negative values of Eh match well with the zone of higher benzene concentration. At the same time, nitrate concentrations are very low around the site except in the zone of lower hydraulic conductivity, where Eh values are positive and benzene has not been detected until now. Very low dissolved oxygen concentrations and the absence of nitrate are conforming to the hypothesis that benzene degradation under aerobic and nitrate-reducing conditions has mainly occurred in the past. Considering the high sulphate concentrations around the Flémalle site, it seems reasonable to think that benzene degradation under sulphate reduction conditions is ongoing.

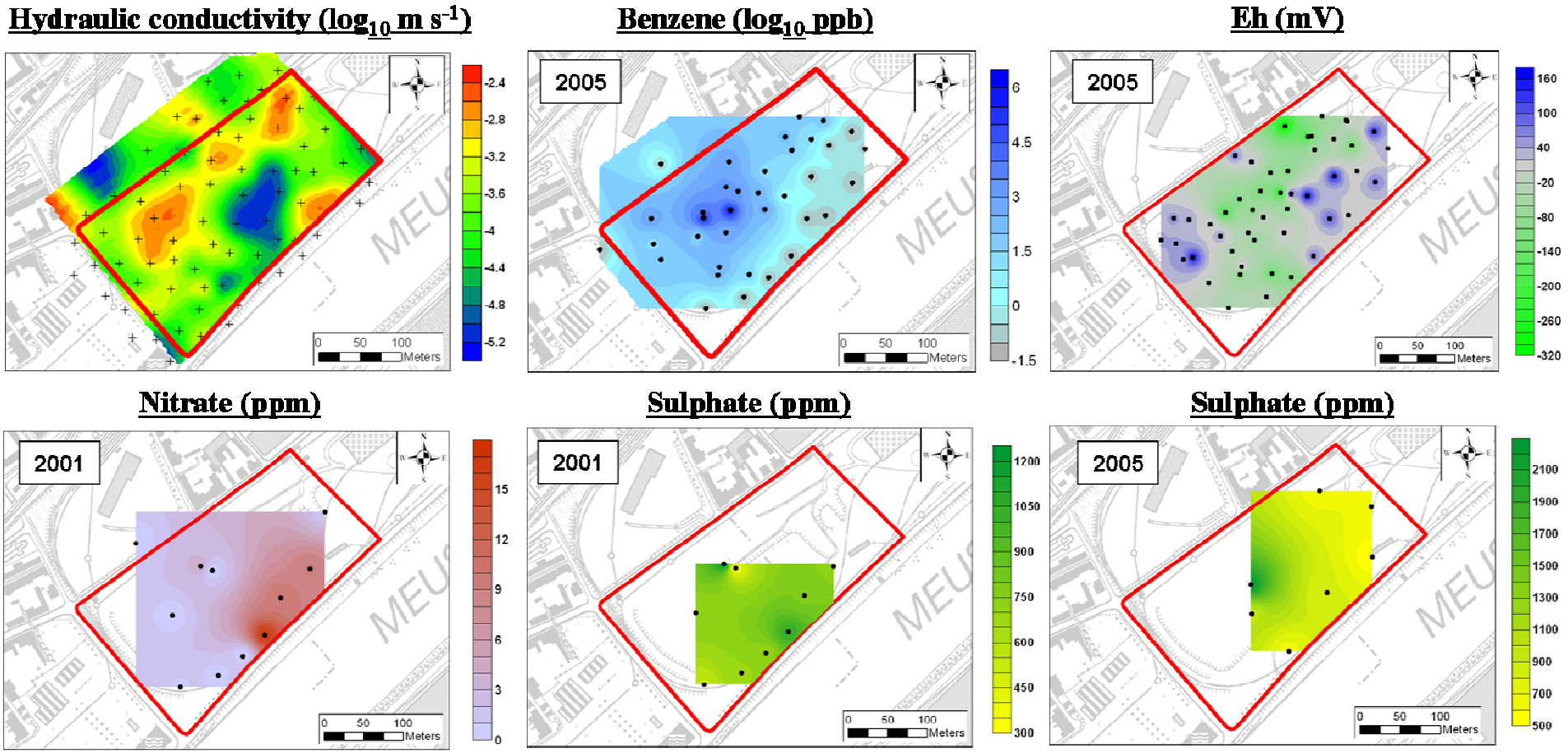

Figure 5.23. Electron donor –ED- (benzene) and electron acceptors –EAs- (nitrate and sulphate) concentration; Eh values are also presented as evidence of biodegradation. Spatial distribution of the hydraulic conductivity is shown for comparison and easy establishment of relations between parameters. The interpolation method used is the inverse distance weighted (crosses represent pilot points location, and dots represent sampling points).

5.3.3.2. Boundary conditions and spatial discretisation for benzene transport modelling

The transport model used for benzene is also based on the groundwater flow model. The area of the model corresponds to the zone where the pilot point approach was used during the transient calibration process of the groundwater flow model (Figure 5.10), with local dimensions of 550 × 380 m. The model domain is subdivided in 159 columns and 113 rows, with variable grid refinement 0.5m × 0.5m in the benzene source zone to 10m × 10m at the limits of the model, with a total of 17,967 active cells.

Boundary conditions have been considered in a similar way as for the model used to model tracer tests: a Fourier boundary condition in the contact between the Meuse River and the aquifer (SE boundary) and prescribed time-varying piezometric levels for the other boundaries (NE, NW and SW).

5.3.3.3. Modelling hypothesis and location of pollutant sources

Three main hypotheses could explain the fact that benzene and others organic pollutants have not been observed yet close to the Meuse River:

1. The benzene plume is still progressing in the alluvial aquifer but it has not reached yet the limit of the site;
2. Biodegradation processes are sufficient to attenuate benzene before reaching the river;
3. Variations of river-stage contribute to “pushing back” the benzene plume into the aquifer. In addition, biodegradation might be accelerated due to the fluctuation of the water table leading to dissolution of oxygen from entrapped air bubbles and due to the infiltration of oxygen-rich river water.

The first hypothesis seems not possible since organic pollutants have been released to the subsurface from the beginning of industrial works in Flémalle site (1922). Concerning the second and third hypothesis, the most probable is that both contribute simultaneously together to the benzene attenuation.

Location of benzene pollution sources and control planes (A, B, C, D and E) used for benzene concentration evaluation are presented in Figure 5.24.

The possible locations of pollution sources were presented in Chapter 2. Although three main source zones were defined, only pollution sources B and C are considered here in transport simulations because their location is more trustworthy. Modelling of pollution source B will serve to characterise the evolution of benzene with transient conditions, as well as to evaluate

its attenuation to the Meuse River. Modelling of pollution source C will have two main goals: (1) to highlight the influence of aquifer heterogeneity on the evolution of the contaminant plume, and (2) to investigate if, as already mentioned in Chapter 2, the origin of aquifer pollution found upstream of the brownfield can be related to the site. Pollution source B is located at 165 m from the Meuse River, and control planes A to E are located at 25, 50, 80, 115 and 160 m from the pollution source, respectively. Pollution source C is located at 200 m distance of the Meuse River, and two control planes (F and G) have been placed at 40 and 70 meters upstream from the plume originated in pollution source C. Although the maximum solubility of benzene is equal to 1780 mg L^{-1}, the benzene concentration released from both sources has been set equal to 750 mg L^{-1}, which corresponds to the maximum benzene concentration measured in the upper part of the alluvial aquifer.

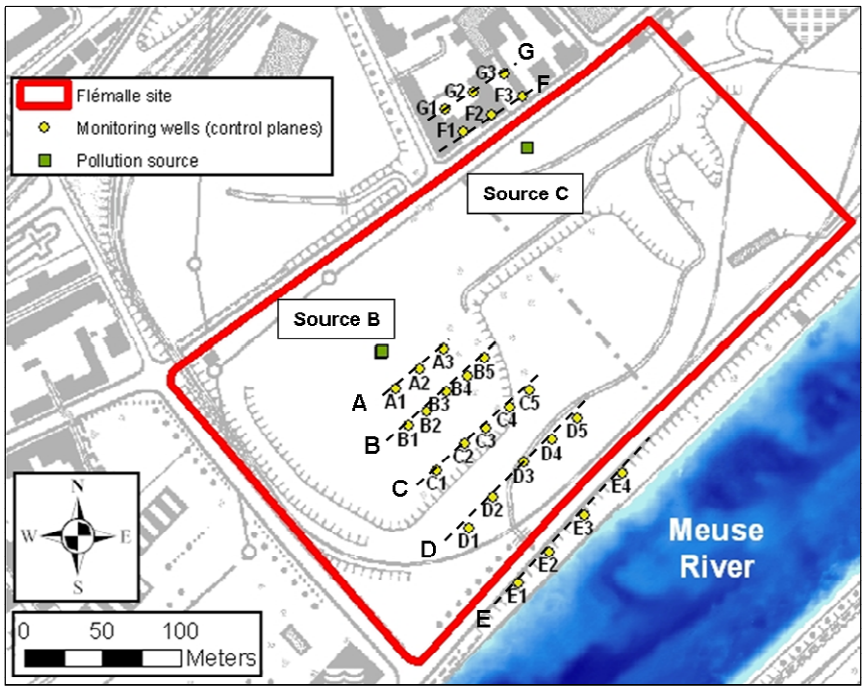

Figure 5.24. Location of pollution sources considered in the groundwater transport model and control planes for benzene relative mass loss evaluation.

Benzene, as the rest of organic and inorganic pollutants present in the aquifer, was released into the subsurface and groundwater more than 25 years ago, when industrial activities were still going on. In a first step, the groundwater flow model was run in steady state conditions and the groundwater transport in a transient state for a period of 25 years. Doing so, it is expected to obtain steady state benzene plumes. This situation will serve later as a starting condition for the subsequent transient groundwater flow model.

5.3.3.4. Results on benzene transport modelling (steady state conditions)

Three different scenarios were considered to simulate the transport of benzene in the aquifer (Table 5.6).

Table 5.6. Benzene transport scenarios considered under steady state conditions (ADE: advection dispersion equation; MIM: mobile immobile water).

Scenario	ADE	MIM	Sorption	Biodegradation
1	✓	✓ ($\alpha = 1\times10^{-7}$ s^{-1})	× ($R_{fc} = 1$)	×
2	✓	✓ ($\alpha = 1\times10^{-7}$ s^{-1})	× ($R_{fc} = 3$)	×
3	✓	✓ ($\alpha = 1\times10^{-7}$ s^{-1})	× ($R_{fc} = 3$)	✓ ($\lambda_B = 3\times10^{-7}$ s^{-1})
3.1	✓	✓ ($\alpha = 1\times10^{-7}$ s^{-1})	× ($R_{fc} = 3$)	✓ ($\lambda_B = 3\times10^{-8}$ s^{-1})
3.2	✓	✓ ($\alpha = 1\times10^{-7}$ s^{-1})	× ($R_{fc} = 3$)	✓ ($\lambda_B = 3\times10^{-6}$ s^{-1})

A mean biodegradation constant rate calculated by CHYN (Daniel Hunkeler and Barbara Morasch) of 3×10^{-7} s^{-1} will be used as representative of the scenario 3. A sensitivity analysis for the biodegradation constant rate will be performed in scenarios 3.1 and 3.2, using minimum and maximum biodegradation rates, 3×10^{-8} and 3×10^{-6} s^{-1}, respectively. Hydrodispersive and retardation parameters used for these scenarios are summarised in Table 5.7. These values correspond to mean values obtained from the calibration of radially converging flow tracer tests.

Table 5.7. Hydrodispersive and retardatation parameters used in the benzene transport simulatioins.

Hydrodispersive and retardation parameters	
θ_m (-)	0.04
θ_{im} (-)	0.1
α_L (m)	2.5
α_T (m)	0.5
α (s^{-1})	1×10^{-7}
p (-)	0.95
R_{fc} (-)	1 - 3
K_d (m^3 kg^{-1})	4.15×10^{-5}
K_{oc} (m^3 kg^{-1})	0.083
f_{oc} (%)	0.05
ρ_b (kg m^{-3})	2,000
λ_B (s^{-1})	3×10^{-8} - 3×10^{-6}

The K_d value has been obtained using Equation (5.10):

$$K_d = K_{oc} f_{oc} \tag{5.10}$$

where K_{oc} is the soil sorption coefficient for soil organic carbon, and f_{oc} is the fraction of soil organic carbon. Because K_{oc} and f_{oc} values are not known for Flémalle, theoretical approximations representative of alluvial aquifers are considered (Alvarez and Illman, 2006, D. Hunkeler, personal communication).

INFLUENCE OF SORPTION AND BIODEGRADATION IN BENZENE PLUME DEVELOPMENT

Figure 5.25 presents the benzene concentration at control planes A, B, C, D and E for scenarios 1 and 2 (R_{fc} = 1 and R_{fc} = 3, respectively). Effects of the attenuation, corresponding to the scenario 3, are presented in Figure 5.26. The Figure 5.26 is the same as Figure 5.25 but benzene concentrations are represented in a logarithmic, which was necessary due to the important attenuation of the benzene under biodegradation processes. As expected, the time to achieve stabilisation of the benzene plume considering a retardation factor of 3 is longer than considering a retardation factor of 1 (no sorption). The time needed to stabilisation without considering sorption is from 1 year in control plane A to 7 years in control plane E, next to the river. With a retardation factor equal to 3, the time need for stabilisation is of 10 years in control plane A and up to 25 years in control plane E.

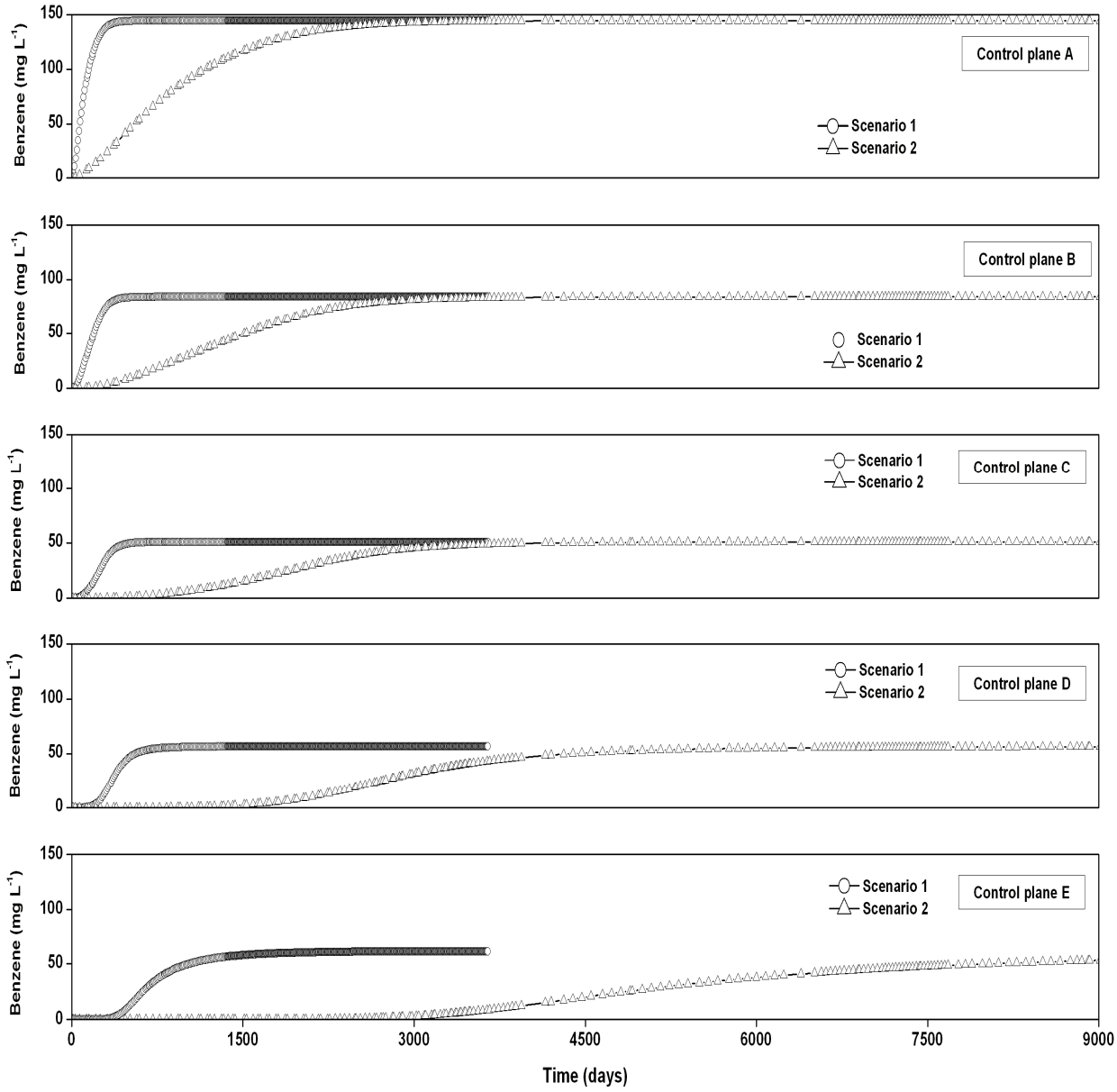

Figure 5.25. Benzene concentration at control planes A, B, C, D and E for scenarios 1 (no sorption) and 2 (R_{fc} = 3).

Benzene plume stabilisation in scenario 3 (R_{fc} = 3; λ_B = 3×10^{-7} s^{-1}) is achieved ealier compared to the scenarios where degradation was not considered, less than a year. These results seem to confirm the effectiveness of benzene biodegradation processes occurring in the alluvial aquifer of the Flémalle site, and *a priori*, it contributes to explain why benzene has never been detected close to the river.

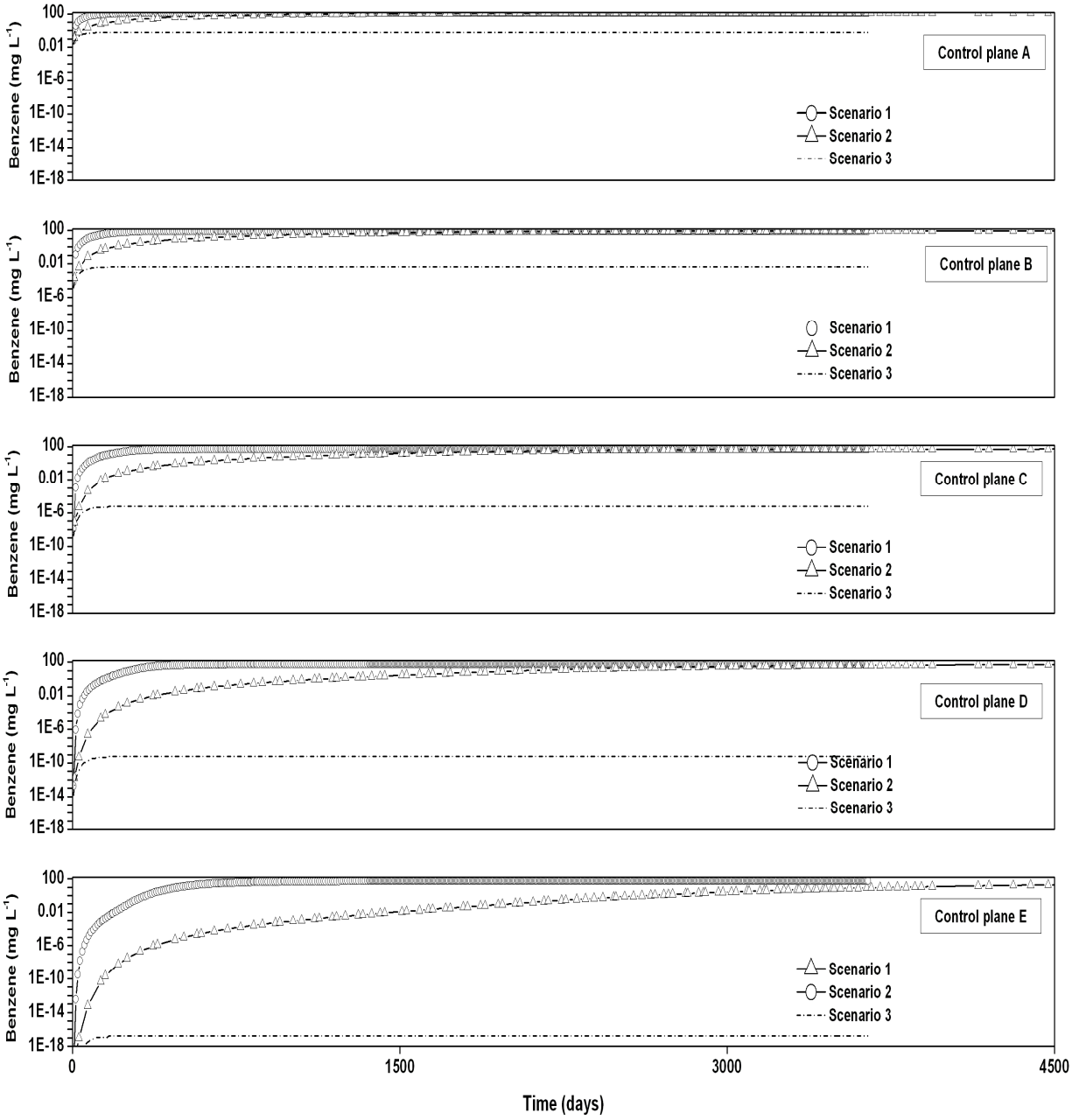

Figure 5.26. Benzene concentration at control planes A, B, C, D and E for scenarios 1 (no sorption), 2 (R_{fc} = 3) and 3 (R_{fc} = 3; $\lambda_B = 3\times10^{-7}$ s^{-1}).

Figure 5.27 presents the spatial extent of the benzene plumes after 50 days, 1 year, and 10 years for scenarios 1 (no sorptioin) and 2 (R_{fc} = 3), while Figure 5.28 presents the benzene plume stabilised after 1 year for the scenario 3 (R_{fc} = 3; $\lambda_B = 3\times10^{-7}$ s^{-1}). At the beginning, as expected, the plume modelled in scenario 1 is more developed. After 10 years, however, benzene plumes corresponding to scenarios 1 and 2 have an important spatial extension, reaching the Meuse River. It is interesting to note the strong influence of aquifer heterogeneity in the spatial development of the benzene plume originated from source C. The benzene plume travels mostly following the high hydraulic conductivity area and later turns to the Meuse River, by-passing the low hydraulic conductivity area.

Contrary to scenarios 1 and 2, the benzene plume in scenario 3 (R_{fc} = 3; $\lambda_B = 3\times10^{-7}$ s^{-1}) is much less developed because of the attenuation due to biodegradation processes, and does not reach the Meuse River.

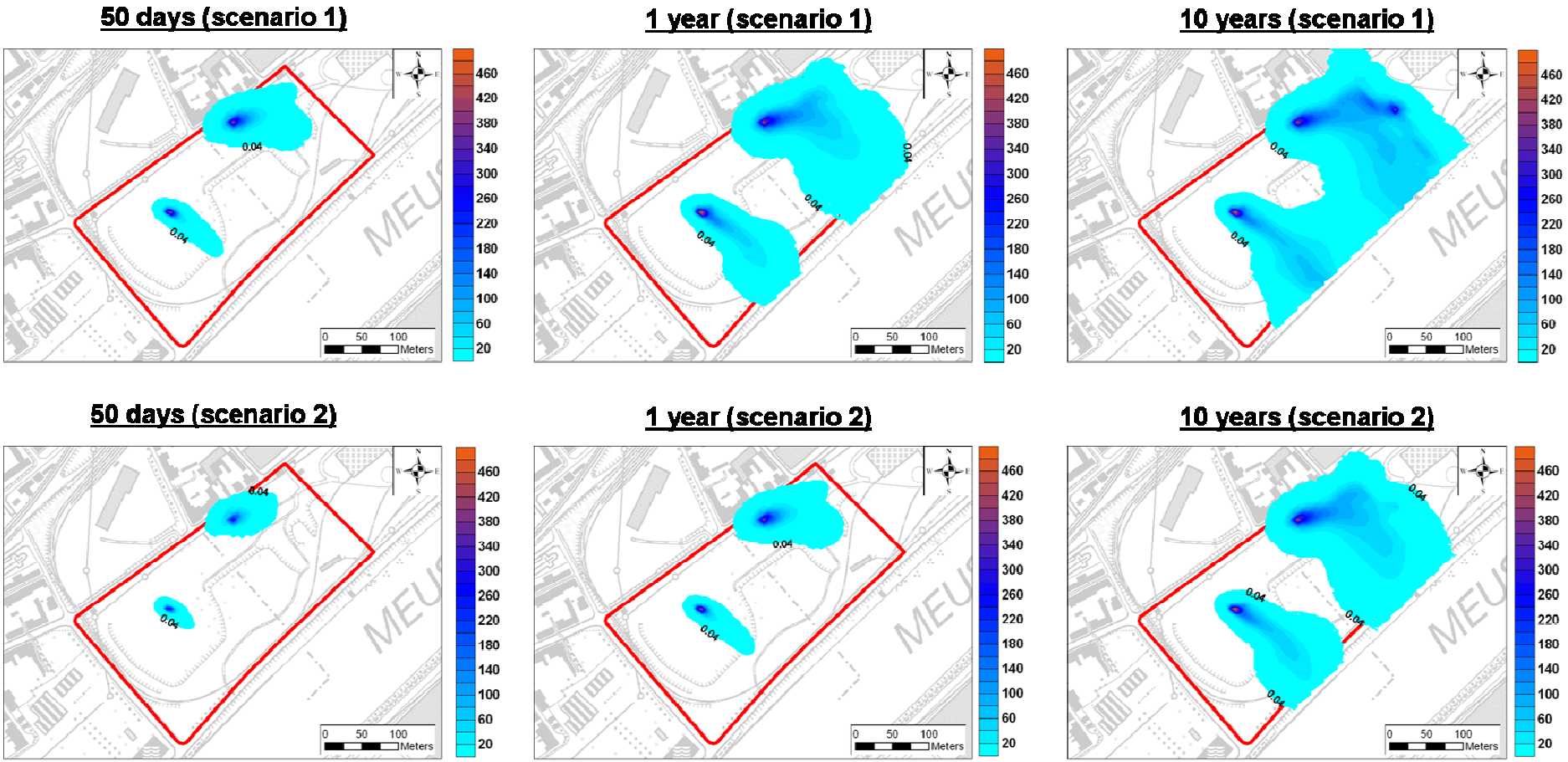

Figure 5.27. Scenario 1 and 2: steady state evolution of benzene plume after 50 days, 1 year and 10 years for scenario 1 (no sorption) and scenario 2 (R_{fc} = 3). Benzene concentrations are in mg L^{-1}.

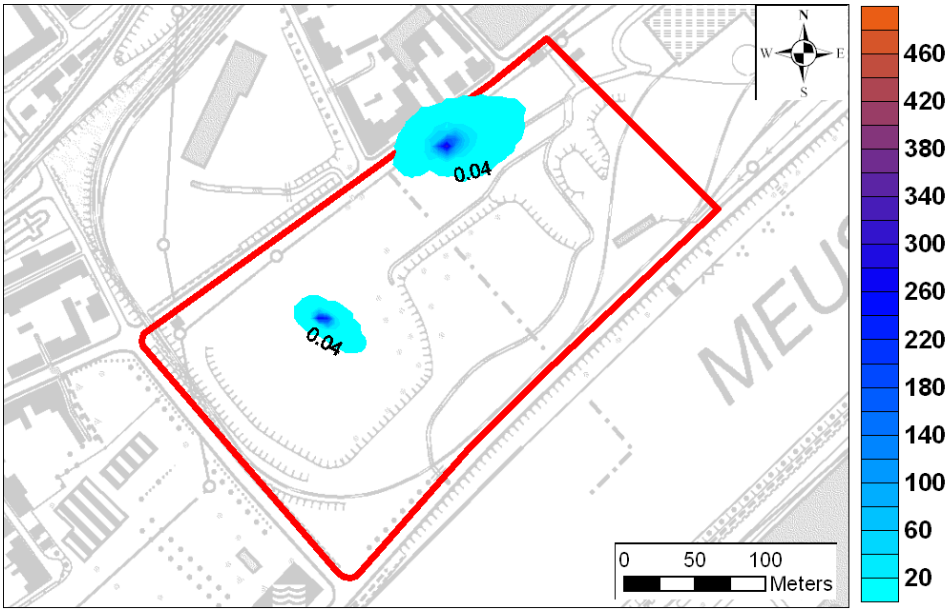

Figure 5.28. Scenario 3: benzene plume stabilisation after 1 year (R_{fc} = 3; λ_B = 3×10^{-7} s^{-1})

SENSITIVITY ANALYSIS OF THE BIODEGRADATION CONSTANT

Three scenarios will be here compared: scenario 3 (λ_B = 3×10^{-7} s^{-1}), scenario 3.1 (λ_B = 3×10^{-8} s^{-1}) and scenario 3.2 (λ_B = 3×10^{-6} s^{-1}), corresponding to the mean, minimum and maximum biodegradation constants calculated by Morasch *et al.* (2007a) and Morasch *et al.* (2007b). As already mentioned, these biodegradation constants correspond to overall degradation processes, making no distinction of explaining reaction processes. Nevertheless, the absence of oxygen and the low concentration of nitrate (almost restricted to the low *K* zone) indicate that aerobic or nitrate reducing conditions do not occur anymore in the site. On the contrary, sulphate is present in excess (Figure 5.23) and it can be expected that sulphate-reducing conditions drive the degradation of benzene. The degradation rate measured by CHYN thus probably reflects sulphate-reducing conditions.

Benzene concentrations for scenarios 3, 3.1 and 3.2 at control planes A, B and C are presented in Figure 5.29, in conjunction with concentrations corresponding to the scenario 2 (R_{fc} = 3; no biodegradation), helping for comparison of the effectiveness of biodegradation processes in reducing benzene concentrations. The spatial development of the benzene plume is presented in Figure 5.30 for scenarios 3, 3.1 and 3.2.

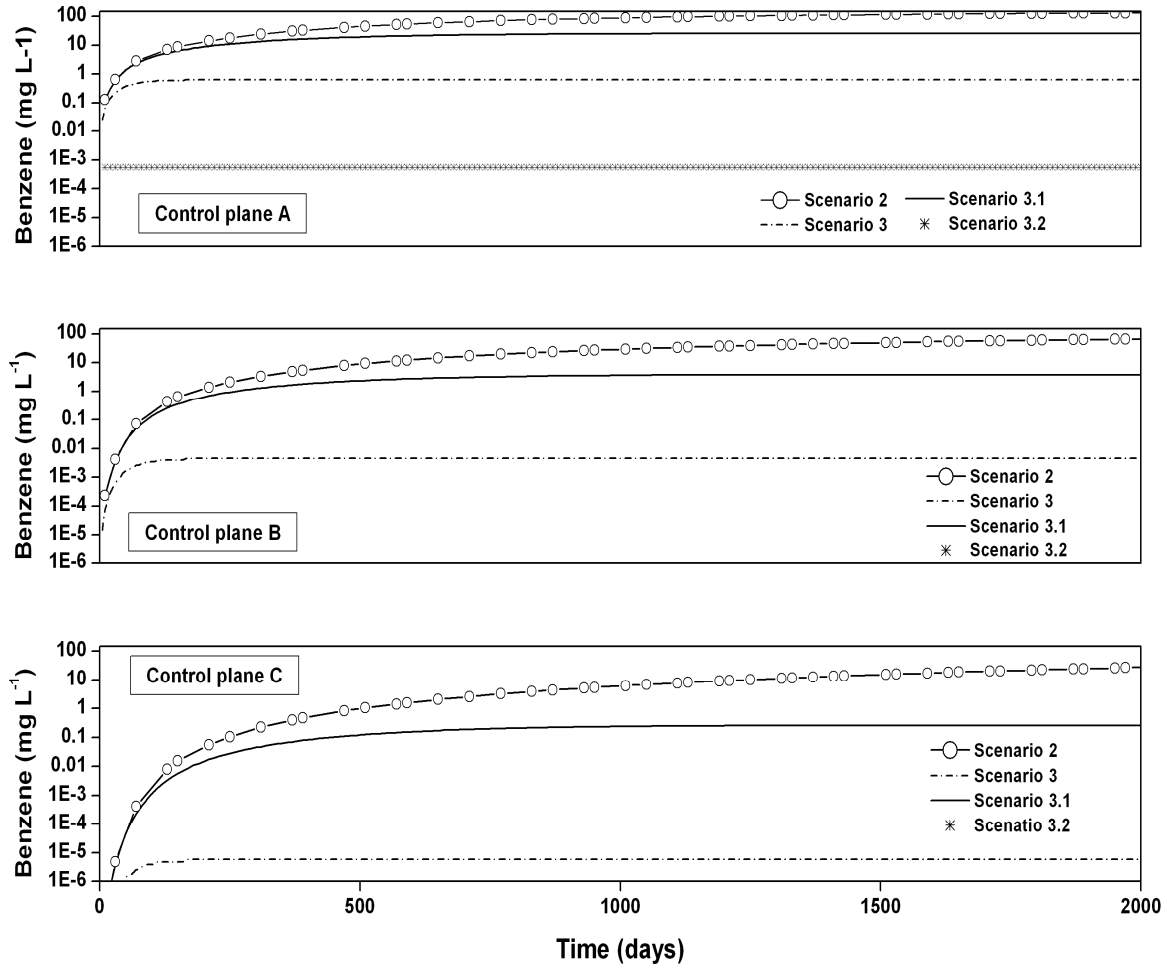

Figure 5.29. Benzene concentration at control planes A, B and C, for scenarios 3 ($\lambda_B = 3\times10^{-7}$ s^{-1}), 3.1 ($\lambda_B = 3\times10^{-8}$ s^{-1}) and 3.2 ($\lambda_B = 3\times10^{-6}$ s^{-1}). Results of scenario 2 ($R_{fc} = 3$) are also presented.

As expected, the benzene attenuation is higher in scenario 3.2 ($\lambda_B = 3\times10^{-6}$ s^{-1}), with concentrations very low (below 1×10^{-12} mg L^{-1} in the control plane B) compared to those of the scenario 3.1 ($\lambda_B = 3\times10^{-8}$ s^{-1}).

The spatial development of the benzene plumes is done accordingly to concentrations beforementioined. In scenario 3.1 ($\lambda_B = 3\times10^{-8}$ s^{-1}) the plume clearly flows to the Meuse River, while in scenario 3.2 ($\lambda_B = 3\times10^{-6}$ s^{-1}), the benzene plume is almost stationary. Between these two contrasted situations, we have the scenario 3 ($\lambda_B = 3\times10^{-7}$ s^{-1}).

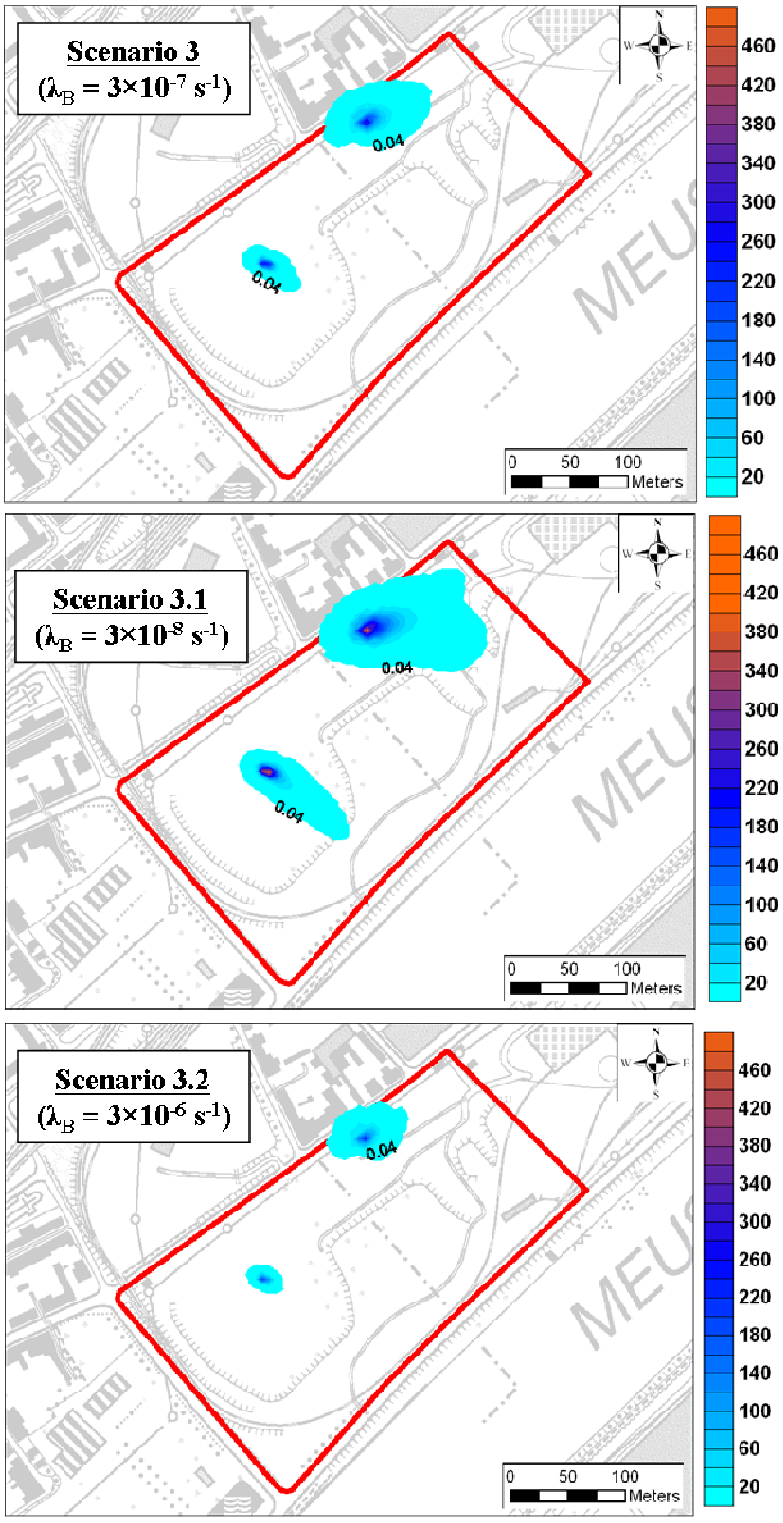

Figure 5.30. Stabilised steady state benzene plume after 1 year for scenarios 3 ($\lambda_B = 3\times10^{-7}$ s^{-1}), 3.1 ($\lambda_B = 3\times10^{-8}$ s^{-1}) and 3.2 ($\lambda_B = 3\times10^{-6}$ s^{-1}). Benzene concentrations are given in mg L^{-1}.

The next step in this research is to consider the stabilised benzene plume for scenarios 3, with a mean biodegradation constant equal to 3×10^{-7} s^{-1}, as starting benzene concentration for the groundwater transient conditions.

5.3.3.5. Influence of the groundwater – surface water dynamics on the transport of benzene

The groundwater flow and transport model has been run for a period corresponding to 10th March 2005 to 29th June 2007, for which daily Meuse River level and groundwater level fluctuations are available. Benzene concentrations in the central observation well for each control plane are presented in Figure 5.31 for scenario 3 ($\lambda_B = 3\times10^{-7}$ s^{-1}).

The evolution of the benzene plume is strongly influenced by Meuse River level fluctuations, this influence being observed in all control planes drawn across the benzene plume. Lower benzene concentrations are observed during high river water levels, and high benzene concentrations are observed during low river water levels. When river water level increase, even thought the hydraulic gradient is not inversed, the benzene plume is pushed insite, which explains the observed reduction of benzene concentration. On the contrary, during periods where river water level remains low, benzene plume move forward to the river. This situation is shown in Figure 5.32, where two contrasted situations are presented: one corresponding to low (or regular) river water level (~ 59.4 m a.s.l.), the other to high river water level (~ 61.0 m). For low water river level the benzene plume B is narrow and well developed forward to the river. On the contrary, when river water level rises the benzene plume moves insite, becoming shorter and wider. The same situation is observed for benzene plume C.

As mentioned in Chapter 2, the benzene pollution (and other organic pollutants) has been observed in groundwater “upstreasm” of the Flémalle site, in the opposite direction of the Meuse River with no concomitant soil pollution at the same location. As clearly shown in Figure 5.31, the benzene plume issued from source C extends outside the brownfield in the “upstream” direction.

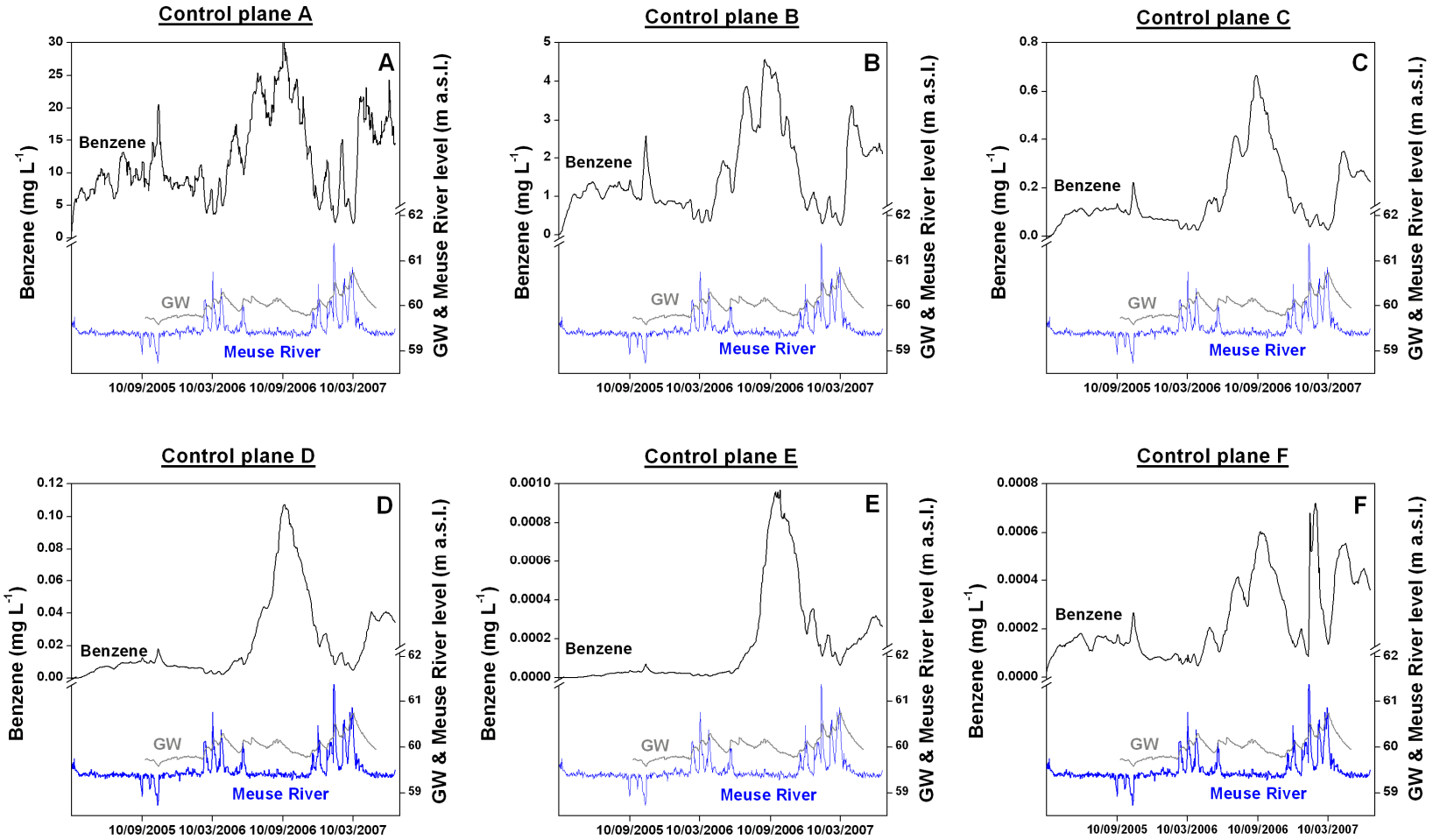

Figure 5.31. Scenario 3 ($\lambda_B = 3\times10^{-7}$ s^{-1}) under transient conditions: benzene concentrations in control planes A, B, C, D and E (for benzene source B) and control plane F (for benzene source C).

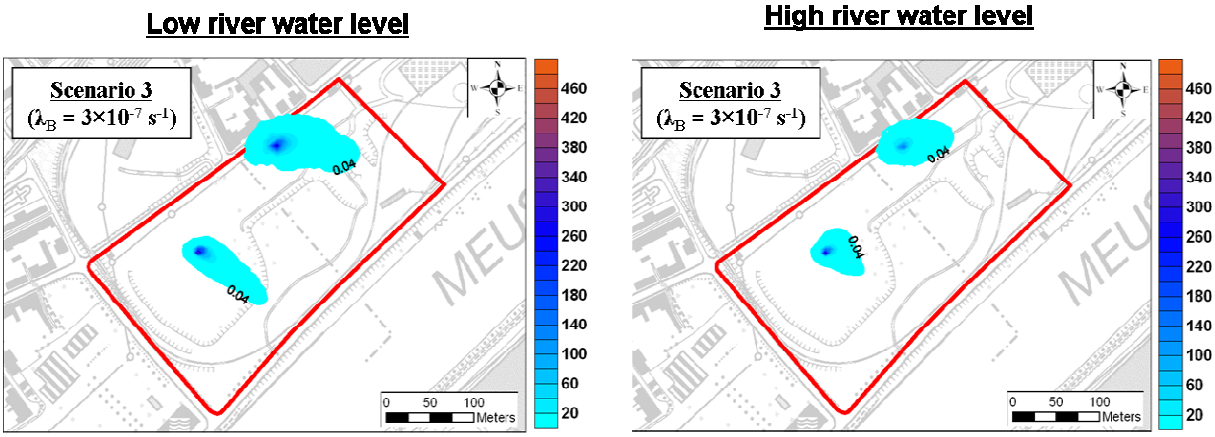

Figure 5.32. Scenarios 3-4-5: spatial development of benzene plumes for low river water level (left) and high river water level (right) conditions.

The back and forward movement of the benzene plume also possibly explains apparently anomalous sampling results obtained during different sampling campaigns performed in the Flémalle site (previously mentioned in Chapter 2). For example, even if benzene concentrations seem to decrease with time in several monitored wells, the contrary is sometimes observed. The well P3 is a clear example of this fact: benzene was measured at 36 at 26 μg L^{-1} in year 2001, while in 2005 the benzene concentration was below 0.2 μg L^{-1}. Unfortunately, no more data of benzene concentration is available for well P3. Another example is the well A2, where benzene was observed at 0.35 μg L^{-1} in 1992, while following the benzene plume direction, in well U9, benzene was observed at 120 μg L^{-1} in year 2005. Again, a continuous sampling in this wells was not performed, which could supply very interesting data about the back and forward movement of the benzene plume. Nevertheless, the location of these wells (between control planes C and E) and their benzene concentrations seems to be in relatively good agreement with concentrations presented in Figure 5.31, indicating that the biodegradation constant of 3×10^{-7} s^{-1} is representative enough of the biodegradation processes occurring in the aquifer.

Results of the groundwater transport model are also in good agreement with results obtained from VITO Aquaterra partner (Vanbroekhoven *et al.*, 2007), who performed batch tests using aquifer material and groundwater from Flémalle to study the fate of heavy metals in the Flémalle site. Zn and Cd were not detected in groundwater in the benzene source area C, but they were observed downstream (Figure 5.33). On the contrary, As was detected in groundwater in the benzene source area C but not downstream. One possible hypothesis to this fact is that, at the location where the organic pollutants are present in groundwater at high

concentrations (source area), all potential electron acceptors are used (oxygen, nitrate and sulphate). Consequently, reducing conditions prevail in this area due to sulphate-reducing biodegradation of organic compounds (sulphate is reduced into sulphide). This leads to immobilisation of divalent metals like Zn and Cd in the form of metasulphides. However, it does have an effect of mobilisation of As in its reduced trivalent form -As(III)-. Downstream, towards the Meuse River, organic pollutants are not present, and oxidising conditions prevail. In the presence of sulphate the reduced As(III) is reoxidised and immobilised again. This process could be also influenced downstream by the possible input of surface water into the aquifer.

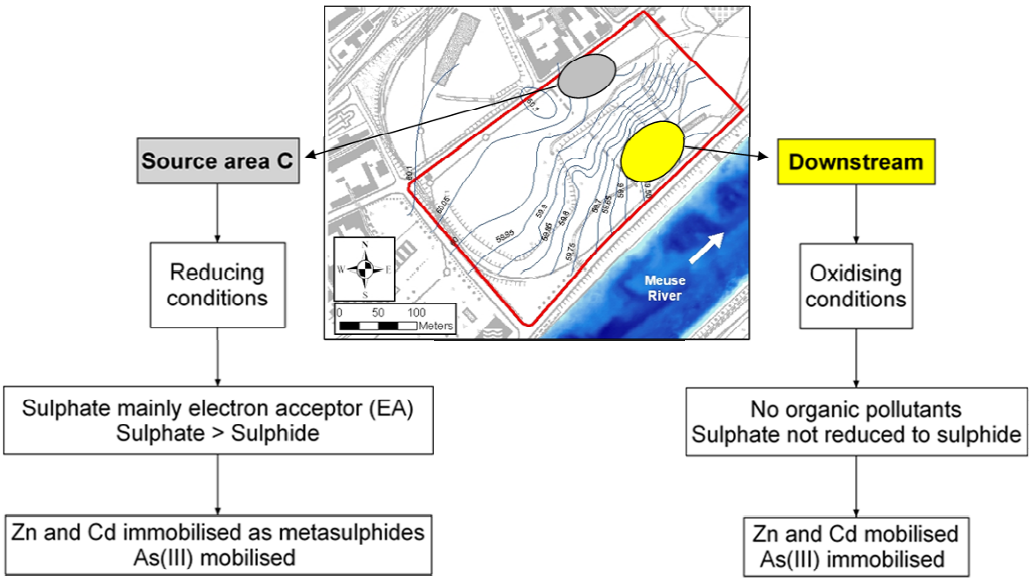

Figure 5.33. Schematisation of the possible relation between organic and inorganic pollutants in the Flémalle site.

5.4. Conclusions to chapter 5

Numerical modelling has confirmed and provided valuable information on the aquifer heterogeneity and on dissolved pollutant transport in the alluvial aquifer. Three main factors are responsible of the spatial and time evolution of dissolved pollutants in groundwater: (1) ongoing biodegradation processes; (2) aquifer heterogeneity; and (3) transient conditions of the river – aquifer system. Although geochemical conditions are also responsible for the mobility of heavy metals, this factor is rather a consequence of the first factor beforementioned, which controls geochemical conditions in the source area and downstream.

Biodegradation processes are mainly related to sulphate-reducing conditions, since oxygen and nitrate are almost depleted in the source area and downstream. If nowadays conditions remain constant, it seems that the risk of contaminant dispersion to the Meuse River through groundwater discharge is low. However, it is reasonable to suppose that, because dissolved oxygen and nitrate are almost depleted in the source area, benzene was first degraded oxidising conditions and subsequently under nitrate-reducing conditions. Similarly, sulphate-reducing conditions will continue until sulphate will be almost depleted. Once sulphate will be depleted, only the back and forward movement of the benzene plume will be active, which is probably not effectively enough to avoid pollutants reaching the river. Furthermore, any subsequent organic pollutants migration in direction of the river could lead to a shift from oxidised to reduced geochemical conditions, and following the hypothesis before stated, some heavy metals like Zn and Cd mobilised.

5.5. References to chapter 5

Alvarez, P. J. J. & Illman, W. A. (2006). Bioremediation and natural attenuation: process fundamentals and mathematical models. Environmental Science and Technology. John Wiley & Sons. Hoboken, New Jersey, USA. 609 pp.

Barlow, P. M., DeSimone, L. A. & Moench, A. F. (2000). Aquifer response to stream-stage and recharge variations. II. Convolution method and applications. *J. Hydrol.* **230**: 211-229.

Barlow, P. M. & Moench, A. F. (1998). Analytical solutions and computer programs for hydraulic interactions of stream-aquifer systems. *US Geol. Survey Open File Report 98-415A*. USGS, Marlborough, Massachusetts, USA. 99 pp.

Batlle-Aguilar, J. & Brouyère, S. (2007). Assessing groundwater - surface water interaction and groundwater discharge in a contaminated site in an industrial, sub-urbanized area. *In* Proc. of Groundater Quality 2007: securing groundwater quality in urban and industrial environments. Fremantle, Western Australia. 17 pp.

Berthier, E., Dupont, S., Mestayer, P. G. & Andrieu, H. (2006). Comparison of two evapotranspiration schemes on a sub-urban site. *J. Hydrol.* **328**: 635-646.

Brouyère, S. (2001). Etude et modélisation du transport et du piégeage des solutés en milieu souterrain variablement saturé (study and modelling of transport and retardation of solutes in variably saturated media). Ph.D thesis. Faculté des Sciences Appliquées. Laboratoire de géologie de l'ingénieur, d'Hydrogéologie et de Prospection géophysique, Université de Liège, Liège (Belgium). 640 pp.

Brouyère, S. (2003). Modeling tracer injection and well-aquifer interactions: a new mathematical and numerical approach. *Water Resour. Res.* **39**(3): doi:10.1029/2002WR001813.

de Marsily, G., Lavedan, G., Boucher, M. & Fasanino, G. (1984). Interpretation of interference tests in a well field using geostatistical techniques to fit the permeability distribution in a reservoir model. *In* Proceedings of Geostatistics for natural resources characterization. Verly *et al.* (ed.). D. Reidel Pub. Co. **Part 2**. 831-849 pp.

Devlin, J. F. & McElwee, C. D. (2007). Effects of measurement error on horizontal hydraulic gradient estimates. *Ground Water* **45**(1): 62-73.

Doherty, J. (2003). Ground water model calibration using pilot points and regularization. *Ground Water* **41**(2): 170-177.

Dupond, S., Guilloteau, E., Mestayer, P. G., Berthier, E. & Andrieu, H. (2006). Parameterization of the urban water budget by using the force-restore method. *J. Appl. Meteor. Climatol.* **45**: 624-648.

Grimmond, C. S. B. & Oke, T. R. (1991). An evapotranspiration-interception model for urban areas. *Water Resour. Res.* **27**(7): 1739-1755.

Grimmond, C. S. B. & Oke, T. R. (2002). Turbulent heat fluxes in urban areas: observations and a Local-scale Urban Meteorological Parameterization Scheme (LUMPS). *Journal of Applied Meteorology* **41**: 792-810.

Harbaugh, A. W., Banta, E. R., Hill, M. C. & McDonald, M. G. (2000). MODFLOW-2000: The U.S. Geological Survey modular ground-water model. User guide to modularization concepts and the ground-water flow process. *Open-File Report 00-92*. U.S. Geological Survey, Reston, Virginia. 121 pp.

Käss, W. (1998). Tracing technique in geohydrology. A.A.Balkema P.O.Box 1675, 3000 BR Rotterdam, Netherlands. 581 pp.

Lu, G., Clement, T. P., Zheng, C. & Wiedemeier, T. H. (1999). Natural attenuation of BTEX compounds: model development and field-scale application. *Ground Water* **27**(5): 707-717.

Morasch, B., Höhener, P. & Hunkeler, D. (2007a). Evidence for in situ degradation of mono- and polyaromatic hydrocarbons in alluvial sediments baed on microcosm experiments with ^{13}C-labeled contaminants. *Environ. Pollut.* **148**(3): 739-748.

Morasch, B., Höhener, P., Hunkeler, D. & Langenhoff, A. (2007b). Quantitative evaluation of biodegradation at the BASIN site of Flémalle. *Report BGC5.10*. AquaTerra (Integrated Project FP6 no. 505428). 15 pp.

Ragab, R., Rosier, P., Dixon, A., Bromley, J. & Cooper, J. D. (2003). Experimental study of water fluxes in a residential area: 2. Road infiltration, runoff and evaporation. *Hydrological processes* **17**: 2423-2437.

Vanbroekhoven, K., Van Roy, S., Gielen, C., Maesen, M., Ryngaert, A., Diels, L. & Seuntjens, P. (2007). Microbial processes as key drivers for metal (im)mobilization along a redox gradient in the saturated zone. *Environ. Pollut.* **148**(3): 759-769.

Zheng, C. (1990). MT3D: A Modular, Three-Dimensional Transport Model for Simulation of Advection, Dispersion and Chemical Reactions of Contaminants in Groundwater Systems. U.S. Environmental Protection Agency, Ada, Oklahoma (USA). 169 pp.

Zheng, C. & Wang, P. P. (1999). MT3DMS: a modular three-dimensional multispecies transport model for simulation of advection, dispersion, and chemical reactions of contaminants in groundwater systems; documentation and user's guide. *Contract Report SERDP-99-1*. U.S. Army Engineer Research and Development Center, Vicksburg, Massachussests (USA). 202 pp.

If you believe in what you are doing, then let nothing hold you up in your work. Much of the best work of the world has been done against seeming impossibilities. The thing is to get the work done.

Dale Carnegie

Writer (1888-1955)

6. CONCLUSIONS & PERSPECTIVES

MAIN RESEARCH OUTCOME

The main goal of this research was to study the risk of contaminant dispersion through a groundwater – surface water system. Considering the characteristics of the studied brownfield, three specific objectives were fixed: (1) to confirm groundwater – surface water interactions and to contribute to a better understanding and quantification of such interactions; (2) to estimate and quantify groundwater discharge fluxes to the Meuse River; and (3) to determine factors contributing to pollutant mobility and attenuation and to evaluate their relative importance.

From 1984 to 2002, various characterisation campaigns were performed on the site of Flémalle. These campaigns provided already a very good knowledge on the nature, amplitude and extent of contamination issues in soils and groundwater in the alluvial aquifer, together with useful and detailed information of the geometry and composition of underground deposits and of piezometric levels for this site.

However, all the information collected during these investigations did not allow one to have a clear global view and understanding of the dynamic of water and pollutants, in particular in the alluvial aquifer. Because of that, it was difficult to really define efficient measures for pollution control and remediation in the site.

With all the experiments and measurements performed in the Flémalle site in the scope of this research, a part of the gap and missing information have been closed. In particular, the collected information has provided a more quantitative view and understanding of hydrodynamic and hydrodispersive properties of the alluvial aquifer, of its heterogeneity and of the very dynamic nature of groundwater – surface water interactions in the test site. The numerical finite difference model has allowed to integrate all the information available (this research, former studies and AquaTerra partners -CHYN and VITO- studies in the site -e.g.: field scale assessment of benzene degradation-), in order to run reliable scenarios of contaminant dispersion (benzene) through groundwater.

DYNAMICS OF GROUNDWATER LEVELS

Time series analysis applied to groundwater heads and river water levels have shown that groundwater heads were mainly controlled by river stage fluctuations. Rainfall and direct groundwater recharge explained only the 20% of the groundwater head dynamics, while the 80% correspond to water river fluctuations. Under regular conditions (river water level ~ 59.4 m a.s.l.), the groundwater is discharged into the river, but inversions of hydraulic gradient are likely to be observed when river water levels increase over 60 m a.s.l. Simultaneously, using temperature as a tracer, changes in groundwater temperature, superposed to the annual trend variability of this parameter, indicate zones of preferential interactions between the river and the aquifer. These changes in groundwater temperature also seem to indicate that the entrance of surface water in site is restricted to the first 25 meters of the alluvial aquifer with respect to the river.

Pumping tests were also relatively influenced by the presence of the Meuse River, but also by the spatial heterogeneity of the hydraulic conductivity of the alluvial aquifer.

MOBILITY AND ATTENUATION OF BENZENE AND OTHER TYPICAL CONTAMINANTS IN THE FLÉMALLE SITE

Based on the detailed investigations performed and advanced modelling results, one can conclude that biodegradation processes, geochemical conditions and transient hydraulic conditions prevailing in the aquifer – river system are the main factors controlling the risk of downstream organic (benzene) contaminant dispersion in the studied brownfield. Geochemical conditions are mainly conditioned by biodegradation processes that have been related mainly to sulphate-reducing conditions, since oxygen and nitrate are almost depleted in the benzene source area. If nowadays conditions remain constant, it seems that the risk of contaminant dispersion to the Meuse River through groundwater discharge is not a special threat. However, based on sampling it is reasonable to suppose that benzene was degraded from the beginning under oxidising conditions, and subsequently under nitrate-reducing conditions, until the complete depletion of these electron acceptors in the source area and in the aquifer around. Today, sulphate-reducing conditions can be considered as main responsible for benzene degradation.

Degradation of PAHs present in the aquifer, such as naphthalene and acenaphthene, was also demonstrated in laboratory by CHYN, although their degradation rates were lower than benzene. As occurs with benzene, high concentrations of these substances are observed in the source area, while they have not been observed close to the river up to now. It is expected that

the risk of dispersion of PAHs is also low since these compounds are less mobile than benzene in groundwater. This should be checked using the model with appropriate degradation and sorption parameters.

The integration of different field techniques and groundwater modelling has enabled to well characterise the brownfield and understand the attenuation of benzene. This methodology and results arising from this work can be of a valuable interest for end-users face up to study brownfields with similar characteristics as the one here presented, often encountered in industrialised countries.

ADVANCES IN FIELD INVESTIGATIONS AND MODELLING

The use of detailed monitoring of groundwater heads and surface water for a long period of time has provided complete and useful dataset, enabling to obtain valuable information of the groundwater – surface water dynamics. Such monitoring scheme is cost-effective, easy to implement in the field and, as shown in this research, it provides very concluding data and modelling results. In contexts such as in Flémalle, continuous groundwater and surface water monitoring, as well as monitoring of complementary parameters such as temperature, is thus highly recommended.

An interesting outcome of field investigations was the development of a new tracer technique (FVPDM) for the quantification of Darcy fluxes in groundwater. It was demonstrated that this technique provides a control of the injection conditions together with complementary information on groundwater flows in the vicinity of the well.

The sensitivity to the experimental conditions makes of the FVPDM a candidate for studying and monitoring changes in Darcy fluxes and groundwater flows in transient conditions, such as changes in hydraulic gradients, with potential applications in monitoring the dynamics of groundwater – surface water interactions in the hyporheic zone. Another important issue of the technique is its combined use, for a relatively long period of time, with passive flux meters for a better assessment of cumulated contaminant fluxes at the vicinity of the monitoring well.

In regard to modelling works, the gap of existing data at a regional scale (outside the studied brownfield) was overcome using a double-scale approach in the automatic parameter estimation process, based on zonation, at the regional scale, and pilot points, at the local scale. Doing so, the regional approach gives enough flexibility to the model in adjusting piezometric levels around the brownfield, at the same time as it avoids overparameterisation of the model, while the local scale approach provides efficient parameterisation for highlighting the strong

heterogeneity of the aquifer and its consequence on groundwater flow and contaminant transport in the site.

VALIDITY OF MONITORED NATURAL ATTENUATION (MNA)

In order to assess the viability of natural attenuation of benzene, the following investigations and monitoring operations should be performed. First, it would be interesting to complete the monitoring network in the alluvial aquifer in order to have efficient control planes in the field, downstream from the sources, where mass reduction could be monitored and confirmed (i.e. in the zone where the numerical model predicts the main extension of the benzene plumes). Second, it would be necessary to evaluate the available "stock" of sulphate and to see if it is likely to be fully depleted as it was the case for nitrate and oxygen, in which case, one could probably not just rely on hydrodynamics processes to expect further and sufficient attenuation of the benzene plume.

The concomitant effects of organic and inorganic contaminants should also be examined further since any shift in geochemical conditions, from oxidised to reduced conditions, could cause the turnover of several heavy metals, such Zn and Cd, accelerating their mobility in the aquifer and the associated risk of dispersion off site. To do so, more advanced multi-component reactive transport modelling could certainly contribute to a more detailed and reliable risk assessment of contaminant dispersion in the brownfield. This could however require further investigations in the field, such as, again, control plane monitoring of contaminants.

ANNEX 1

Complement on GW – SW monitoring pictures of Chapter 4

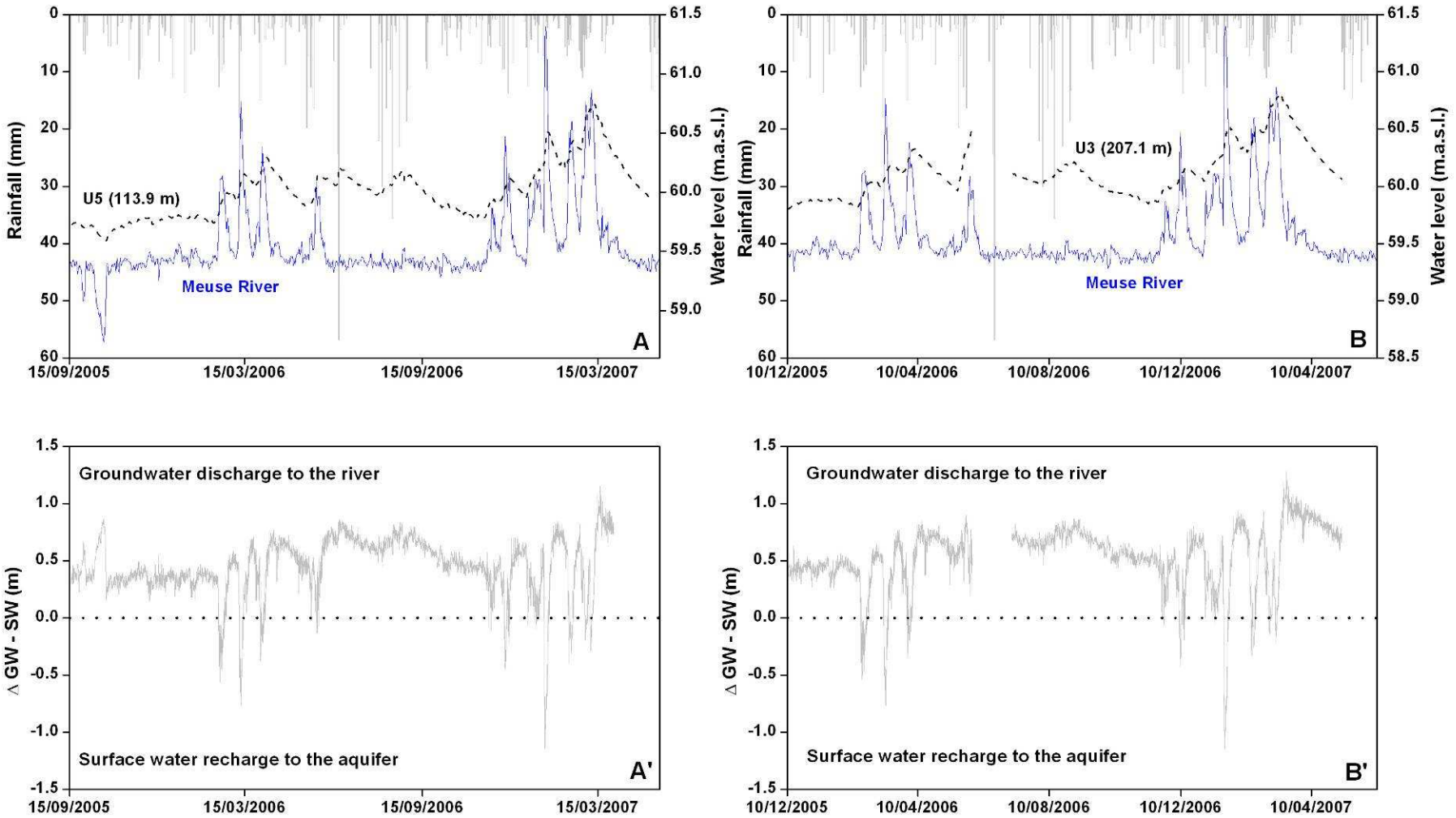

Daily groundwater level (GW) and, Meuse River levels (SW), and rainfall (Ivoz-Ramet dam), for observation wells U5 (A) and U3 (B). Difference between groundwater and Meuse River levels (Δ GW – SW), calculated with hourly data, is also presented (A' and B', respectively).

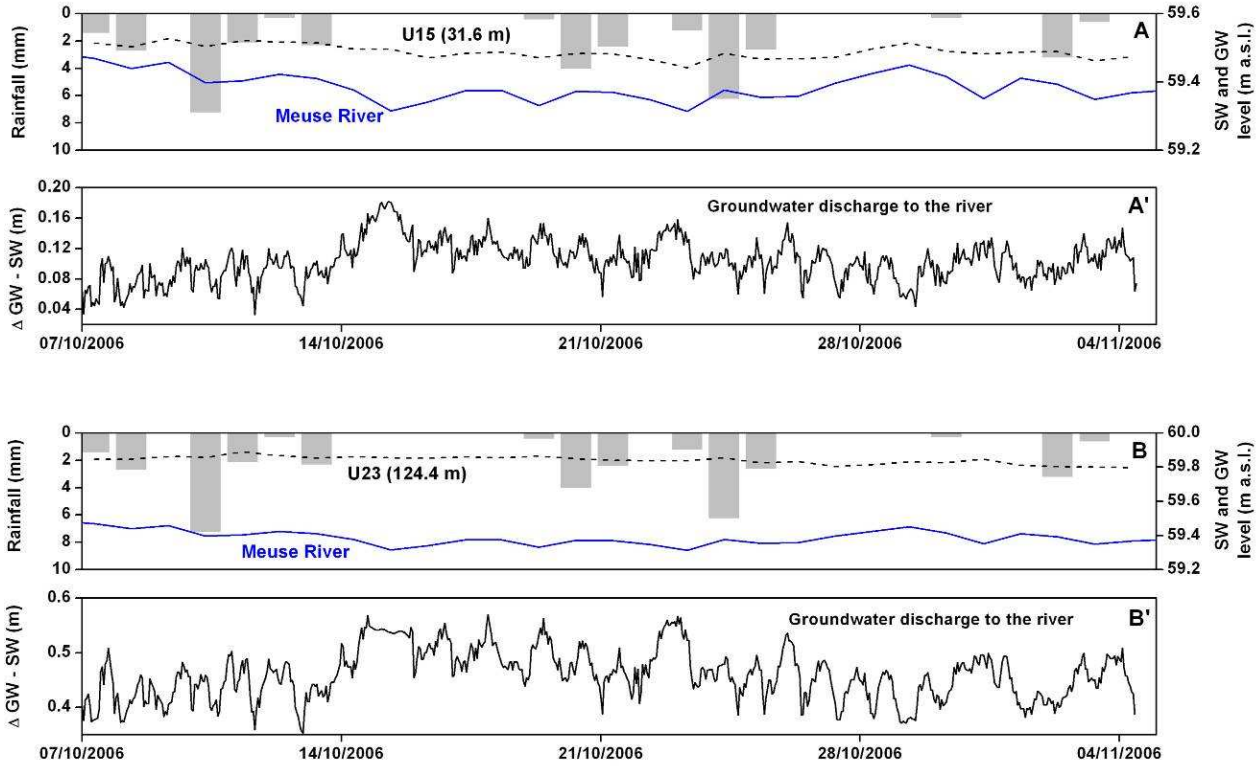

Daily groundwater (GW) and Meuse River levels (SW), and rainfall (Ivoz-Ramet dam), for observation wells U15 (A) and U23 (B). Difference between groundwater and Meuse River levels (Δ GW – SW), calculated with hourly data, is also presented (A' and B', respectively).

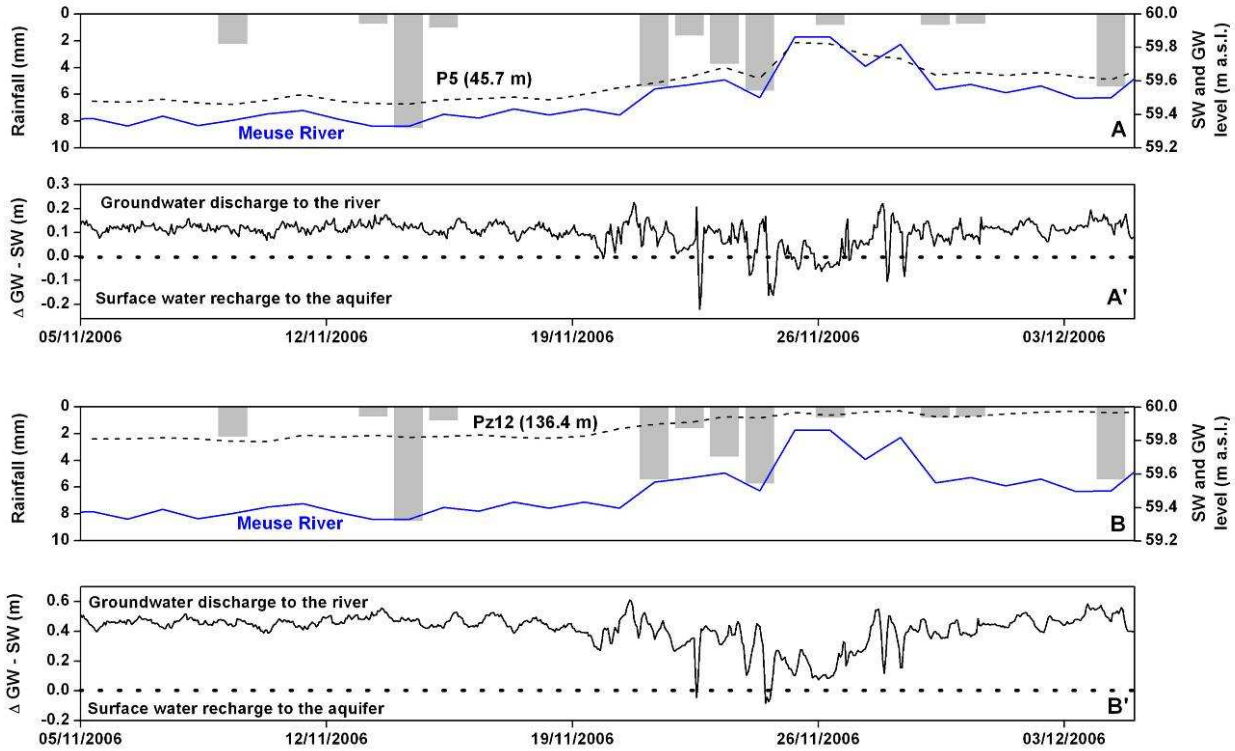

Daily groundwater (GW) and Meuse River levels (SW), and rainfall (Ivoz-Ramet dam), for observation wells P5 (A) and Pz12 (B). Difference between groundwater and Meuse River levels (Δ GW – SW), calculated with hourly data, is also presented (A' and B', respectively).

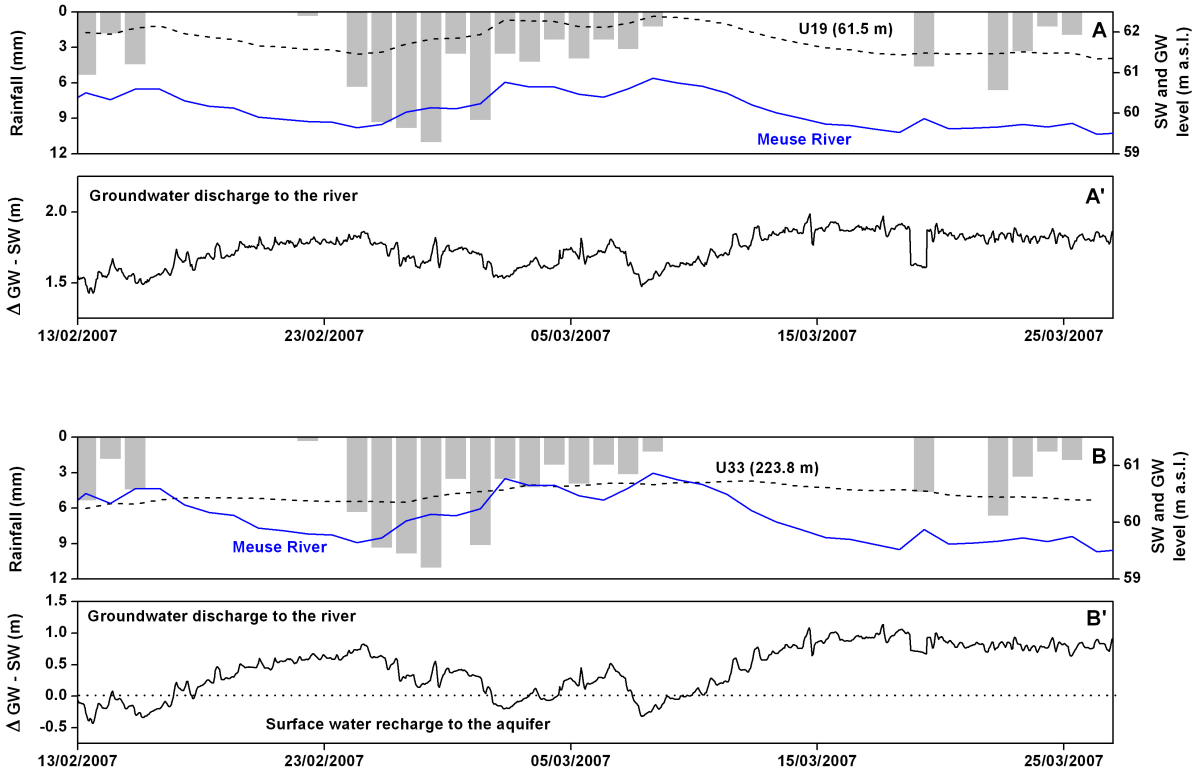

Daily groundwater (GW) and Meuse River levels (SW), and rainfall (Ivoz-Ramet dam), for observation wells U19 (A) and U33 (B). Difference between groundwater and Meuse River levels (Δ GW – SW), calculated with hourly data, is also presented (A' and B', respectively).

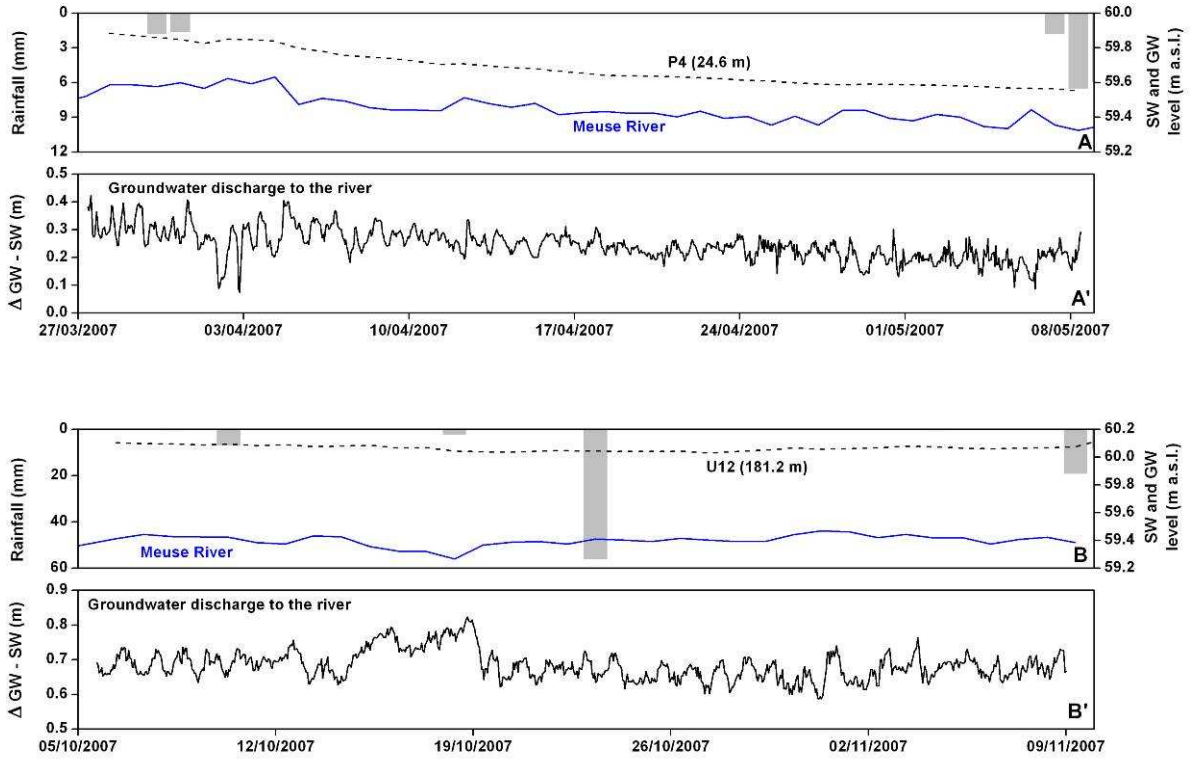

Daily groundwater (GW) and Meuse River levels (SW), and rainfall (Ivoz-Ramet dam), for observation wells P4 (A) and U12 (B). Difference between groundwater and Meuse River levels (Δ GW – SW), calculated with hourly data, is also presented (A' and B', respectively).

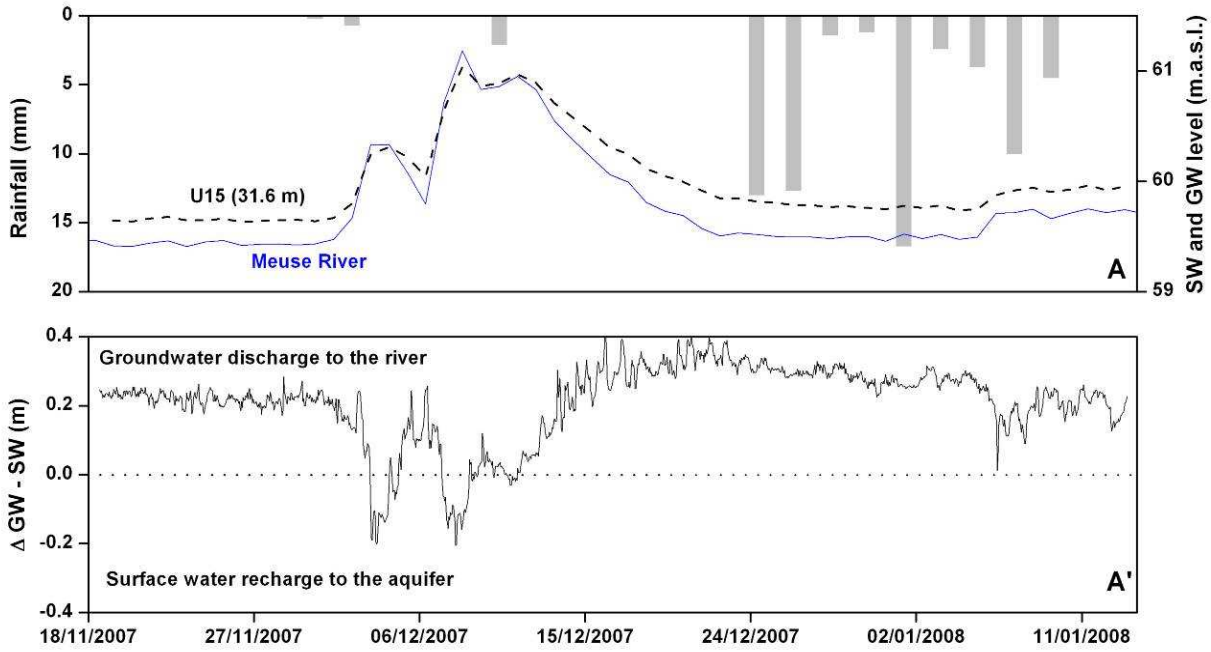

Daily groundwater (GW) and Meuse River levels (SW), and rainfall (Ivoz-Ramet dam), for observation well U15 (A). Difference between groundwater and Meuse River levels (Δ GW – SW), calculated with hourly data, is also presented (A').

ANNEX 2

Published article in Hydrogeology Journal

In the scope of the AquaTerra project, the University of Liège was also involved, into the sub-project TREND, in the study of the development and estimation of groundwater quality trends, with application to datasets available for different groundwater bodies in the Walloon Region. It was into this research where the first time of my Ph.D was spent.

A statistical approach was proposed and applied for trend detection and quantification in groundwater quality (nitrate) datasets in the Geer basin (Belgium), based on a three-step statistical analysis methodology. This work has been published in Hydrogeology Journal, and a copy of this manuscript is here attached.

The statistical analysis provided point-by-point estimates of nitrate trends, in the form of slopes expressed by an increase or a decrease in nitrate concentration per year. In the Geer basin, a general upward trend is observed in the entire basin. Two zones can be distinguished in the basin: the Southern part corresponding to the unconfined part of the chalk aquifer where high nitrate concentrations are observed, and the Northern part corresponding to the confined part of the aquifer, where nitrate has not been detected (or at very low concentrations only).

A rough estimation of the time remaining before the threshold concentration of 50 mg L^{-1} would be exceeded, and was calculated based on a point-by-point extrapolation of current nitrate contamination levels using nitrate trend estimates. To do so, the present contamination level was estimated at the different groundwater abstraction points used for drinking water production. This estimation was based on a point-by-point calculation of mean nitrate concentration over the period 1999-2003, a period for which the nitrate dataset is well furnished. Then, using the calculated slope value at the nearest available point, an estimation of the year at which the drinking limit will be reached was performed.